



UNIVERSITÀ DEGLI STUDI DI SALERNO



UNIVERSITÀ DEGLI STUDI DI SALERNO
Dipartimento di Farmacia

Dottorato di Ricerca
in **Scienze del Farmaco**
Ciclo XXIX — Anno accademico 2016/2017

Tesi di Dottorato in

Design, synthesis, biological evaluation and binding studies of new small-molecule modulators of KDMs (lysine-specific demethylases)

Dottorando

Dott. *Amodio Luca Balzano*

Tutore

Chiar.mo Prof. *Gianluca Sbardella*

Coordinatore: Chiar.mo Prof. *Gianluca Sbardella*

ABSTRACT	VII
CHAPTER 1 - INTRODUCTION	9
1.1. <i>Epigenetic</i>	10
1.2. <i>The genome organization</i>	10
1.3. <i>The epigenetic enzymes</i>	11
1.4. <i>Histone methylation</i>	13
1.5. <i>Histone demethylase proteins (HDMs)</i>	15
1.6. <i>Histone lysine demethylases (KDMs)</i>	16
1.6.1. Lysine specific demethylases (LSDs)	16
1.6.2. Jumonji-C domain-containing histone demethylase (JHDMs)	19
1.7. <i>The Jumonji-C domain-containing protein 2 family (JMJD2)</i>	21
1.7.1. The physiological role of KDM4s	23
1.7.2. The pathological role of KDM4s	24
1.8. <i>KDM4s: a relevant therapeutic target</i>	25
1.8.1. The 2OG derivatives	25
1.8.2. 8-Hydroxyquinoline-based KDM4s inhibitors	27
1.8.3. Other Fe-chelating KDM4s inhibitor scaffolds	28
1.8.4. KDM4s inhibitors of natural origin	29
1.8.5. Noncatalytic domain targeting KDM4s inhibitors	30
1.8.6. Substrate competitive inhibitors	31
1.8.7. Other inhibitors of KDM4s	31
1.9. <i>Specific demethylation assays used in lead discovery</i>	32
1.9.1. Indirect demethylation methods	33
1.9.2. Direct demethylation methods	35
CHAPTER 2 - AIM OF WORK	36

2.1.	<i>High-Throughput Screening for the identification of new hits</i>	37
2.2.	<i>Fragment-based ligand discovery</i>	38
2.3.	<i>Hit validation process and further derivatizations</i>	41
CHAPTER 3 - CHEMISTRY		45
3.1.	<i>Synthesis of thiophene-2-sulfonamide derivatives</i>	46
3.2.	<i>Synthesis of quinoxaline derivative</i>	47
3.2.1.	Construction of the quinoxaline core	48
3.2.2.	Synthesis of 2-amino-N-hydroxybenzamide (33)	55
3.2.2.1.	Synthesis and deprotection of 2-amino-N-(benzyloxy)benzamide (127a)	56
3.2.2.2.	Synthesis and deprotection of 2-amino-N-((tetrahydro-2H-pyran-2-yl)oxy)benzamide (127b)	58
3.3.	<i>Synthesis of triazole derivatives</i>	59
3.4.	<i>Synthesis of N-(5-ethyl-1-(2-morpholinoethyl)-3-oxoindolin-2-yl)acetamide</i>	60
3.5.	<i>Synthesis of 3-hydroxy-2,3-dihydroquinazolin-4(1H)-one derivatives (1-30)</i>	61
3.5.1.	Synthesis of quinazolin-4(3H)-one derivatives	64
3.5.2.	Synthesis of non-commercially available aldehydes	64
CHAPTER 4 - BIOLOGY		69
4.1.	<i>Biochemical evaluation of chimera molecules</i>	70
4.1.1.	Orthogonal screening platform	71
4.2.	<i>Hit validation process</i>	72
4.2.1.	Chemical stability assay	73
4.2.2.	Parallel artificial membrane permeability assay	74
4.2.3.	Secondary screening	75

4.3. Preliminary SARs _____	76
4.3.1. Structure-activity relationships of triazole derivatives _____	77
4.3.2. Structure-activity relationships of 3-hydroxy-2,3-dihydroquinazolin-4(1H)-one derivatives _____	78
4.3.3. Binding hypothesis and design of new derivatives _____	80
4.4. Biochemical evaluation _____	81
4.4.1. Determination of solubility _____	82
4.4.2. AlphaLISA homogeneous proximity immunoassay _____	85
4.5. Biological evaluation _____	86
4.5.1. Analysis of histone modifications by mass spectrometry _____	87
4.5.2. Cell cycle analysis _____	92
4.5.3. Analysis of histone modifications by Western blot _____	93
CHAPTER 5 - CONCLUSION _____	96
CHAPTER 6 - EXPERIMENTAL PART _____	101
6.1. General information _____	102
6.2. Procedures to obtain thiophene-2-sulfonamide derivatives _____	102
6.3. Procedures to obtain quinoxaline derivative (97) _____	107
6.4. Procedures to obtain triazole derivatives _____	112
6.5. Procedures to obtain N-(5-ethyl-1-(2-morpholinoethyl)-3-oxindolin-2-yl)acetamide _____	117
6.6. Procedure to obtain 3-hydroxy-2,3-dihydroquinazolin-4(1H)-one derivatives _____	119
6.7. Histone processing and mass spectrometry analysis _____	140
6.8. AlphaLISA KDM4 assay _____	141
6.9. Hit validation stability assays _____	142
6.10. PAMPA _____	143

6.11. Nephelometric assay	144
6.12. NMR data	144
ACKNOWLEDGEMENTS	204
REFERENCES	206

ABSTRACT

JHDMs (JmjC-domain-containing histone demethylases) are the largest class of demethylase enzymes, contain a Jumonji C (JmjC) domain and catalyze lysine demethylation of histones through an oxidative reaction that requires Fe(II) ion and α -ketoglutarate (2OG) as cofactors. The misregulation of these enzymes, in particular JMJD2 subfamily, has been significantly implicated in cancer initiation and progression. Potent and specific inhibitors of these enzymes have not been identified yet, most of them inhibiting many other Fe(II)/2OG dependent oxygenases or being affected by undesirable characteristics.

Here, we describe the discovery by high throughput screening (HTS) of a bunch of novel hit compounds active against KDM4s and the subsequent hit validation stage to select the most interesting ones for further derivatization. The use of a multiple combined approach of different in vitro techniques led us to select the hit **EML586** as starting point for the development of novel optimized derivatives.

The substitution of quinoxaline ring with more aliphatic portions gave derivatives such as **EML678** and **EML684**, which demonstrate a better activity against *h*KDM4A compared to the starting hit compound. Furthermore, they induced a marked reduction in methylation of lysines H3K9 and H3K27 in a cell-based assay together with a marked arrest in the S phase of cell cycle

CHAPTER 1

INTRODUCTION

1.1. Epigenetic

Almost all nucleated cells of human body contains the complete genome sequence; epigenetic changes, among other mechanisms, enable the differentiation of pluripotent stem cells into the somatic cells that make up different organs and tissues in the body¹.

Etymologically, the term *epigenetics* is derived from the Greek επί (epì) γενετικός (genetikòs), which literally means “above or beyond genetics”. The term was first coined in 1942 by Conrad Waddington, defining it as “causal interactions between genes and their products which bring the phenotype into being”². Over the years, the concept of epigenetics has been repeatedly expanded and revised. To date, the most comprehensive definition is that formulated by Bird in 2007, according to which epigenetic events are “the structural adaptation of chromosomal regions so as to register, signal or perpetuate altered activity states”³. This definition does not include the concept of “inheritance”, peculiar characteristic of many epigenetic alterations but not of all of them.

1.2. The genome organization

DNA within eukaryotic cells is condensed in chromatin. The nucleosome is the core unit of chromatin and is composed of an octamer of four different histones (H3, H4, H2A, and H2B), around which DNA is wound with a length of approximately 140–150 base pairs (Figure 1.1)⁴.

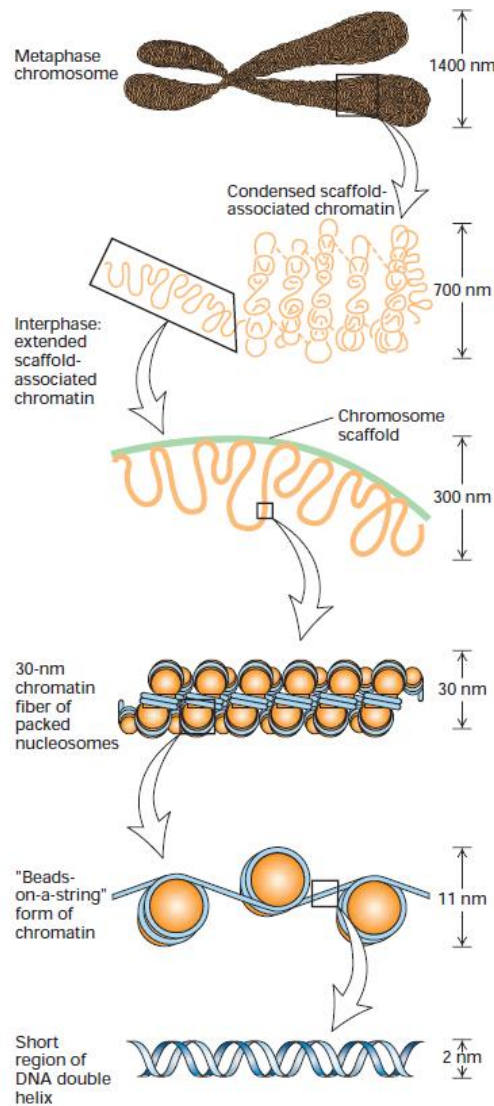


Figure 1.1. The gene organization. Pictures modified from Lodish, H et al.
Molecular cell biology 1999.

For many years, the main function of the histone packaging of DNA was considered to be to compact the double helix into a repressive structure; now we understand that the nucleosome is an active participant in both repression and activation of eukaryotic genes, and that the proper coordination of gene expression involves the dynamic action of hundreds of chromatin protein factors⁵.

1.3. The epigenetic enzymes

DNA and histone proteins can undergo various post-synthetic modifications. These modifications, along with histone variants and nucleosome remodelers, can strongly influence chromatin structure and transcriptional regulation without changing the underlying DNA sequence, in a process called “epigenetic regulation”. Epigenetic regulation can be separated into three inter-related layers: nucleosome positioning, histone modifications, and DNA methylation⁶. It is widely accepted that these mechanisms are intricately interrelated, working together to determine the status of gene expression and to decide cell fate⁷.

Ever since Allfrey’s pioneering studies in the early 1960s, we have known that histones are post-translationally modified. There are a large number of different histone post-translational modifications (PTMs), including methylation, acetylation, phosphorylation and ubiquitination⁸. Distinct histone modifications can generate synergistic or antagonistic interaction affinities for chromatin-associated proteins, which in turn dictate dynamic transitions between transcriptionally active or silent chromatin states. The combinatorial nature of histone modifications thus suggests a “histone code” that considerably extends the information potential of the genetic code⁹.

Histone modifications are catalyzed by a large variety of histone-modifying enzymes, which are able to read, add or remove covalent modifications to histone proteins⁴. They are generally divided into three categories: enzymes that add chemical marks to histone substrates, the so-called *writers* such as histone acetyltransferases (HATs) and histone methyltransferases (HTMs); enzymes that remove such chemical covalent modification from histone substrates—namely, *erasers* such as histone deacetylases (HDACs) and histone lysine demethylases (KDMs); and proteins that recognize and react to specific modified histone residues at epigenetic code level, the *readers*¹⁰ (Figure 1.2).

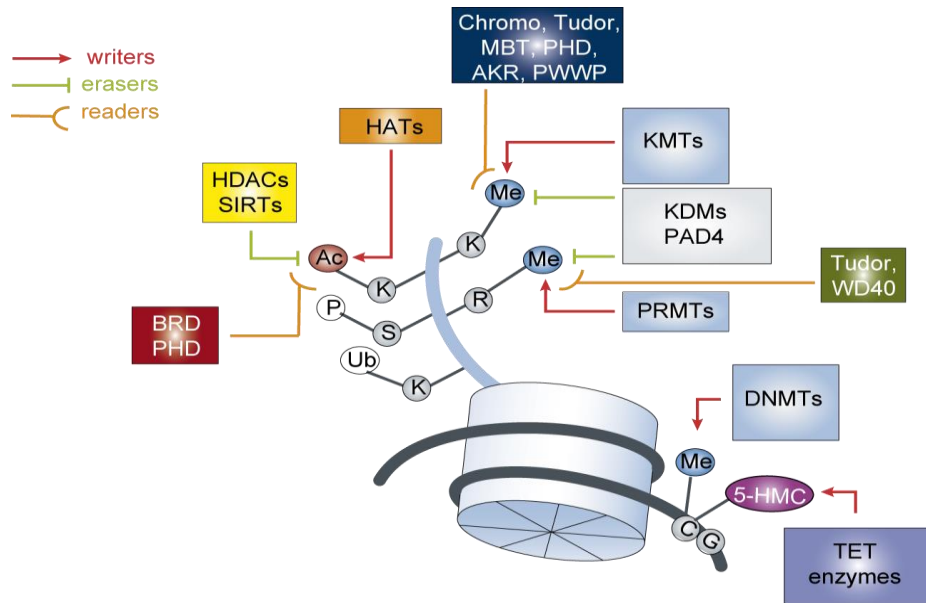


Figure 1.2. Classification of epigenetic enzyme. Pictures modified from Copeland, R. A. et al. *Nat Rev Drug Discovery* 2009.

1.4. Histone methylation

Histone methylation is an important epigenetic modification in chromatin. Lysine and arginine residues can be methylated. The number of methyl groups that can be incorporated at a specific residue is different and seems to be determinant to transcription. Thus, the ϵ -amino group of lysines can be mono-, di-, or trimethylated, while the guanidino- ϵ -amino groups of arginines can accommodate two methyl groups in a symmetric or asymmetric manner (Figure 1.3)¹¹.

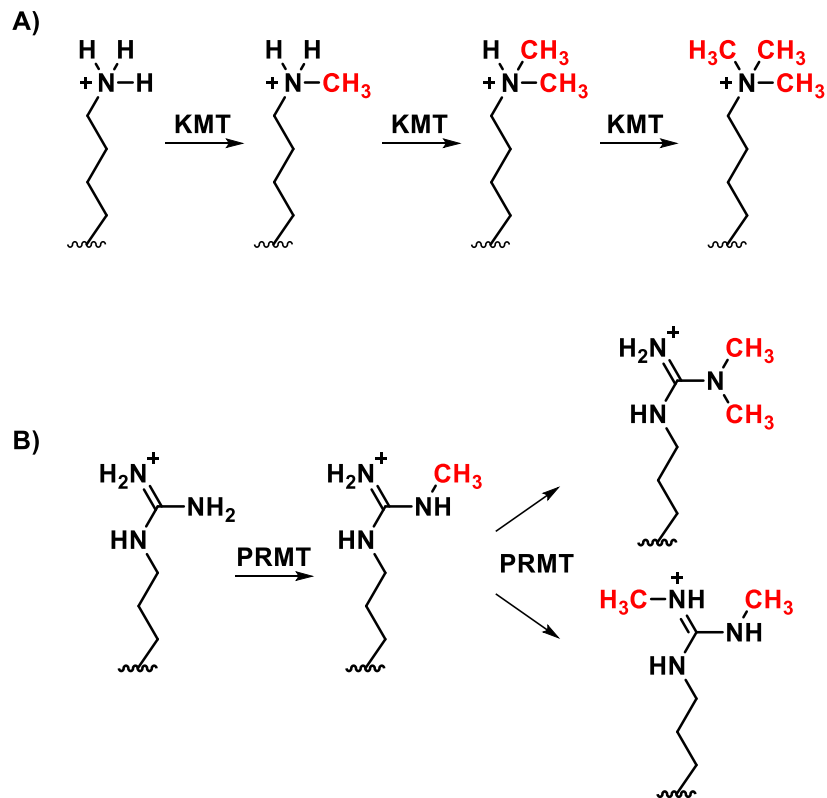


Figure 1.3. Lysine (A) and arginine (B) methylation states.

Histone methylation is regulated by a complex network that involves a large number of site-specific methylases (HMTs), demethylases (HDMs) and methyl recognition proteins¹², which play an important role in many biological processes, including cell-cycle regulation, DNA damage- and stress response, embryonic development and cellular differentiation^{4, 13}.

Arginine/lysine methylation is catalysed by S-adenosyl-methionine-dependent methyltransferases (HMTs), that can be grouped into two divergent families: histone lysine methyltransferases (HKMTs) catalyzing the methylation of lysine residues and protein arginine methyltransferases (PRMTs) catalyzing the methylation of arginine residues¹¹.

The introduction of a methyl group, despite not altering the amino acid charge, induces alterations in the chromatin architecture. In contrast with acetylation/deacetylation of the histone tails, where in general acetylation reduces

DNA–nucleosomal interactions to facilitate transcription, methylation on either lysine or arginine residues of the histone tails can be associated with either condensation or relaxation of the chromatin structure. Since several sites for methylation are present on each tail, different combinations are possible¹⁴⁻¹⁵.

Furthermore, it should also be remembered that methylation of lysine and arginine residues is not only limited to histones. Several methyltransferases have been identified to methylate many non-histone proteins including RelA, p53, estrogen receptors and TAF10, regulating moreover distinct functions of NF- κ B¹⁶⁻¹⁸.

1.5. Histone demethylase proteins (HDMs)

HDMs are enzymes that, as the name suggests, remove methyl groups from lysine and arginine residues in both histone and non-histone proteins.

Although for many years N-methylation was thought to be a stable, irreversible modification, the reversal of lysine methylation is now well established. In 2004, the first mammalian histone lysine demethylase (KMD) was reported to be a flavin-containing amino oxidase (AO) that specifically demethylated mono or dimethylated lysine 4 at histone H3 (H3K4me1 and H3K4me2) and has been named LSD1 (lysine-specific demethylase 1)/KDM1A¹⁹.

Since then this area of research has grown exponentially with the identification of a second flavin-dependent H3K4me1/2 demethylase called LSD2/KDM1B²⁰ and a larger and more versatile family of KDMs, structurally different from LSD1, working through a Fe(II)/2-oxoglutarate (2OG) mechanism for catalysis²¹⁻²².

In contrast to lysine methylation, the extent to which arginine methylation is dynamic is much less clear. The peptidyl-arginine deiminases (PADs) catalyse the hydrolysis of the guanidino arginine side chain to the urea group of citrulline²³⁻²⁴. In this reaction, demethylination is not a ‘true’ demethylation reaction: it removes but does not reverse N-methylation because produces neutral citrulline,

which has considerably different chemical properties compared to unmethylated arginine.

Recently, some KDMs have been reported to catalyze methylarginine demethylation²⁵⁻²⁷; however, their biological role in these processes is still controversial and it merits further investigation.

1.6. Histone lysine demethylases (KDMs)

Removal of the N-methyl tag on lysine residues of histone proteins is carried out by two different classes of oxidative enzymes. LSDs (Lysine specific demethylases) are a class of enzymes that directly reverse histone H3K4 or H3K9 modifications by an oxidative demethylation reaction in which flavin adenine dinucleotide (FAD) is a cofactor¹⁹. JHDMs (JmjC-domain-containing histone demethylases) are the second class of oxidative demethylase enzymes. These enzymes catalyse demethylation through a reaction that requires iron Fe(II) and 2OG as cofactors²².

1.6.1. Lysine specific demethylases (LSDs)

Mammals contain so far only two flavoenzyme demethylases: LSD1 and LSD2 known also as KDM1A and KDM1B¹⁹⁻²⁰.

In the early 60s, it was observed for the first time a demethylase activity that could demethylate modified lysine by an amine oxidase (AO) reaction in tissue extracts. It was proposed a mechanism in which FAD was a cofactor and formaldehyde and unmethylated lysine were reaction products²⁸. The reaction was catalyzed by an enzyme called LSD1, identified several years later as a component of a histone deacetylase (HDAC) protein complexes²⁹⁻³⁰. Based on the presence of LSD1 in chromatin-modifying complexes and its predicted FAD-dependent AO function, it was proposed as the long-sought-after FAD-dependent histone demethylase enzyme¹⁹.

LSD1 shows a robust demethylase activity with specificity towards histone H3 methylated on lysine 4 (H3K4), but it can demethylate also non-histone targets, such as K370me1 and K370me2 on p53³¹, Lys1096 on DNA methyltransferase 1 (DNMT1)³² and Lys185 on E2F1³³.

The other LSD family member, LSD2 (KDM1B) has so far only been shown to demethylate H3K4me1 and H3K4me2^{20, 34}. Furthermore, characterization of the LSD2 complex reveals that LSD2 forms active complexes with euchromatic histone methyltransferases G9a and NSD3 as well as cellular factors involved in transcription elongation. These data provide a possible molecular mechanism linking LSD2 to transcriptional regulation after initiation³⁵.

These enzymes are related to the well-characterized monoamine oxidases (MAOs). Structurally, both LSDs consist of an N-terminal SWIRM domain and an amine oxidase-like (AOL) domain containing 2 sites to bind the methylated substrate and the FAD cofactor, respectively (Figure 1.4).

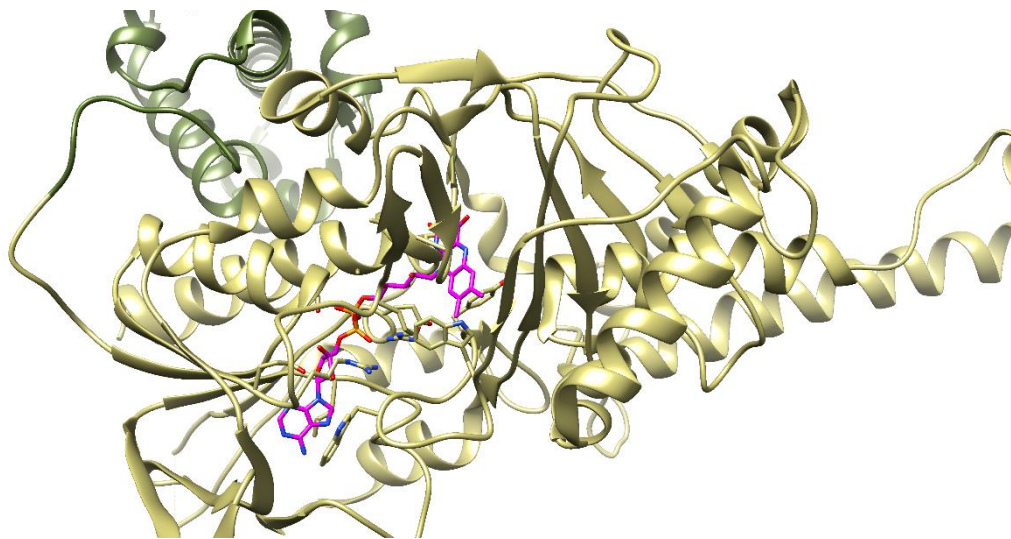


Figure 1.4. Crystallographic structure of LSD1: amine oxidase-like (AOL) domain with FAD (magenta) and SWIRM domain (green). PDB: 2HKO.

Only in LSD1, between these 2 sites in the AOL domain, there are 2 antiparallel α -helices project away as a unique feature forming the Tower domain, crucial for the interaction of LSD1 with other proteins and for the ability to

demethylate nucleosomal substrates^{10, 36-38}. Otherwise, LSD2 has an amino-terminal zinc finger domain of unknown function³⁹.

The catalytic activity resides in the AOL domain, which uses an oxidation mechanism that is dependent on the cofactor FAD to catalyse the removal of methyl groups from histone lysine residues. The catalytic mechanism relies on a lone electron pair on the lysine ϵ -nitrogen atom, and for this reason the LSD enzymes can demethylate mono- and demethylated lysines but not trimethylated lysines (Figure 1.5)⁴⁰.

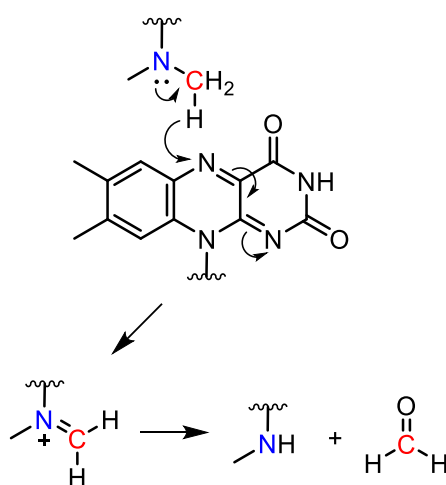


Figure 1.5. Mechanism of action of LSDs.

Given the structural similarities with MAOs, amongst the first reported KDM1 inhibitors there were structures as phenelzine and tranylcypromine (PCPA)⁴¹. Subsequent studies supported by crystallographic analyses, have utilized tranylcypromine as a scaffold for the development of a good number of analogues, modified on both the aromatic ring and amino groups. These inhibitors display both improved potency, especially against KDM1A, and, in some cases, also selectivity (Figure 1.6)⁴².

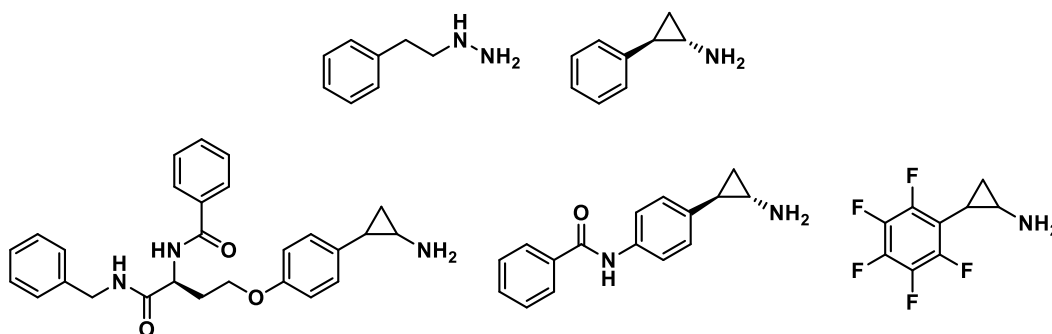


Figure 1.6. Some inhibitors of LSD1.

Interestingly, the LSD1 inhibitor ORY-1001 is currently in a phase I/IIA clinical trial in patients with relapsed or refractory acute leukemia⁴³.

1.6.2. Jumonji-C domain-containing histone demethylase (JHDMs)

JHDMs are the second and largest class of demethylase enzymes. They contain a Jumonji C (JmjC) catalytic domain and catalyse lysine demethylation of histones through an oxidative reaction that requires iron Fe(II) and 2-oxoglutarate as cofactors^{21-22, 44}.

The name of this family is correlated with the high conserved JmjC-domain that was first identified in the protein JARID2⁴⁵. *Jumonji* means cruciform in Japanese: the gene was so named because mutant mice on *jmj* locus develop an abnormal cross-like neural tube⁴⁵.

This enzyme class is part of a much larger superfamily, the 2OG oxygenases, whose members (about 80 genes in the human genome) catalyse a diverse range of oxidation reactions⁴⁶, e.g. enzymes involved in the hypoxic response pathway⁴⁷⁻⁴⁹. Among the 30 JmjC domain-containing proteins identified so far within the human genome, about 20 have been found to possess histone demethylase activity. Six different subfamilies (JMJD1s, JMJD2s, JARID1s, UTX/Y-JMJD3, PHFs, and FBXLs) of JHDMs have been described, which have different histone sequence and methylation state selectivities (Figure 1.7)⁵⁰⁻⁵¹.

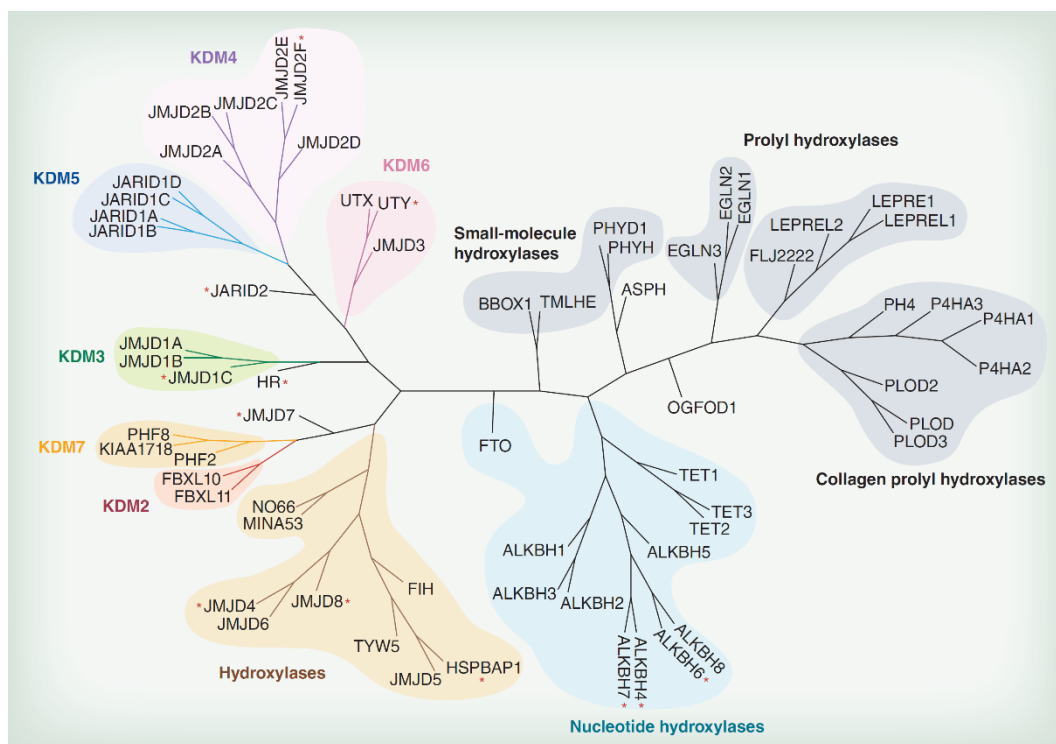


Figure 1.7. Phylogenetic tree of JHDMs. Pictures modified from Johansson, C. et al. *Epigenomics* **2014**.

The JmjC domain is characterized by a double-stranded β -helical (DSBH) fold, also called the “jelly-roll” fold, composed of eight β -strands which are arranged antiparallel to each other to form a β -sandwich structure⁵². The active site is located at one end of the DSBH fold, employing a two-histidine-one-carboxylate “facial triad” to coordinate the catalytic Fe(II) center, while 2OG interacts with two residues that are also conserved among the members of the JHDM family^{40, 49}.

Most JHDMs also contain additional secondary structure elements, including at least one helix to the C-terminal side of the DSBH, that surround the domain and define the different subfamilies⁵³⁻⁵⁴.

The catalytic mechanism for JHDMs is provided in Figure 1.8. The two cofactors, Fe(II) and 2-oxoglutarate, react with dioxygen to form a highly active oxoferryl (Fe(IV)=O) intermediate that hydroxylates the methyl groups of the methylated lysine substrate^{53, 55}. The resulting lysyl hemiaminal is unstable and is hydrolyzed to release the methyl group from nitrogen in the form of formaldehyde.

This mechanism allows for the demethylation of lysines in all three methylation states (mono-, di- and trimethylated lysines)⁵⁶⁻⁵⁷.

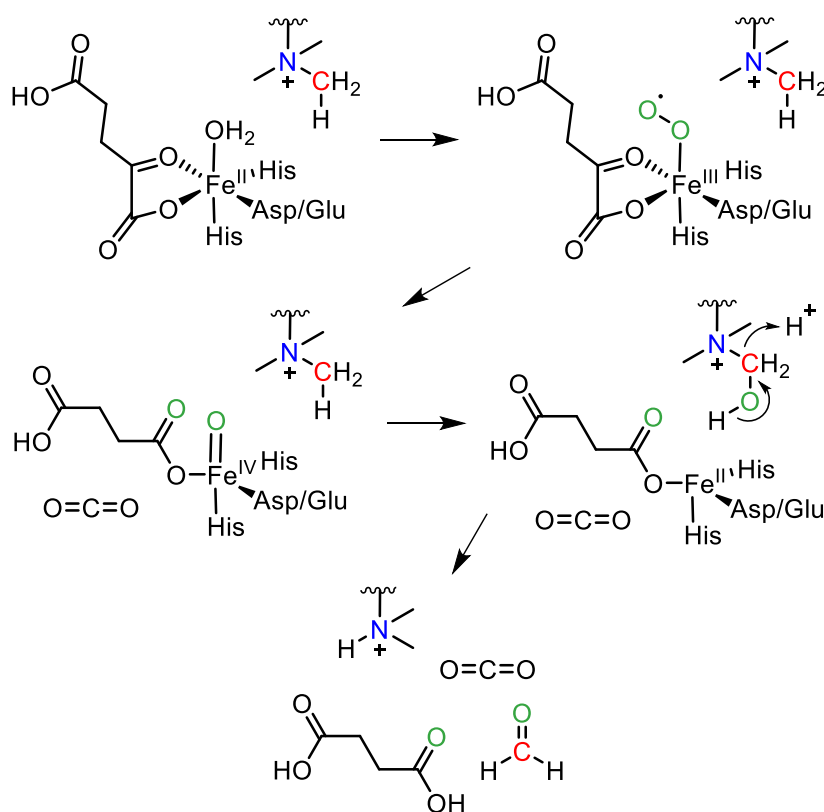


Figure 1.8. Catalytic mechanism of JHDMS.

Although this reaction is common to JHDM enzymes, crystallographic analyses have shown that variations in the size of the active site region are in part responsible for the methylation state selectivity⁵³. Similarly, also the presence of non-catalytic domains, including the PHD, Tudor, CXXC, FBOX, ARID, LRR, as well as JmjN domains, regulates demethylase selectivity to particular residues⁵⁸⁻⁵⁹.

Furthermore, mounting evidence suggests that some JmjC demethylases are also able to demethylate non-histone substrates⁶⁰.

1.7. The Jumonji-C domain-containing protein 2 family (JMJD2)

The subfamily of JMJD2s (called KDM4s in an alternative, more recent, nomenclature) is one of the largest among the JHDMs⁶¹. Six *Jmjd2* genes are present in the human genome, coding for as many different isoforms classified according to an alphabetical order from A to F⁶².

Jmjd2E and *-F*, whose gene products are very similar to KDM4D, are considered pseudogenes and, only recently, *Jmjd2E* expression has been observed, suggesting its role as a functional gene. However, the catalytic domain of human KDM4E is highly active and shows similar substrate specificities as KDM4D⁶³.

KDM4 subfamily enzymes are highly conserved; KDM4A–C orthologues exist in all genome-sequenced vertebrates with earlier animals containing only a single KDM4 enzyme. Contrarily, KDM4D orthologues only exist in eutherians placental mammals where they are conserved, including proposed substrate sequence-determining residues⁶³.

The KDM4A–C proteins share more than 50% sequence identity and contain JmjN, two plant homeodomains (PHD) and two Tudor domains in addition to the JmjC domain. KDM4D–F, in contrast, contain only the JmjN and JmjC domains. As for the other JHDMs, the JmjC domain bears catalytic function in KDM4s, while the JmjN domain interacts extensively with JmjC and provides structural integrity (Figure 1.9)^{57, 61}. Phylogenetic analysis shows that KDM4A and KDM4C are more similar to one another than KDM4B and KDM4D. They all contain the conserved amino acids that are associated with Fe(II) coordination⁵⁶.

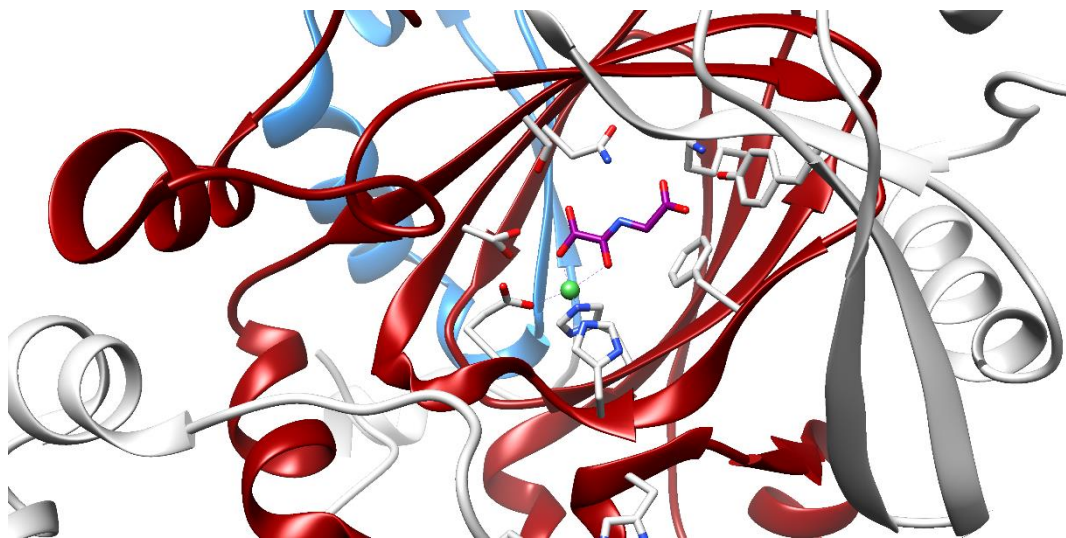


Figure 1.9. Active site of KDM4A with 2OG (magenta). JmjC domain (red) and JmjN domain (blue) are visible. PDB: 2Q8E.

Crystallographic data of KDM4A revealed that the active site of this subfamily enzymes is larger and more open than other JHDM demethylases due to the presence of an adjacent aliphatic subpocket⁶⁴. Moreover, there is a secondary Cys3-His Zn(II) binding site close to the N-methyl lysine-residue binding site. Bioinformatic analyses indicated that none of the other JHDM subfamilies (or indeed other 2OG oxygenases) identified to date have a comparable Zn-binding site close to their catalytic domain (although some do have structurally diverse Zn(II) binding sites in other domains likely involved in binding to chromatin)⁶⁵. This site can be may be involved in substrate recognition.

Biochemical studies indicate that KDM4A-C catalyze the removal of H3K9 and H3K36 di- and trimethyl marks, while KDM4D can only demethylate H3K9me3/me2. KDM4E meanwhile, catalyzes the removal of two methyl groups from H3K9me3 and H3K56me3⁶⁶.

Beyond the catalytic core of KDM4A-C, the C-terminal PHD and Tudor domains bear important histone reader functions. Structural and biochemical studies have demonstrated that the Tudor domains of KDM4A can recognize and bind two unrelated histone marks, H3K4me3/me2 and H4K20me3/me2, by means of distinct binding mechanisms⁶⁷⁻⁶⁹. Furthermore, the PHD domains in other histone regulatory proteins have been demonstrated to bind unmodified or modified histone residues on one or more histone tails, offering flexibility in directing epigenetic modifications⁷⁰. However, to date, no functional studies of the KDM4s PHD domains have been reported, highlighting the need to clarify the molecular function of these domains.

1.7.1. The physiological role of KDM4s

Kdm4 genes are expressed in various human tissues; KDM4A-C are broadly expressed in the spleen, ovary and colon, while KDM4D is predominantly

expressed in the testes⁷¹. KDM4 proteins can be found in multiprotein complexes known to participate in transcriptional regulation and epigenetic remodeling.

KDM4A is the most abundant and the most studied isoform. Through H3K9me3 demethylation, it promotes an open chromatin state, contributing to the transcription activation of promoter regions. Contrarily, the outcome of KDM4A-mediated demethylation of H3K36 is less clear⁷². KDM4A is also implicated in replication timing and genomic stability⁷³.

KDM4A abundance is cell cycle-dependent, and this protein antagonizes the function of heterochromatin protein 1 gamma (HP1g)⁷³. Additionally, KDM4A is involved in the DNA damage response together with KDM4B through their Tudor domains that bind to the methylated residues of H4. After DNA damage, KDM4A/B is ubiquitinated by RNF8 and RNF168 and degraded by the proteasome, allowing the binding of 53BP1 to H4K20me2. Furthermore, KDM4A overexpression abrogates 53BP1 recruitment to DNA damage sites, suggesting a possible role of KDM4A in the DNA damage response⁷⁴.

KDM4A has also been found to play a key role in the regulation of p53 through its function, in complex with a F-box protein, as a novel E3 ubiquitin ligase targeting methylated p53 for degradation at the late senescent stage⁷⁵.

More recently, it was proposed that KDM4A possesses the potential to act as an oxygen sensor in the context of chromatin modifications, with possible implications for epigenetic regulation in hypoxic disease states⁷⁶.

1.7.2. The pathological role of KDM4s

Perturbations in heterochromatin and histone methylation are common characteristics of tumor cells⁷⁷⁻⁷⁸. Global changes in histone methylation patterns can be found in several tumor types, such as breast, prostate, lung, and ovarian cancer⁷⁹⁻⁸¹. In particular, there is an abundance of data linking aberrations in H3K9 methylation to cancer⁸²⁻⁸³.

The KDM4 proteins are capable of modifying the epigenetic landscape, and several tumor types have been identified that overexpress one of these demethylases. For example, KDM4B levels are increased in colorectal cancer⁸⁴ and medulloblastoma⁸⁵ and functions as an oncogene in breast cancer⁸⁶⁻⁸⁷. In particular, KDM4B mRNA levels are higher in ER α -positive breast cancer where there is a cooperative interaction between KDM4B and ER α to allow the transcription of several oncogenes and anti-apoptotic genes⁸⁷.

KDM4A overexpression plays a key role in prostate cancer progression. KDM4A and KDM4B are overexpressed in prostate cancer and KDM4A and KDM4D both bind the androgen receptor (AR), stimulating AR-induced transcription that is the driving force behind the development and progression of pathology⁸⁸⁻⁸⁹.

Also KDM4C is overexpressed in several tumor types including breast cancer⁹⁰, esophageal squamous cell carcinoma⁹¹, and Hodgkin lymphoma⁹².

The association of KDM4 overexpression with malignancy is a reflection of their role in promoting cellular proliferation. For each of KDM4A–D, forced overexpression is associated with increased cellular proliferation and anchorage-independent growth⁸⁹. Moreover, knockdown of the overexpressed KDM4 proteins reduces these oncogenic characteristics^{87, 93-94}.

Aberrant KDM4s activity is also associated with cardiac hypertrophy⁹⁵, cellular response to hypoxia⁷⁶ and DNA damage response⁹⁴.

1.8. KDM4s: a relevant therapeutic target

Given the role of KDM4s in various diseases, especially cancer, the development of specific KDM4 inhibitors is the focus of several research groups. In the following section will be presented a summary of the main inhibitor class described so far in the literature.

1.8.1. The 2OG derivatives

First promising results in the research for KDM4 inhibitors were provided, as often happens, from the efforts to target the cofactors essential for the activity of this class of enzymes. This strategy aims to obtain cofactor analogues that could interact with the catalytic domain of KDM4s, where 2OG is normally bound, but unable to take part in the reaction of demethylation.

N-oxalylglycine (NOG) is a closely related analogue of 2OG wherein the C-3 methylene group is replaced with an NH group. It was one of the first disclosed JmjC demethylase inhibitors and represents the simplest compound within this class (Figure 1.10). NOG mimics the initial coordination of the 2OG, occupying the same position and forming the same set of hydrogen bonds, but it does not initiate the hydroxylation process⁹⁶. Although first described as a prolyl hydroxylase (PHD) inhibitor, NOG is a broadspectrum inhibitor of many 2OG oxygenases and was then mostly used as a biochemical tool compound for in vitro testing⁹⁷.

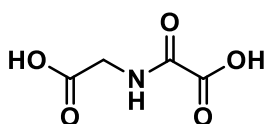


Figure 1.10. Structure of NOG.

The identification of suberanilohydroxamic acid (SAHA), a histone deacetylase (HDAC) inhibitor, as a KDM4E inhibitor, together with the knowledge that hydroxamic acids are good iron chelators, led to the design of inhibitors where the 2-oxoacid group of 2OG is replaced with a hydroxamic acid moiety. The resulting compounds containing the hydroxamic acid scaffold show good selectivity for the KDM4 family over the related 2OG oxygenases, improved by the addition of a carbon linker bearing a protonated tertiary amine likely function (Figure 1.11)⁹⁸⁻⁹⁹. However, the presence of a carboxylic acid function makes these compounds poor chemical probes because of their poor cell permeability.

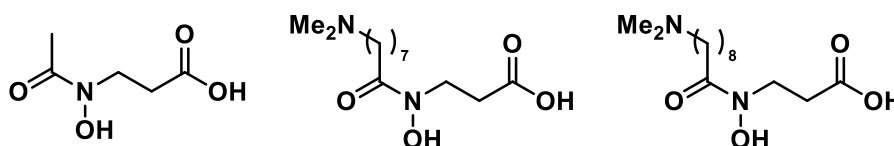


Figure 1.11. Hydroxamic acid derivatives.

Pyridine dicarboxylates are more rigid 2OG analogues than NOG and the acyclic hydroxamic acids, although they share the same mechanism of action. The pyridine-2,4-dicarboxylic acid (2,4-PDCA) is the broadest-spectrum 2OG oxygenase inhibitor, and is an inhibitor of most JHDMs. Its JHDM activity has also been confirmed in cell through the use of ester prodrugs¹⁰⁰. Subsequent derivatizations have led to 3-substituted and bipyridine compounds; although there has been improvement in potency, these inhibitors remain unselective towards the 2OG-dependent oxygenases (Figure 1.12)¹⁰¹⁻¹⁰².

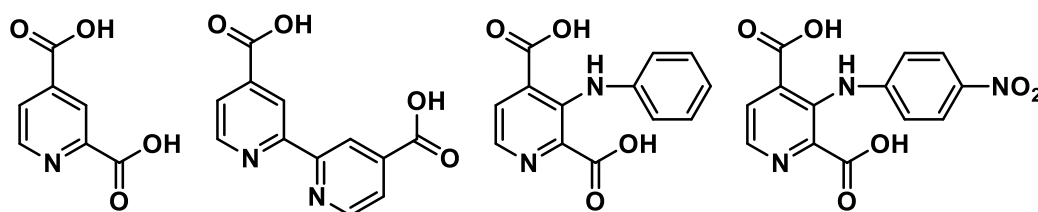


Figure 1.12. Pyridine dicarboxylates derivatives.

1.8.2. 8-Hydroxyquinoline-based KDM4s inhibitors

Interestingly, variously substituted 8-hydroxyquinoline derivatives have been identified as KDM4 inhibitors through a high-throughput screen campaign (Figure 1.13). Among them, the 5-carboxy-8-hydroxyquinoline (IOX1) was the most active inhibitor displayed an IC₅₀ of 0.2 μ M in vitro and cellular activity (HeLa cells), despite its poor cellular permeability. The IOX1 inhibitory mechanism was linked to its capacity to chelate Fe(II) in the enzyme active site in a bidentate manner via its quinoline nitrogen and phenol oxygen atoms. For the same reason, IOX1 is active against many other 2OG-dependent enzymes (KDM3A, KDM6A, KDM2A, PHF8, KDM5C and BBOX1)¹⁰³.

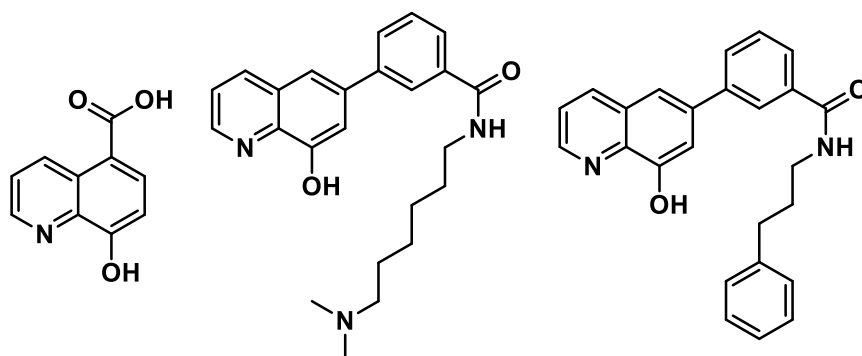


Figure 1.13. IOX1 and other 8-hydroxyquinoline derivatives.

Recently, research for novel JMJD2A inhibitors by using IOX1 as active moiety led to a novel series of 2-substituted derivatives with a potent JHDMS inhibitory activity and selectivity over PHD2 (Figure 1.14). Despite the better physico-chemical properties compared to IOX1, these compounds are still limited by poor cellular permeability¹⁰⁴.

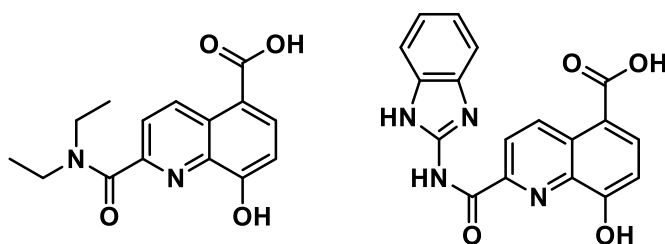


Figure 1.14. Novel 2-substituted 5-carboxy-8-hydroxyquinoline derivatives.

1.8.3. Other Fe-chelating KDM4s inhibitor scaffolds

Triazolopyridines have been reported as a potent scaffold for JHDMS inhibition¹⁰⁵. In these compounds the alternative triazole metal binding motif was incorporated to the known 2,2'-bipyridine-4-carboxylate scaffold. Crystallographic studies demonstrated that they bind KDM4A active site via metal chelation. A good number of analogues were synthesized leading to selective KDM2 and KDM5 inhibitors; unfortunately no one of them has shown selectivity against KDM4s (Figure 1.15)¹⁰⁵.

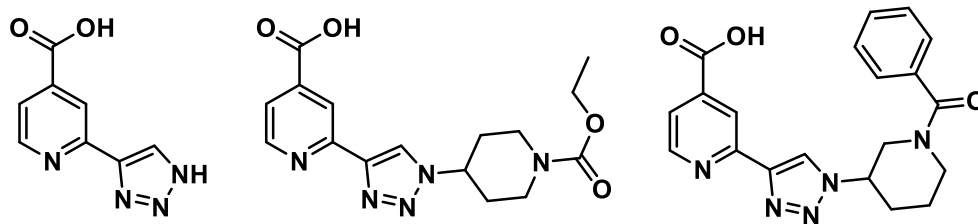


Figure 1.15. Triazolopyridines development.

Towards a rational approach, a tetrazolylhydrazide scaffold compound has been identified to be active against KDM4A, with 4-fold and 41-fold selectivity over KDM5A and KDM6B, respectively (Figure 1.16)¹⁰⁶. However, this scaffold provided limited opportunity for expansion into unexplored space having few points of appendage variation; the terminal hydrazide substitution was not tolerated and the alkyl chain extension lead to less than 2-fold potent compounds¹⁰⁶.

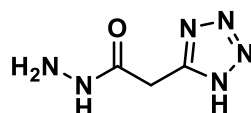


Figure 1.16. 2-(1H-tetrazol-5-yl)acetohydrazide as the most active compound of this class

1.8.4. KDM4s inhibitors of natural origin

In the last few years, a lot of natural products as flavonoids and catechols have been demonstrated to inhibit a number of 2OG oxygenases, including the KDM4s¹⁰⁷. In one of these studies, a catechol series, caffeic acid derivatives, was found to inhibit KDM4C and KDM6A but not PHF8 (Figure 1.17)¹⁰⁸. These compounds didn't compete directly with 2OG and it is possible that multiple factors contribute to their inhibitory effect¹⁰⁸.

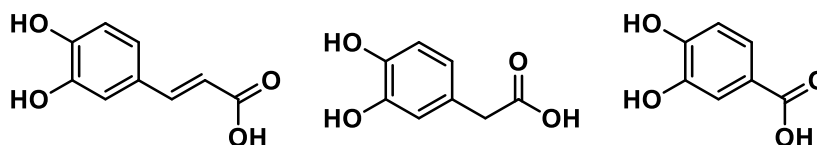


Figure 1.17. Catechols with inhibitory activity against KDM4s.

Recently, the natural product Tripartin, a dichlorinated indanone isolated from *Streptomyces* sp. associated with a larva of a dung beetle, has been reported as a KDM4 inhibitor (Figure 1.18). Activity in a cell-based assay against KDM4 has been reported, but we have no evidence about the mechanism of action and selectivity¹⁰⁹.

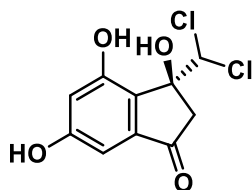


Figure 1.18. Tripartin, a KDM4 Inhibitor from a bacterium associated with a dung beetle larva.

1.8.5. *Noncatalytic domain targeting KDM4s inhibitors*

Among the KDM4s inhibitors described in the literature, there are also compounds, such as Disulfiram and Ebselen, approved or investigated for the treatment of other pathologies (Figure 1.19).

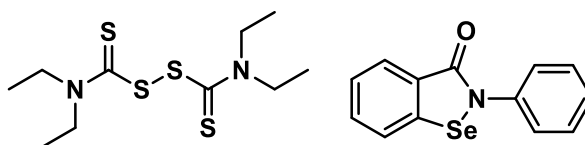


Figure 1.19. Disulfiram (left) and Ebselen (right).

Disulfiram is an aldehyde dehydrogenase inhibitor that was used to treat alcoholism by producing an extremely aversive reaction when taken in the presence of alcohol, and thus considered a deterrent¹¹⁰.

Ebselen mimics glutathione peroxidase activity and catalyzes several essential reactions for the protection of cellular components from oxidative and free

radical damage. It is currently under clinical trials for the prevention and treatment of various disorders such as cardiovascular diseases, arthritis, stroke, atherosclerosis, and cancer¹¹¹.

The inhibitory effect of these compounds was conferred by their ability to fit into the Cys3-His Zn(II) binding site, close to the active site, displacing the Zn²⁺ ion. This causes a conformational change in the protein so that binding of N-methylated lysine at the close active site is altered.

This allosteric inhibition occurred only in KDM4s because, as mentioned in Paragraph 1.7, none of the other JHDM subfamilies have a comparable Zn-binding site close to their catalytic domain⁶⁵.

1.8.6. Substrate competitive inhibitors

Recently, highly conjugated arylalkenes, including curcumin derivatives, have been identified as competitive inhibitors with respect to histone H3K9me3 against KDM4A and KDM4B (Figure 1.20). These compounds shown induced apoptosis in cancer cells and negatively regulated androgen receptor (AR)-responsive genes¹¹²⁻¹¹³.

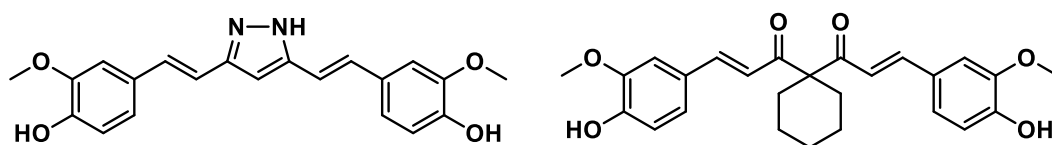


Figure 1.20. Arylalkenes derivatives as KDM4 inhibitors.

However, curcumins are known to be promiscuous inhibitors highlighted as pan-assay interference (PAINS) compounds¹¹⁴.

1.8.7. Other inhibitors of KDM4s

In the last years, also cyclic peptide sequences were selected as novel inhibitor scaffolds for the KDM4s¹¹⁵. Interestingly, these peptides, with a good in vitro potency but no activity in cells, bind KDM4s in “allosteric sites”¹¹⁵.

Recently, also metal-containing inhibitors of KDM4s were reported, as for some iridium(III) complexes. However, discrepancy between the data obtained and the unclear mechanism of action suggest that these molecules are able to interact with other proteins¹¹⁵.

1.9. Specific demethylation assays used in lead discovery

The identification of JHDMs modulators over the last decade has been supported by the development of several screening methods in order to evaluate compounds potency, selectivity, binding and mechanism of action.

Biochemical assays are the most common ones, as they give a quantitative measure of the ability of the compound to influence target activity. In most cases, activity was related to the level of reaction products (methylated peptides, formaldehyde) or reagents (2OG), that can be measured in a direct or indirect manner.

On the other hand, biophysical methods are capable of measuring the equilibrium binding constants between pairs of molecules crucial for molecular recognition processes, encompassing protein–protein, protein–small molecule, and protein–nucleic acid interactions, and several can be used to measure the kinetic or thermodynamic components controlling these biological processes. For a full characterization of a binding process, determinations of stoichiometry, binding mode, and any conformational changes associated with such interactions are also required. The suite of biophysical methods that are now available represents a powerful toolbox of techniques which can effectively deliver this full characterization¹¹⁶.

In the following paragraphs, it will be presented a summary of the main JHDMs-specific screening technique described so far in the literature, highlighting on advantages and disadvantages that could affect the outputs.

1.9.1. Indirect demethylation methods

Indirect methods are well-established in many areas of drug discovery and are often amenable to high-throughput screening according to their advantageous characteristics (high versatility, fast results, low costs).

The FDH-coupled assay is a miniaturized fluorescence-based assay used for the identification of new JHDMS inhibitors. In this assay, formaldehyde released from demethylation of the histone peptide substrate was detected by converting it to formic acid using a second enzyme: formaldehyde dehydrogenase (FDH). The oxidation of formaldehyde is coupled to the reduction of nicotinamide adenine dinucleotide (NAD^+) to NADH, which is monitored by fluorescence spectroscopy (Figure 1.21)^{97, 107, 117}.

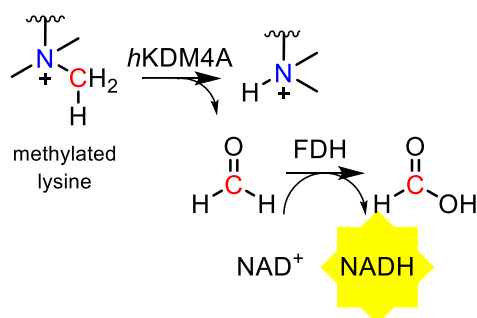


Figure 1.21. Principle of FDH-coupled inhibition assay.

However, FDH-coupled assay can be problematic due to its vulnerability to measurement errors and lack of reliability. The screening results could be easily affected by interferences arising from factors including compound auto-fluorescence, noisy/partial concentration responses, false positives acting on the coupled-enzyme component of the assay, and promiscuous inhibitors or potent metal chelators¹⁰³. To this end, the combined use of an orthogonal assay greatly increases the reliability of data obtained.

Other assays capable of detecting and quantifying formaldehyde, generating fluorescent adducts, have become available over the past few years. However, they share the same limitations discussed above.

The AlphaLISA homogeneous proximity immunoassay is another commonly used indirect assay. In this assay, the photosensitizer phthalocyanine is dissolved on a polystyrene donor bead. Excitation with 680 nm light induces phthalocyanine to convert ambient oxygen to singlet oxygen molecules with a 4 μ s half-life. These molecules can diffuse 200 nm freely through solution. If a polystyrene acceptor bead is within the lifetime of the singlet oxygen species, the singlet oxygen will react with an Europium chelate. The Europium (Eu) chelate is directly excited by the 340 nm light resulting from the conversion of thioxene to a di-ketone derivative following its reaction with singlet oxygen. The excited Europium chelate generates an intense light detectable within a much narrower wavelength bandwidth centred around 615 nm. In the KDM4-specific catalytic assay, a streptavidin-coated donor and anti-H3K9me2-coated acceptor bead pair were used to detect the demethylation of biotinylated H3K9me3 peptide (Figure 1.22)¹¹⁸.

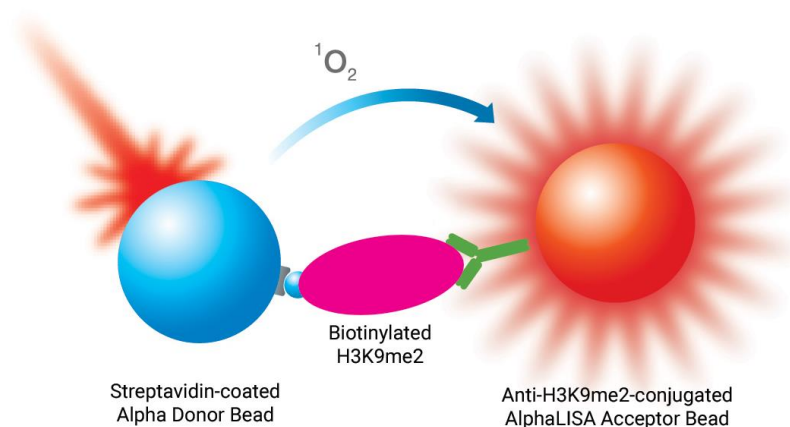


Figure 1.22. Principle of the AlphaLISA homogeneous proximity immunoassay technology.

However, also AlphaLISA may be sensitive to different types of interferences. For example, antioxidants or other quenchers of reactive oxygen

species like metal ions can strongly affect the emitted signal, as well as biotin-like compounds can compete for the interaction of biotinylated substrate with Donor beads. Moreover, colored compounds absorbing in the 500-600 nm wavelength range can artificially decrease the signal and therefore may be detected as false positives¹¹⁹.

1.9.2. Direct demethylation methods

Direct methods are more specific and, generally, reliable alternatives to quantify JHDMs activity. These techniques have less problems of false positives and negatives, but are generally more expensive in terms of time and money. For this reason, direct methods are used most frequently in advanced-stages of drug discovery.

Mass spectrometry methods are widely used to determinate histone modifications, in both enzymatic and cell-based assays. LC-MS and MALDI-TOF represent an alternative approach that can address the complexity of histone PTMs in single experimental set and overcome some of the limitations of antibody-based methods (such as specificity, availability, limited dynamic range and by problems in detecting multiple modifications). However, they require more complex sample preparation methods, longer times, and more material compared to other methods, resulting in more difficulties for high-throughput.

Nondenaturing mass spectrometry has been used to assess binding of potential inhibitors to JMJD2s, but also to explore the extend of binding pocket though a disulfide exchange based dynamic combinatorial-mass spectrometry (DCMS) screen. In this method, a compound that binds to the active site (the support ligand) which contains a thiol is allowed to react (either on the enzyme in the active site, or in solution) with a set of thiols to form a mixture of disulfides. Nondenaturing ESI-MS is then used to analyze which disulfides bind preferentially to the enzyme¹²⁰. However, In these ESI-MS analyses, it is important to appreciate that different types of noncovalent interaction survive the transition from solution to gas phase differently.

CHAPTER 2

AIM OF WORK

Several KDM4s inhibitors have been identified over the last few years, as described in Paragraph 1.8. In most cases, these molecules are recognized within the active site by residues that interact with 2OG and are, for this reason, capable to compete with it. Despite their clear inhibitory activity in various biochemical assays, the use of these compounds in cell-based assays in order to clarify the role of KDM4s in pathological processes is limited by their undesirable characteristics. In particular, many inhibitors described in literature have poor cell permeability, which limits their applicability as chemical probes and their potential therapeutic development. Moreover, these structures are often unselective; to be useful as probes, KMD4s inhibitors should not inhibit at least some of the other Fe(II)/2OG dependent oxygenases, e.g., those involved in the hypoxic response pathway, including the factor-inhibiting HIF (FIH) and the human HIF prolyl hydroxylase domain 2 (PHD2).

In this regard, the aim of my PhD project was to develop new selective and cytopermeable small-molecule modulators of KDM4 subfamily enzymes in order to obtain a useful chemical probe that could help us to elucidate the role of demethylation in cell-based assays.

2.1. High-Throughput Screening for the identification of new hits

In 2012, a commercially available library of compounds preselected for epigenetic target was screened using an indirect fluorescence assay for human KDM4 (*hKDM4*) in the laboratory of Professor Axel Ihmof at Ludwig-Maximilians-Universität (Munich, Germany). From this high-throughput screening (HTS) campaign it has been possible to identify a pool of eight hits (Figure 2.1), all characterized by a good inhibitory potency, with an IC_{50} in the low micromolar range (Table 2.1).

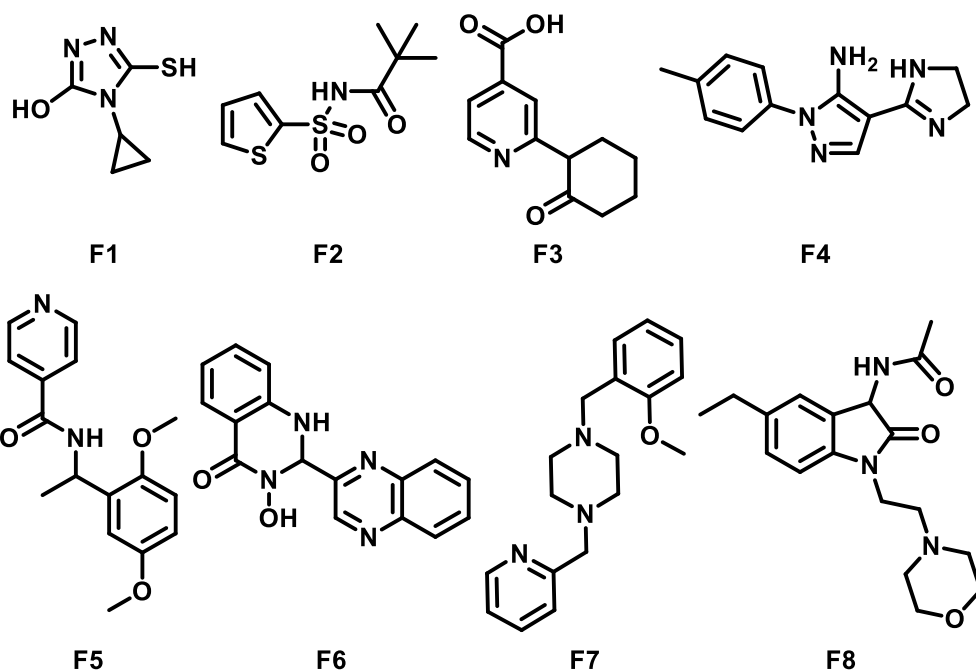


Figure 2.1. Initial hits identified by high-throughput screening.

Table 2.1. IC₅₀ values of hits identified by HTS.

hits	IC ₅₀ (μM)	hits	IC ₅₀ (μM)
F1	2.4	F5	6.4
F2	0.5	F6	6.4
F3	3.7	F7	9.3
F4	15.8	F8	6.6

2.2. Fragment-based ligand discovery

Identified hits have low molecular weight and very simple structure, meeting fully or partially to the “rule of three”, useful to classify a molecule like “fragment”¹²¹⁻¹²². For this reasons, we decided to describe these compounds as *pseudo-fragments*, using gathered information as starting point for development of a fragment-based ligand discovery (FBLD) campaign.

In FBLD, identification of active fragments is generally supported by information about their binding mode. With this information, it is possible to guide the development of larger and more complex structures that target additional interactions in the active site of the protein. This strategy appears to be particularly appropriate in the case of biological targets for which very little is known about selectivity, although there is the possibility of generating inactive or less active compounds compared to starting hits. Furthermore, a diverse range of scaffolds should provide a higher chance for discovery of small-molecule biological functional modulators¹²³.

For this reason, in collaboration with Professor Rino Ragno of Università degli Studi di Roma “La Sapienza”, an efficient in silico model was generated on the basis of the crystallographic data available in the literature (PDB IDs: 2GP5, 2OQ7, 2OS2, 2OT7, 2OX0, 2PXJ, 2Q8C, 2Q8D, 2Q8E, 2VD7, 2WWJ, 2YBK, 2YBP, 2YBS, 3NJY, 3PDQ, 3RVH, 3U4S, 4AI9, 4GD4). A cross-docking study was performed and the software PLANTS(CHEMPLP) was selected based on two parameters: docking accuracy (DA) and average value of root-mean-square deviation (RMSD). Despite the computational studies are not the first choice in this kind of approach, the availability of solved crystallographic structures along with the possibility to use multiple templates to build models have improved the quality of our in silico model. The *pseudo-fragments* have been docked in this model, highlighting the hypothetical key interactions that they create within the active site. Different docking poses were generated and the ones with the lowest free energy were selected for further studies.

Based on computational data, we have combined crucial non-overlapping moieties and designed a small library of chimera compounds (Figure 2.2), with the aim to establish the maximum amount of skeletal diversity and structural complexity, but also to build more complex structures, key factors toward improving the selectivity for novel therapeutic leads screening.

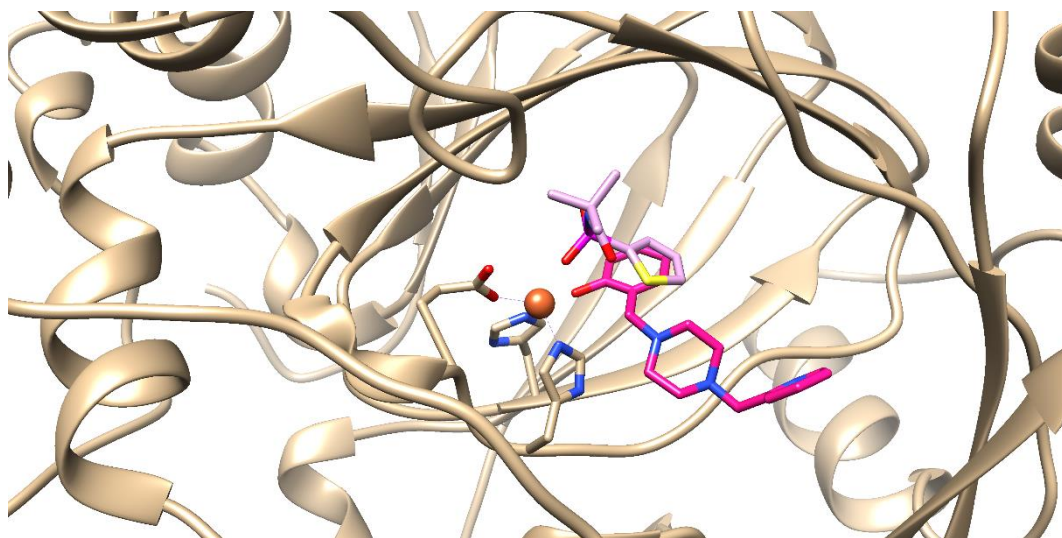
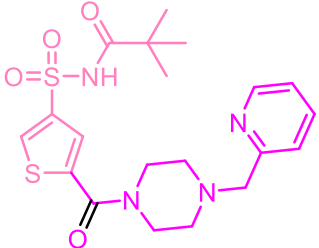
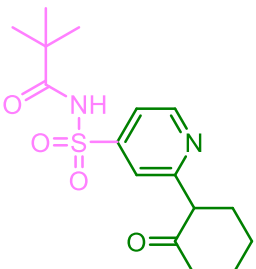
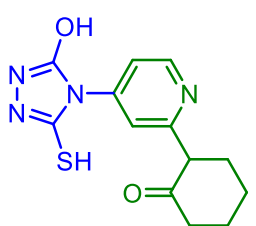


Figure 2.2. Overlap of hits F2 (plum) and F7 (deep pink) within the catalytic domain.

The designed chimera compounds have been docked with the same computational model, in order to predict and classify binding affinity of molecules (Table 2.2). Structures with the lowest free energy have been synthesized and screened against *h*KDM4 (Chapters 3 and 4).

Table 2.2. Best scored chimera molecules.

Compounds	parent fragments	binding free energy
 <chem>CC(C)(C)NS(=O)(=O)c1ccc2nc3c(ncn3C(=O)Nc4ccccc4)cn21</chem>	F2 and F6	-164,602
 <chem>CC(C)(C)C(=O)NS(=O)(=O)c1cc2sc(cc2s1)C(=O)N3CCN(CC3Cc4ccccn4)C5=CC=CC=C5</chem>	F2 and F7	-149,881

	F2 and F7	-147,161
	F2 and F3	-133,463
	F1 and F3	-111,426

Unfortunately, as will be described in Chapter 4, biochemical evaluation of chimera molecules certified their complete absence of inhibitory activity. These results could depend from excessive structural rigidity of derivatives than starting pseudo-fragments, as well as from some mistakes in initially formulated hypotheses.

2.3. Hit validation process and further derivatizations

To better understand negative results, chimera molecules together with the starting hits, was further investigated by Imhof and collaborators through a more reliable, direct screening platform, based on mass spectrometry (MS), as triage tool to confirm inhibition and identify true positives. It was found a good inhibitory potency only for three among the eight initial hits, whereas other two were endowed with modest activity and the remaining three compounds resulted completely inactive (Figure 2.3). No activity has been found for chimera molecules either.

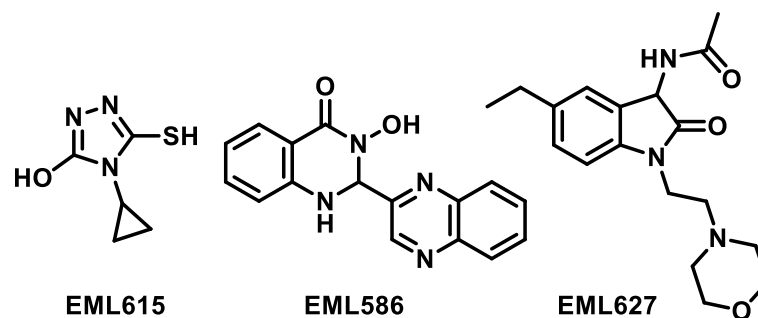


Figure 2.3. Real actives from HTS campaign.

Nevertheless, this result is not so surprising. The indirect assay initially used, despite advantageous characteristics in terms of speed, cost and versatility, also has disadvantages; artifacts from the coupled enzyme reaction can easily lead to false positives and negatives, which require a thorough counter-screen to eliminate. Furthermore, experience had shown that not all the “actives” discovered through HTS are of equal value in terms of progression in the Hit-to-Lead (HtL) phase.

Therefore, we decided to take a step back restarting from real actives identified during HTS campaign, focusing this time on the validation of active compounds as well as on the evaluation of hit classes on the basis of both target-independent and target-dependent criteria, following generic rules described in literature¹²⁴⁻¹²⁵. The goal was to identify the most promising lead candidates in order to increase possibilities to obtain potent and selective KDM4 inhibitors.

Therefore, hits were re-synthesized, structurally confirmed and evaluated for purity and stability by NMR, MS and HPLC experiments. Compounds with reactive functionality or other undesirable chemotypes were removed. Also biophysical and biochemical assays were performed to evaluate cell permeability, synthetic accessibility, activity, selectivity and preliminary structure-activity relationships (SARs).

This process is significantly expensive in terms of time and money, but it is also more promising and it was considered necessary in relation to the results initially obtained.

As will be widely described in Chapter 4, compound **EML586 (F6)** has been selected for further derivatization over the other two. Starting from its 3-hydroxy-2,3-dihydroquinazolin-4(1H)-one scaffold, we designed a small library of novel analogues (Figure 2.4) as will be discussed in Chapter 4.

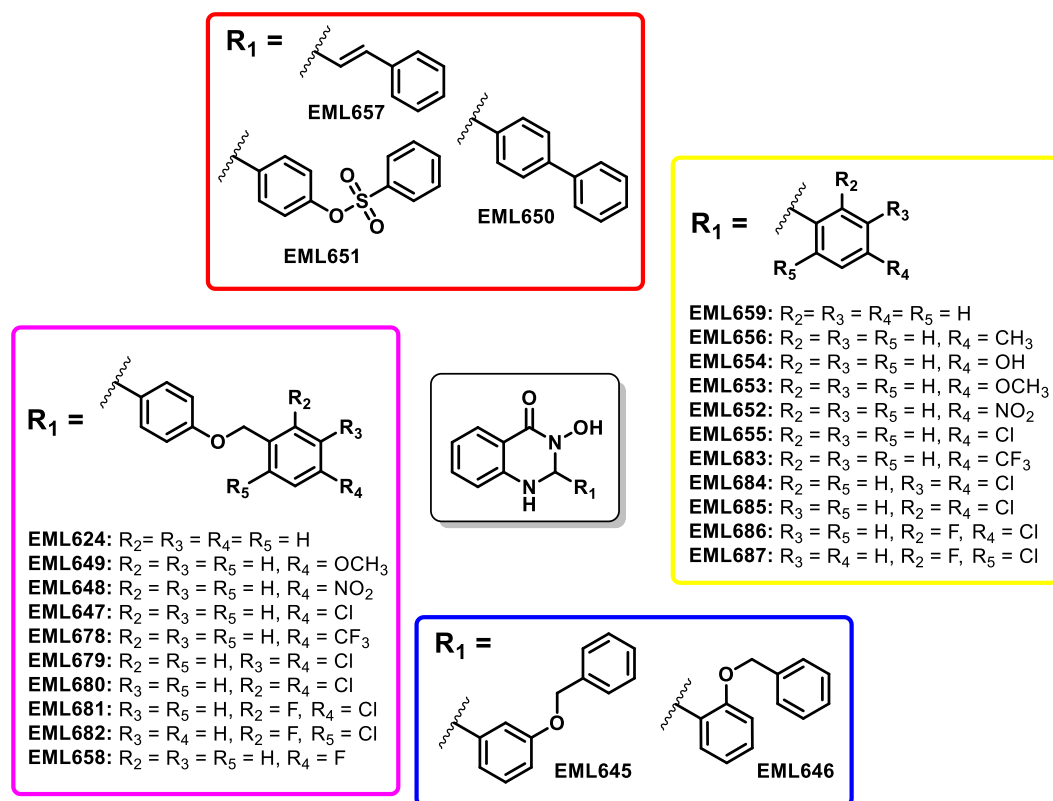


Figure 2.4. The library of 3-hydroxy-2,3-dihydroquinazolin-4(1H)-one derivatives synthesized.

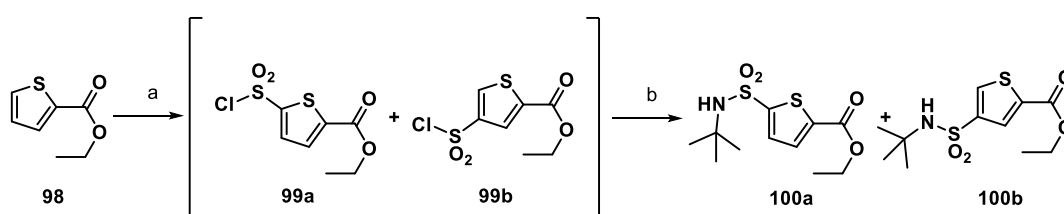
CHAPTER 3

CHEMISTRY

3.1. Synthesis of thiophene-2-sulfonamide derivatives

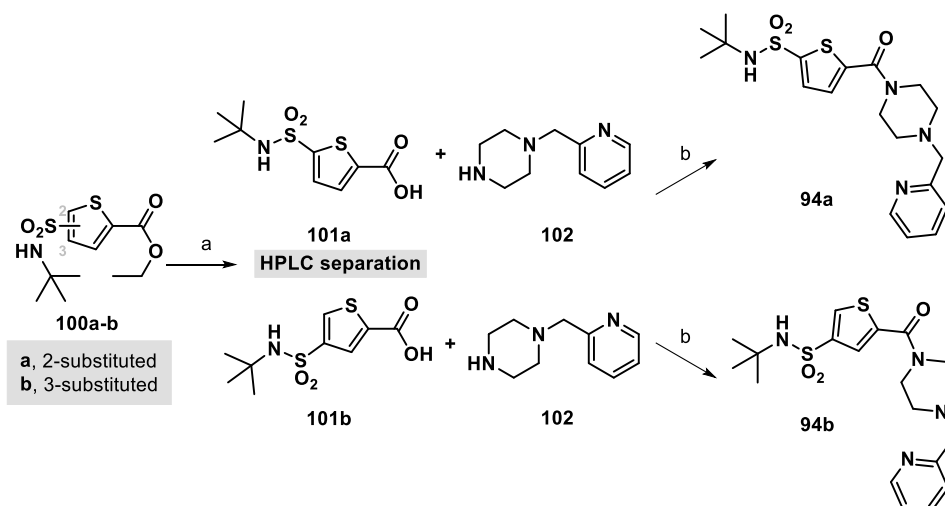
The first derivatives that have been synthesized were designed by the combination of fragment **F2** and **F7** (Chapter 2). These chimeras are characterized by a thiophene core.

The synthesis of the thiophene-2-sulfonamide derivatives **96a-b** has been developed starting from the ethyl thiophene-2-carboxylate **98**, which was treated with chlorosulfonic acid and then with in chloroform to yield a mixture of regioisomers **99a-b**. After removing the excess acid through liquid-liquid extraction, the mixture was used without further purification. Finally, the reaction with *tert*-butylamine in dry tetrahydrofuran gave corresponding sulfonamides **100a-b** (Scheme 3.1).



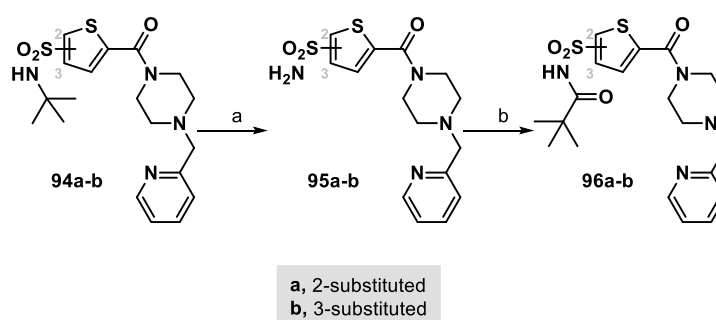
Scheme 3.1. Reagents and conditions: (a) chlorosulfuric acid, CH₂Cl₂, room temperature, overnight; (b) *tert*-butylamine, triethylamine, dry THF, room temperature, 0.5 h (60%^a over two steps). ^a100a:100b 1:1 ratio as determined by NMR analysis.

The regioisomeric mixture of sulfonamides **100a-b** was treated with lithium hydroxide to hydrolyse the ester function and the corresponding acids (**101a-b**) were separated by preparative high performance liquid chromatography (HPLC). Coupling reaction with the 1-(pyridin-2-ylmethyl)piperazine (**102**) in the presence of *N,N'*-dicyclohexylcarbodiimide (DCC) and 4-(dimethylamino)pyridine (DMAP) furnished thiophene-2-sulfonamide derivatives **94a** and **94b** (Scheme 3.2).



Scheme 3.2. Reagents and conditions: (a) lithium hydroxide, THF/H₂O, room temperature, 2 h (95%); (b) DCC, DMAP, dry CH₂Cl₂, room temperature, overnight (75%).

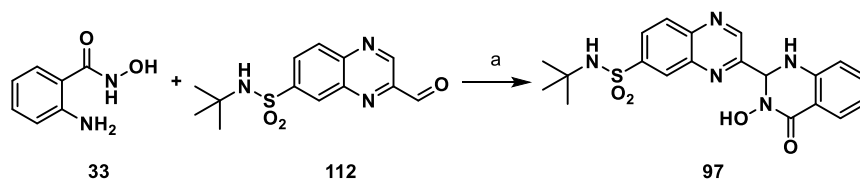
Tert-butyl group was removed with trifluoroacetic acid and the corresponding sulfonamides sulfonimides **95a-b** were acylated with pivaloyl chloride in the presence of triethylamine to yield the desired *N*-(thiophenylsulfonyl)pivalamides **96a** and **96b** (Scheme 3.3).



Scheme 3.3. Reagents and conditions: (a) trifluoroacetic acid, CH₂Cl₂, room temperature, overnight (95%); (b) pivaloyl chloride, triethylamine, dry CH₂Cl₂, room temperature, overnight (70%).

3.2. Synthesis of quinoxaline derivative

The second chimera compound was designed from apposition of the fragments **F2** and **F6** and it was characterized by a quinoxaline core. It was obtained through a convergent synthesis in which the key step was the condensation of the 2-amino-*N*-hydroxybenzamide **33** with the 2-formylquinoxaline **112** in methanol at room temperature (Scheme 3.4)¹²⁶. Product was readily purified by column chromatography and recovered in good yields.



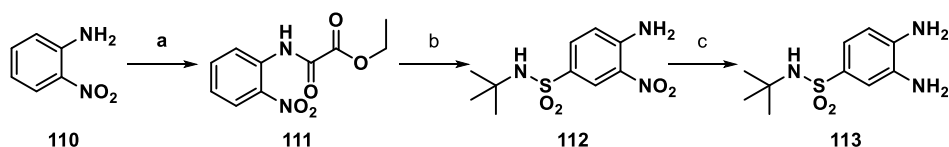
Scheme 3.4. Reagents and conditions: (a) MeOH, room temperature, 2 h (68%).

The following paragraphs will describe the synthesis optimization of the key intermediates.

3.2.1. Construction of the quinoxaline core

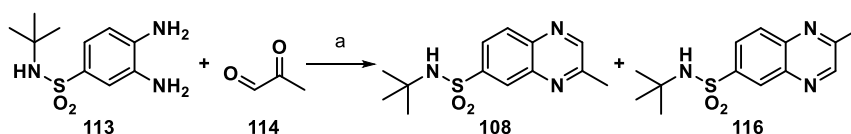
Initially, we tried to build quinoxaline ring following classical procedures that involve the condensation of an aromatic ortho-diamine with an α -dicarbonyl derivatives¹²⁷⁻¹²⁸. This kind of reactions are generally very accessible having simple reaction conditions, good yield and using readily available starting materials and reagents.

According to this, o-diamine derivative **113** was prepared from 2-nitroaniline (**110**) in a three-step sequence. Treatment with mono-ethyl oxalyl chloride to give **111** was followed by chlorosulfonation to give intermediate **112** in good yield. Subsequent nitro reduction with zinc powder in acetic acid easily gave compound **113** (Scheme 3.5). All the compounds were readily purified through liquid-liquid extraction and subsequent recrystallization.



Scheme 3.5. Reagents and conditions: (a) mono-ethyl oxalyl chloride, Et₂O, room temperature, 3 h (99%); (b) chlorosulfuric acid, neat, 80 °C, 3 h then *tert*-butylamine, triethylamine, dry THF, room temperature, 0.5 h (78%); (c) zinc powder, acetic acid, room temperature, 0.5 h (95%).

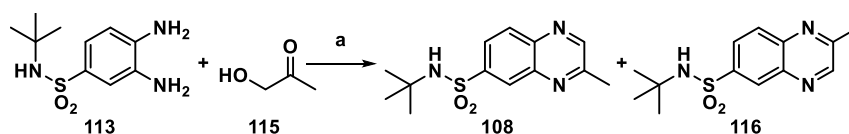
Ortho-diamine derivative **113** was then treated with methylglyoxal (**114**) in acetonitrile at room temperature to give the 7-substituted-2-methylquinoxaline **108**. As expected, the coupling reaction gave a mixture of regioisomers, affording also the 2,6-disubstituted derivative **116** (Scheme 3.6) in a 50:50 ratio. Contrary to what happened with the thiophene derivatives, in this case it was not possible to separate the molecules exploiting HPLC, due to their very similar chromatographic profiles.



Scheme 3.6. Reagents and conditions: (a) ACN, room temperature, 1 h (90%^a).

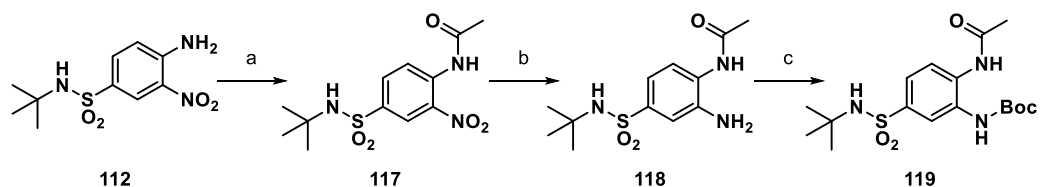
^a108:116 = 45:55 ratio as determined by NMR analysis.

Trying to exploit the differential nucleophilicity of amino function on the ortho-diamine derivative **113**, we developed a different strategy in which it was treated with the commercially available α -hydroxy acetone **115**, at low temperature. Also in these conditions, the outcome of reaction was the mixture of regioisomers, although in different ratio 70:30 (Scheme 3.7).



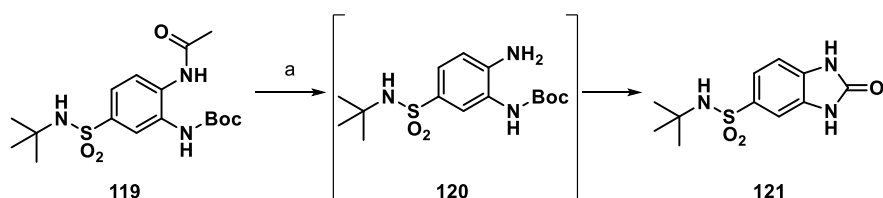
Scheme 3.7. Reagents and conditions: (a) ACN, 0 °C, 1 h (80%^a). ^a108:116 = 70:30 ratio as determined by NMR analysis.

Subsequently, we tried to use a pair of orthogonal protecting groups, to selectively access to single amine, but also this approach ultimately failed. Acylation of 2-nitroaniline derivative **112** with acetic anhydride gave compound **117** which was sequentially reduced using zinc powder and acetic acid, at room temperature, to afford amine **118**. The second amino function was then protected with di-*tert*-butyl dicarbonate to give compound **119** in low yield (Scheme 3.8).



Scheme 3.8. Reagents and conditions: (a) acetic anhydride, acid acetic, reflux, 2.5 h (90%); (b) zinc powder, acetic acid, room temperature, 0.5 h (77%); (c) di-*tert*-butyl dicarbonate, iodine, MeOH, room temperature, overnight (25%).

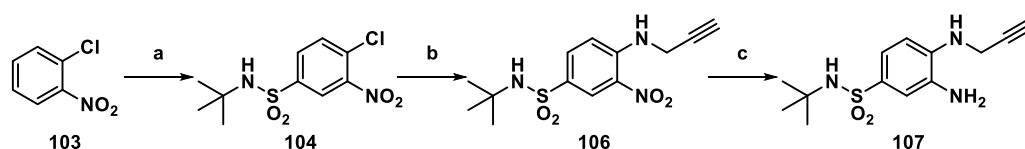
Unexpectedly, isolation of compound **120**, obtained by selective removal of the acetyl group, was not possible due to a side intramolecular reaction. In fact, the Boc group, stable under the conditions of removal of the acetyl, reacts with the amine function released and hydroxybenzoimidazole **121** was obtained as a main product (Scheme 3.9).



Scheme 3.9. Reagents and conditions: (a) lithium hydroxide, THF/H₂O, room temperature, overnight.

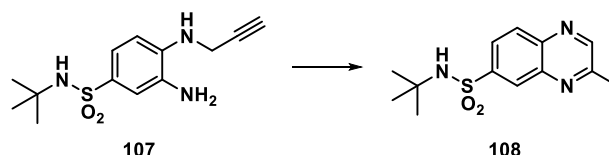
Therefore, to obtain 7-substituted-2-methylquinoxaline we look for different synthesis methods. Finally, we succeeded in obtaining the desired compound using an intra-molecular copper-catalysed hydroamination. Starting from the procedure of Knapp et al.¹²⁹, the reported procedure was modified improving yield, decreasing reaction time and enhancing atom economy lowering copper-catalyst required. In the following paragraph details have been reported.

Sulfonamide derivative **104** was obtained by chlorosulfonation of commercially available 2-chloronitrobenzene (**103**) according to the procedure already described for compound **112**. After chloride substitution with propargylamine (**105**), nitro group was reduced with iron sulphate in ammonia aqueous solution yielded 3-amino-N-(tert-butyl)-4-(prop-2-yn-1-ylamino)benzenesulfonamide (**107**) in good yield (Scheme 3.10).



Scheme 3.10. Reagents and conditions: (a) chlorosulfuric acid, neat, 120 °C, 1 h then *tert*-butylamine, triethylamine, THF dry, room temperature, 0.5 h (85%); (b) propargylamine, triethylamine, EtOH, 120 °C (mw), 1.5 h (65%); (c) iron(II) sulfate heptahydrate, ammonium hydroxide solution, H₂O, EtOH, reflux, 1 h (90%).

As reported by Knapp, the primary amino group of **107** intramolecularly reacts with the triple bond in a hydroamination reaction catalyzed by a cuprous salt used in stoichiometric amount (Scheme 3.11).



Scheme 3.11. Hydroamination reaction to yield the quinoxaline ring.

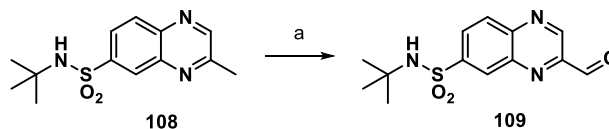
Despite large related literature, there are few cases of hydroamination employing a cuprous catalyst. Moreover, examples of this intramolecular reaction to build heterocycles are still less. For these reasons, together with the need to improve initially low yield (9%), we made a methodology work to optimize the reaction, which results are reported in Table 3.1.

Table 3.1. Optimization of hydroamination reaction. ^aNumber of microwave heating cycles are indicated. ^bIsolated yield after chromatographic purification. ^cUnreacted starting material.

copper salt	temperature (°C)	solvent	time^a (h)	Yield^b (%)	starting material^c
Tetrakis(acetonitrile)copper(I) tetrafluoroborate (1.00 eq)	90	dry toluene	20	9	-
Tetrakis(acetonitrile)copper(I) tetrafluoroborate (1.00 eq)	90 (mw)	dry toluene	4x0.5	23	-
Tetrakis(acetonitrile)copper(I) tetrafluoroborate (1.00 eq)	90 (mw)	dry acetonitrile	0.5	33	-
Tetrakis(acetonitrile)copper(I) tetrafluoroborate (1.00 eq)	90	dry acetonitrile	5	31	-
Tetrakis(acetonitrile)copper(I) tetrafluoroborate (1.00 eq)	90 (mw)	dry ethanol	0.5	29	-
Tetrakis(acetonitrile)copper(I) tetrafluoroborate (0.10 eq)	90 (mw)	dry acetonitrile	4x0.5	49	-
Tetrakis(acetonitrile)copper(I) tetrafluoroborate (0.10 eq)	90 (mw)	dry acetonitrile	2x0.5	13	77
Tetrakis(acetonitrile)copper(I) tetrafluoroborate (0.10 eq)	90	dry acetonitrile	11	67	8
Tetrakis(acetonitrile)copper(I) tetrafluoroborate (0.10 eq)	90 (mw)	dry ethanol	5x0.5	39	18
Tetrakis(acetonitrile)copper(I) tetrafluoroborate (0.10 eq)	90 (mw)	dry acetonitrile	3x0.5	33	9
Copper(I) iodide (0.10 eq)	90 (mw)	dry acetonitrile	3x0.5	40	-
Copper(I) iodide (0.10 eq)	90 (mw)	dry ethanol	8x0.5	43	9
Copper(I) iodide (0.10 eq)	90 °C	dry acetonitrile	9	54	2

Copper(II) tetrafluoroborate hydrate (0.10 eq)	90 °C	dry acetonitrile	4x0.5	38	9
Copper(I) iodide (0.10 eq)	130 °C	dry acetonitrile	0.25	41	3
Copper(I) iodide (0.10 eq)	130 °C	dry acetonitrile	0.125	29	24

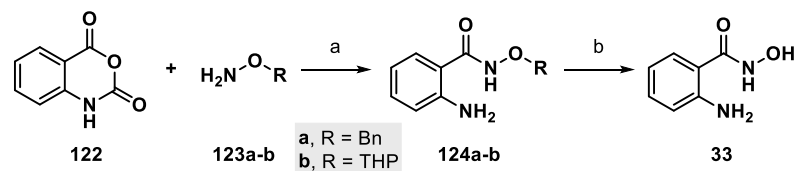
With the proper 7-substituted-2-methylquinoxaline **108** in hand, the desired key synthon **109** was easily obtained by oxidation of methyl substituent using selenium dioxide in reflux toluene (Scheme 3.12).



Scheme 3.12. Reagents and conditions: (a) selenium dioxide, dioxane/H₂O, reflux, 1 h (81%).

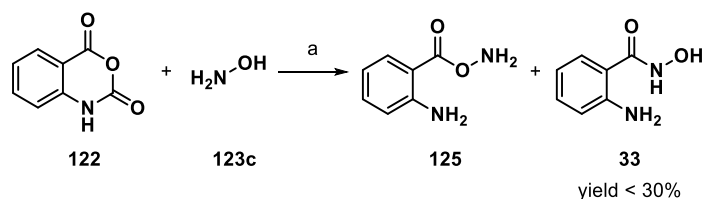
3.2.2. Synthesis of 2-amino-*N*-hydroxybenzamide (**33**)

2-amino-*N*-hydroxybenzamide (**33**) was the second building block required for the synthesis of the chimera compound **97**. Starting from commercially available isatoic anhydride (**122**), which was coupled with O-protected hydroxylamine, hydroxamic acid **33** was obtained by deprotection of the protected intermediate **124** (Scheme 3.13).



Scheme 3.13. Reagent and conditions: (a) ACN, reflux, 3 h (90-95%); (b) various reagents and conditions.

The protection of hydroxy group was necessary because direct reaction between isatoic anhydride (**122**) and hydroxylamine (**123c**) leads to the formation of 2-((aminooxy)carbonyl)aniline (**125**) as main product (Scheme 3.14).

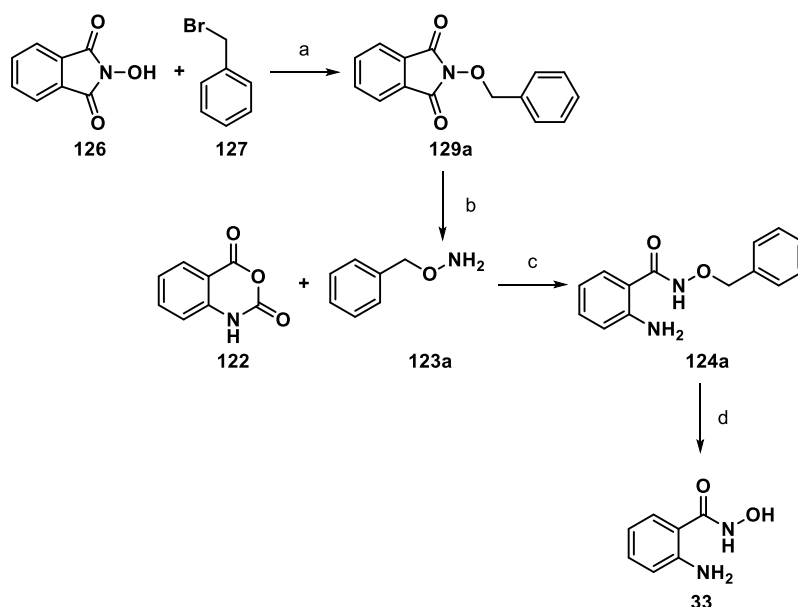


Scheme 3.14. Reagent and conditions: (a) ACN, reflux, 3 h (25%).

Two different protecting groups, the benzyl (Bn) and the tetrahydro-2H-pyran-2-yl (THP) groups, were considered. As will be described in detail below, both protecting groups can be easily added, but only the THP can be readily removed.

3.2.2.1. Synthesis and deprotection of 2-amino-N-(benzyloxy)benzamide (127a)

Scheme 3.15 describes the synthetic strategies used to obtain 2-amino-N-(benzyloxy)benzamide protected on the oxygen with the benzyl group (**124a**) and its subsequent deprotection.



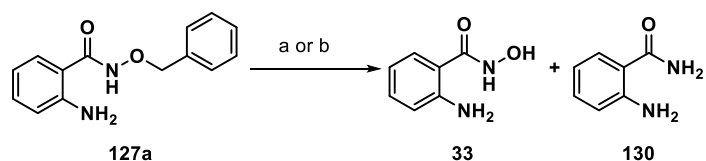
Scheme 3.15. Reagents and conditions: (a) K_2CO_3 , DMF, room temperature, 5 h (96%); (b) $NH_2NH_2 \cdot H_2O$, Et_2O , room temperature, 2 h (99%); (c) ACN, reflux, 3h (90%); (d) various reagents and conditions.

Alkylation of N-hydroxy phthalimide **126** with benzyl bromide (**127**) in DMF straightforwardly gave compounds **129a**, which can be easily precipitated by

adding water to the reaction mixture and recovered in good yield and purity. Without any purification step, it was treated with hydrazine monohydrate at room temperature in diethyl ether to afford compound **123a**. After removing the main impurities by liquid-liquid extraction, pure compound was recovered by evaporation of solvents under reduced pressure.

The coupling reaction between isatoic anhydride (**122**) and O-benzyl hydroxylamine (**123a**) gave the compound **124a**, readily purified by column chromatography. Unfortunately, it was not possible to find an efficient strategy to remove the benzyl group. Different procedures were carried out; always product **33** has been obtained in moderate yield after long purification processes due to the presence of the side product **130**.

Below, the most relevant deprotection procedures will be briefly described (Scheme 3.16).



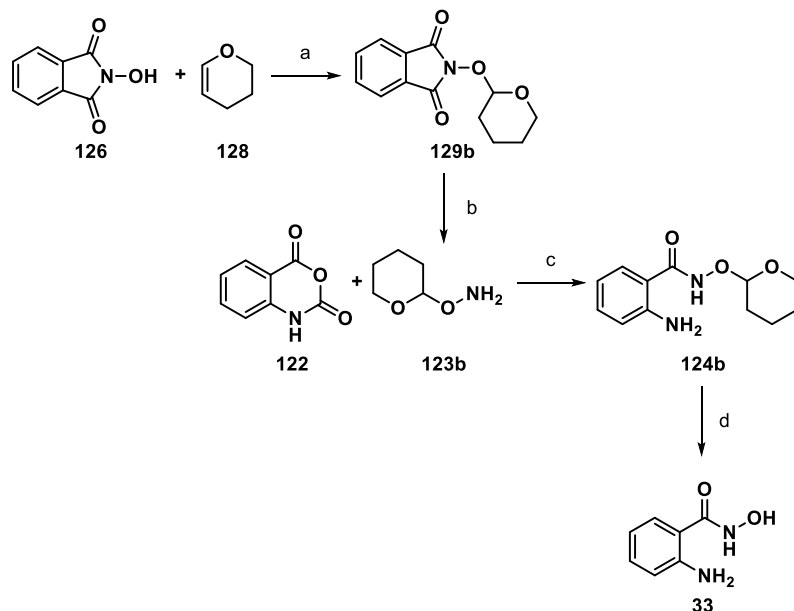
Scheme 3.16. Reagents and conditions: (a) H₂, Pd/C 10%, EtOH, room temperature, overnight (45%); (b) 1,4-cyclohexadiene, Pd/C 10%, MeOH, 120 °C (mw), 4 min, (53%).

2-amino-*N*-(benzyloxy)benzamide (**124a**) has been deprotected under hydrogen atmosphere, using palladium on active carbon (10%) as catalyst. The reaction gave compound **33** together with the side product **130** in moderate yield. A similar result was also obtained under microwave-assisted catalytic transfer hydrogenation conditions, using 1,4-cyclohexadiene as mild hydrogen donor.

For above mentioned reasons, it was considered appropriate to change the protecting group, trying the tetrahydropyranyl as possible substitute.

3.2.2.2. Synthesis and deprotection of 2-amino-N-((tetrahydro-2H-pyran-2-yl)oxy)benzamide (127b)

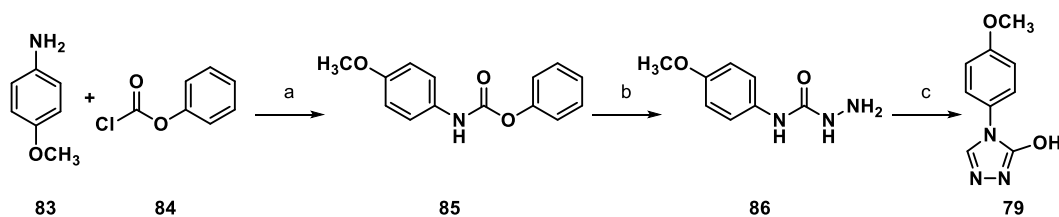
The use of THP protecting group follows a similar synthetic route compared to benzyl group just described (Scheme 3.17).



Scheme 3.17. Reagents and conditions: (a) *para*-toluensulfonic acid, CH₂Cl₂/dioxane, room temperature, 3.5 h (99%); (b) (b) NH₂NH₂·H₂O, Et₂O, room temperature, 2 h (99%); (c) ACN, reflux, 3h (90%); (d) Amberlyst® 15 hydrogen form, MeOH, 50 °C, 3h (95%).

According to literature procedures¹³⁰, *O*-THP hydroxylamine **124b** can be conveniently synthesized treating commercially available *N*-hydroxy phthalimide (**126**) with 3,4-dihydro-2*H*-pyran (**128**) in the presence of a catalytic amount of *para*-toluensulfonic acid. As described before for benzyl derivative, compound **129b** was treated with hydrazine monohydrate at room temperature in diethyl ether to afford the corresponding *O*-protected hydroxylamine **123b**.

The coupling reaction between isatoic anhydride (**122**) and *O*-THP hydroxylamine (**123b**) gave the compound **124b** in high yield, readily purified by recrystallization.

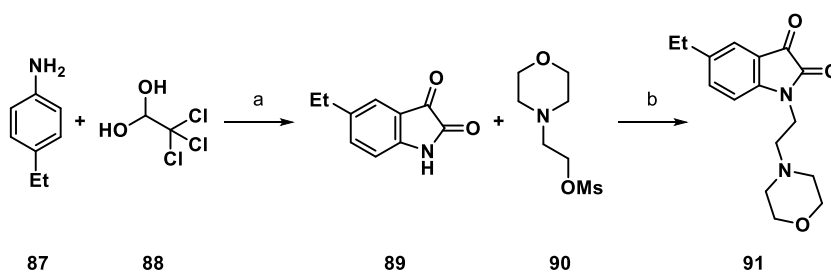


Scheme 3.19. Reagents and conditions: (a) dry THF, room temperature, 1 h (55%); (b) hydrazine hydrate, EtOAc, room temperature, 4 h (90%); (c) formamidine acetate salt, acetic acid, DMF, 80 °C, 8 h (60%).

Para-methoxyaniline (**83**) was converted to phenylcarbamate **85** by reacting with phenyl chloroformate (**84**) at room temperature. Compound **85** was then treated with hydrazine hydrate to give semicarbazide **86**, which was subsequently reacted with formamidine acetate in the presence of DMF at 80 °C to give the triazolone **79**.

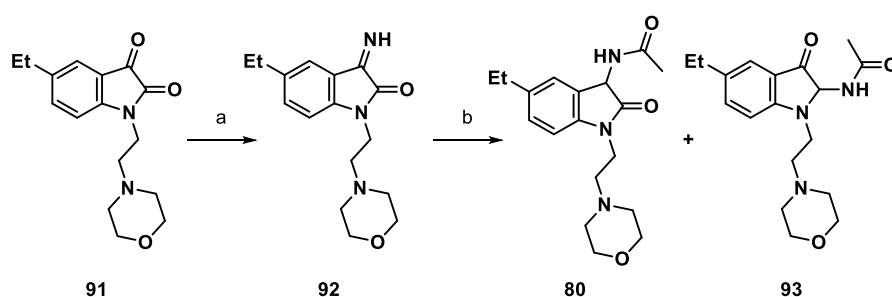
3.4. Synthesis of *N*-(5-ethyl-1-(2-morpholinoethyl)-3-oxoindolin-2-yl)acetamide

The synthesis of hit **F8** (**80**) has been developed starting from the 5-ethyl isatin (**91**), which was synthesized from *para*-ethyl aniline (**87**) and chloral hydrate (**88**) exploiting the classical Sandmeyer isatin synthesis¹³³. Isatin **89** was subsequently *N*-alkylated with 2-morpholinoethan-1-ol, previously activated with methanesulfonyl chloride (**90**), to give compound **91** in good yield (Scheme 3.20).



Scheme 3.20. Reagents and conditions: (a) hydroxylamine hydrochloride, sodium sulfate, HCl aqueous solution 5%, H₂O, 95 °C, 2 h, then H₂SO₄ conc., 80 °C, 0.5 h (65%); (b) potassium carbonate, DMF/THF, 80 °C, overnight, (70%).

5-ethyl-1-(2-morpholinoethyl)indoline-2,3-dione (**91**) was then treated with ammonia solution in methanol to yield the corresponding imide **92**, which was quickly treated with sodium cyanoborohydride at -78 °C in tetrahydrofuran. After a proper reduction time, the very unstable amino intermediate was directly acylated with acetic anhydride without any purification step. Anhydride was added at -78 °C and the mixture was allowed to slowly warm to ambient temperature while stirring. This two-step reaction yielded a mixture of isomers as described in Scheme 3.21.

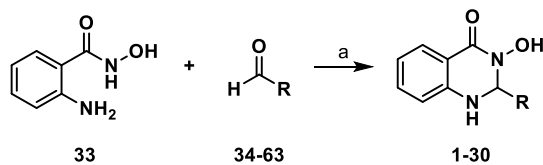


Scheme 3.21. Reagents and conditions; (a) saturated ammonia solution in MeOH, formic acid (catalytic), room temperature, 3 h (80%); (b) sodium cyanoborohydride, dry THF, -78 °C, 6 h, then acetic anhydride, room temperature, overnight (20%).

Finally, separation of isomers by preparative HPLC provided compound **80** in low yield.

3.5. Synthesis of 3-hydroxy-2,3-dihydroquinazolin-4(1H)-one derivatives (1-30)

The key step for the synthesis of 3-hydroxy-2-(quinoxalin-2-yl)-2,3-dihydroquinazolin-4(1H)-one derivatives **1-30** was the condensation of the 2-amino-*N*-hydroxybenzamide **33** with the proper aldehyde (**34-63**) in methanol at room temperature (Scheme 3.22)¹²⁶. The reaction times varied according to aldehyde solubility from 1 to 24 hours. All the compounds were readily purified by column chromatography and recovered in good yields (65-90%).



Scheme 3.22. Reagents and conditions: (a) MeOH, room temperature, 1-24 h (65-90%).

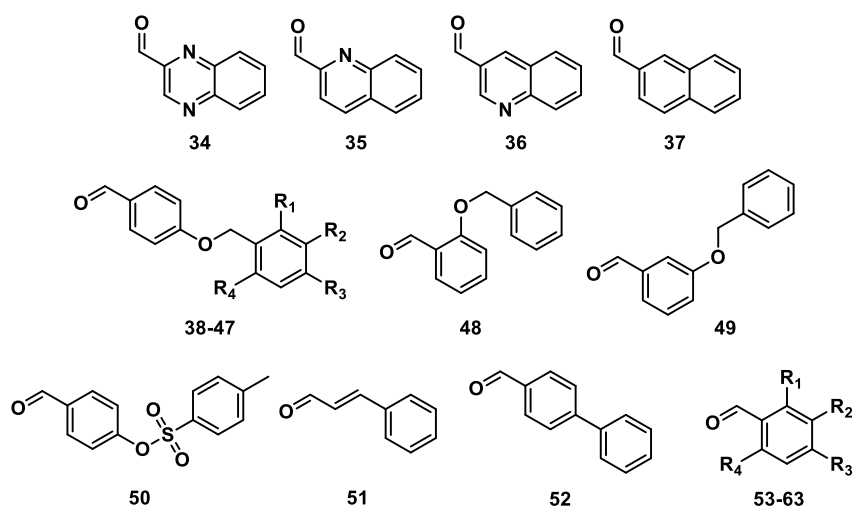


Figure 3.1. Aldehydes used for the synthesis of compounds **1-30**

Table 3.2. All 3-hydroxy-2,3-dihydroquinazolin-4(1*H*)-one derivatives synthesized. ^aIsolated yield.

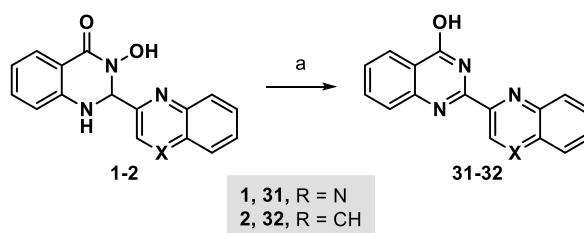
entry	compound	aldehyde	R ₁	R ₂	R ₃	R ₄	yield ^a (%)
1	EML586	34	-	-	-	-	84
2	EML621	35	-	-	-	-	87
3	EML622	36	-	-	-	-	85
4	EML623	37	-	-	-	-	90
5	EML624	38	H	H	H	H	77

6	EML647	39	H	H	Cl	H	81
7	EML648	40	H	H	NO ₂	H	83
8	EML649	41	H	H	OCH ₃	H	79
9	EML658	42	H	H	F	H	80
10	EML678	43	H	H	CF ₃	H	85
11	EML679	44	H	Cl	Cl	H	81
12	EML680	45	Cl	H	Cl	H	82
13	EML681	46	F	H	Cl	H	85
14	EML682	47	F	H	H	Cl	80
15	EML645	48	-	-	-	-	74
16	EML646	49	-	-	-	-	77
17	EML651	50	-	-	-	-	65
18	EML657	51	-	-	-	-	82
19	EML650	52	-	-	-	-	88
20	EML659	54	H	H	H	H	68
21	EML655	55	H	H	Cl	H	71
22	EML652	56	H	H	NO ₂	H	73
23	EML653	57	H	H	OCH ₃	H	70
24	EML654	53	H	H	OH	H	67
25	EML656	58	H	H	CH ₃	H	71
26	EML683	59	H	H	CF ₃	H	75
27	EML684	60	H	Cl	Cl	H	73
28	EML685	61	Cl	H	Cl	H	77

29	EML686	62	F	H	Cl	H	74
30	EML687	63	F	H	H	Cl	73

3.5.1. Synthesis of quinazolin-4(3H)-one derivatives

Aromatic analogues **31-32** were obtained from oxidation with selenium dioxide of compounds **1** and **2** respectively, in toluene (Scheme 3.23)

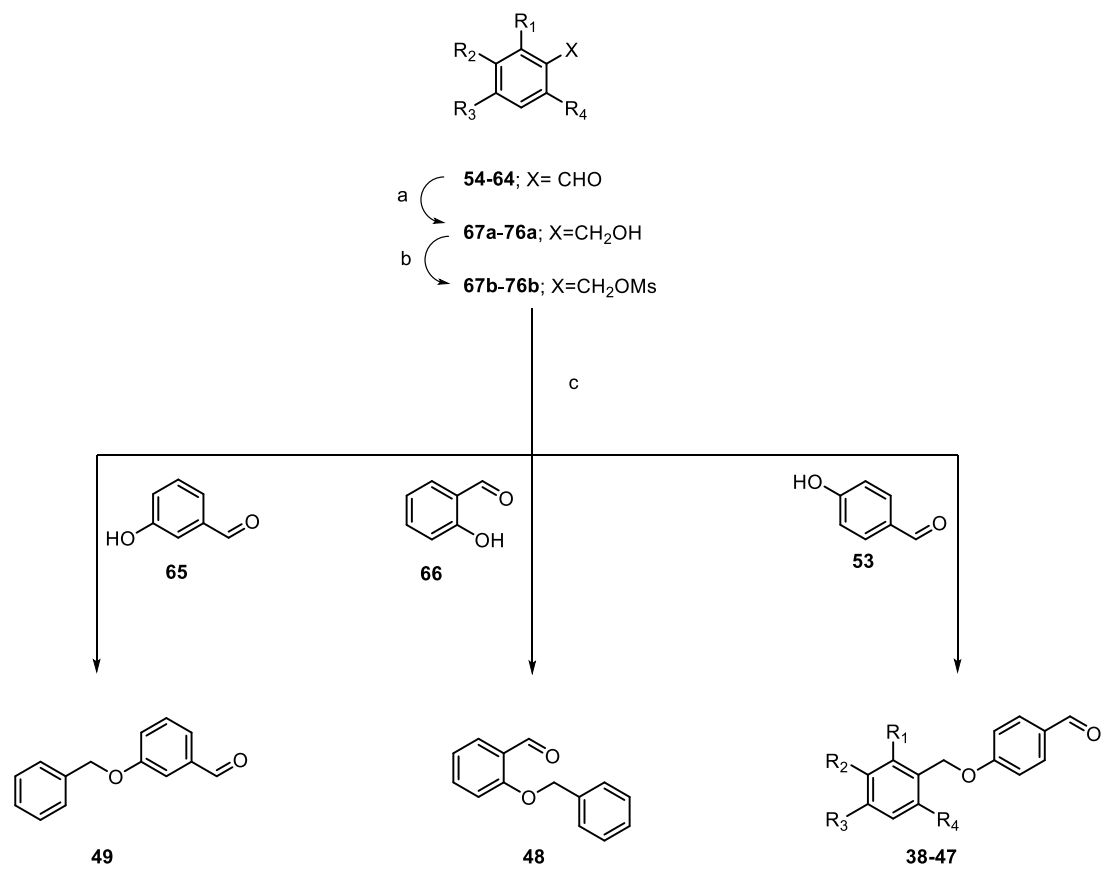


Scheme 3.23. Reagents and conditions: (a) selenium dioxide, toluene, reflux, 4 h (80%).

Compounds are readily purified by column chromatography and collected in good yield.

3.5.2. Synthesis of non-commercially available aldehydes

While aldehydes **34-37** and **51-63** are commercially available, aldehydes **38-49** were prepared according to the general synthetic procedure reported in Scheme 3.24.



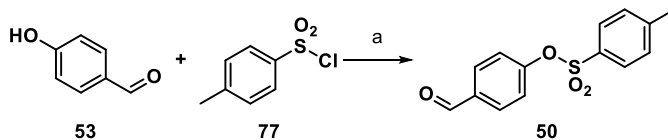
Scheme 3.24. Reagents and conditions: (a) NaBH₄, MeOH, room temperature, 0.5 h (95-99%); (b) mesyl chloride, triethylamine, dry CH₂Cl₂, 0° C, 3.5 h (95-99%); (c) potassium carbonate, acetone, reflux, 1 h (75-85%).

Commercially available aldehydes **54-64** have been readily reduced using sodium borohydride in methanol to give the corresponding benzyl alcohols **67a-76a** with quantitative yield. The alcohol group was then activated with methanesulfonyl chloride (derivatives **67b-76b**) and reacted with proper hydroxybenzaldehyde (**55, 65-66**) to give products **38-49**. Reactions were carried out in acetone with potassium carbonate. After chromatographic purification, aldehydes derivatives were collected in good yields (Table 3.3).

Table 3.3. Non-commercially available aldehydes synthesized. ^aIsolated yield.

Product	starting aldehyde	R ₁	R ₂	R ₃	R ₄	yield ^a (%)
38	54	H	H	H	H	77
39	55	H	H	Cl	H	85
40	56	H	H	NO ₂	H	79
41	57	H	H	OCH ₃	H	84
42	64	H	H	F	H	81
43	57	H	H	CF ₃	H	88
44	58	H	Cl	Cl	H	77
45	59	Cl	H	Cl	H	75
46	60	F	H	Cl	H	84
47	61	F	H	H	Cl	75
48	-	-	-	-	-	79
49	-	-	-	-	-	83

Finally, reaction between *para*-hydroxybenzaldehyde **53** and tosyl chloride (**77**) in CH₂Cl₂ in presence of triethylamine gave aldehyde **50** in high yield (Scheme 3.25).



Scheme 3.25. Reagents and conditions: (a) triethylamine, dry CH₂Cl₂, room temperature, 3 h (96%).

CHAPTER 4

BIOLOGY

4.1. Biochemical evaluation of chimera molecules

As described in Chapter 2, the identification of eight hit compounds by HTS guided us toward a FBLD approach, supported by molecular docking studies.

A small pool of chimera molecules has been designed combining non-overlapping binding portions of different fragments and then have been docked with the same computational model, in order to predict and classify their binding affinity. According to computational prioritization, the most promising ones have been synthesized, as described in Chapter 3 (Figure 4.1).

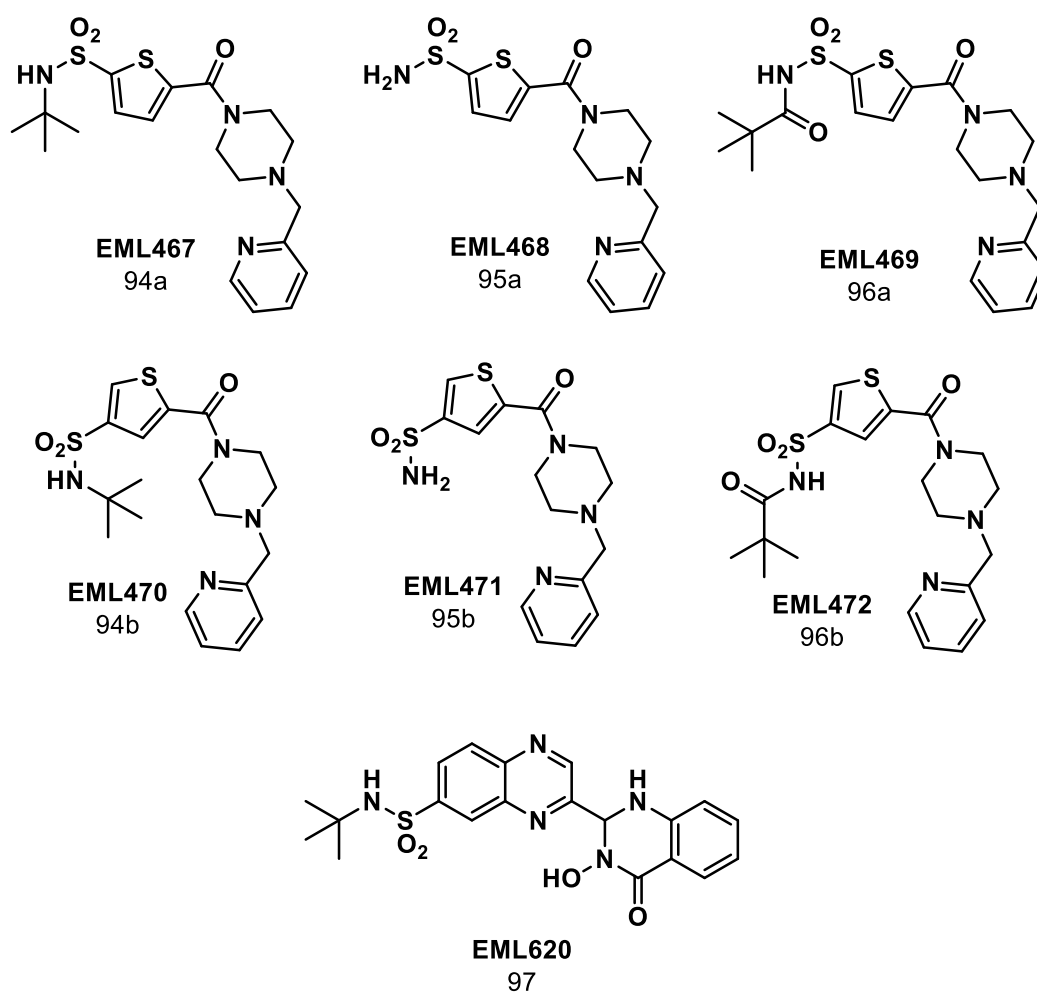


Figure 4.1. Chimera compounds synthesized.

Chimera molecules, together with some reaction intermediates, have been screened against *hKDM4A* by the FDH-coupled assay, in collaboration with Professor Axel Imhof at Ludwig-Maximilians-Universität (Munich, Germany).

Unfortunately, no inhibitory activity was found for any of the prepared compounds. These results could depend from excessive structural rigidity of derivatives than starting pseudo-fragments, as well as from some mistakes in initially formulated hypotheses.

4.1.1. Orthogonal screening platform

In order to better understand negative results and increase the reliability of data obtained, a new and more reliable screening platform has been developed in the lab of Professor Imhof, to orthogonal confirm compounds activity by mass spectrometry. To this aim, the activity of the *hKDM4A* was calculated, in the presence and without inhibitors, by LC-MS and MALDI-TOF through the direct measurement of the level of histone methylation. MALDI-TOF was also used to quantify the activity of KDM4A of *Drosophila* (*dKDM4A*).

Exploiting these assays, chimera molecules have been tested again, showing no activity in all the three different conditions. At the same time, we also evaluated the activity of initial hit compounds by the new screening platform. Results have confirmed a good inhibitory potency only for three of them (Figure 4.2), certifying modest activity for other two and a total absence of that for the other three molecules.

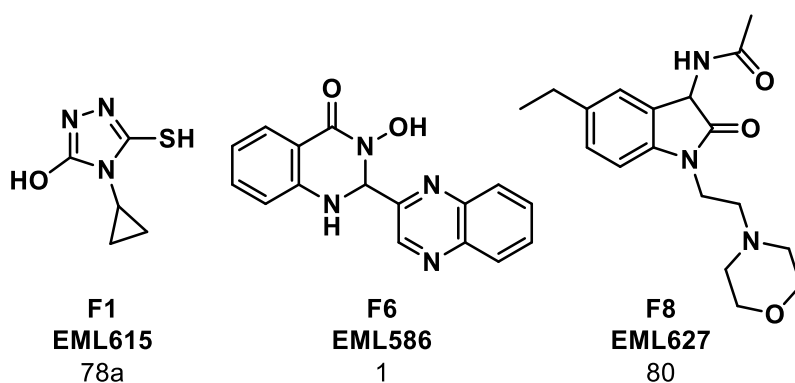


Figure 4.2. Real active identified by orthogonal screening

Unfortunately, our combined molecules are composed, partially or totally, by the inactive hits identified as false positives. This may explain the total lack of activity of them.

4.2. Hit validation process

The identification of only three real positives, among the eight hit compounds selected by HTS, persuaded us to take a step back and focus our attention on the prioritization of the hits in order to identify the most promising lead candidates and increase possibilities to obtain potent and selective KDM4 inhibitors.

This process is significantly expensive in terms of time and money, but it generally allows to avoid high attrition rate during the lead optimization phase.

To this aim, we evaluated hits on the basis of both target-independent and dependent criteria, following the generic rules described in the literature (Table 4.1)¹²⁴⁻¹²⁵.

Table 4.1. Generic Criteria for Hit Validation

-
1. structural identity confirmed
 2. tractable synthetic route established
 3. purity and stability established
 4. structure free of reactive/undesirable chemotypes
 5. structure reasonably drug-like
 6. activity confirmed on solids
 7. not a promiscuous inhibitor
 8. logical structure-activity relationship (SAR)
-

At first, actives were re-synthesized. As described in Chapter 3, compounds **EML615** and **EML586** are synthetically accessible in high yields. On the contrary,

the synthesis of **EML627** was affected by the formation of a mixture of two regioisomers, that lowered yield and increased purification time.

All compounds were structurally confirmed and evaluated for purity by NMR and HPLC experiments.

4.2.1. Chemical stability assay

The stability of compounds has been evaluated after incubation in phosphate-buffered saline (PBS) aqueous solution. Small molecule compounds can be unstable in aqueous solutions with respect to hydrolysis and this was considered a major issue because can significantly affect their application as molecular probes.

Therefore, compounds **EML586**, **EML615** and **EML627** were incubated with PBS solution, at room temperature. The presence of degradation products in the samples was evaluated by HPLC analysis after 5, 15, 30, 60 minutes and 24 h (Figure 4.3).

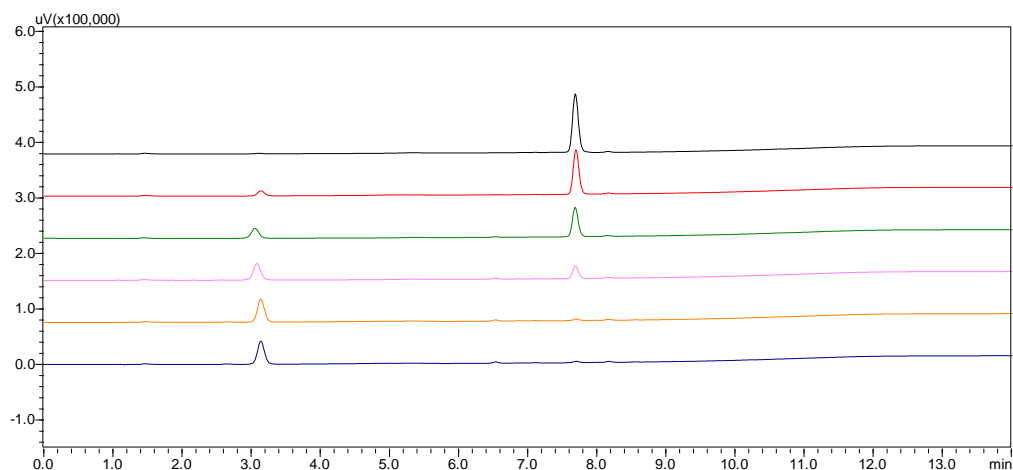


Figure 4.3. HPLC chromatograms obtained for compound **EML627** injected immediately after the dissolution in PBS, after 5, 15, 30, 60 minutes and 24 h. Spectra were recorded at 220 nm.

Experimental results indicated that the compounds **EML586** and **EML615** were stable under the conditions routinely used in biological assays (see Chapter

6). On the contrary, the high susceptibility of **EML627** to degradation in aqueous buffer appeared as a strong limitation, considering its incompatibility with all cellular assays conditions. Therefore, in addition of its poor synthetic accessibility, we decided to discard its chemotype for further derivatization.

4.2.2. *Parallel artificial membrane permeability assay*

Subsequently, we evaluated the cell permeability of **EML586** and **EML615**. To this aim, the well-validated parallel artificial membrane permeability assay (PAMPA) technique was employed¹³⁴⁻¹³⁵. The highly permeable drug propranolol and the poorly permeable drug furosemide were used as references (Table 4.2).

In PAMPA, a donor compartment, containing a buffer solution of selected compound, was separated by a filter plate coated with a liquid artificial membrane from an acceptor compartment, containing initial fresh buffer solution. Permeability was determined by measuring the delivery rate of chemical permeated into the acceptor compartment from the donor one during an incubation of 24 h at room temperature. A solution of dodecane was used as artificial membrane, providing significant correlations with gastrointestinal absorption in humans.

Table 4.2. Apparent permeability values of **EML586** and **EML615** with respect to standards propranolol and furosemide.

Compound	P_{app} (cm/s)
Propranolol	4.1 x 10 ⁻⁶
EML586	1.5 x 10 ⁻⁶
EML615	0.2 x 10 ⁻⁶
Furosemide	0.09 x 10 ⁻⁶

The compound **EML586** showed an apparent permeability value (P_{app}) of 1.5×10^{-6} cm/s, similar to that of propranolol ($P_{app} = 4.1 \times 10^{-6}$ cm/s), and very different from furosemide ($P_{app} = 0.09 \times 10^{-6}$ cm/s).

On the other side, **EML615** showed a poor apparent permeability value ($P_{app} = 0.2 \times 10^{-6}$ cm/s), probably due its more hydrophilic structure.

4.2.3. Secondary screening

Once both chemical stability and cell permeability were established, **EML586** and **EML615** have been tested against a panel of non-metal catalysed in-house epigenetic enzymes (PRMT1, PRMT3) and, again, on hKDM4A, using a different biochemical assay: the AlphaLISA homogeneous proximity immunoassay.

As described in Chapter 1, this type of assay measured enzyme activity by detecting the methylation grade of a biotinylated histone H3 peptide using streptavidin-coated donor beads and AlphaLISA acceptor beads conjugated to an antibody directed against the modified substrate.

This additional independent biochemical assay was useful to confirm on solid activity against *hKDM4A*, as well as to elucidate a perspective on potential promiscuity of the inhibitors against other epigenetic targets.

Compounds have been tested at the fixed dose of 100 μ M (5% DMSO) and results are summarized in Figure 4.4.

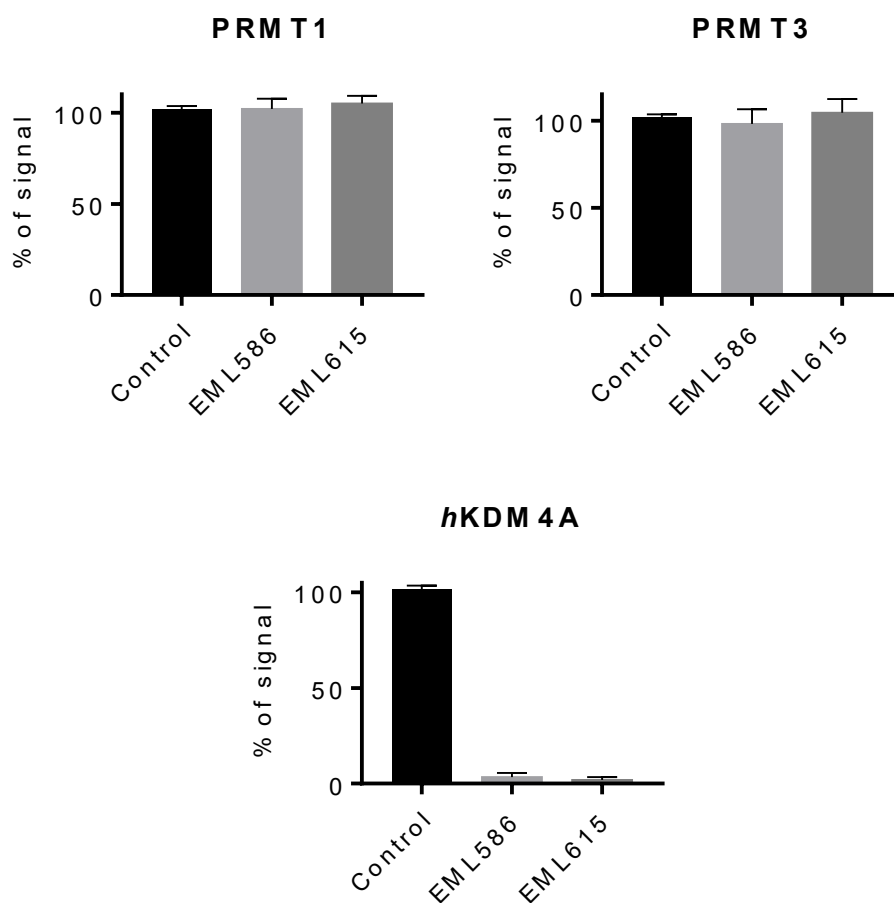


Figure 4.4. AlphaLISA assay performed with the *hKDM4*, PRMT1 and PRMT3. Enzyme activity percentage determined at 100 μ M (5% DMSO) with respect to DMSO. The results reported are the means \pm SD determined for at least two separate experiments.

Both the compounds have been shown no activity against PRMT enzyme, while they were able to completely inhibit *hKDM4* activity at this concentration.

4.3. Preliminary SARs

Hit validation last stage was to identify consistent SARs of actives to corroborate structure-based activity and develop a pharmacophore hypothesis. To

meet this, we designed and synthesized a small pool derivatives containing **EML586** and **EML615** scaffolds.

4.3.1. Structure-activity relationships of triazole derivatives

The active **EML615** was characterized by a very simple structure. For this reason, we decided to apply a molecular complication strategy to generate more complex derivatives, in order to explore the space availability into the active pocket. To meet this aim, we introduced an aromatic ring in place of the cyclopropane on the nitrogen N1, directly connected to the triazole moiety or separated by an alkyl chain (1 or 2 carbon atoms). Subsequently, we decided to explore the importance of the sulfhydryl group, in order to verify its possible role in metal-interactions. All designed derivatives are summarized in Figure 4.5.

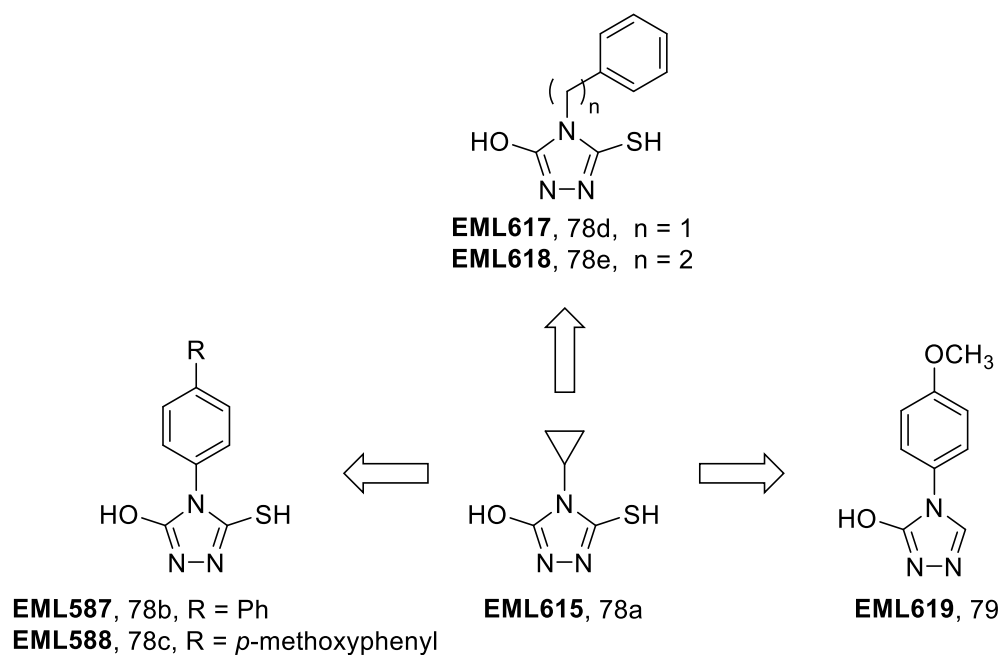


Figure 4.5. Derivatives of active **EML615**.

The compounds were synthesized (Chapter 3) and tested using the AlphaLISA homogeneous proximity immunoassay against *hKDM4A* at 50 μM (5% DMSO) fixed concentrations (data shown in Table 4.3).

Table 4.3. Effects of **EML615** derivatives on the activity of hKDM4A. Enzyme activity percentage determined at fixed dose of 50 μ M (5% DMSO) with respect to DMSO. The results reported are the means \pm SD determined for at least two separate experiments.

Compound	% residual activity hKDM4A
EML615	20.8 \pm 2.3
EML587	43.8 \pm 5.8
EML588	47.9 \pm 4.0
EML617	no inhibition
EML618	no inhibition
EML619	no inhibition

All derivatives synthesized were less active than **EML615**. Removal of the sulfhydryl group led to inactive compound **EML619**. On the other hand, introduction of an aromatic ring resulted in moderately active compounds (**EML587** and **EML588**), but only when it was directly bound to the triazole ring. In fact, the insertion of an alkyl chain gave the inactive derivatives **EML617** and **EML618**, suggesting a limited space availability into the active pocket.

These results led us to discard also triazole moiety for further derivatization because this scaffold provided limited opportunity for expansion into unexplored space having few points of appendage variation.

4.3.2. Structure-activity relationships of 3-hydroxy-2,3-dihydroquinazolin-4(1H)-one derivatives

The development of **EML586** derivatives has initially involved the replacement of one or both nitrogen atoms on quinoxaline to obtain the corresponding quinoline and naphthalene derivatives, in order to elucidate their role

in metal-interactions. Furthermore, hydroxamic function in 3-hydroxy-2,3-dihydroquinazolin-4(1H)-one ring has been removed to obtain 4-hydroxyquinazoline derivatives through dehydration (Figure 4.6).

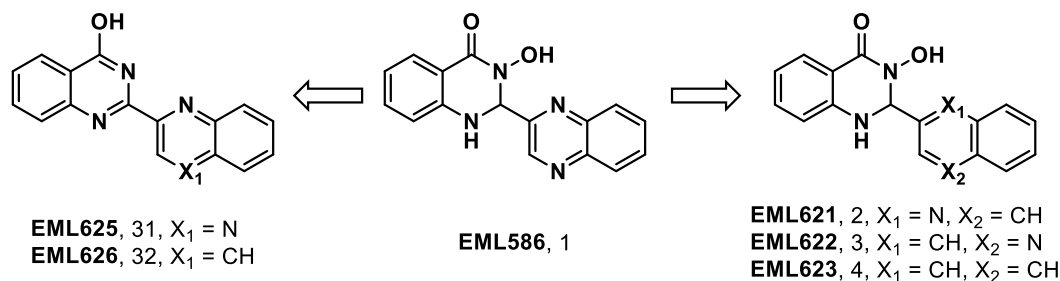


Figure 4.6. Derivatives of active **EML586**.

As for the triazole derivatives, compounds have been tested using the AlphaLISA homogeneous proximity immunoassay against *hKDM4A* at 50 μ M (5% DMSO) fixed concentrations (data shown in Table 4.4).

Table 4.4. Effects of compounds on the activity of *hKDM4A*. Enzyme activity percentage determined at fixed dose of 50 μ M (5% DMSO) with respect to DMSO. The results reported are the means \pm SD determined for at least two separate experiments.

Compound	% residual activity <i>hKDM4A</i>
EML586	38,7 \pm 8,4
EML621	19,7 \pm 8,1
EML622	19,8 \pm 7,8
EML623	4,8 \pm 16,0
EML625	no inhibition
EML626	no inhibition

Removal of hydroxamic acid group in compounds **EML625** and **EML626** resulted in a complete loss of activity, thus On the contrary, quinoline and naphthalene derivatives showed a better inhibitory activity against *h*KDM4A than **EML586**. In particular, the number of nitrogen atoms in the cycle on the right-side appeared to be not essential for the activity. In fact, the derivative with a naphthyl substituent was more active than the corresponding quinolyl-substituted analogues and even more active than the starting quinoxaline hit.

4.3.3. Binding hypothesis and design of new derivatives

These data are in agreement with crystallographic studies that identified an aliphatic subpocket adjacent to the active site in KDM4s extending into the substrate binding groove (see Paragraph 1.7)¹³⁶. It is probable that the naphthyl substituent fits into this pocket.

According to these preliminary SARs and with the aim to investigate the effects on potency induced by substitution of quinoxaline-ring in compound **EML586**, we designed a small library of novel analogues planning to replace the quinoxaline ring with more lipophilic functions (Figure 4.7).

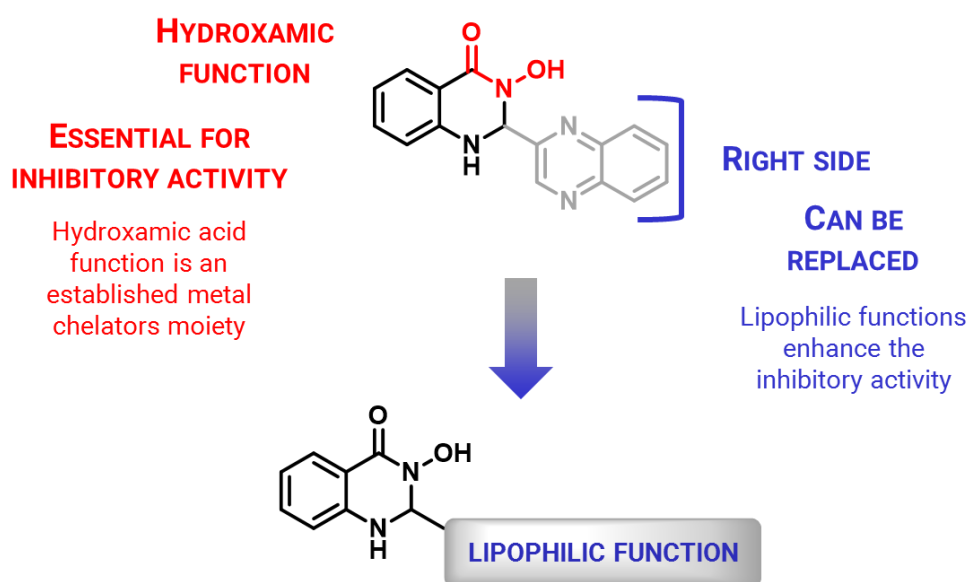


Figure 4.7. Design of novel “lipophilic” inhibitors of KDM4.

Novel derivatives were synthesized according to the previously reported procedures using a pool of selected aldehydes. We chose both short- and long-chain aldehydes, always characterized by variously functionalized aromatic rings, in order to explore a wide range of the lipophilic, electronic and steric properties (Figure 4.8).

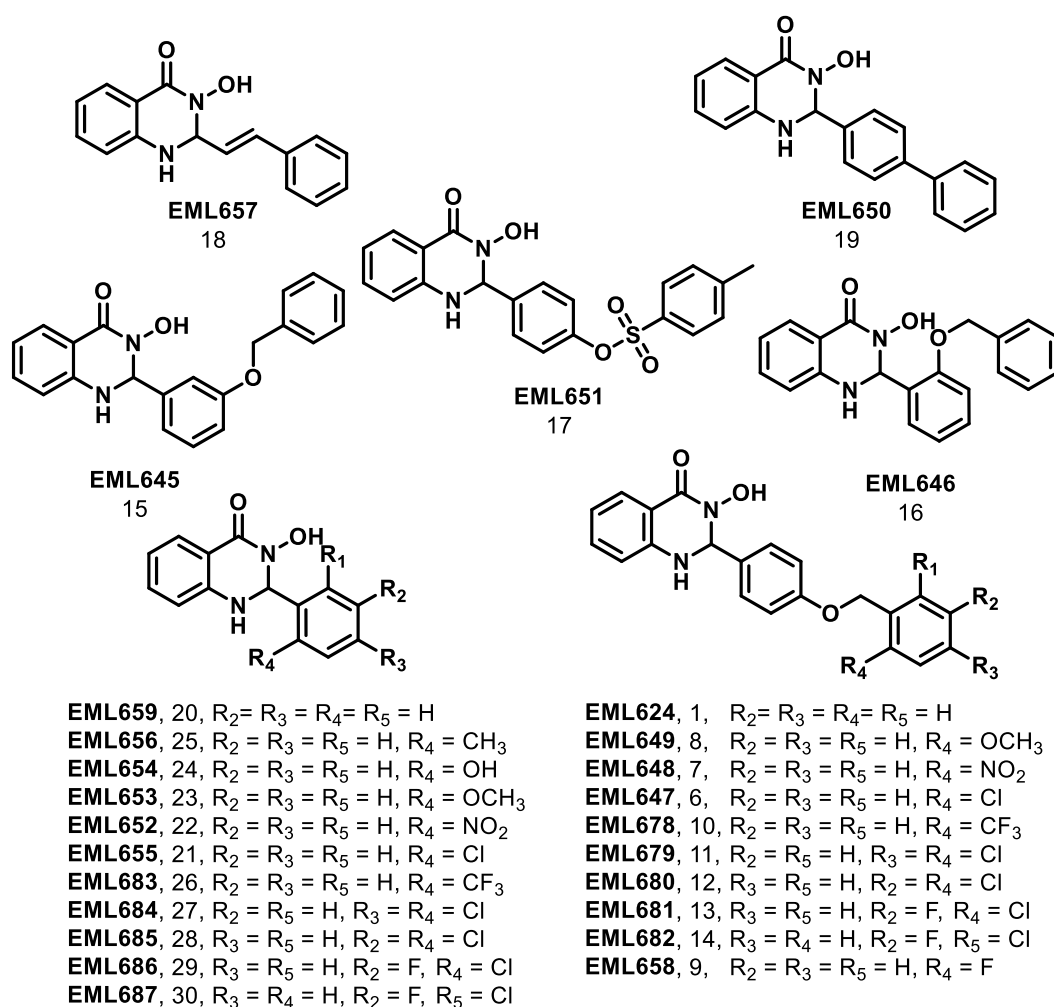


Figure 4.8. Novel library of derivative compounds for lead optimization.

4.4. Biochemical evaluation

All derivatives have been synthesized according to procedures described in Chapter 3 and then screened against *h*KDM4A using the AlphaLISA homogeneous proximity immunoassay.

To enhance the robustness of the results, firstly solubility of all derivatives has been evaluated both in water and in the assay buffer, using a nephelometer according to published procedures¹³⁷⁻¹³⁸.

4.4.1. Determination of solubility

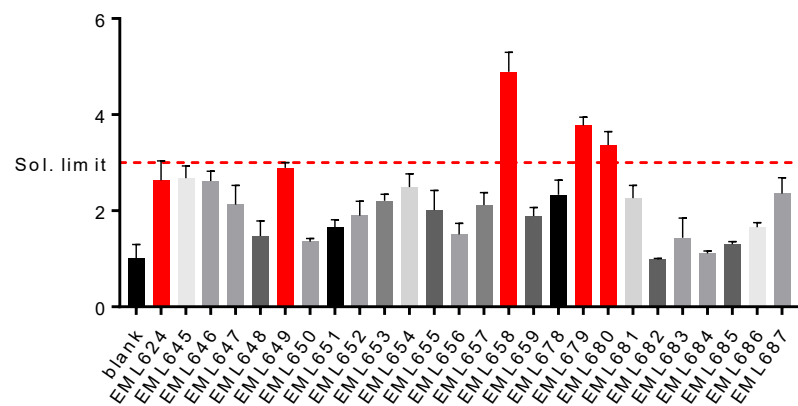
In drug discovery, solubility is an important parameter to take into account because compounds must be dissolved to undergo pharmacological processes. Precipitation decreases the concentration in solution, resulting in a reduction of compound to bind to the protein of interest. If the compound is partially dissolved or is supersaturated, the SARs, pharmacokinetics or in vivo potency may be unreliable¹³⁹. Considering the lipophilic character of novel derivatives, the solubility of them has been evaluated before the biochemical assays.

Solution conditions may largely affect this parameter. Solubility is determined by the interactions of the molecules with themselves in the crystal, the interactions with themselves in solution, and by the interactions of solute and solvent molecules in solution. For these reasons, the measure of solubility under the assay conditions has been considered crucial to assist data interpretation¹³⁹. Thus, solubility has been evaluated both in water and in AlphaLISA buffer solution using a nephelometric assay.

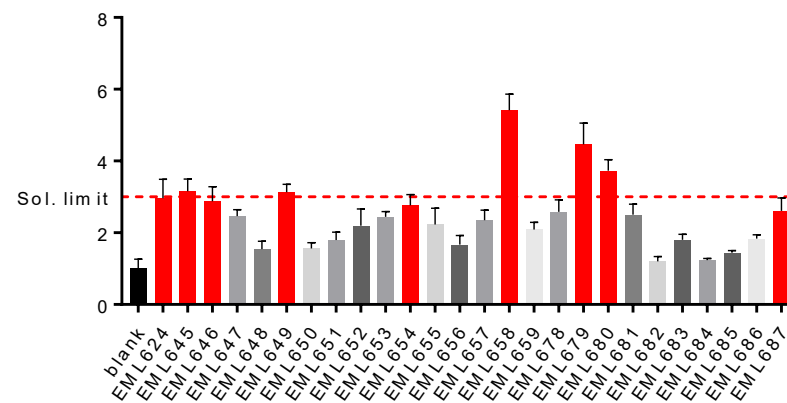
This method measures the intensity of scattered visible light, the light reflected by illuminated suspended particles, in a given medium in order to determine concentration, size, and shape of disperse particles in disperse systems. For light scattering measurements, a signal-to noise ratio (S/N) equals to or >3 was used to indicate the presence of precipitation.

Solubility has been measured at the fixed dose of 25 μ M, with the 5% of DMSO in both the experimental conditions (water and AlphaLISA buffer). Measures have been done immediately after the preparation of samples and after an incubation time of 1 h at room temperature. Collected data are summarized in Figure 4.9.

Water solubility T0



Water solubility 1 h



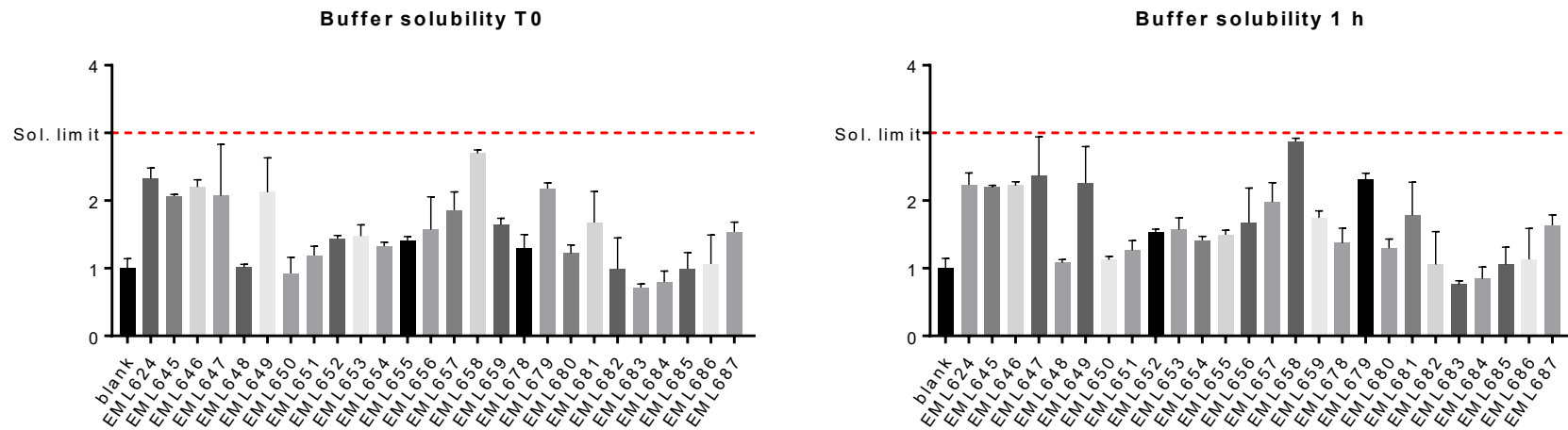


Figure 4.9. Solubility in water and AlphaLISA buffer. Two incubation times were examined: 0 and 60 minutes. Insoluble compounds are highlighted in red. The results reported are the means \pm SD determined for at least two separate experiments.

As expected, several derivatives showed a poor solubility profile in pure water, which decreases in a time-dependent manner. However, all derivatives have been found soluble in AlphaLISA buffer at the concentration of 25 μM (5% DMSO).

4.4.2. AlphaLISA homogeneous proximity immunoassay

All synthesized compounds were screened against *hKDM4A* using the AlphaLISA homogeneous proximity immunoassay.

In agreement to solubility data and expecting a better activity of novel compounds with respect to those of the first library, we selected a fixed 25 μM (5% DMSO) concentration as cut-off for the biochemical activity evaluation. The results are summarized in Figure 4.10.

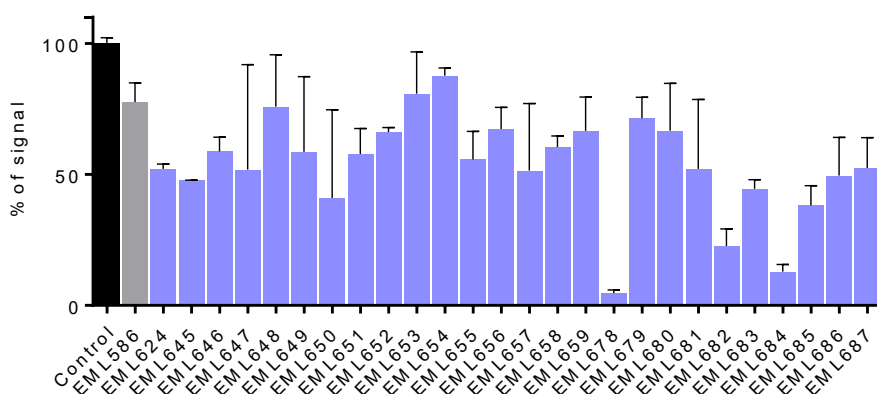


Figure 4.10. AlphaLISA assay performed with the *hKDM4*. Enzyme activity percentage determined at 25 μM (5% DMSO) with respect to DMSO. The results reported are the means \pm SD determined for at least three separate experiments.

Most active compounds were selected and their activity has been measured over a range of concentrations from which IC_{50} values were determined (Table 4.5).

Table 4.5. Compounds were tested in 10-dose IC₅₀ mode with threefold serial dilutions starting at 200 μ M (5% DMSO). The results reported are the means \pm SD determined for at least two separate experiments.

Compound	IC ₅₀ (μ M)
EML586	39.7 \pm 1.1
EML621	30.5 \pm 1.1
EML622	37.7 \pm 1.1
EML623	38.2 \pm 1.1
EML624	33.0 \pm 1.1
EML649	140.0 \pm 1.2
EML678	20.8 \pm 1.2
EML682	20.4 \pm 1.3
EML684	22.7 \pm 1.3

The data suggested that derivatives with more bulky and lipophilic substituents were endowed with the highest inhibitory activity. In particular, compounds **EML678**, **EML682** and **EML684** were about 2-fold more potent than **EML586** against *hKDM4A* in this biochemical assay. These data are in agreement with the binding hypothesis discussed in Paragraph 4.3.3.

4.5. Biological evaluation

Pursuing my efforts toward the identification of new interesting molecular probes to elucidate the role of KDM4s, I've spent a period of six months abroad, as a visiting PhD student in the laboratory of Professor Axel Imhof at the Ludwig Maximilian University of Munich. At Imhof lab, I had the opportunity to test some selected inhibitors in a cell-based assay in order to analyze the effects of them on the histone methylation pattern by mass spectrometry.

At the same time, an independent analysis of histone methylation levels in cells by antibody-based methods, after the treatment with inhibitors, has been

performed in collaboration with Professor Lucia Altucci of Seconda Università degli Studi di Napoli.

Both the experiments have demonstrated the ability of synthesized compounds to affect the level of histone methylation in cells. In the following paragraphs, details have been reported.

4.5.1. Analysis of histone modifications by mass spectrometry

The analysis of histone modifications in cells is normally performed using antibody-based methods like immunoblotting, immunoprecipitation, ELISA, or immunofluorescence and is constrained by problems, such as specificity, availability, limited dynamic range and by problems in detecting multiple modifications on different sites at the same time¹⁰⁰. Mass spectrometry (MS) provides an alternative experimental approach that can address the complexity of histone PTMs in single experimental set and overcome some of the limitations of antibody-based methods.

In collaboration with the group of Professor Axel Imhof, we used a well-established procedure to isolate histones from cells, prepare them for MS analysis and interpret the results.

HEK 293 cell line has been selected as suitable for the treatment. At first, it has been chosen to test only three compounds; hit compound **EML586**, its direct analogue **EML621**, in which only one nitrogen from the quinoxaline ring was removed, and the more lipophilic compound **EML684**, one of the most powerful derivatives identified from my biochemical studies, have been selected as starting points. Having no idea of correlation between biochemical and biological activities, experiments with 4 different concentrations of inhibitors (200, 100, 50 and 25 μ M, with final 0.5% DMSO concentration) have been performed and compared to a control (0.5% DMSO).

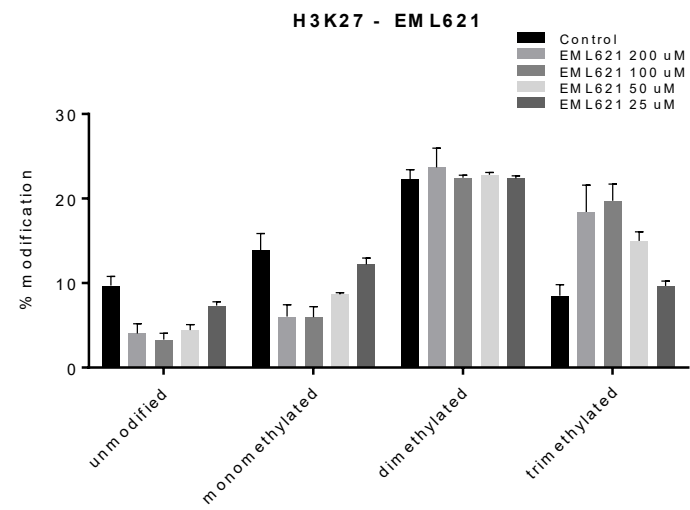
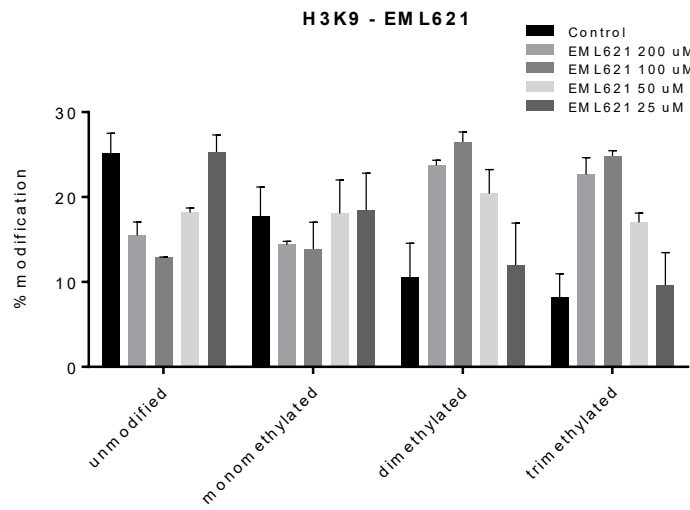
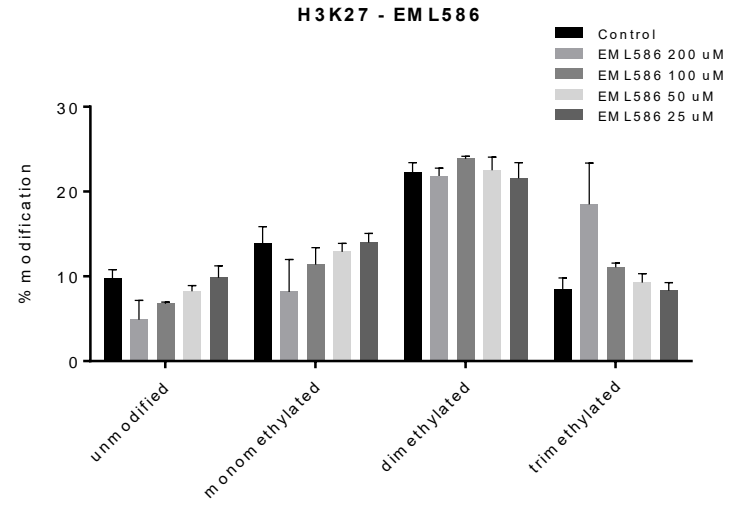
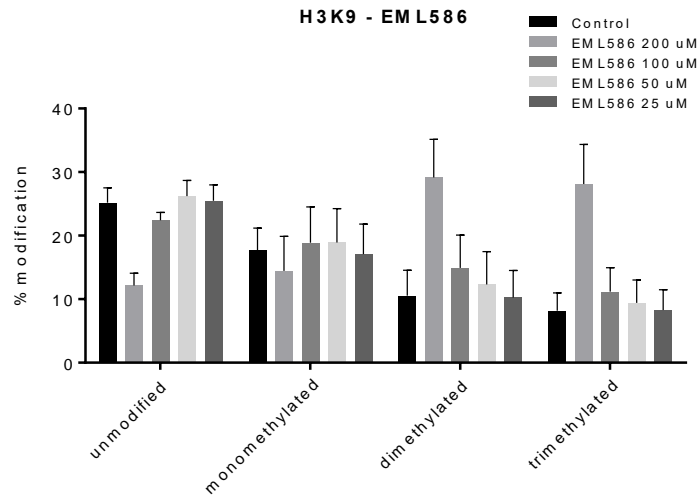
After an incubation time of 24 h at 36 °C, treated cells were collected and histones were isolated from biological tissues by acid extraction. The extraction was performed using hydrochloric acid (HCl), due to histones basicity¹⁴⁰, starting

with whole cells to minimize losses due to handling. Further separation by SDS-PAGE gel and Coomassie staining showed a characteristic pattern of histones, that were isolated from the other basic proteins. The corresponding bands were excised from the gel to undergo protease digestion prior to MS analysis. Digestion was lead using trypsin to cut proteins in smaller peptides. To avoid generation of peptides too short that cannot be analyzed efficiently by MS (trypsin cleave proteins after lysine and arginine, very abundant in histone tails), a treatment with propionic anhydride was performed to block lysines from tryptic cleavage. Un-methylated and mono-methylated lysines react to form propionic amides that are not recognized by trypsin, as well as di- and tri-methylated lysines.

After digestion, the peptides were released from the gel pieces into the supernatant through different chemicals and prepared for MS analysis. Samples were concentrated and the peptide mixtures were desalted by reversed phase absorption/elution.

Samples were then separated by C18 reversed phase chromatography and the eluting peptides were directly ionized and infused into the mass spectrometer, which measures the mass-to-charge ratio (m/z) of them.

Data generated by MS-analysis are summarized in Figure 4.11.



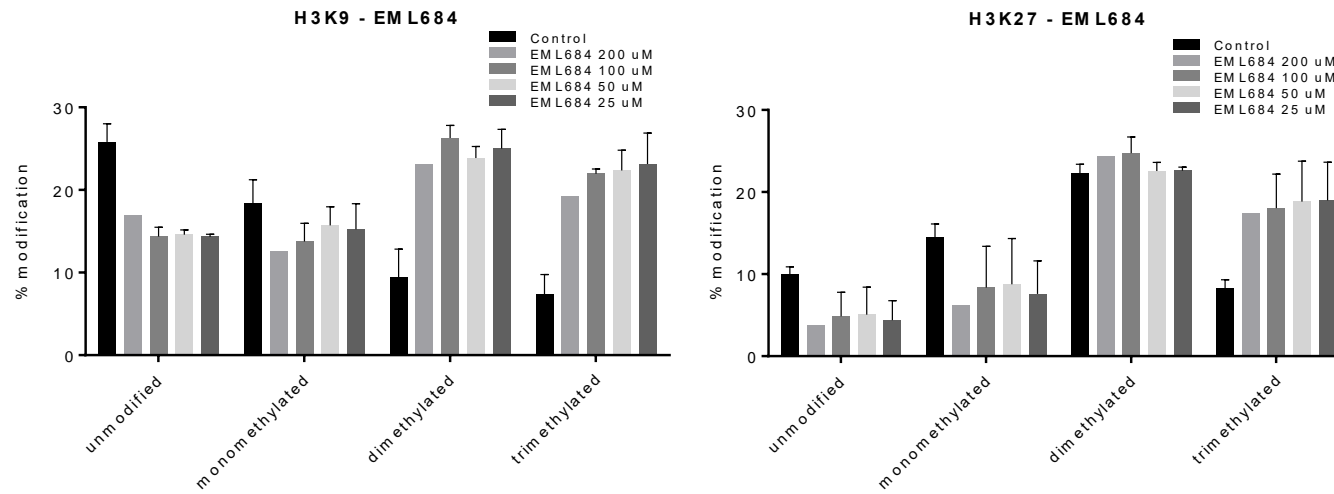


Figure 4.11. H3K9 and H3K27 methylation levels in treated HEK293 compared to control. The results reported are the means \pm SD determined for at least three separate experiments.

The treatment with inhibitors resulted in a dose-dependent increase of methyl marks H3K9me3 and H3K27me3 in HEK 293 cells compared to a control group. If the increase in H3K9 methylation is in agreement with the inhibition of KDM4 enzymes, a different state of H3K27 methylation may be associated with the inhibition of one or more different JHDM enzymes (i.e. KDM6 subfamily). Curiously, these 2 effects appear to occur at the same concentrations.

Similarly to what we observed in the biochemical assay, the trend of cellular activity could be related to the lipophilicity of substituents on the dihydroquinazolinone moiety, with compound **EML684** being more active than **EML621** and **EML586**, respectively. Moreover, despite the methylation levels never exceeded a certain threshold, **EML684** seemed to completely inhibit the enzymatic activity at concentration of 25 μ M, suggesting that lower concentrations may also be effective. Using this concentration as cut-off, the inhibiting capability of other 12 molecules (**EML622**, **EML624**, **EML645**, **EML646**, **EML652**, **EML655**, **EML657**, **EML659**, **EML678**, **EML683**, **EML685** and **EML686**) against JHDMs was tested in HEK 293 cell line (Figure 4.12).

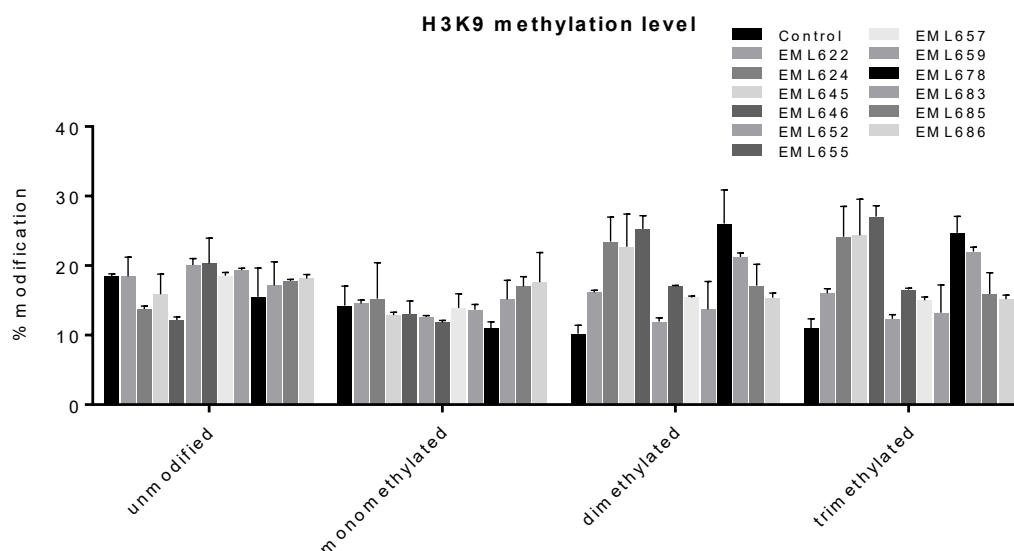


Figure 4.12. H3K9 methylation levels in treated HEK 293 compared to control. The results reported are the means \pm SD determined for at least three separate experiments.

Treatment with compounds **EML624**, **EML645**, **EML646**, **EML678** and **EML683** increased H3K9me3 and H3K27me3 levels in a comparable manner to that of **EML684**.

4.5.2. Cell cycle analysis

To better understand the effects of these compounds in cell-based assays, cell viability experiments has been conducted in parallel with MS-analysis using the Trypan blue assay. Interestingly, it was observed that inhibitors induced a concentration-dependent loss in cellular viability at the same dose that led to reduction of the methylation level (Figure 4.13).

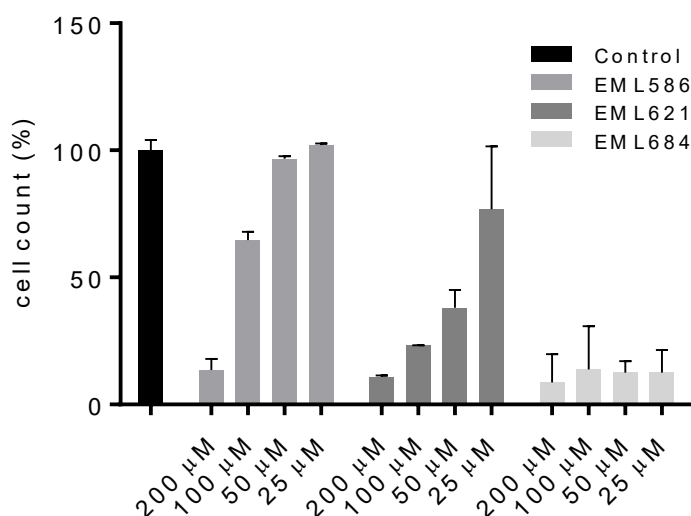


Figure 4.13. Cells vitality percentage measured with trypan blue assay at different concentration with respect to DMSO. The results reported are the means \pm SD determined for at least three separate experiments.

To further investigate treatment-induced cell death, cell cycle analysis has been performed by FACS on HEK 293 cells treated with inhibitors. Flow cytometry analysis showed an increase in the percentage of cells blocked in S phase and a decrease in the percentage of cells in G1 phase or G2 phase (Figure 4.14).

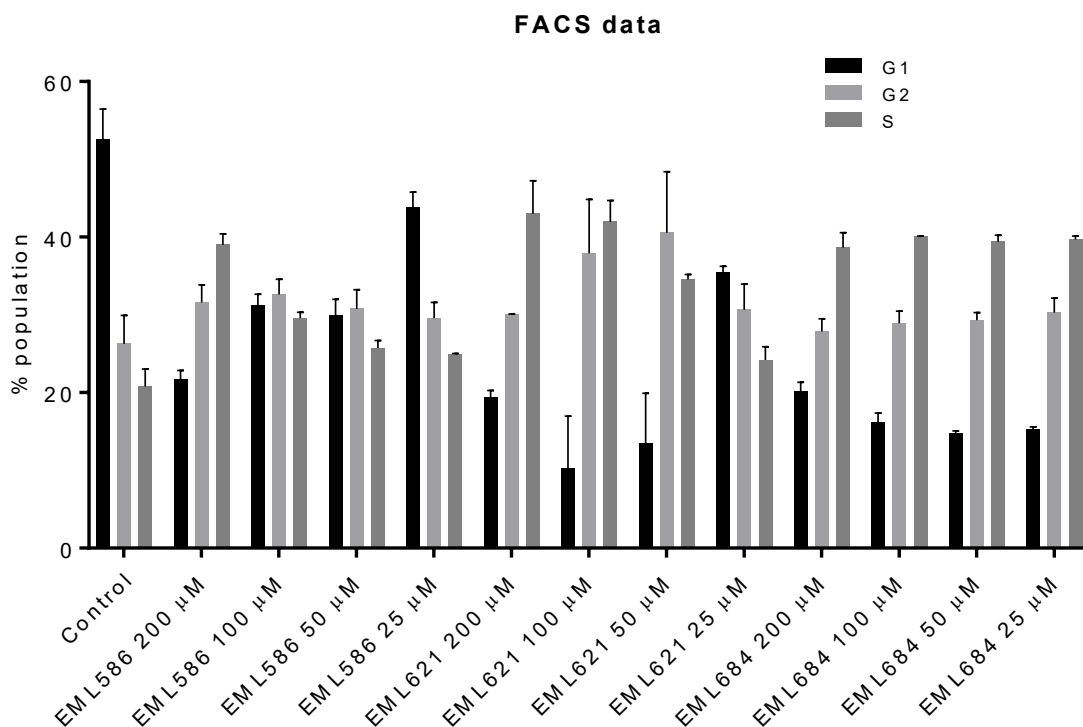


Figure 4.14. FACS analysis data for HEK 293 cells treated with inhibitors at different concentration with respect to DMSO. The results reported are the means \pm SD determined for at least two separate experiments.

As for the effect on the cellular viability, S-block was present only at the concentrations that led to reduction of the methylation level, suggesting that there may be a correlation between them.

4.5.3. Analysis of histone modifications by Western blot

A second biological screening, on a different cell line, was carried out in collaboration with Professor Altucci of Seconda Università di Napoli (Naples, Italy).

The effects of compounds **EML621**, **EML622**, **EML652**, **EML683** and **EML685** on cellular histone methylation have been investigated using modification-specific antibodies against H3K9me3, H3K9me2 and H4 in human colon cancers cells HCT-116. Cells were incubated for the 24 h with the inhibitors (50 μ M, 0.1% DMSO) and the histone extracts were then immunoblotted with antibodies to specific histone acetylation sites (Figure 4.15).

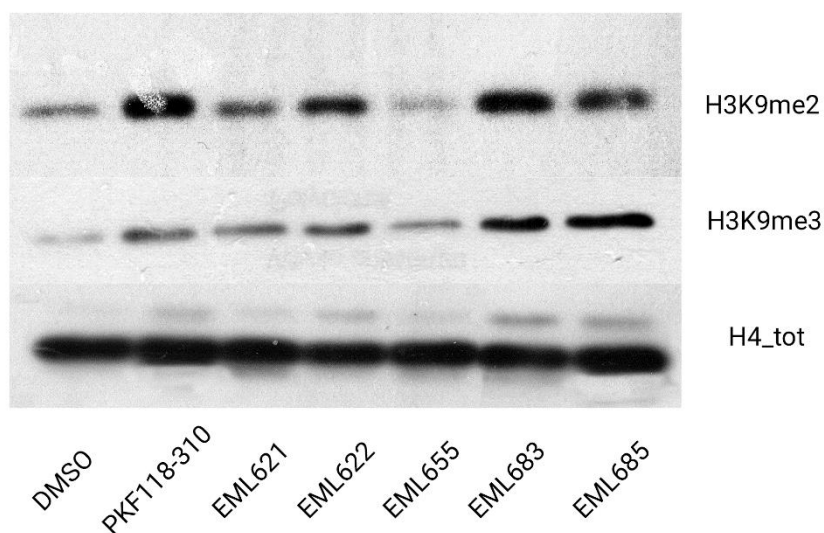


Figure 4.15. Western blot analyses performed with inhibitors at 50 μ M for 24 h on the methylation of the specific lysine residues H3K9 in histone extracts from HCT-116 cells.

Methylation was detected by immunoblotting with antibodies specific for histone methylation sites as indicated. Total histone H4 was used to check for equal loading.

PKF118-310 (1 μ M) was used as a reference compound.

It was observed that all compounds, in particular **EML683**, induced a marked increase in the level of lysine H3K9me2 and H3K9me2 in HCT-116 cells.

CHAPTER 5

CONCLUSION

‘Readers’, ‘writers’, and ‘erasers’ are the mediators of epigenetic mechanisms in physiological and disease conditions. Fine-tuning their activity is the goal of epigenetic drug discovery, and huge advances are continually being made. While HDAC inhibitors are already in clinical use, the understanding of methylation regulators has lagged somewhat behind. The scientific community shares the view that histone methylation is one of the major crossroads in gene expression and regulation. However, the finer features of players involved in molecular machinery, known collectively as demethylase enzymes, are yet to be clarified. Investigators are looking for small molecules able to modulate these enzymatic families.

Among demethylases, KDM4 enzymes play an important role in regulation of H3K9 and H3K36 methylation, key events for active gene transcription. The aberrant activity of these enzymes has been significantly implicated in cancer initiation and progression and, as a consequence, they are currently one of the main targets investigated in drug discovery. However, only a few inhibitors have been identified to date, most of them inhibiting many other Fe(II)/2OG dependent oxygenases or being affected by undesirable characteristics, such as poor cell permeability, which limit their applicability as chemical probes and their potential therapeutic development. Potent and selective inhibitors are, therefore, highly needed.

Starting from a preliminary HTS campaign using an indirect fluorescence assay for human KDM4 (*hKDM4*) subfamily, and the subsequent hit validation stage using a more reliable method based on LC-MS and MALDI-TOF, we were able to identify a cell-permeable compound, namely **EML586**, as a promising lead candidate for the development of a new series of KDM4 inhibitors. A small library of derivatives was then synthesized and tested against *hKDM4A* compared to the lead compound using an AlphaLISA homogeneous proximity immunoassay. Cytopermeability was also assessed using a parallel artificial membrane permeability assay (PAMPA). This led us to generate a binding mode hypothesis, which posited that hydroxamic acid function cannot be replaced, suggesting the possibility of an active role in the formation of coordination bonds with Fe(II). On the contrary, replacement of quinoxaline ring with more lipophilic functions resulted in more active compounds, probably because of a better interaction into the

aliphatic subpocket adjacent to the active site in KDM4s. These data are in agreement with crystallographic studies performed by other groups,¹³⁶ that identified an aliphatic subpocket adjacent to the active site in KDM4s extending into the substrate binding groove.

Subsequent derivatization of the 3-hydroxy-2,3-dihydroquinazolin-4(1H)-one moiety with variously functionalized aromatic rings resulted in the discovery of potent inhibitors **EML678** and **EML684**, which showed a better activity against *h*KDM4A compared to the lead compound in the AlphaLISA homogeneous proximity immunoassay.

Then, to better characterize the activity profile of the compounds and analyze the effects on histone modifications avoiding the typical issues occurring with antibody-based methods (specificity, availability, limited dynamic range and problems in detecting multiple modifications on different sites at the same time¹⁰⁰), we tested the selected molecules in a cell-based assay to analyze the effects on the histone methylation pattern through a MS-based method. We found that the treatment with the selected inhibitors enables simultaneous and dose-dependent increases in levels of H3K9me2/3 and H3K27me2/3 in HEK 293 and HCT116 colon cancer cells. Further experiments are ongoing, in order to determine the IC₅₀ values and selectivity profiles over other 2OG-dependent oxygenases and epigenzymes. In fact, if the increase in H3K9 methylation is in agreement with the inhibition of KDM4s, a different state of H3K27 methylation could be related to a downregulation of one or more different JHDM enzymes (i.e. KDM6 subfamily) as well as to compensatory effects related to other mechanism, such as an upregulation of methyltransferases (HMTs). Furthermore, cytometric analysis also showed that these compounds led to a marked arrest in the S phase of cell cycle and a concentration-dependent loss in cellular viability. The mechanism of this effects and their correlation with the increase of methylation level are still unknown and will be subjects of further studies.

These results are promising and stimulate our research toward the identification of even more potent, cell permeable, and selective inhibitors of the KDM4 subfamily with which to study the role of KDM4 enzyme function in cancer

biology and to further explore the potential of such compounds as anticancer agents. The advantage of using such inhibitors for cancer treatment may lie in their ability to achieve a synergistic effect in combination with other methylation regulators, such as (for example) the inhibitor of KDM6B GSK-J4¹⁴¹. This evidence highlights the growing interest to develop combination therapies as viable approaches to increase the effectiveness of a histone methylation modulator. Since several aberrant histone modifications are involved in cancer, the effect of combination therapy is synergistic, targeting simultaneously 2 or more epi-modifications. In addition, combo-therapies are useful to overcome drug resistance and minimize toxicities and side effects.

Future efforts will be directed towards two main objectives. The first will be the chiral resolution of the most active derivatives, obtained as a mixture of enantiomers from the coupling between 2-amino-N-hydroxybenzamide and achiral aldehydes, in order to assess which enantiomer is more active. The second aim will be the decoration of the left side of our scaffold. With the aim to improve the occupation of the enzyme catalytic site, including the binding site of the methylated lysine substrate, and consequently increase selectivity, the left side will decorate with various aliphatic chains of different lengths linked to methylated lysine mimetic moieties.

CHAPTER 6

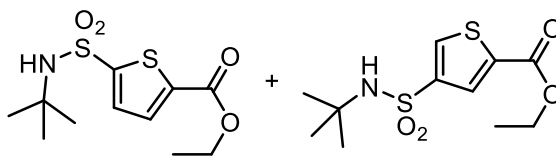
EXPERIMENTAL PART

6.1. General information

All chemicals were purchased from Sigma Aldrich (Milan, Italy) or from Fluorochem Ltd (Hadfield, United Kingdom) and were of the highest purity. All solvents were reagent grade and, when necessary, were purified and dried by standard methods. All reactions requiring anhydrous conditions were conducted under a positive atmosphere of nitrogen in oven-dried glassware. Standard syringe techniques were used for anhydrous addition of liquids. Reactions were routinely monitored by TLC performed on aluminum-backed silica gel plates (Merck DC, Alufolien Kieselgel 60 F254) with spots visualized by UV light ($\lambda = 254, 365$ nm) or using a KMnO_4 alkaline solution. Solvents were removed using a rotary evaporator operating at a reduced pressure of ~ 10 Torr. Organic solutions were dried over anhydrous Na_2SO_4 . Chromatographic purification was done on an automated flash chromatography system (IsoleraOne™, Biotage) using cartridges packed with KP-SIL, 60 Å (40–63 μm particle size). High performance liquid chromatography (HPLC) was performed on a Shimadzu SPD 20A UV/vis detector ($\lambda = 220$ nm) using C-18 column Phenomenex Synergi Fusion RP 80A (75mm \times 4.60 mm; 4 μm) at 25 °C using a mobile phase A (water + 0.1% TFA) and B (MeCN + 0.1% TFA) at a flow rate of 1 mL/min. Melting points were determined on a Stuart SMP30 melting point apparatus in open capillary tubes and are uncorrected. ^1H NMR spectra were recorded at 300 MHz on a Bruker Avance 300 spectrometer or at 400 MHz on a Bruker AVANCE III HD. Chemical shifts are reported in δ (ppm) relative to the internal reference tetramethylsilane (TMS). When compounds were tested as salts, NMR data refer to the free base. Mass spectra were recorded on a Finnigan LCQ DECA ThermoQuest (San Jose, USA) mass spectrometer in electrospray positive and negative ionization modes (ESI-MS). Purity of tested compounds was established by combustion analysis, confirming a purity $\geq 95\%$.

6.2. Procedures to obtain thiophene-2-sulfonamide derivatives

Synthesis of ethyl 5-(N-(tert-butyl)sulfamoyl)thiophene-2-carboxylate and 2-((5-(ethoxycarbonyl)thiophene)-3-sulfonamido)-2-methylpropan-1-ylidium mixture (100a-b)

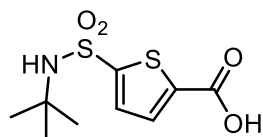


To a stirred solution of ethyl thiophene-2-carboxylate (**98**; 1.00 g, 6.40 mmol) in DCM (15.0 mL), chlorosulfonic acid (14.0 mL) was added slowly. The reaction mixture was stirred at room temperature overnight, then was poured in water (200 mL) at 0 °C and extracted with CH₃Cl (3 x 70 mL). The organic phase was dried (Na₂SO₄), filtered, and concentrated in vacuo. The residue was dissolved in dry THF (10 mL) then *tert*-butylamine (1.87 g, 25.60 mmol) was added to stirring solution. The resulting white suspension was stirred vigorously for 1 h, then the reaction mixture was taken up with EtOAc (100 mL), washed with saturated aqueous solution of NaHCO₃ (3 x 30 mL) and brine (30 mL), dried, filtered, and concentrated in vacuo. The crude was purified by silica gel chromatography (DCM/EtOAc) to give the title compounds in ratio 1:1 in 60% yield as a brown oil. ¹H NMR (300 MHz, CDCl₃) δ 8.11 (s, 1H), 8.01 (s, 1H), 7.70 (d, J = 3.9 Hz, 1H), 7.57 (d, J = 3.9 Hz, 1H), 4.49 – 4.37 (m, 5H), 1.35 (d, J = 3.2 Hz, 16H), 1.31 (s, 7H). MS ESI m/z: 292 [M + H]⁺.

Synthesis of ethyl 4-(chlorosulfonyl)thiophene-2-carboxylate and ethyl 5-(chlorosulfonyl)thiophene-2-carboxylate (**101a-b**)

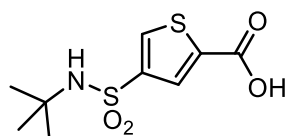
To a stirred solution of ethyl 5-(chlorosulfonyl)thiophene-2-carboxylate and ethyl 4-(chlorosulfonyl)thiophene-2-carboxylate mixture (0.50 g, 1.71 mmol) in THF (5 mL) was added a lithium hydroxide water solution (5 mL, 1.4 M). The resulting mixture was stirred overnight at room temperature. The organic solvent was evaporated and resulting aqueous solution was washed with DCM (3 x 2 mL). The crude was recovered by acidification of the aqueous phase with HCl 12 N and filtration of the white precipitate. Final purification by preparative HPLC allowed us to obtain all of the designed compounds in quantitative yield.

5-(N-(*tert*-butyl)sulfamoyl)thiophene-2-carboxylic acid 101a



$^1\text{H NMR}$ (300 MHz, CDCl_3) δ 7.76 (d, $J = 3.9$ Hz, 1H), 7.58 (d, $J = 3.9$ Hz, 1H), 4.79 (s, 1H), 1.33 (s, 9H). MS ESI m/z : 264 $[\text{M} + \text{H}]^+$.

4-(N-(tert-butyl)sulfamoyl)thiophene-2-carboxylic acid 101b

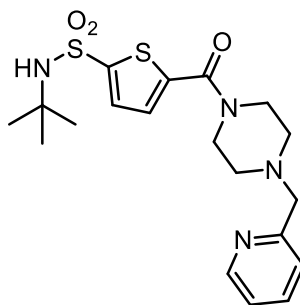


$^1\text{H NMR}$ (300 MHz, CDCl_3) δ 8.79 (s, 1H), 8.38 – 8.25 (m, 1H), 4.59 (d, $J = 7.1$ Hz, 1H), 1.48 (t, $J = 7.1$ Hz, 9H). MS ESI m/z : 264 $[\text{M} + \text{H}]^+$.

General procedure for the synthesis of N-(tert-butyl)-5-(4-(pyridin-2-ylmethyl)piperazine-1-carbonyl)thiophene sulfonamides 94a-b

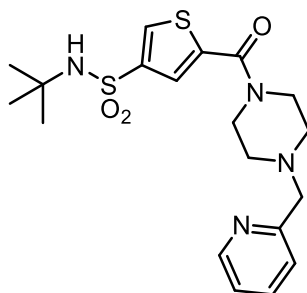
To a stirring solution of thiophene carboxylic acid (**101a-b**; 0.30 g, 1.15 mmol), 1-(pyridin-2-ylmethyl)piperazine (**102**; 0.11 g, 0.95 mmol) and N,N-dimethylpyridin-4-amine (0.01 g, 0.10 mmol) in dry DCM (15.0 mL) was added N,N'-methane Diylidene dicyclohexanamine. The mixture was stirred at room temperature overnight. The white precipitate was removed by filtration and the crude was readily purified by silica gel chromatography (DCM/MeOH) to give the title compounds in 75% yield as a brown solid.

N-(tert-butyl)-5-(4-(pyridin-2-ylmethyl)piperazine-1-carbonyl)thiophene-2-sulfonamide 94a



^1H NMR (300 MHz, DMSO- d_6) δ 8.50 (d, J = 3.9 Hz, 1H), 7.90 (s, 1H), 7.78 (t, J = 7.0 Hz, 1H), 7.58 – 7.42 (m, 2H), 7.36 (d, J = 3.6 Hz, 1H), 7.30 – 7.23 (m, 1H), 3.64 (s, 6H), 1.17 (s, 9H). MS ESI m/z : 423 $[\text{M} + \text{H}]^+$.

N-(tert-butyl)-5-(4-(pyridin-2-ylmethyl)piperazine-1-carbonyl)thiophene-3-sulfonamide 94b

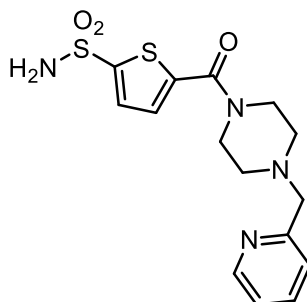


^1H NMR (300 MHz, DMSO- d_6) δ 8.84 (d, J = 4.0 Hz, 1H), 8.60 (s, 1H), 8.12 (t, J = 7.2 Hz, 1H), 7.88 (s, 1H), 7.85 – 7.76 (m, 2H), 7.68 – 7.56 (m, 1H), 3.99 (s, 6H), 1.45 (s, 9H). MS ESI m/z : 423 $[\text{M} + \text{H}]^+$.

General procedure for the synthesis of 5-(4-(pyridin-2-ylmethyl)piperazine-1-carbonyl)thiophene sulfonamides 95a-b

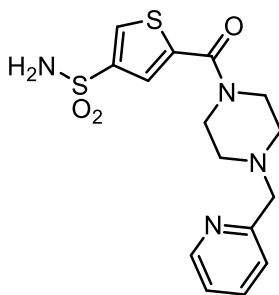
To a stirring solution of sulfonamide (**94a-b**; 0.11 g, 0.27 mmol) in DMC (5.0 mL) was added trifluoroacetic acid (5.0 mL). The mixture was stirred at room temperature overnight. After the evaporation of the solvent, water (20 mL) was added and title compound was extracted with EtOAc (3 x 7 mL), washed with brine (10 mL), dried, filtered, and concentrated in vacuo. The desired product was obtained as white solid in 95% yield after recrystallization from EtOAc.

5-(4-(pyridin-2-ylmethyl)piperazine-1-carbonyl)thiophene-2-sulfonamide 95a



^1H NMR (300 MHz, DMSO- d_6) δ 8.68 (d, J = 5.0 Hz, 1H), 7.94 (t, J = 7.6 Hz, 1H), 7.86 (s, 2H), 7.65 – 7.50 (m, 4H), 4.40 (s, 2H), 3.88 (s, 4H). MS ESI m/z : 367 $[\text{M} + \text{H}]^+$.

5-(4-(pyridin-2-ylmethyl)piperazine-1-carbonyl)thiophene-3-sulfonamide
95b

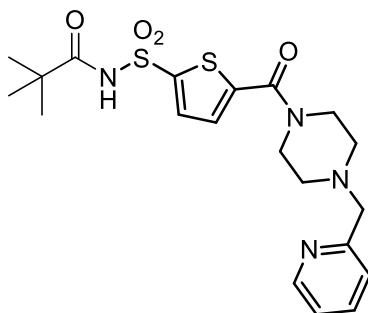


^1H NMR (300 MHz, DMSO- d_6) δ 8.68 (d, J = 4.4 Hz, 1H), 8.27 (s, 1H), 7.94 (t, J = 7.7 Hz, 1H), 7.65 (s, 1H), 7.59 – 7.37 (m, 4H), 4.43 (s, 2H), 3.89 (s, 4H). MS ESI m/z : 367 $[\text{M} + \text{H}]^+$.

General procedure for the synthesis of N-((5-(4-(pyridin-2-ylmethyl)piperazine-1-carbonyl)thiophenyl) sulfonyl)pivalamides (96a-b)

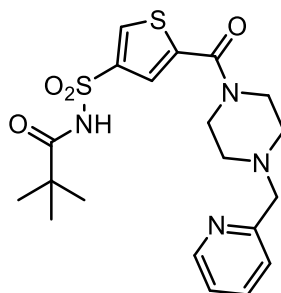
To a stirring suspension of sulfonamide (**95a-b**; 0.12 g, 0.26 mmol) in dry DMC (6.0 mL) were added, in this order, triethylamine (0.05 g, 0.52 mmol) and pivaloyl chloride (0.04 g, 0.31 mmol). The yellow solution thus obtained was stirred at room temperature overnight. After the removal of solvent under reduced pressure, crude was purified by silica gel chromatography (DCM/MeOH) to give the title compounds in 70% yield as a white solid.

N-((5-(4-(pyridin-2-ylmethyl)piperazine-1-carbonyl)thiophen-2-yl)sulfonyl)pivalamide 96a



^1H NMR (300 MHz, DMSO- d_6) δ 11.68 (s, 1H), 8.52 (s, 1H), 8.41 (s, 1H), 7.79 (s, 1H), 7.54 (s, 1H), 7.47 (d, $J = 7.6$ Hz, 1H), 7.29 (s, 1H), 3.65 (s, 6H), 1.05 (d, $J = 1.1$ Hz, 9H). MS ESI m/z : 451 $[\text{M} + \text{H}]^+$.

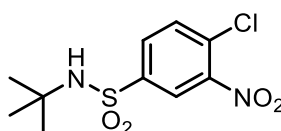
N-((5-(4-(pyridin-2-ylmethyl)piperazine-1-carbonyl)thiophen-3-yl)sulfonyl)pivalamide 96b



^1H NMR (300 MHz, CDCl_3) δ 8.60 – 8.44 (m, 1H), 7.71 (d, $J = 4.0$ Hz, 1H), 7.65 – 7.53 (m, 1H), 7.31 (d, $J = 7.8$ Hz, 1H), 7.18 (s, 1H), 7.12 (dd, $J = 8.2, 4.5$ Hz, 2H), 3.66 (d, $J = 11.8$ Hz, 6H), 1.10 (d, $J = 2.1$ Hz, 9H). MS ESI m/z : 451 $[\text{M} + \text{H}]^+$.

6.3. Procedures to obtain quinoxaline derivative (97)

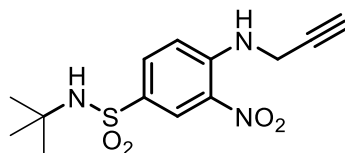
Synthesis of *N*-(*tert*-butyl)-4-chloro-3-nitrobenzenesulfonamide 104



A slurry of 1-chloro-2-nitrobenzene (**103**; 2.00 g, 12.69 mmol) and chlorosulfonic acid (10.0 mL) was stirred at 150 °C for 8 h. The mixture was poured in water (200 mL) and chloride derivative was extracted with EtOAc (3 x 75 mL), washed with brine (10 mL), dried, filtered, and concentrated in vacuo. Crude intermediate was dissolved in dry THF (10.0 mL) then triethylamine (5.13 g, 50.76 mmol) was added. Orange suspension was stirred at room temperature for 1 h, after that solvent was removed under reduced pressure. Crude mixture was dissolved in EtOAc (100 mL) and organic phase was washed with water (3 x 30 mL) brine (30 mL), dried, filtered, and concentrated in vacuo. Pure compound was recovered without further purification in 85% yield as yellow solid.

$^1\text{H NMR}$: (300 MHz, DMSO- d_6) δ 8.47 (d, $J = 1.0$ Hz, 1H), 8.09 (dd, $J = 8.4$, 1.2 Hz, 1H), 8.00 (d, $J = 8.4$ Hz, 1H), 7.94 (s, 1H), 1.13 (s, 9H). MS ESI m/z : 293 $[\text{M} + \text{H}]^+$.

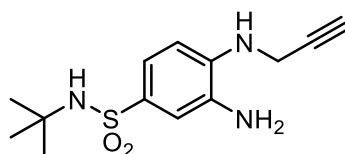
Synthesis of *N*-(*tert*-butyl)-3-nitro-4-(prop-2-yn-1-ylamino)benzenesulfonamide **106**



A 40 mL CEM pressure vessel equipped with stirrer bar was charged with intermediate **104** (1.12 g, 3.81 mmol), propargylamine (**105**; 0.39 mL, 6.10 mmol), triethylamine (0.77 mL, 5.53 mmol) and ethanol (20 mL). The microwave vial was sealed and heated in a CEM Discover microwave synthesizer to 120 °C (measured by the vertically focused IR temperature sensor) for 1.5 h. After cooling to room temperature, solvent was removed and crude was purified by silica gel chromatography (Hex/EtOAc) to give the title compounds in 65% yield as a orange solid.

$^1\text{H NMR}$ (300 MHz, DMSO- d_6) δ 8.72 (t, $J = 5.3$ Hz, 1H), 8.48 (d, $J = 2.0$ Hz, 1H), 7.92 (dd, $J = 9.0$, 1.7 Hz, 1H), 7.54 (s, 1H), 7.25 (d, $J = 9.1$ Hz, 1H), 4.29 (dd, $J = 5.3$, 1.7 Hz, 2H), 3.28 (d, $J = 2.0$ Hz, 1H), 1.11 (s, 9H). MS ESI m/z : 312 $[\text{M} + \text{H}]^+$.

Synthesis of 3-amino-*N*-(*tert*-butyl)-4-(prop-2-yn-1-ylamino)benzenesulfonamide **107**

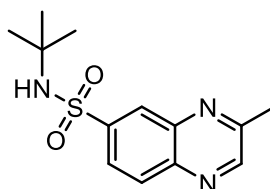


A boiling solution of the intermediate **106** (1.34 g, 4.31 mmol) in ethanol (20 ml) was added to a suspension of iron(II) sulfate heptahydrate (12.0 g, 43.1 mmol) in water (20.0 ml) and 32% ammonium hydroxide (2.0 ml). The reaction mixture was heated under reflux for 4 h while 32% ammonium hydroxide was dropped (20.0

ml). The hot mixture was filtered and the inorganic material was washed with boiling ethanol. The solution was partially evaporated and then extracted with chloroform (3 x 100 ml). The combined organic layers were washed with water followed by a saturated sodium chloride solution, dried over anhydrous sodium sulfate and evaporated to give pure compound **107** without any other purification in 90% yield (yellow solid).

^1H NMR (300 MHz, DMSO- d_6) δ 7.05 – 6.92 (m, 3H), 6.56 (d, J = 8.9 Hz, 1H), 5.55 (t, J = 5.4 Hz, 1H), 4.90 (s, 2H), 3.96 (dd, J = 5.4, 2.0 Hz, 2H), 3.13 (t, J = 2.0 Hz, 1H), 1.07 (s, 9H). MS ESI m/z : 282 $[\text{M} + \text{H}]^+$.

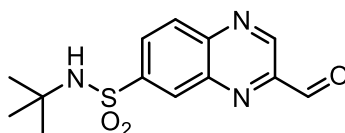
Synthesis of *N*-(*tert*-butyl)-3-methylquinoxaline-6-sulfonamide **108**



Intermediate **107** (0.09 g, 0.32 mmol) and tetrakis(acetonitrile)copper(I) tetrafluoroborate (0.10 g, 0.03 mmol) were suspended in toluene (5.0 mL) in a close vessel and mixture stirred at 90 °C for 11 h. The hot mixture was filtered through Celite and the crude was purified by silica gel chromatography (Hex/EtOAc) to give the title compounds in 67% yield as brown solid.

^1H NMR (300 MHz, DMSO- d_6) δ 8.99 (s, 1H), 8.38 (s, 1H), 8.24 (d, J = 8.9 Hz, 1H), 8.12 (d, J = 8.9 Hz, 1H), 7.88 (br s, 1H), 2.75 (s, 3H), 1.11 (s, 9H). MS ESI m/z : 280 $[\text{M} + \text{H}]^+$.

Synthesis of *N*-(*tert*-butyl)-3-formylquinoxaline-6-sulfonamide **109**

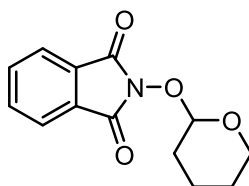


To a hot suspension of selenium dioxide (0.08 g, 0.72 mmol) in dioxane (1.5 mL) was added a solution of compound **108** (0.10 g, 0.36 mmol) in dioxane (0.5 mL). The mixture was refluxed for 4 h. The hot mixture was filtered through Celite

and the crude was purified by silica gel chromatography (Hex/EtOAc) to give the title compounds in 81% yield as reddish solid.

^1H NMR (300 MHz, DMSO- d_6) δ 10.20 (s, 1H), 9.45 (s, 1H), 8.72 – 8.24 (m, 3H), 8.03 (s, 1H), 1.14 (s, 9H). MS ESI m/z : 294 $[\text{M} + \text{H}]^+$.

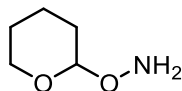
Synthesis of 2-((tetrahydro-2H-pyran-2-yl)oxy)isoindoline-1,3-dione **129b**



To a stirring solution of *N*-hydroxyphthalimide **126** (10.00 g, 61.30 mmol) in DCM/dioxane (250.0 mL, ratio 4:3) were added 3,4-dihydro-2H-pyran (**128**; 6.70 g, 79.69 mmol) and *para*-toluenesulfonic acid monohydrate (0.23 g, 1.23 mmol). The reaction mixture was stirred at room temperature for 3.5 h. Saturated aqueous solution of NaHCO_3 (200 mL) was added to the reaction mixture and organic layer was separated. The aqueous layer was further extracted with DCM (2 x 70 mL) and the combined organic phase was washed with water followed by a saturated sodium chloride solution, dried over anhydrous sodium sulfate and evaporated to give pure compound **129b** as a white solid (99%).

^1H NMR (300 MHz, DMSO- d_6) δ 1.62–1.64 (3H, m), 1.77–1.81 (2H, m), 1.91–1.93 (1H, m), 3.58 (1H, d, $J=10.2$ Hz), 4.28–4.33 (1H, m), 5.32 (1H, s), 7.88 (4H). MS ESI m/z : 118 $[\text{M} + \text{H}]^+$.

Synthesis of *O*-((tetrahydro-2H-pyran-2-yl)hydroxylamine) **123b**

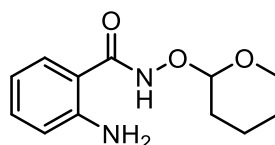


To a stirring solution of compound **129b** (15.00 g, 61.30 mmol) in Et_2O (150.0 mL) was added hydrazine monohydrate (6.20 g, 110.60 mmol). The mixture was stirred at room temperature for 2 h. The white precipitate was removed by filtration and the yellowish solution thus obtained was concentrated under

controlled pressure to afford compound **123b** as a yellow oil (99%), which was used for the next steps without further purification.

^1H NMR (300 MHz, DMSO- d_6) δ 5.99 (2H, s), 4.56–4.57 (1H, m), 3.73–3.80 (1H, m), 3.40–3.46 (1H, m), 1.54–1.65 (2H, m), 1.43–1.44 (4H, m). MS ESI m/z : 248 $[\text{M}+\text{H}]^+$.

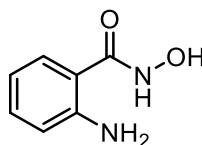
Synthesis of 2-amino-*N*-((tetrahydro-2*H*-pyran-2-yl)oxy)benzamide **124b**



A suspension of isatoic anhydride (**122**; 5.00 g, 30.66 mmol) and hydroxylamine **123b** (7.18 g, 61.32 mmol) in ACN (45.0 mL) was refluxed for 2 h and then concentrated in vacuo. The residue was treated with EtOAc (100.0 mL) and washed with water (3 x 30 mL) saturated sodium chloride solution (30.0 mL). The organic layer was dried over anhydrous sodium sulfate and evaporated. Compound **124b** was collected as white solid (90%) after recrystallization from toluene.

^1H NMR (300 MHz, DMSO- d_6) δ 7.35 (d, $J = 7.9$ Hz, 1H), 7.15 (t, $J = 7.7$ Hz, 1H), 6.70 (d, $J = 8.3$ Hz, 1H), 6.49 (t, $J = 7.5$ Hz, 1H), 6.23 (s, 2H), 4.96 (s, 1H), 1.71 (m, 3H), 1.54 (m, 3H); MS ESI m/z : 237 $[\text{M}+\text{H}]^+$.

Synthesis of 2-amino-*N*-hydroxybenzamide **33**

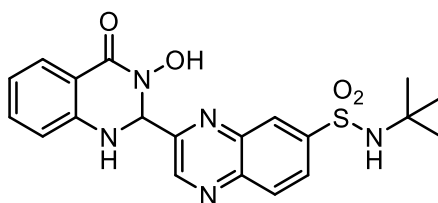


To a solution of compound **127b** (6.00 g, 25.39 mmol) in MeOH (50.0 mL) was added the resin Amberlyst® 15 hydrogen form wet (3.00 g, 1.7 meq/mL by wetted bed volume). The resulting solution was gently stirred at 50 °C for 3.5 h. The resin was removed by filtration and the solvent concentrated under reduced

pressure. Pure compound **33** was collected as white solid (95%) after recrystallization from toluene.

^1H NMR (300 MHz, DMSO- d_6) δ 10.70 (s, 1H), 8.85 (s, 1H), 7.30 (dd, J = 7.9, 1.6 Hz, 1H), 7.12 (ddd, J = 8.5, 7.1, 1.6 Hz, 1H), 6.69 (dd, J = 8.3, 1.2 Hz, 1H), 6.52 – 6.43 (m, 1H), 6.22 (s, 2H); MS ESI m/z : 153 $[\text{M}+\text{H}]^+$.

Synthesis of N-(tert-butyl)-3-hydroxy-4-oxo-2-(quinoxalin-2-yl)-1,2,3,4-tetrahydroquinazoline-7-sulfonamide **97**



To a solution of 2-amino-N-hydroxybenzamide (**33**; 0.10 g, 0.66 mmol) in methanol (5.0 mL) was added quinoxaline (**109**; 0.11 g, 0.73 mmol). The mixture was stirred at room temperature for 2 h, then the solvent was removed in vacuo. The crude was readily purified by silica gel chromatography (DCM/MeOH) to give the title compound as reddish solid.

^1H NMR (300 MHz, DMSO- d_6) δ 9.97 (s, 1H), 9.24 (d, J = 1.5 Hz, 1H), 8.40 (s, 1H), 8.33 (d, J = 8.8 Hz, 1H), 8.22 (d, J = 8.9 Hz, 1H), 7.92 (s, 1H), 7.74 (d, J = 7.9 Hz, 1H), 7.67 (s, 1H), 7.27 (t, J = 7.2 Hz, 1H), 6.77 (t, J = 7.6 Hz, 1H), 6.70 (d, J = 8.2 Hz, 1H), 6.28 (s, 1H), 1.11 (s, 9H). MS ESI m/z : 428 $[\text{M}+\text{H}]^+$.

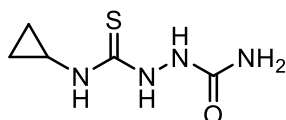
6.4. Procedures to obtain triazole derivatives

General procedure for the synthesis of thiobiureas **82a-e**

To a suspension of sodium acetate (0.22 g, 2.63 mmol) and semicarbazide (0.29 g, 2.63 mmol) in acetonitrile (10.0 mL) was added the proper isothiocyanate **81a-e** (2.63 mmol), and the reaction mixture was stirred for 24 h. The solvent was removed by rotary evaporation, and the resulting residue was dissolved in 2 M NaOH aqueous solution (30 mL) and filtered through activated charcoal to remove any unreacted isothiocyanate. The filtrate was acidified with 1 N HCl (40 mL). The

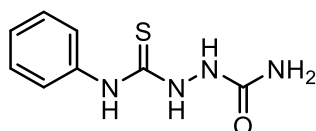
precipitate was collected and washed with water (3 × 20 mL) and hexanes (2 × 20 mL) to afford the title compound as a white solid (95%).

2-(cyclopropylcarbamothioyl)hydrazine-1-carboxamide 82a



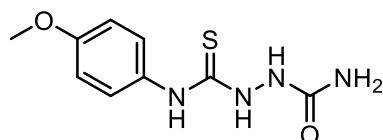
¹H NMR (300 MHz, DMSO-d₆) δ 9.07 (s, 1H), 7.89 (s, 1H), 7.76 (s, 1H), 5.93 (s, 2H), 3.00 (s, 1H), 1.39 – 0.28 (m, 4H). MS ESI m/z: 175 [M+H]⁺.

2-(phenylcarbamothioyl)hydrazine-1-carboxamide 82b



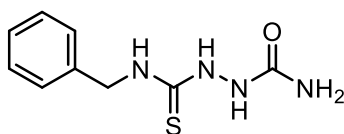
¹H NMR (300 MHz, DMSO-d₆) δ 9.63 (s, 1H), 9.38 (s, 1H), 8.01 (s, 1H), 7.52 (d, J = 7.3 Hz, 1H), 7.31 (t, J = 7.8 Hz, 2H), 7.13 (t, J = 7.3 Hz, 1H), 6.04 (s, 2H). MS ESI m/z: 211 [M+H]⁺.

2-((4-methoxyphenyl)carbamothioyl)hydrazine-1-carboxamide 82c



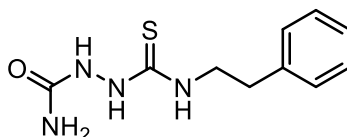
¹H NMR (300 MHz, DMSO-d₆) δ 12.61 (s, 1H), 7.20 (d, J = 8.5 Hz, 2H), 7.02 (d, J = 8.9 Hz, 2H), 3.80 (s, 3H). MS ESI m/z: 241 [M+H]⁺.

2-(benzylcarbamothioyl)hydrazine-1-carboxamide 82d



¹H NMR (300 MHz, DMSO-d₆) δ 9.54 (s, 1H), 9.38 (s, 1H), 7.37 – 7.24 (m, 5H), 7.22 (s, 1H), 6.22 (s, 2H), 4.75 (s, 2H). MS ESI m/z: 225 [M+H]⁺.

2-(phenethylcarbamothioyl)hydrazine-1-carboxamide 82e

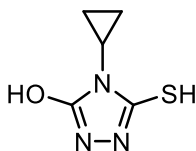


^1H NMR (300 MHz, DMSO- d_6) δ 7.83 (s, 1H), 7.58 (s, 1H), 7.21 (d, J = 18.5 Hz, 6H), 6.22 (s, 2H), 3.77 (t, J = 7.6 Hz, 2H), 2.77 (d, J = 7.6 Hz, 2H). MS ESI m/z : 239 $[\text{M}+\text{H}]^+$.

General procedure for the synthesis of 3-hydroxy-5-thiol derivatives 78a-e

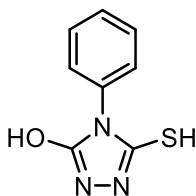
The proper 2-thiobiurea compound **82a-e** (1.88 mmol) in 2 M NaOH aqueous solution (20.0 mL) was stirred at reflux for 6 h. The reaction mixture was allowed to cool to room temperature and then acidified with 1 N HCl. The resulting precipitate was collected by filtration and washed with water (3×20 mL), hexanes (2×20 mL), 1:1 hexanes/ diethyl ether (20 mL) successively and dried in vacuo to afford the title compound as a white solid (95%).

4-cyclopropyl-5-mercapto-4H-1,2,4-triazol-3-ol 78a (EML615)



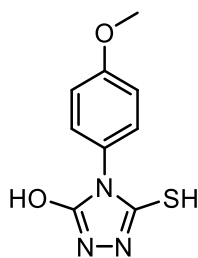
^1H NMR (300 MHz, DMSO- d_6) δ 2.77 – 2.15 (m, 1H), 1.19 – 0.65 (m, 2H), 0.65 – 0.34 (m, 2H). MS ESI m/z : 157 $[\text{M}+\text{H}]^+$.

5-mercapto-4-phenyl-4H-1,2,4-triazol-3-ol 78b



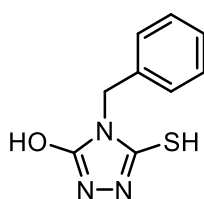
^1H NMR (300 MHz, DMSO- d_6) δ 12.77 (s, 2H), 8.01 – 6.47 (m, 5H). MS ESI m/z : 194 $[\text{M}+\text{H}]^+$.

5-mercapto-4-(4-methoxyphenyl)-4H-1,2,4-triazol-3-ol 78c



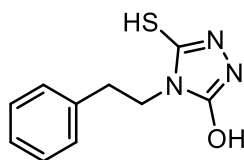
^1H NMR (300 MHz, DMSO- d_6) δ 7.21 (d, J = 8.5 Hz, 2H), 7.04 (d, J = 8.9 Hz, 2H), 3.82 (s, 3H). MS ESI m/z : 224 $[\text{M}+\text{H}]^+$.

4-benzyl-5-mercapto-4H-1,2,4-triazol-3-ol 78d



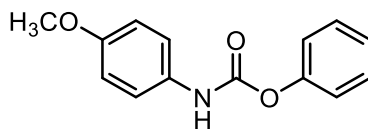
^1H NMR (300 MHz, DMSO- d_6) δ 13.07 (s, 2H), 7.94 – 6.83 (m, 5H), 4.85 (s, 2H). MS ESI m/z : 208 $[\text{M}+\text{H}]^+$.

5-mercapto-4-phenethyl-4H-1,2,4-triazol-3-ol 78e



^1H NMR (300 MHz, DMSO- d_6) δ 13.03 (s, 2H), 7.74 – 6.86 (m, 5H), 3.85 (t, J = 7.8 Hz, 2H), 2.93 (t, J = 7.8 Hz, 2H). MS ESI m/z : 222 $[\text{M}+\text{H}]^+$.

Synthesis of phenyl (4-methoxyphenyl)carbamate 85

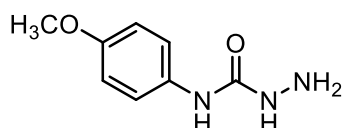


Phenyl chloroformate (1.72 g, 10.98 mmol) was added dropwise to a stirred mixture of *p*-ethoxyaniline (1.37 g, 9.99 mmol), pyridine (0.85 g, 10.98 mmol) and EtOAc (20.0 mL) at 0 °C. The mixture was stirred for 3 h at room temperature, then washed with water (3 x 20 mL), dried over anhydrous Na_2SO_4 , and filtrated.

The solvent was evaporated under reduced pressure and the deposited solid were collected and washed with hexane to give **85** as yellow solid (55%). The product can be used directly in the next step without further purification.

^1H NMR (300 MHz, DMSO- d_6) δ 10.06 (s, 1H), 7.39-7.44 (m, 4H), 7.19-7.26 (m, 3H), 6.90 (d, 2H, $J = 9.0$ Hz), 3.71 (s, 3H). MS ESI m/z : 244 $[\text{M}+\text{H}]^+$.

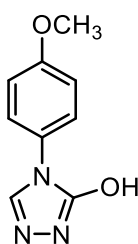
Synthesis of N-(4-methoxyphenyl)hydrazinecarboxamide **86**



A mixture of compound **85** (1.80 g, 7.41 mol), 33% hydrazine hydrate (0.74 mL) and dimethoxyethane (12.0 mL) was stirred for 24 h. The solvent was evaporated under reduced pressure and the residue was washed with EtOAc. The title compound was collected as a pink solid (90%) after recrystallization from ethanol.

^1H NMR (300 MHz, DMSO- d_6) δ 8.45 (s, 1H), 7.41 (d, 2H, $J = 8.7$ Hz), 7.29 (s, 1H), 8.82 (d, 2H, $J = 8.7$ Hz), 4.31 (s, 2H), 3.71 (s, 3H). MS ESI m/z : 182 $[\text{M}+\text{H}]^+$.

Synthesis of 4-(4-methoxyphenyl)-4H-1,2,4-triazol-3-ol **79**

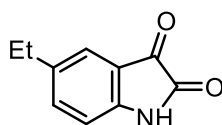


A mixture of compound **86** (7.56 g, 0.05 mol), formamidine acetate (22.0 g, 0.2 mol) and DMF (250.0 mL) was stirred at room temperature for 30 min. AcOH (15 mL) was added, and the resulting mixture was heated for 8 h at 80 °C. The solvent was evaporated under reduced pressure and the residue was poured into the ice water. After filtration, the crude was purified by silica gel chromatography (DCM/EtOAc) to give the title compounds **79** as pale yellow solid (60%).

^1H NMR (300 MHz, DMSO- d_6) δ 9.69 (s, 1H), 7.73 (d, $J = 7.5$ Hz, 1H), 7.10 (d, $J = 7.5$ Hz, 1H), 3.79 (s, 3H). MS ESI m/z : 192 $[\text{M}+\text{H}]^+$.

6.5. Procedures to obtain *N*-(5-ethyl-1-(2-morpholinoethyl)-3-oxoindolin-2-yl)acetamide

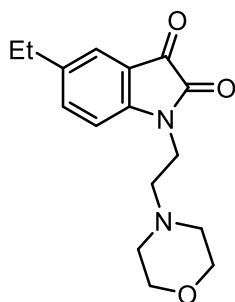
Synthesis of 5-ethylindoline-2,3-dione **89**



To a 60 mL aqueous solution of chloral hydrate (3.60 g, 22.00 mmol) were added 52.00 g sodium sulfate, 4-ethylaniline (2.42 g, 20.00 mmol), 2.0 mL HCl 1 N, and a 20.0 mL aqueous solution of hydroxylamine hydrochloride (4.40 g, 63.00 mmol), successively. This solution was gradually heated, and refluxed for 1 min. Upon cool, the precipitate was filtered. The dark brown solid was added to 20 mL sulfuric acid at 50 °C in small portions, and heated at 80 °C for 10 min. The resulting solution was cooled to room temperature, and dropwise added to ice, and the precipitate was filtrated to give title compound as orange solids in 65% yield.

^1H NMR (300 MHz, CDCl_3) δ 7.81 (s, 1H), 7.46 (s, 1H), 7.38-7.41 (d, 1H), 6.81-6.83 (d, 1H), 2.59-2.67 (q, 2H), 1.20-1.25 (t, 3H). MS ESI m/z : 176 $[\text{M}+\text{H}]^+$.

Synthesis of 5-ethyl-1-(2-morpholinoethyl)indoline-2,3-dione **91**

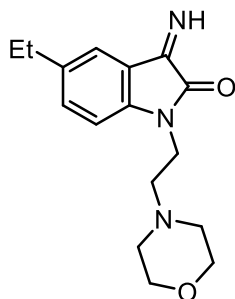


To a stirring suspension of compound **89** (0.22 g, 1.25 mmol) and potassium carbonate (0.22 g, 1.62 mmol) in dry DMF (5.0 mL) was added 2-morpholinoethyl methanesulfonate (**90**; 0.31 g, 1.38 mmol) in dry THF solution (12.0 mL). The

mixture was heated at 70 °C overnight and then concentrated in vacuo. The residue was treated with EtOAc (100 mL) and washed with saturated aqueous solution of NaHCO₃ (3 x 30 mL) saturated sodium chloride solution (30 mL). The organic layer was dried over anhydrous sodium sulfate and evaporated. The crude was readily purified by silica gel chromatography (DCM/MeOH) to give the title compounds in 70% yield as a orange oil.

¹H NMR (300 MHz, CDCl₃) δ 7.39 (d, J = 8.2 Hz, 2H), 6.83 (dd, J = 7.8, 0.9 Hz, 1H), 3.81 (t, J = 6.6 Hz, 2H), 3.61 (d, J = 4.7 Hz, 4H), 2.59 (td, J = 7.5, 7.0, 3.8 Hz, 4H), 2.52 – 2.42 (m, 4H), 1.20 (t, J = 7.6 Hz, 3H). MS ESI m/z: 289 [M+H]⁺.

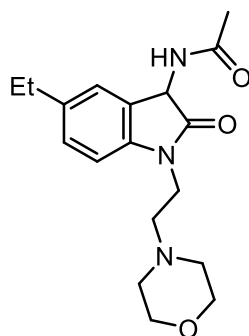
Synthesis of 5-ethyl-3-imino-1-(2-morpholinoethyl)indolin-2-one **92**



Compound **91** (0.25 g, 0.83 mmol) and formic acid (0.08 mmol) were stirred in a saturated solution of ammonia in methanol (5.0 mL) at room temperature for 3 h. The mixture was concentrated in vacuo to give the title compound in 80% yield as yellowish oil. Due to its poor stability, the product was used directly in the next step without further purification.

¹H NMR (300 MHz, CDCl₃) δ 7.66 (d, J = 1.8 Hz, 1H), 7.32 – 7.21 (m, 1H), 6.87 (t, J = 8.6 Hz, 1H), 3.79 (t, J = 6.9 Hz, 2H), 3.73 – 3.58 (m, 2H), 3.48 (s, 2H), 2.65 (q, J = 7.4 Hz, 2H), 2.49 – 2.33 (m, 4H), 1.95 – 1.75 (m, 2H), 1.56 – 1.06 (m, 3H). MS ESI m/z: 288 [M+H]⁺.

Synthesis of N-(5-ethyl-1-(2-morpholinoethyl)-2-oxoindolin-3-yl)acetamide **80**



A solution of compound **92** (0.80 g, 2.78 mmol) in THF (5.0 mL) was prepared and cooled to $-78\text{ }^{\circ}\text{C}$, then sodium cyanoborohydride (0.35 g, 5.56 mmol) was added. The mixture was stirred at $-78\text{ }^{\circ}\text{C}$ for 6 h, then acetic anhydride was added. The mixture was allowed to slowly warm to ambient temperature while stirring overnight. After the removal of solvent under reduced pressure, the resulting residue was dissolved in DCM and washed with saturated aqueous solution of NaHCO_3 (3 x 30 mL) and brine (30 mL). The organic layer was dried over anhydrous sodium sulfate and evaporated. Final purification by preparative HPLC allowed us to obtain the title compound in 20% yield as white solid.

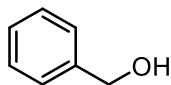
^1H NMR (300 MHz, DMSO-d_6) δ 9.57 (s, 1H), 8.94 (d, $J = 8.0$ Hz, 1H), 7.17 (d, $J = 8.2$ Hz, 1H), 7.06 (d, $J = 7.4$ Hz, 1H), 5.08 (d, $J = 7.7$ Hz, 1H), 4.24 – 3.82 (m, 4H), 3.77 – 3.48 (m, 4H), 3.48 – 3.27 (m, 2H), 3.27 – 3.02 (m, 2H), 2.57 (q, 2H), 1.89 (s, 3H), 1.15 (t, $J = 7.6$ Hz, 3H). MS ESI m/z : 332 $[\text{M}+\text{H}]^+$.

6.6. Procedure to obtain 3-hydroxy-2,3-dihydroquinazolin-4(1H)-one derivatives

General procedure for the synthesis of alcohol 67a-76a

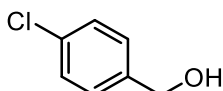
A solution of proper aldehyde (**54-64**; 9.42 mmol) in MeOH (25.0 mL) was prepared and cooled to $0\text{ }^{\circ}\text{C}$, then sodium borohydride (0.72 g, 18.84 mmol) was added portionwise. The mixture was allowed to slowly warm to room temperature while stirring for 30 min. After the removal of solvent under reduced pressure, the resulting residue was dissolved in DCM (50 mL) and washed with water (3 x 15 mL) and brine (15 mL). The organic layer was dried over anhydrous sodium sulfate and evaporated to afford the title compound as colorless oil (95-99%).

Phenylmethanol 67a



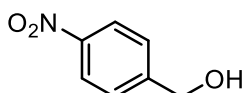
Colorless oil, 95% yield. $^1\text{H-NMR}$ (300 MHz, CDCl_3) δ 7.26 (m, 5H) 4.51 (s, 2H) 3.18 (s, 1H)¹⁴². MS ESI m/z : 109 $[\text{M}+\text{H}]^+$.

(4-chlorophenyl)methanol 68a



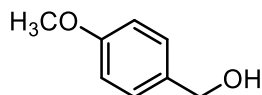
White solid, 98% yield. $^1\text{H-NMR}$ (300 MHz, CDCl_3) δ 7.26–7.32 (m, 4H), 4.67 (s, 2H)¹⁴². MS ESI m/z : 143 $[\text{M}+\text{H}]^+$.

(4-nitrophenyl)methanol 69a



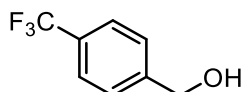
Yellow solid, 95% yield. $^1\text{H-NMR}$ (300 MHz, CDCl_3) δ 8.22 (d, $J = 8.4$ Hz, 2H), 7.53 (d, $J = 8.4$ Hz, 2H), 4.84 (s, 2H)¹⁴². MS ESI m/z : 154 $[\text{M}+\text{H}]^+$.

(4-methoxyphenyl)methanol 70a



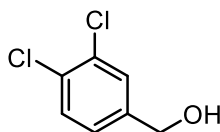
Colorless oil, 98% yield. $^1\text{H-NMR}$ (300 MHz, CDCl_3) δ 7.23 (d, $J = 8.5$ Hz, 2H), 6.86 (d, $J = 8.5$ Hz, 2H), 3.77 (s, 3H), 4.53 (s, 2H)¹⁴². MS ESI m/z : 139 $[\text{M}+\text{H}]^+$.

(4-(trifluoromethyl)phenyl)methanol 71a



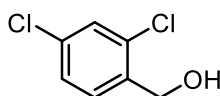
Colorless oil, 98% yield. $^1\text{H-NMR}$ (300 MHz, CDCl_3) δ 7.60 (d, $J = 8.4$ Hz, 2H) 7.46 (d, $J = 8.4$ Hz, 2H), 4.75 (s, 2H)¹⁴². MS ESI m/z : 177 $[\text{M}+\text{H}]^+$.

(3,4-dichlorophenyl)methanol 72a



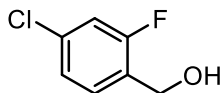
White solid, 95% yield. $^1\text{H-NMR}$ (300 MHz, CDCl_3) δ 7.42 (d, $J = 1.9$ Hz 1H), 7.39 (d, $J = 8.3$ Hz 1H) 7.15 (td, $J = 8.3$ 1.9 0.6 Hz 1H), 4.61 (d, $J = 0.9$ Hz, 2H)¹⁴². MS ESI m/z : 177 $[\text{M}+\text{H}]^+$.

(2,4-dichlorophenyl)methanol 73a



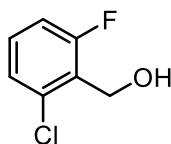
White solid, 99% yield. $^1\text{H-NMR}$ (300 MHz, CDCl_3) δ 7.38 (d, $J = 8.1$ Hz, 1H), 7.36 (d, $J = 2.1$ Hz, 1H), 7.25 (dd, $J = 8.1$ Hz $J = 2.1$ Hz, 1H), 4.71 (s, 2H), 2.31 (s, 1H)¹⁴². MS ESI m/z : 177 $[\text{M}+\text{H}]^+$.

(4-chloro-2-fluorophenyl)methanol 74a



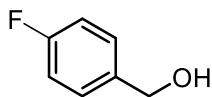
White solid, 98% yield. $^1\text{H-NMR}$ (300 MHz, CDCl_3) δ 7.38 (t, $J = 8.1$ Hz, 1H), 7.15 (dd, $J = 8.2$, 2.1 Hz, 1H), 7.09 (dd, $J = 9.8$, 2.0 Hz, 1H), 4.73 (d, $J = 4.2$ Hz, 2H), 1.76 (d, $J = 6.7$ Hz, 1H). MS ESI m/z : 161 $[\text{M}+\text{H}]^+$.

(2-chloro-6-fluorophenyl)methanol 75a



Yellowish oil, 98% yield. $^1\text{H-NMR}$ (300 MHz, CDCl_3) δ 7.45 – 6.94 (m, 1H), 4.90 (s, 1H), 2.12 (s, 1H)¹⁴². MS ESI m/z : 161 $[\text{M}+\text{H}]^+$.

(4-fluorophenyl)methanol 76a



White solid, 97% yield. $^1\text{H-NMR}$ (300 MHz, CDCl_3) δ 4.65 (s, 2H), 7.00–7.04 (m, 2H), 7.29–7.33 (m, 2H)¹⁴². MS ESI m/z : 127 $[\text{M}+\text{H}]^+$.

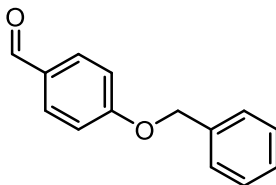
General procedure for the synthesis of methanesulfonate derivatives 67b-76b

A solution of proper alcohol (**67a-76a**; 9.42 mmol) in dry DCM (25.0 mL) was prepared and cooled to 0 °C, then triethylamine (2.6 mL, 18.84 mmol) and mesyl chloride (0.9 mL, 11.30 mmol) were added respectively. The mixture was allowed to slowly warm to room temperature while stirring for 3.5 h, then was washed with water (3 x 10 mL) and brine (10 mL). The organic layer was dried over anhydrous sodium sulfate and evaporated to afford the title compound as colorless oil (95-99%) which was used for the next steps without further purification.

General procedure for the synthesis of aldehydes 38-49

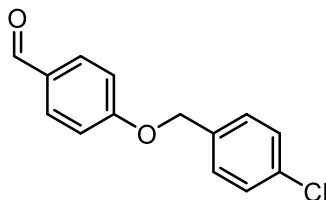
To stirring suspension of proper hydroxybenzaldehyde (**55**, **65-66**; 0.50 g, 4.10 mmol) and potassium carbonate (1.13 g, 8.20 mmol) in acetone (20.0 mL) was added a solution of proper methanesulfonate derivative (**67b-76b**; 4.91 mmol) in acetone (1 M). The mixture was refluxed for 1 h, then the solvent was removed in vacuo, the residue was dissolved in DCM (50 mL) and washed with water (3 x 15 mL) and brine (15 mL). The organic layer was dried over anhydrous sodium sulfate and evaporated. The crude was readily purified by silica gel chromatography (Hexane/EtOAc) to give the title compound.

4-(benzyloxy)benzaldehyde 38



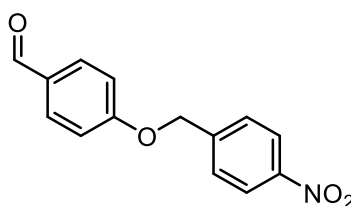
White solid, 77% yield. $^1\text{H-NMR}$ (300 MHz, $\text{DMSO-}d_6$) δ 9.87 (s, 1H), 7.87 (d, $J = 8.8$ Hz, 2H), 7.50-7.34 (m, 5H), 7.21 (d, $J = 8.8$ Hz, 2H), 5.23 (s, 2H)¹⁴³. MS ESI m/z : 213 $[\text{M}+\text{H}]^+$.

4-((4-chlorobenzyl)oxy)benzaldehyde 39



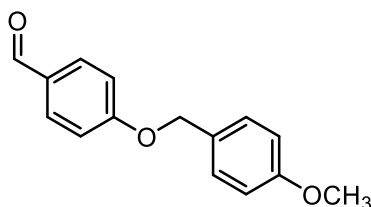
White solid, 85% yield. $^1\text{H-NMR}$ (300 MHz, $\text{DMSO-}d_6$) δ 9.87 (s, 1H), 7.88 (d, $J = 8.6$ Hz, 2H), 7.56 – 7.43 (m, 4H), 7.20 (d, $J = 8.4$ Hz, 2H), 5.24 (s, 2H)¹⁴⁴. MS ESI m/z : 247 $[\text{M}+\text{H}]^+$.

4-((4-nitrobenzyl)oxy)benzaldehyde 40



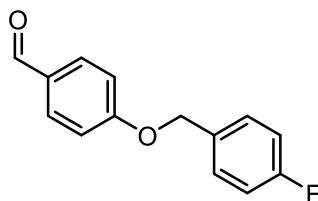
Yellow solid, 79% yield. $^1\text{H-NMR}$ (300 MHz, $\text{DMSO-}d_6$) δ 9.88 (s, 1H), 8.28 (d, $J = 8.5$ Hz, 2H), 7.89 (d, $J = 8.6$ Hz, 2H), 7.74 (d, $J = 8.4$ Hz, 2H), 7.23 (d, $J = 8.6$ Hz, 2H), 5.42 (s, 2H)¹⁴⁴. MS ESI m/z : 258 $[\text{M}+\text{H}]^+$.

4-((4-methoxybenzyl)oxy)benzaldehyde 41



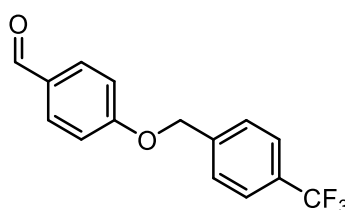
White solid, 84% yield. $^1\text{H-NMR}$ (300 MHz, $\text{DMSO-}d_6$) δ 9.86 (s, 1H), 7.86 (d, $J = 8.7$ Hz, 1H), 7.40 (d, $J = 8.6$ Hz, 1H), 7.19 (d, $J = 8.7$ Hz, 1H), 6.96 (d, $J = 8.4$ Hz, 1H), 5.14 (s, 1H), 3.76 (s, 1H)¹⁴⁵. MS ESI m/z : 243 $[\text{M}+\text{H}]^+$.

4-((4-fluorobenzyl)oxy)benzaldehyde 42



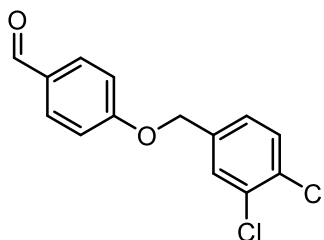
White solid, 81% yield. $^1\text{H-NMR}$ (300 MHz, CDCl_3) δ 9.89 (s, 1H), 7.84 (d, $J = 8.8$ Hz, 2H), 7.43 (d, $J = 8.8$ Hz, 1H), 7.39 (d, $J = 8.4$ Hz, 1H), 7.13-7.04 (m, 4H), 5.10 (s, 2H)¹⁴⁶. MS ESI m/z : 231 $[\text{M}+\text{H}]^+$.

4-((4-(trifluoromethyl)benzyl)oxy)benzaldehyde 43



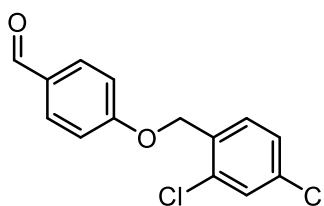
White solid, 88% yield. $^1\text{H-NMR}$ (300 MHz, CDCl_3) δ 9.90 (s, 1H), 7.86 (dd, $J = 7.0$ e 1.8 Hz, 2H), 7.67 (d, $J = 8.8$ Hz, 2H), 7.55 (d, $J = 8.0$ Hz, 2H), 7.07 (dd, $J = 6.6$ e 1.8 Hz, 2H), 5.21 (s, 2H)¹⁴⁶. MS ESI m/z : 281 $[\text{M}+\text{H}]^+$.

4-((3,4-dichlorobenzyl)oxy)benzaldehyde 44



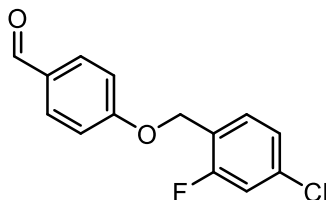
White solid, 77% yield. $^1\text{H-NMR}$ (300 MHz, $\text{DMSO-}d_6$) δ 9.88 (s, 1H), 7.88 (d, $J = 8.4$ Hz, 2H), 7.76 (s, 1H), 7.68 (d, $J = 8.3$ Hz, 2H), 7.49 – 7.44 (m, 1H), 7.21 (d, $J = 8.4$ Hz, 2H), 5.25 (s, 2H)¹⁴⁷. MS ESI m/z : 282 $[\text{M}+\text{H}]^+$.

4-((2,4-dichlorobenzyl)oxy)benzaldehyde 45



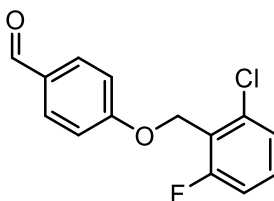
White solid, 75% yield. $^1\text{H-NMR}$ (300 MHz, CDCl_3) δ 9.89 (s, 1H), 7.85 (d, 2H, $J = 8.6$ Hz), 7.42–7.48 (m, 2H), 7.26–7.30 (m, 1H), 7.07 (d, 2H, $J = 8.6$ Hz), 5.19 (s, 2H)¹⁴⁸. MS ESI m/z : 282 $[\text{M}+\text{H}]^+$.

4-((4-chloro-2-fluorobenzyl)oxy)benzaldehyde 46



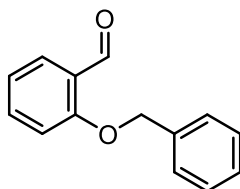
White solid, 84% yield. $^1\text{H-NMR}$ (300 MHz, $\text{DMSO-}d_6$) δ 9.89 (d, $J = 1.1$ Hz, 1H), 7.92 – 7.85 (m, 2H), 7.62 (t, $J = 8.1$ Hz, 1H), 7.55 – 7.49 (m, 1H), 7.39 – 7.33 (m, 1H), 7.26 – 7.21 (m, 2H), 5.26 (s, 2H). MS ESI m/z : 265 $[\text{M}+\text{H}]^+$.

4-((2-chloro-6-fluorobenzyl)oxy)benzaldehyde 47



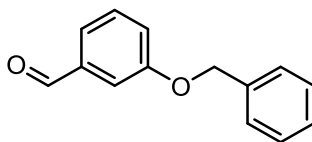
White solid, 75% yield. $^1\text{H-NMR}$ (300 MHz, $\text{DMSO-}d_6$) δ 9.90 (s, 1H), 7.90 (d, $J = 8.8$ Hz, 2H), 7.59 – 7.30 (m, 3H), 7.26 (d, $J = 8.4$ Hz, 2H), 5.28 (d, $J = 1.9$ Hz, 2H); MS ESI m/z : 265 $[\text{M}+\text{H}]^+$.

2-(benzyloxy)benzaldehyde 48



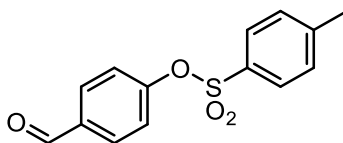
White solid, 79% yield. $^1\text{H-NMR}$ (300 MHz, CDCl_3) δ 10.55 (s, 1 H), 7.86–6.99 (m, 9 H), 5.17 (s, 2 H)¹⁴⁹. MS ESI m/z : 213 $[\text{M}+\text{H}]^+$.

3-(benzyloxy)benzaldehyde 49



White solid, 83% yield. $^1\text{H-NMR}$ (300 MHz, CDCl_3) δ 9.98 (s, 1H), 7.34–7.49 (m, 8H), 7.23–7.32 (m, 1H), 5.13 (s, 2H)¹⁵⁰. MS ESI m/z : 213 $[\text{M}+\text{H}]^+$.

Synthesis of 4-formylphenyl 4-methylbenzenesulfonate **50**



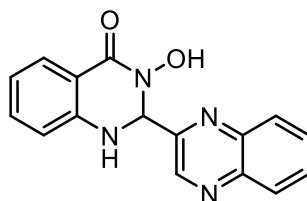
A suspension of 4-hydroxybenzaldehyde (0.50 g, 4.10 mmol) in dry DCM (25.0 mL) was prepared and cooled to 0 °C, then triethylamine (1.1 mL, 8.20 mmol) and tosyl chloride (**77**; 0.86 g, 4.51 mmol) were added respectively. The mixture was allowed to slowly warm to room temperature while stirring for 1 h, then was washed with water (3 x 10 mL) and brine (10 mL). The organic layer was dried over anhydrous sodium sulfate and evaporated. The crude was purified by silica gel chromatography (Hexane/EtOAc) to give the title compounds as white solid in 96% yield.

$^1\text{H-NMR}$ (300 MHz, $\text{DMSO-}d_6$) δ 9.97 (s, 1H), 7.98 – 7.88 (m, 2H), 7.77 (d, $J = 8.4$ Hz, 2H), 7.48 (d, $J = 8.0$ Hz, 2H), 7.30 – 7.24 (m, 2H), 2.42 (s, 3H)¹⁵¹. MS ESI m/z : 277 $[\text{M}+\text{H}]^+$.

General procedure for the synthesis of 3-hydroxy-2,3-dihydroquinazolin-4(1H)-one derivatives

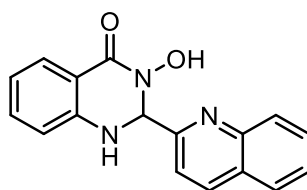
To a solution of 2-amino-N-hydroxybenzamide (**33**; 0.10 g, 0.66 mmol) in methanol (5.0 mL) was added the proper aldehyde. The mixture was stirred at room temperature for 1-24 h, then the solvent was removed in vacuo. The crude was readily purified by silica gel chromatography (DCM/MeOH) to give the title compound as reddish solid.

3-hydroxy-2-(quinoxalin-2-yl)-2,3-dihydroquinazolin-4(1H)-one 1
(EML586)



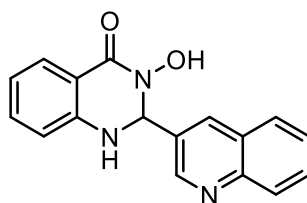
Yield: 84%. ^1H NMR (400 MHz, DMSO- d_6) δ 9.94 (s, 1H), 9.11 (s, 1H), 8.18 – 8.10 (m, 1H), 8.09 – 7.99 (m, 1H), 7.93 – 7.85 (m, 2H), 7.74 (dd, J = 7.8, 1.6 Hz, 1H), 7.66 (d, J = 2.1 Hz, 1H), 7.27 (ddd, J = 8.1, 7.2, 1.6 Hz, 1H), 6.77 (ddd, J = 8.0, 7.2, 1.0 Hz, 1H), 6.70 (dd, J = 8.2, 1.0 Hz, 1H), 6.21 (d, J = 2.1 Hz, 1H). ^{13}C NMR (101 MHz, DMSO) δ 163.22, 153.12, 145.67, 144.42, 141.87, 140.46, 133.51, 130.69, 130.56, 128.99, 128.89, 127.19, 117.85, 114.26, 113.98, 75.11. MS ESI m/z : 293 $[\text{M}+\text{H}]^+$.

3-hydroxy-2-(quinolin-2-yl)-2,3-dihydroquinazolin-4(1H)-one 2 (EML621)



Yield: 87%. ^1H NMR (400 MHz, DMSO- d_6) δ 9.84 (s, 1H), 8.41 (d, J = 8.5 Hz, 1H), 7.99 (ddd, J = 8.0, 2.0, 1.1 Hz, 2H), 7.78 (ddd, J = 8.4, 6.9, 1.4 Hz, 1H), 7.71 (dd, J = 7.8, 1.6 Hz, 1H), 7.69 – 7.54 (m, 3H), 7.23 (ddd, J = 7.8, 7.2, 1.6 Hz, 1H), 6.72 (td, J = 7.5, 1.0 Hz, 1H), 6.68 (dd, J = 8.2, 1.0 Hz, 1H), 6.06 (d, J = 2.1 Hz, 1H). ^{13}C NMR (101 MHz, DMSO) δ 162.76, 158.79, 146.50, 145.79, 137.22, 133.36, 129.87, 128.76, 127.87, 127.72, 127.09, 126.87, 118.81, 117.40, 114.05, 113.72, 76.77. MS ESI m/z : 292 $[\text{M}+\text{H}]^+$.

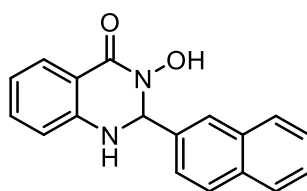
3-hydroxy-2-(quinolin-3-yl)-2,3-dihydroquinazolin-4(1H)-one 3 (EML622)



Yield: 85%. ^1H NMR (400 MHz, DMSO- d_6) δ 9.85 (s, 1H), 9.02 (d, J = 2.3 Hz, 1H), 8.37 (dd, J = 2.3, 0.7 Hz, 1H), 8.08 – 7.97 (m, 2H), 7.79 (ddd, J = 8.4, 6.9,

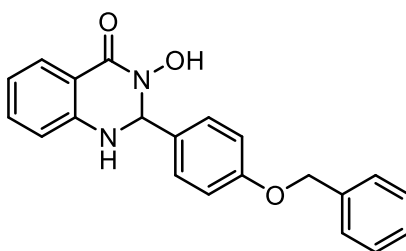
1.5 Hz, 1H), 7.74 – 7.68 (m, 1H), 7.64 (ddd, J = 8.1, 6.9, 1.3 Hz, 1H), 7.57 (d, J = 1.8 Hz, 1H), 7.30 (ddd, J = 8.0, 7.3, 1.6 Hz, 1H), 6.85 – 6.66 (m, 2H), 6.21 (d, J = 1.7 Hz, 1H). ¹³C NMR (101 MHz, DMSO) δ 163.32, 149.97, 147.61, 146.19, 134.39, 133.58, 132.30, 129.92, 128.66, 128.24, 127.32, 127.02, 126.98, 117.78, 114.28, 113.79, 73.46. MS ESI m/z: 292 [M+H]⁺.

3-hydroxy-2-(naphthalen-2-yl)-2,3-dihydroquinazolin-4(1H)-one 4
(EML623)



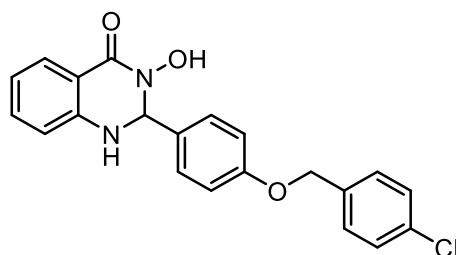
Yield: 90%. ¹H NMR (400 MHz, DMSO-d₆) δ 9.75 (s, 1H), 8.01 – 7.78 (m, 4H), 7.69 (dd, J = 8.0, 1.6 Hz, 1H), 7.63 (dd, J = 8.6, 1.7 Hz, 1H), 7.59 – 7.51 (m, 2H), 7.49 (d, J = 1.8 Hz, 1H), 7.26 (ddd, J = 8.2, 7.2, 1.6 Hz, 1H), 6.81 – 6.61 (m, 2H), 6.09 (d, J = 1.8 Hz, 1H). ¹³C NMR (101 MHz, DMSO) δ 162.80, 146.19, 137.22, 133.36, 133.03, 132.38, 127.98, 127.91, 127.52, 127.18, 126.37, 126.27, 124.69, 117.34, 114.07, 113.68, 75.15. MS ESI m/z: 291 [M+H]⁺.

2-(4-(benzyloxy)phenyl)-3-hydroxy-2,3-dihydroquinazolin-4(1H)-one 5
(EML624)



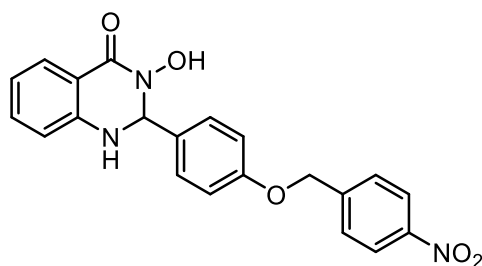
Yield: 77%. ¹H NMR (400 MHz, DMSO-d₆) δ 9.65 (s, 1H), 7.64 (dd, J = 8.1, 1.6 Hz, 1H), 7.46 – 7.29 (m, 8H), 7.27 – 7.14 (m, 1H), 7.01 – 6.91 (m, 2H), 6.75 – 6.62 (m, 2H), 5.84 (d, J = 1.8 Hz, 1H), 5.10 (s, 2H). ¹³C NMR (101 MHz, DMSO) δ 162.68, 158.50, 146.21, 136.99, 133.23, 132.13, 128.40, 128.26, 127.78, 127.57, 127.09, 117.19, 114.41, 114.04, 113.70, 74.48, 69.16. MS ESI m/z: 347 [M+H]⁺.

2-(4-((4-chlorobenzyl)oxy)phenyl)-3-hydroxy-2,3-dihydroquinazolin-4(1H)-one 6 (EML647)



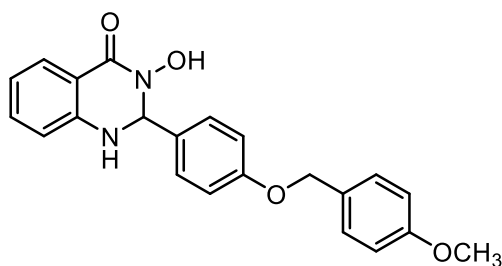
Yield: 81%. ^1H NMR (400 MHz, DMSO- d_6) δ 9.65 (s, 1H), 7.64 (dd, J = 8.0, 1.6 Hz, 1H), 7.48 – 7.42 (m, 4H), 7.41 – 7.29 (m, 3H), 7.24 (ddd, J = 8.2, 7.2, 1.6 Hz, 1H), 7.10 – 6.92 (m, 2H), 6.85 – 6.64 (m, 2H), 5.84 (d, J = 1.8 Hz, 1H), 5.10 (s, 2H). ^{13}C NMR (101 MHz, DMSO) δ 162.69, 158.29, 146.20, 136.06, 133.25, 132.33, 132.27, 129.38, 128.40, 128.28, 127.10, 117.20, 114.43, 114.05, 113.70, 74.45, 68.31. MS ESI m/z : 381 $[\text{M}+\text{H}]^+$.

3-hydroxy-2-(4-((4-nitrobenzyl)oxy)phenyl)-2,3-dihydroquinazolin-4(1H)-one 7 (EML648)



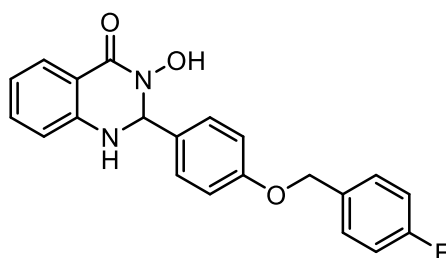
Yield: 83%. ^1H NMR (400 MHz, DMSO- d_6) δ 9.67 (s, 1H), 8.25 (d, J = 8.4 Hz, 2H), 7.70 (d, J = 8.3 Hz, 2H), 7.64 (dd, J = 8.0, 1.5 Hz, 1H), 7.39 – 7.30 (m, 3H), 7.29 – 7.13 (m, 1H), 7.10 – 6.95 (m, 2H), 6.80 – 6.59 (m, 2H), 5.85 (d, J = 1.7 Hz, 1H), 5.28 (s, 2H). ^{13}C NMR (101 MHz, DMSO) δ 162.68, 158.05, 146.98, 146.18, 144.98, 133.26, 132.56, 128.34, 128.13, 127.10, 123.59, 117.22, 114.47, 114.05, 113.70, 74.41, 68.00. MS ESI m/z : 392 $[\text{M}+\text{H}]^+$.

3-hydroxy-2-(4-((4-methoxybenzyl)oxy)phenyl)-2,3-dihydroquinazolin-4(1H)-one 8 (EML649)



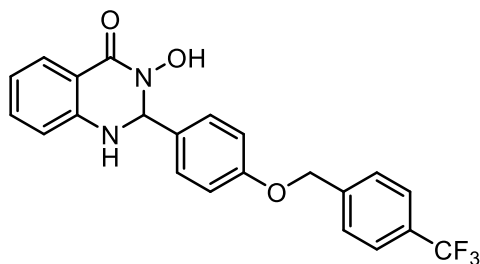
Yield: 79%. ^1H NMR (400 MHz, DMSO- d_6) δ 9.64 (s, 1H), 7.64 (dd, J = 8.0, 1.6 Hz, 1H), 7.41 – 7.30 (m, 5H), 7.24 (ddd, J = 8.1, 7.2, 1.6 Hz, 1H), 7.03 – 6.86 (m, 4H), 6.78 – 6.64 (m, 2H), 5.84 (d, J = 1.8 Hz, 1H), 5.00 (s, 2H), 3.75 (s, 3H). ^{13}C NMR (101 MHz, DMSO) δ 162.69, 158.94, 158.56, 146.21, 133.24, 131.99, 129.37, 128.83, 128.21, 127.10, 117.19, 114.41, 114.04, 113.79, 113.71, 74.48, 68.94, 55.07. MS ESI m/z : 377 $[\text{M}+\text{H}]^+$.

2-(4-((4-fluorobenzyl)oxy)phenyl)-3-hydroxy-2,3-dihydroquinazolin-4(1H)-one 9 (EML658)



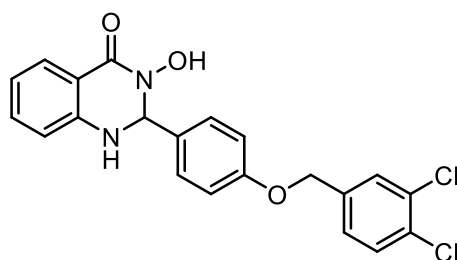
Yield: 80%. ^1H NMR (400 MHz, DMSO- d_6) δ 9.65 (s, 1H), 7.65 (dd, J = 8.1, 1.6 Hz, 1H), 7.56 – 7.42 (m, 2H), 7.35 (dd, J = 8.9, 2.3 Hz, 3H), 7.30 – 7.15 (m, 3H), 7.04 – 6.92 (m, 2H), 6.75 – 6.63 (m, 2H), 5.85 (d, J = 1.8 Hz, 1H), 5.08 (s, 2H). ^{13}C NMR (101 MHz, DMSO) δ 162.92, 162.70, 160.50, 158.40, 146.21, 133.26, 133.20, 132.20, 129.88, 129.80, 128.27, 127.11, 117.22, 115.33, 115.12, 114.42, 114.06, 113.71, 74.46, 68.46. MS ESI m/z : 365 $[\text{M}+\text{H}]^+$.

3-hydroxy-2-(4-((4-(trifluoromethyl)benzyl)oxy)phenyl)-2,3-dihydroquinazolin-4(1H)-one 10 (EML678)



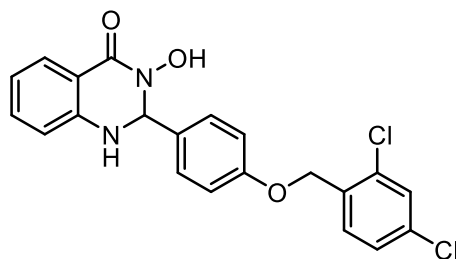
Yield: 85%. ^1H NMR (400 MHz, DMSO- d_6) δ 9.65 (s, 1H), 7.78 – 7.71 (m, 2H), 7.65 (dt, J = 8.0, 1.5 Hz, 3H), 7.40 – 7.29 (m, 3H), 7.24 (ddd, J = 8.2, 7.2, 1.7 Hz, 1H), 7.05 – 6.91 (m, 2H), 6.75 – 6.58 (m, 2H), 5.85 (d, J = 1.8 Hz, 1H), 5.22 (s, 2H). ^{13}C NMR (101 MHz, DMSO) δ 162.70, 158.20, 146.20, 141.94, 133.26, 132.41, 128.34, 127.88, 127.11, 125.33, 125.29, 117.22, 114.44, 114.05, 113.70, 74.44, 68.27. MS ESI m/z : 415 $[\text{M}+\text{H}]^+$.

2-(4-((3,4-dichlorobenzyl)oxy)phenyl)-3-hydroxy-2,3-dihydroquinazolin-4(1H)-one 11 (EML679)



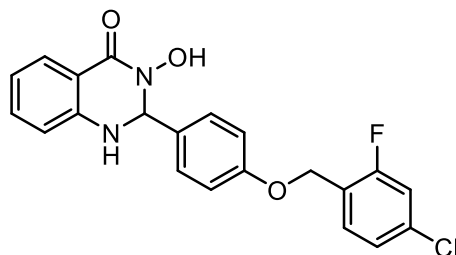
Yield: 81%. ^1H NMR (400 MHz, DMSO- d_6) δ 9.65 (s, 1H), 7.70 (d, J = 2.0 Hz, 1H), 7.65 (dd, J = 8.1, 3.1 Hz, 2H), 7.43 (dd, J = 8.3, 2.0 Hz, 1H), 7.39 – 7.30 (m, 3H), 7.30 – 7.15 (m, 1H), 7.06 – 6.90 (m, 2H), 6.80 – 6.60 (m, 2H), 5.85 (d, J = 1.8 Hz, 1H), 5.12 (s, 2H). ^{13}C NMR (101 MHz, DMSO) δ 162.70, 158.10, 146.19, 138.29, 133.25, 132.44, 131.06, 130.67, 130.29, 129.36, 128.32, 127.70, 127.10, 117.22, 114.44, 114.05, 113.70, 74.43, 67.60. MS ESI m/z : 415 $[\text{M}+\text{H}]^+$.

2-(4-((2,4-dichlorobenzyl)oxy)phenyl)-3-hydroxy-2,3-dihydroquinazolin-4(1H)-one 12 (EML680)



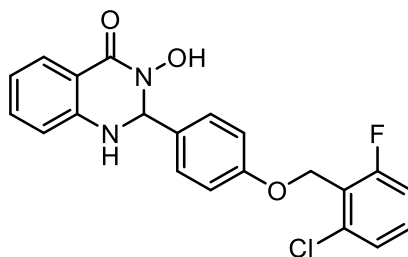
Yield: 82%. ^1H NMR (400 MHz, DMSO- d_6) δ 9.70 (s, 1H), 7.69 (d, J = 2.1 Hz, 1H), 7.66 (dd, J = 8.1, 1.6 Hz, 1H), 7.61 (d, J = 8.3 Hz, 1H), 7.48 (dd, J = 8.3, 2.1 Hz, 1H), 7.43 – 7.32 (m, 3H), 7.30 – 7.17 (m, 1H), 7.10 – 6.89 (m, 2H), 6.81 – 6.60 (m, 2H), 5.87 (d, J = 1.7 Hz, 1H), 5.14 (s, 2H). ^{13}C NMR (101 MHz, DMSO) δ 162.70, 158.17, 146.19, 133.56, 133.49, 133.44, 133.26, 132.58, 131.30, 128.90, 128.36, 127.51, 127.10, 117.21, 114.36, 114.05, 113.69, 74.43, 66.32. MS ESI m/z : 415 $[\text{M}+\text{H}]^+$.

2-(4-((4-chloro-2-fluorobenzyl)oxy)phenyl)-3-hydroxy-2,3-dihydroquinazolin-4(1H)-one 13 (EML681)



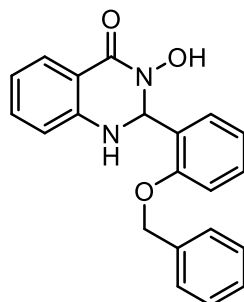
Yield: 85%. ^1H NMR (400 MHz, DMSO- d_6) δ 9.66 (s, 1H), 7.65 (dd, J = 8.1, 1.6 Hz, 1H), 7.57 (t, J = 8.2 Hz, 1H), 7.49 (dd, J = 10.0, 2.1 Hz, 1H), 7.41 – 7.29 (m, 4H), 7.24 (ddd, J = 8.1, 7.3, 1.6 Hz, 1H), 7.07 – 6.93 (m, 2H), 6.70 (ddd, J = 8.1, 5.8, 1.2 Hz, 2H), 5.86 (d, J = 1.8 Hz, 1H), 5.12 (s, 2H). ^{13}C NMR (101 MHz, DMSO) δ 162.68, 161.44, 158.95, 158.17, 146.19, 133.78, 133.68, 133.25, 132.51, 131.76, 131.71, 128.32, 127.10, 124.79, 124.75, 123.13, 122.98, 117.21, 116.22, 115.97, 114.35, 114.05, 113.70, 74.42, 63.06, 63.02. MS ESI m/z : 399 $[\text{M}+\text{H}]^+$.

2-(4-((2-chloro-6-fluorobenzyl)oxy)phenyl)-3-hydroxy-2,3-dihydroquinazolin-4(1H)-one 14 (EML682)



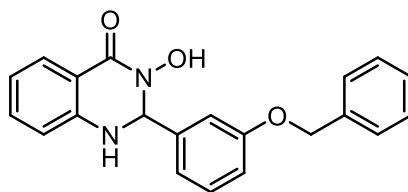
Yield: 80%. ^1H NMR (400 MHz, DMSO- d_6) δ 9.66 (s, 1H), 7.65 (dd, J = 8.1, 1.6 Hz, 1H), 7.51 (td, J = 8.2, 6.2 Hz, 1H), 7.46 – 7.30 (m, 5H), 7.28 – 7.17 (m, 1H), 7.18 – 6.92 (m, 2H), 6.85 – 6.63 (m, 2H), 5.87 (d, J = 1.8 Hz, 1H), 5.14 (d, J = 1.9 Hz, 2H). ^{13}C NMR (101 MHz, DMSO) δ 162.73, 162.59, 160.11, 158.48, 146.21, 135.44, 135.38, 133.27, 132.58, 131.83, 131.73, 128.35, 127.11, 125.71, 121.99, 121.81, 117.22, 114.87, 114.65, 114.21, 114.05, 113.70, 74.46, 60.90, 60.86. MS ESI m/z : 399 $[\text{M}+\text{H}]^+$.

2-(2-(benzyloxy)phenyl)-3-hydroxy-2,3-dihydroquinazolin-4(1H)-one 15
(EML645)



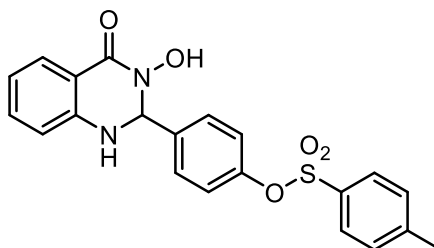
Yield: 74%. ^1H NMR (400 MHz, DMSO- d_6) δ 9.80 (s, 1H), 7.65 (dd, J = 8.0, 1.6 Hz, 1H), 7.51 – 7.18 (m, 8H), 7.09 (dd, J = 2.5, 1.7 Hz, 1H), 7.05 – 6.88 (m, 2H), 6.80 – 6.50 (m, 2H), 5.88 (d, J = 2.0 Hz, 1H), 5.06 (s, 2H). ^{13}C NMR (101 MHz, DMSO) δ 162.48, 158.23, 146.02, 141.60, 136.86, 133.27, 129.32, 128.40, 127.83, 127.72, 127.09, 119.28, 117.28, 114.38, 114.09, 113.76, 113.66, 74.58, 69.22. MS ESI m/z : 347 $[\text{M}+\text{H}]^+$.

2-(3-(benzyloxy)phenyl)-3-hydroxy-2,3-dihydroquinazolin-4(1H)-one 16
(EML646)



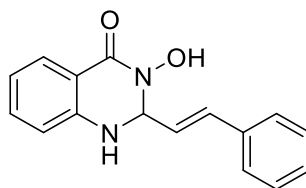
Yield: 77%. ^1H NMR (400 MHz, DMSO- d_6) δ 9.76 (s, 1H), 7.67 (dd, J = 7.7, 1.6 Hz, 1H), 7.51 (ddt, J = 7.5, 1.4, 0.7 Hz, 2H), 7.44 – 7.36 (m, 2H), 7.36 – 7.29 (m, 1H), 7.29 – 7.24 (m, 2H), 7.22 (ddd, J = 8.2, 7.2, 1.7 Hz, 1H), 7.11 (dd, J = 8.4, 1.0 Hz, 1H), 7.05 (d, J = 2.3 Hz, 1H), 6.91 (td, J = 7.5, 1.0 Hz, 1H), 6.77 – 6.65 (m, 2H), 6.31 (d, J = 2.0 Hz, 1H), 5.20 (s, 2H). ^{13}C NMR (101 MHz, DMSO) δ 162.63, 155.68, 145.88, 137.08, 133.14, 129.62, 128.41, 127.70, 127.64, 127.29, 126.99, 126.76, 120.34, 117.17, 114.24, 113.61, 112.69, 69.48, 69.31. MS ESI m/z : 347 $[\text{M}+\text{H}]^+$.

4-(3-hydroxy-4-oxo-1,2,3,4-tetrahydroquinazolin-2-yl)phenyl 4-
methylbenzenesulfonate 17 (EML651)



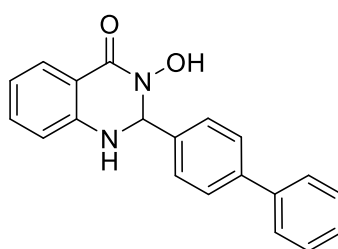
Yield: 65%. ^1H NMR (400 MHz, DMSO- d_6) δ 9.75 (s, 1H), 7.75 (d, J = 8.1 Hz, 2H), 7.64 (dd, J = 7.7, 1.4 Hz, 1H), 7.56 – 7.36 (m, 5H), 7.25 (td, J = 7.6, 1.5 Hz, 1H), 7.05 (d, J = 8.6 Hz, 2H), 6.86 – 6.63 (m, 2H), 5.91 (d, J = 1.8 Hz, 1H), 2.42 (s, 3H). ^{13}C NMR (101 MHz, DMSO) δ 162.66, 149.00, 145.99, 145.78, 139.01, 133.43, 131.59, 130.25, 128.73, 128.09, 127.16, 121.85, 117.46, 114.10, 113.55, 74.13, 21.16. MS ESI m/z : 411 $[\text{M}+\text{H}]^+$.

(E)-3-hydroxy-2-styryl-2,3-dihydroquinazolin-4(1H)-one 18 (EML657)



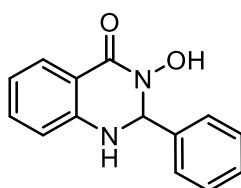
Yield: 82%. ^1H NMR (400 MHz, DMSO- d_6) δ 9.77 (s, 1H), 7.65 (dd, $J = 7.8$, 1.5 Hz, 1H), 7.49 – 7.38 (m, 2H), 7.33 (t, $J = 7.3$ Hz, 2H), 7.30 – 7.21 (m, 3H), 6.76 (d, $J = 8.1$ Hz, 1H), 6.74 – 6.63 (m, 2H), 6.39 (dd, $J = 15.8$, 7.0 Hz, 1H), 5.43 (dd, $J = 7.0$, 1.9 Hz, 1H). ^{13}C NMR (101 MHz, DMSO) δ 162.31, 146.10, 135.56, 133.25, 132.84, 128.69, 128.17, 127.18, 126.65, 125.92, 117.34, 114.35, 113.78, 74.32. MS ESI m/z : 267 $[\text{M}+\text{H}]^+$.

2-([1,1'-biphenyl]-4-yl)-3-hydroxy-2,3-dihydroquinazolin-4(1H)-one 19
(EML650)



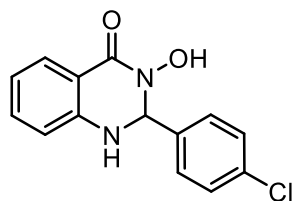
Yield: 88%. ^1H NMR (400 MHz, DMSO- d_6) δ 9.80 (s, 1H), 7.77 – 7.61 (m, 5H), 7.56 – 7.49 (m, 2H), 7.49 – 7.41 (m, 3H), 7.41 – 7.30 (m, 1H), 7.26 (ddd, $J = 8.2$, 7.2, 1.6 Hz, 1H), 6.82 – 6.57 (m, 2H), 5.96 (d, $J = 2.0$ Hz, 1H). ^{13}C NMR (101 MHz, DMSO) δ 162.64, 146.11, 140.46, 139.71, 139.06, 133.34, 128.91, 127.52, 127.15, 126.68, 126.56, 117.32, 114.11, 113.75, 74.53. MS ESI m/z : 317 $[\text{M}+\text{H}]^+$.

3-hydroxy-2-phenyl-2,3-dihydroquinazolin-4(1H)-one 20 (EML659)



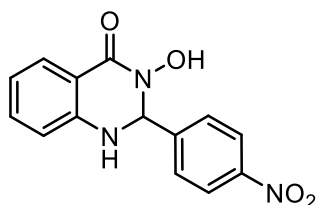
Yield: 68%. ^1H NMR (400 MHz, DMSO- d_6) δ 9.74 (s, 1H), 7.66 (dd, $J = 8.0$, 1.6 Hz, 1H), 7.50 – 7.39 (m, 3H), 7.39 – 7.29 (m, 3H), 7.29 – 7.19 (m, 1H), 6.78 – 6.61 (m, 2H), 5.90 (d, $J = 1.9$ Hz, 1H). ^{13}C NMR (101 MHz, DMSO) δ 162.65, 146.13, 139.91, 133.32, 128.53, 128.21, 127.12, 126.94, 117.29, 114.07, 113.71, 74.84. MS ESI m/z : 241 $[\text{M}+\text{H}]^+$.

2-(4-chlorophenyl)-3-hydroxy-2,3-dihydroquinazolin-4(1H)-one 21
(EML655)



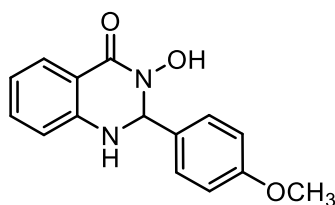
Yield: 71%. ^1H NMR (400 MHz, DMSO- d_6) δ 9.79 (s, 1H), 7.66 (dd, J = 8.0, 1.6 Hz, 1H), 7.50 – 7.40 (m, 5H), 7.26 (ddd, J = 8.1, 7.2, 1.6 Hz, 1H), 6.80 – 6.60 (m, 2H), 5.93 (d, J = 2.0 Hz, 1H). ^{13}C NMR (101 MHz, DMSO) δ 162.68, 145.98, 138.84, 133.41, 133.10, 128.88, 128.21, 127.16, 117.46, 114.13, 113.67, 74.11, 39.52. MS ESI m/z : 275 $[\text{M}+\text{H}]^+$.

3-hydroxy-2-(4-nitrophenyl)-2,3-dihydroquinazolin-4(1H)-one 22
(EML652)



Yield: 73%. ^1H NMR (400 MHz, DMSO- d_6) δ 9.98 (s, 1H), 8.36 – 8.20 (m, 2H), 7.79 – 7.63 (m, 3H), 7.59 (s, 1H), 7.36 – 7.22 (m, 1H), 6.74 (t, J = 7.5 Hz, 2H), 6.11 (d, J = 2.3 Hz, 1H). ^{13}C NMR (101 MHz, DMSO) δ 162.58, 147.60, 147.11, 145.73, 133.55, 128.31, 127.22, 123.49, 117.73, 114.26, 113.68, 73.80. MS ESI m/z : 286 $[\text{M}+\text{H}]^+$.

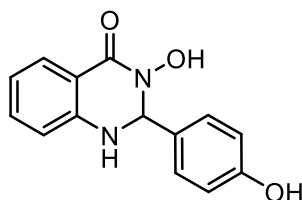
3-hydroxy-2-(4-methoxyphenyl)-2,3-dihydroquinazolin-4(1H)-one 23
(EML653)



Yield: 70%. ^1H NMR (400 MHz, DMSO- d_6) δ 9.64 (s, 1H), 7.65 (dd, J = 8.2, 1.6 Hz, 1H), 7.41 – 7.30 (m, 3H), 7.30 – 7.12 (m, 1H), 7.01 – 6.81 (m, 2H), 6.82 – 6.60 (m, 2H), 5.85 (d, J = 1.8 Hz, 1H), 3.74 (s, 3H). ^{13}C NMR (101 MHz, DMSO)

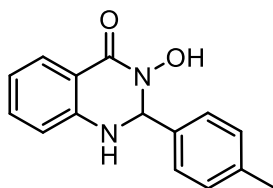
δ 162.71, 159.45, 146.23, 133.24, 131.89, 128.25, 127.10, 117.19, 114.05, 113.71, 113.53, 74.49, 55.13. MS ESI m/z: 271 [M+H]⁺.

3-hydroxy-2-(4-hydroxyphenyl)-2,3-dihydroquinazolin-4(1H)-one 24
(EML654)



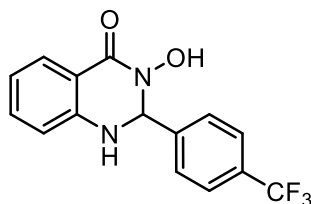
Yield: 67%. ¹H NMR (400 MHz, DMSO-d₆) δ 9.47 (s, 2H), 7.64 (dd, J = 8.1, 1.7 Hz, 1H), 7.43 – 6.91 (m, 4H), 6.80 – 6.36 (m, 4H), 5.78 (s, 1H). ¹³C NMR (101 MHz, DMSO) δ 162.70, 157.68, 146.32, 133.21, 130.18, 128.30, 127.09, 117.09, 114.80, 113.98, 113.63, 74.75. MS ESI m/z: 257 [M+H]⁺.

3-hydroxy-2-(p-tolyl)-2,3-dihydroquinazolin-4(1H)-one 25 (EML656)



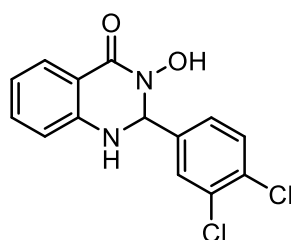
Yield: 71%. ¹H NMR (400 MHz, DMSO-d₆) δ 9.72 (s, 1H), 7.64 (dd, J = 8.1, 1.6 Hz, 1H), 7.38 (d, J = 2.1 Hz, 1H), 7.34 – 7.28 (m, 2H), 7.26 – 7.19 (m, 1H), 7.16 (d, J = 7.9 Hz, 2H), 6.83 – 6.59 (m, 2H), 5.86 (d, J = 1.9 Hz, 1H), 2.28 (s, 3H). ¹³C NMR (101 MHz, DMSO) δ 162.53, 146.10, 137.77, 137.02, 133.19, 128.67, 127.05, 126.82, 117.18, 114.04, 113.77, 74.62, 20.70. MS ESI m/z: 255 [M+H]⁺.

3-hydroxy-2-(4-(trifluoromethyl)phenyl)-2,3-dihydroquinazolin-4(1H)-one 26
(EML683)



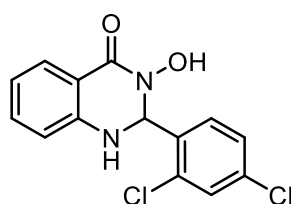
Yield: 75%. ^1H NMR (400 MHz, DMSO- d_6) δ 9.88 (s, 1H), 7.81 – 7.72 (m, 2H), 7.73 – 7.59 (m, 3H), 7.51 (d, J = 2.1 Hz, 1H), 7.34 – 7.19 (m, 1H), 6.73 (td, J = 7.5, 1.1 Hz, 2H), 6.04 (d, J = 2.0 Hz, 1H). ^{13}C NMR (101 MHz, DMSO) δ 162.69, 145.88, 144.39, 133.48, 129.23, 128.91, 128.70, 127.85, 127.19, 125.23, 125.20, 117.58, 114.16, 113.66, 74.14. MS ESI m/z : 309 $[\text{M}+\text{H}]^+$.

2-(3,4-dichlorophenyl)-3-hydroxy-2,3-dihydroquinazolin-4(1H)-one 27
(EML684)



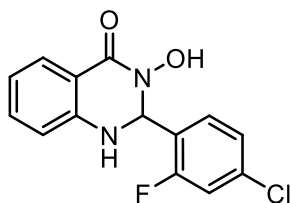
Yield: 73%. ^1H NMR (400 MHz, DMSO- d_6) δ 9.90 (s, 1H), 7.72 – 7.61 (m, 3H), 7.49 (d, J = 2.2 Hz, 1H), 7.45 – 7.37 (m, 1H), 7.33 – 7.21 (m, 1H), 6.85 – 6.49 (m, 2H), 5.98 (d, J = 2.1 Hz, 1H). ^{13}C NMR (101 MHz, DMSO) δ 162.70, 145.79, 140.91, 133.54, 131.08, 130.86, 130.54, 129.15, 127.21, 127.20, 117.71, 114.23, 113.65, 73.51. MS ESI m/z : 309 $[\text{M}+\text{H}]^+$.

2-(2,4-dichlorophenyl)-3-hydroxy-2,3-dihydroquinazolin-4(1H)-one 28
(EML685)



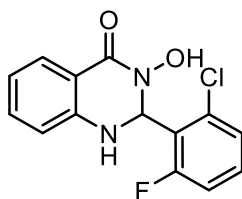
Yield: 77%. ^1H NMR (400 MHz, DMSO- d_6) δ 9.81 (s, 1H), 7.73 – 7.61 (m, 2H), 7.57 – 7.43 (m, 2H), 7.39 (d, J = 2.1 Hz, 1H), 7.27 (ddd, J = 8.1, 7.2, 1.6 Hz, 1H), 6.80 – 6.63 (m, 2H), 6.29 (d, J = 2.0 Hz, 1H). ^{13}C NMR (101 MHz, DMSO) δ 162.92, 145.58, 135.65, 133.95, 133.58, 133.30, 129.73, 129.03, 127.62, 127.19, 117.67, 114.26, 113.27, 71.34. MS ESI m/z : 309 $[\text{M}+\text{H}]^+$.

2-(4-chloro-2-fluorophenyl)-3-hydroxy-2,3-dihydroquinazolin-4(1H)-one 29
(EML686)



Yield: 74%. ^1H NMR (400 MHz, DMSO- d_6) δ 9.84 (s, 1H), 7.68 (dd, J = 7.8, 1.6 Hz, 1H), 7.55 – 7.38 (m, 3H), 7.32 (ddd, J = 8.4, 2.0, 0.8 Hz, 1H), 7.30 – 7.22 (m, 1H), 6.88 – 6.57 (m, 2H), 6.19 (d, J = 2.0 Hz, 1H). ^{13}C NMR (101 MHz, DMSO) δ 162.75, 161.27, 158.77, 145.79, 134.12, 134.01, 133.50, 129.71, 129.69, 129.67, 127.15, 125.93, 125.80, 124.71, 124.70, 124.68, 117.56, 116.38, 116.13, 114.09, 113.32, 68.90. MS ESI m/z : 293 $[\text{M}+\text{H}]^+$.

2-(2-chloro-6-fluorophenyl)-3-hydroxy-2,3-dihydroquinazolin-4(1H)-one 30 (EML687)

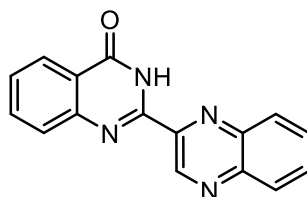


Yield: 73%. ^1H NMR (400 MHz, DMSO- d_6) δ 9.82 (s, 1H), 7.65 (dd, J = 7.8, 1.5 Hz, 1H), 7.50 – 7.38 (m, 2H), 7.36 (dt, J = 8.1, 1.0 Hz, 1H), 7.30 – 7.13 (m, 2H), 6.73 – 6.64 (m, 2H), 6.60 (dd, J = 8.2, 1.0 Hz, 1H). ^{13}C NMR (101 MHz, DMSO) δ 163.20, 161.16, 160.69, 145.77, 133.96, 133.90, 133.15, 131.18, 131.09, 126.86, 125.96, 125.93, 124.58, 124.43, 116.74, 115.63, 115.40, 113.23, 112.79, 69.79. MS ESI m/z : 293 $[\text{M}+\text{H}]^+$.

General procedure for the synthesis of quinazolin-4(3H)-ones (31-32)

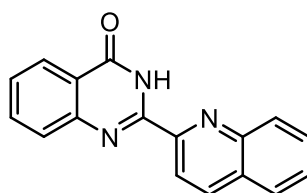
To a suspension of proper 3-hydroxy-2,3-dihydroquinazolin-4(1H)-one (**1-2**; 0.50 mmol) in toluene (10.0 mL) was added selenium dioxide (0.11 g, 1.00 mmol), then the mixture was refluxed for 4 hours. The hot mixture was filtered through Celite and the crude was purified by silica gel chromatography (Hex/EtOAc) to give the title compounds in 80% yield as light brown solid.

2-(quinoxalin-2-yl)quinazolin-4(3H)-one 31 (EML625)



Yield: 80%. ^1H NMR (400 MHz, CDCl_3) δ 10.86 (s, 1H), 10.05 (s, 1H), 8.40 (d, $J = 7.9$ Hz, 0H), 8.27 – 8.21 (m, 1H), 8.21 – 8.13 (m, 1H), 7.98 – 7.80 (m, 4H), 7.66 – 7.53 (m, 1H). ^{13}C NMR (101 MHz, CDCl_3) δ 161.32, 148.92, 147.76, 143.86, 143.78, 142.66, 140.67, 135.03, 131.93, 131.34, 129.73, 128.70, 128.34, 127.03, 122.95, 120.14. MS ESI m/z : 275 $[\text{M}+\text{H}]^+$.

2-(quinolin-2-yl)quinazolin-4(3H)-one 32 (EML626)



Yield: 80%. ^1H NMR (400 MHz, CDCl_3) δ 11.19 (s, 1H), 8.61 (d, $J = 8$ Hz, 1H), 8.34 (t, $J = 8$ Hz, 2H), 8.12 (d, $J = 8$ Hz, 1H), 7.65-7.90 (m, 4H), 7.45-7.65 (m, 2H)¹⁵². ^{13}C NMR (101 MHz, CDCl_3) δ 161.3, 149.1, 148.9, 148.0, 146.7, 137.5, 134.4, 130.4, 129.6, 129.2, 128.2, 127.6, 127.4, 126.7, 122.6, 118.4¹⁵². MS ESI m/z : 274 $[\text{M}+\text{H}]^+$.

6.7 Histone processing and mass spectrometry analysis

Histone bands were separated by SDS-PAGE, stained with Coomassie (Brilliant blue G-250) and excised at appropriate height. Bands were destained in 50% acetonitrile/50% 100 mM ammonium bicarbonate. Histones were chemically modified by propionylation (30 min, room temperature, 2.5% propionic anhydride (Sigma) in ammonium bicarbonate at pH 7.5) to prevent tryptic cleavage. Histone proteins were then digested with trypsin (Promega, 200 ng in 50 mM ammonium bicarbonate) overnight and the supernatant desalted by Carbon TopTips (Glygen) according to manufacturer's instructions. The peptides were injected in an Ultimate 3000 HPLC system (LC Packings Dionex) and separated with a gradient from 5%

to 60% acetonitrile in 0.1% formic acid over 40 min at 300 nl/min on a 75 μm ID X 10 cm ReproSil-Pur C1-AQ analytical column (2.4 μm ; Dr. Maisch GmbH Germany). The effluent from the HPLC was directly electro-sprayed into the Q Exactive™ HF hybrid quadrupole-Orbitrap mass spectrometer (Thermo Fisher Scientific). The MS instrument was operated in the data-dependent mode to automatically switch between full scan MS and MS/MS acquisition. Survey full scan spectra (m/z 250–2000) were acquired in the Quadrupole-Orbitrap with resolution $R = 60\,000$ at m/z 400. For all measurements with the Quadrupole-Orbitrap detector, three lock-mass ions from ambient air ($m/z = 371.10123$, 445.12002 , 519.13882) were used for internal calibration. The six most intense peptide ions with charge state between two and five were sequentially isolated (window = 2.0 m/z) to a target value of 10 000 and fragmented in the linear ion trap by collision-induced dissociation (CID). Fragment ion spectra were recorded in the linear trap of the instrument. A dynamic exclusion time of 180 s was applied. Typical mass spectrometric conditions were: spray voltage 1.4 kV; no sheath and auxiliary gas flow; heated capillary temperature 200 °C; normalized collision energy 35% for CID in linear ion trap. An activation $q = 0.25$ and activation time of 30 ms were used. Data analysis was performed Skyline software (MacCoss Lab Software) by using doubly and triply charged peptide masses for extracted ion chromatograms (XICs). XICs were checked manually and values exported to Excel for further calculations.

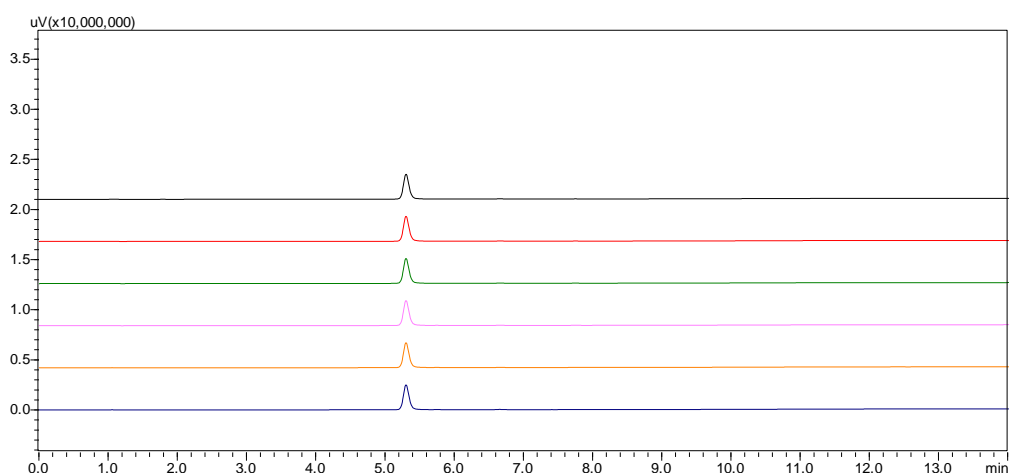
6.8. AlphaLISA KDM4 assay

The assays were performed in white Optiplate-384 (PerkinElmer, # 6007299) at room temperature in a final volume of 20 μL , using the following Assay Buffer: 50 mM Hepes pH 7.5, 0.01% Tween-20, 0.1% BSA. *h*KDM4A (BPS BioScience # 50103) (100 nM, final concentration) was diluted in Assay Buffer, then a mixture of Fe(II) (Sigma # 215406) (5 μM , final concentration), ascorbate (Sigma # 11140) (100 μM , final concentration) and proper inhibitor (5% DMSO, final concentration) was added. After a pre-incubation time of 15 minutes, Histone H3 (1 - 21) lysine 9 tri-methylated peptide, biotinylated (H3K9me3) (AnaSpec # 64360) (200 nM, final

concentration) and 2OG (Sigma # K2000) (5 μ M, final concentration) were added. The reaction was incubated for 1 h, afterwards the Anti-methyl-Histone H3 Lysine 9 (H3K9me2) AlphaLISA Acceptor beads (PerkinElmer # AL117 PerkinElmer # AL117) in Epigenetic Buffer 1X was added in each well, to reach a final concentration of 20 μ g/mL. After an incubation of 1 h, Streptavidin Donor beads (PerkinElmer, # 6760002) were diluted in Epigenetic Buffer 1X and added in each well to reach a final concentration of 20 μ g/mL. After 30 minutes of incubation, the Alpha signal was read with the EnSpire Multilabel plate Reader (PerkinElmer). All incubation steps with AlphaScreen beads were performed at room under subdued lighting condition.

6.9. Hit validation stability assays

Hit compounds **EML586**, **EML620** and **EML627** were dissolved in PBS to reach a final concentration of 100 μ M (5% DMSO). 5 μ L of the prepared solutions were analysed by HPLC after 5, 15, 30, 60 minutes and 24 h. Spectra were recorded on a Shimadzu SPD 20A UV/vis detector ($\lambda = 220$ nm) using C-18 column Phenomenex Synergi Fusion RP 80A (75mm \times 4.60 mm; 4 μ m) at 25 $^{\circ}$ C using a mobile phase A (water + 0.1% TFA) and B (MeCN + 0.1% TFA) at a flow rate of 1 mL/min.



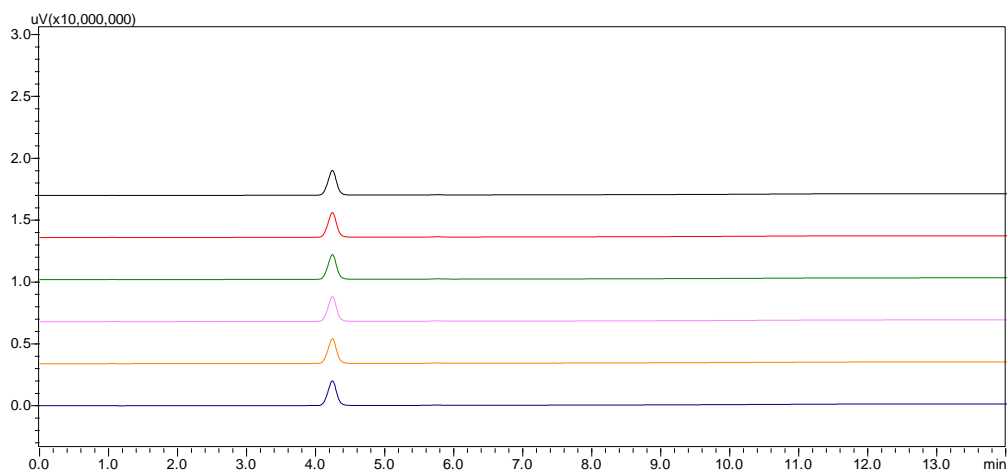


Figure 4.3. HPLC chromatograms obtained for compound **EML586** (up) and **EML615** (down) injected immediately after the dissolution in PBS, after 5, 15, 30, 60 minutes and 24 h. Spectra were recorded at 220 nm.

6.10. PAMPA

Donor solution (0.5 mM) was prepared by diluting 1 mM dimethyl sulfoxide (DMSO) compound stock solution using phosphate buffer (pH 7.4, 0.01 M). Filters were coated with 5 μL of a 1% (w/v) dodecane solution of phosphatidylcholine. Donor solution (150 μL) was added to each well of the filter plate. To each well of the acceptor plate were added 300 μL of solution (50% DMSO in phosphate buffer). Compounds were tested in triplicate. The sandwich was incubated for 24 h at room temperature under gentle shaking. After the incubation time, the sandwich plates were separated and 250 μL of the acceptor plate were transferred to a UV quartz microtiter plate and measured by UV spectroscopy, using a Multiskan GO microplate spectrophotometer (Thermo Scientific) at 250-500 nm at step of 5 nm. Reference solutions (250 μL) were prepared diluting the sample stock solutions to the same concentration as that with no membrane barrier. The apparent permeability value P_{app} is determined from the ratio r of the absorbance of compound found in the acceptor chamber divided by the theoretical equilibrium absorbance (determined independently) applying the Faller modification of Sugano equation:

$$P_{app} = \left(\frac{VD * VR}{(VD + VR) * At} \right) * \ln(1 - r)$$

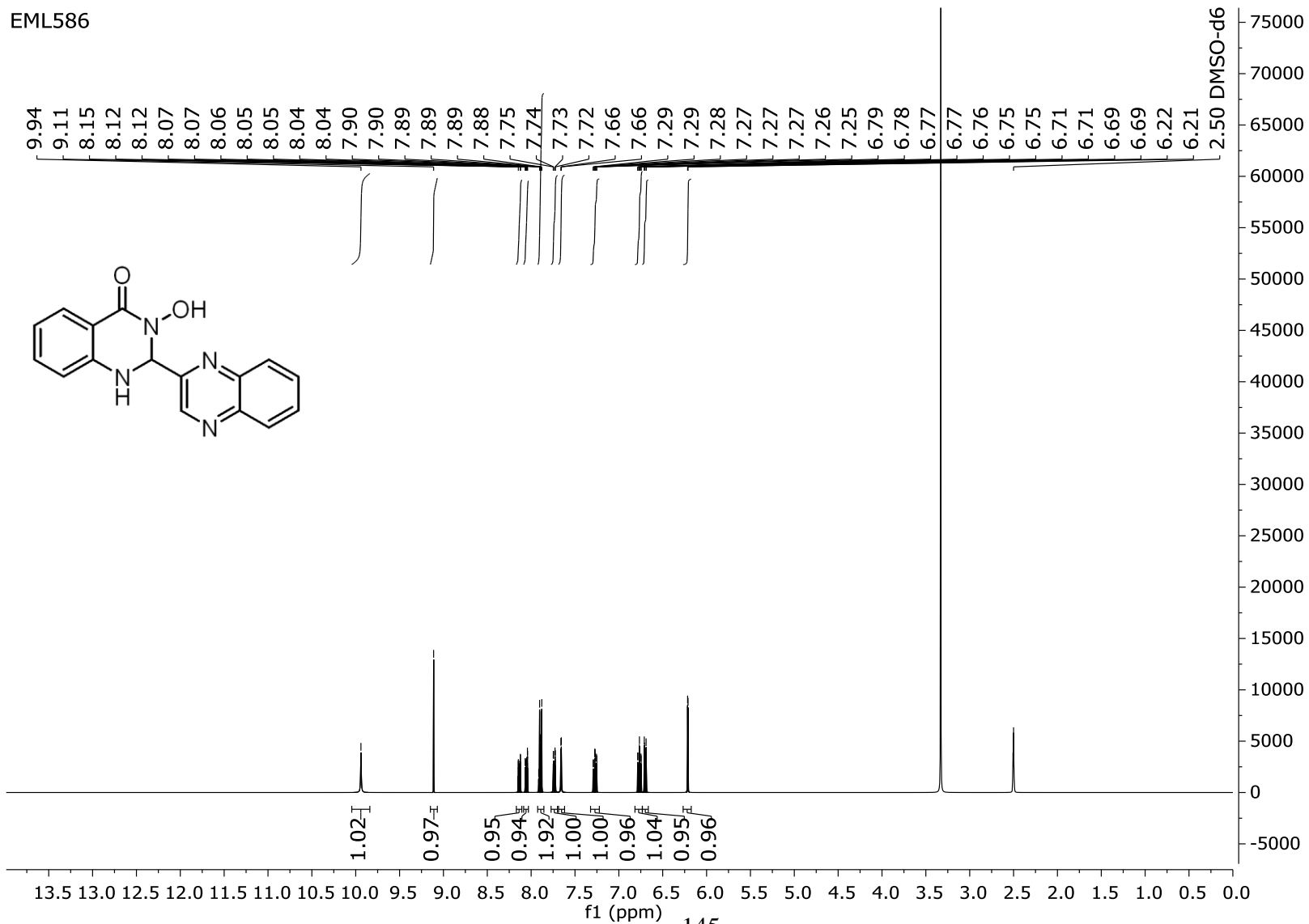
In this equation, VR is the volume of the acceptor compartment (0.3 cm³), VD is the donor volume (0.15 cm³), A is the accessible filter area (0.24 cm²), and t is the incubation time in seconds.

6.11. Nephelometric assay

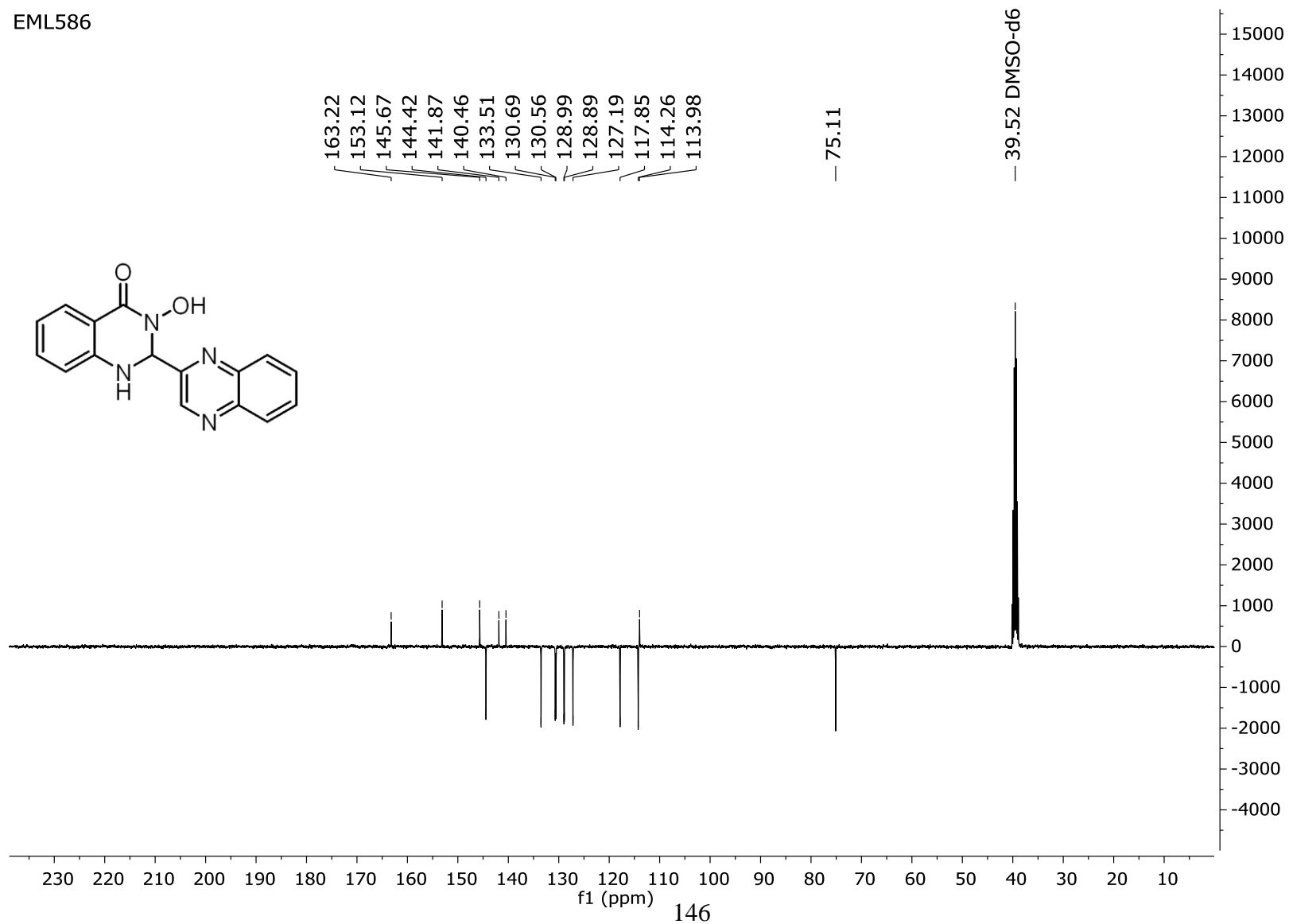
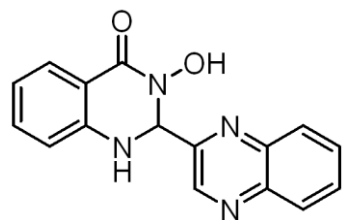
Stock solutions of test compound (500 μM in DMSO) were diluted into water or AlphaLISA Assay Buffer (50 mM Hepes pH 7.5, 0.01% Tween-20, 0.1% BSA) and put in 96 well plates to final concentrations of 25 μM (5% DMSO, 300 μL of each). The mixtures were incubated at room temperature and scattering was measured immediately after preparation of samples (T0) and after 60 min. Each measurement has been preceded by a stirring step (2 min, 600 rpm) to re-suspend any precipitated particles. All tests were performed in duplicate for each sample. Solubility was measured on a Nepheloskan Ascent plate reader equipped with a quartz halogen lamp and photomultiplier detector operating between 580 and 630 nm with a measurement angle of 90 degrees. The instrument settings were the following: PMT voltage 450; lamp voltage 11.0.

6.12. NMR data

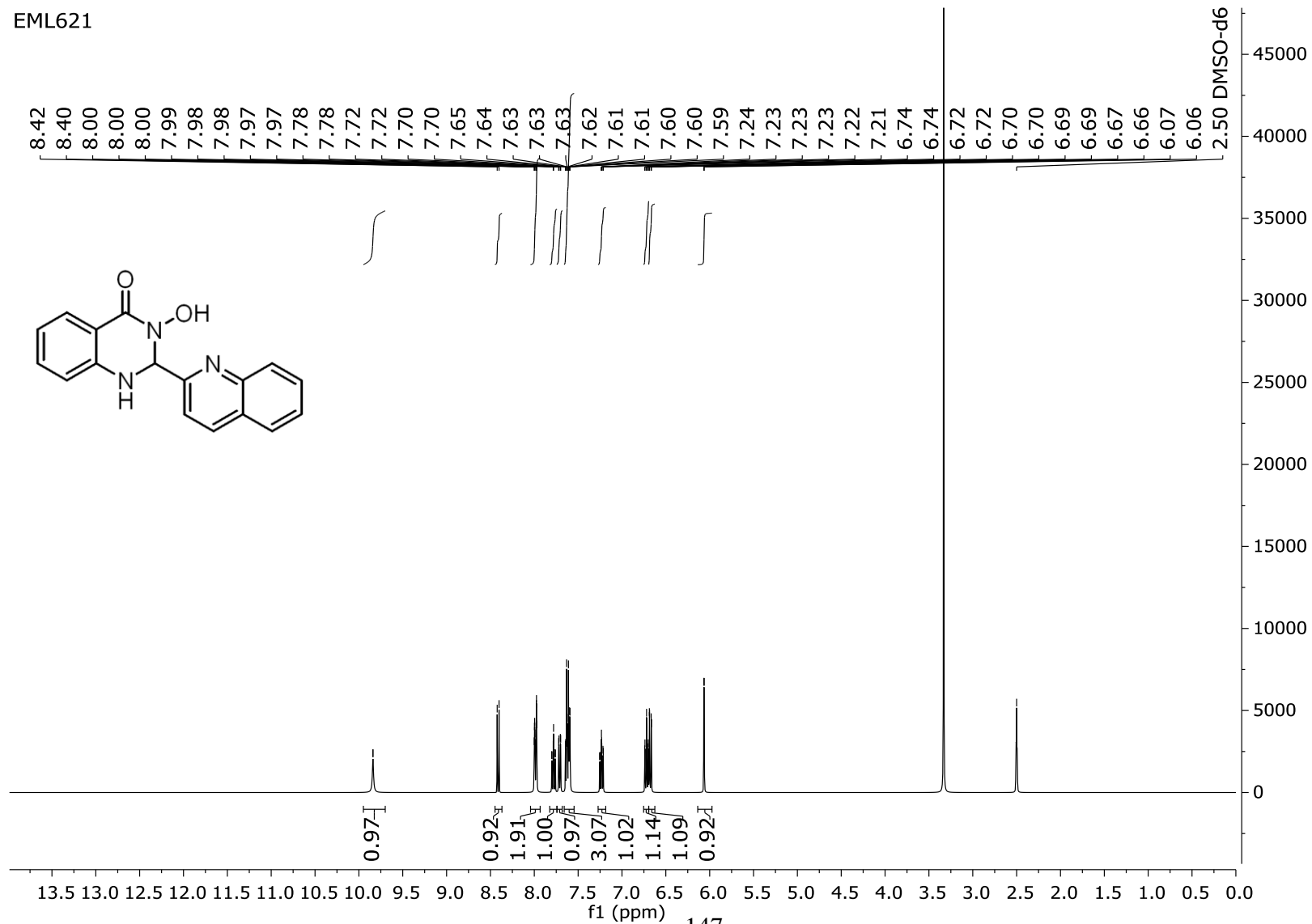
EML586



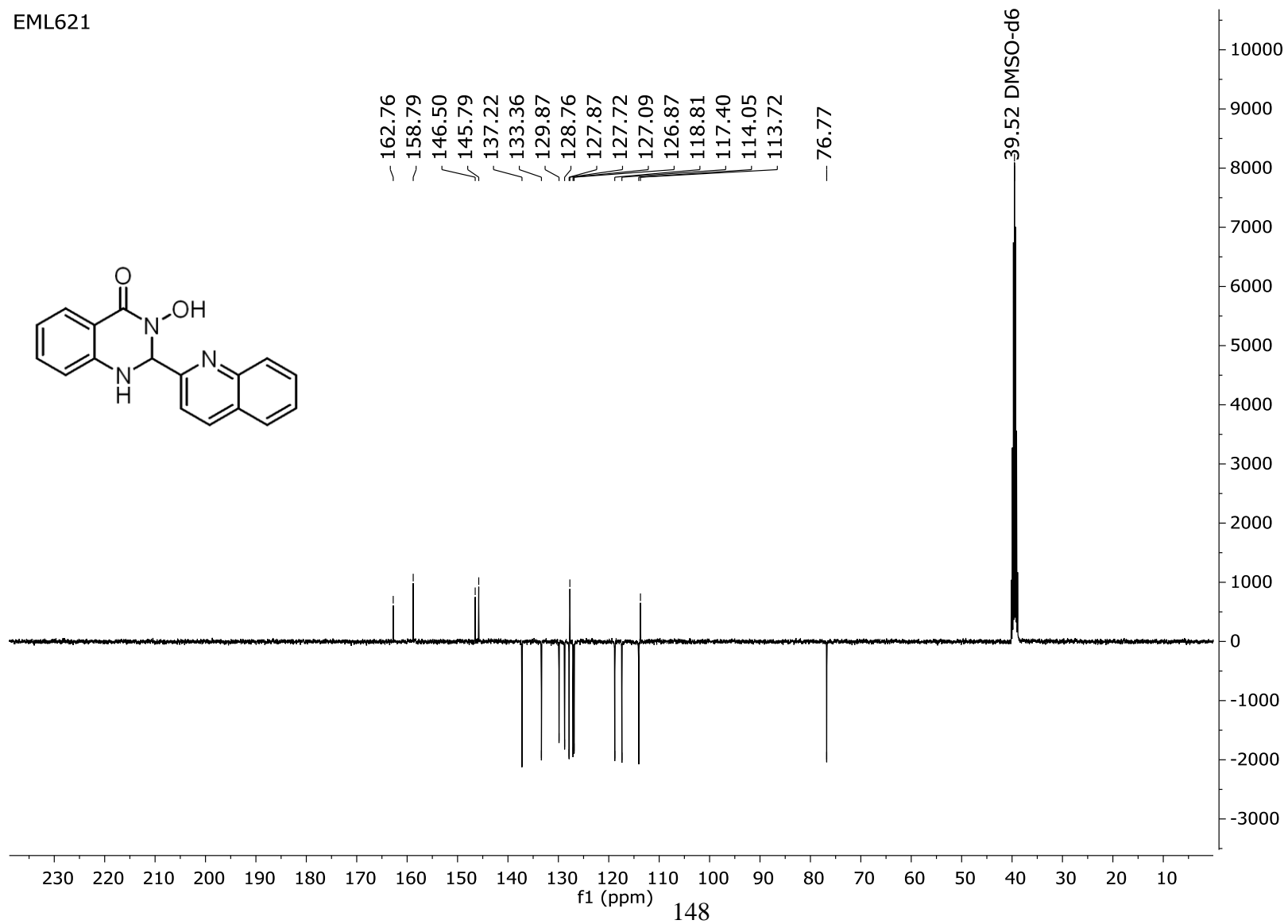
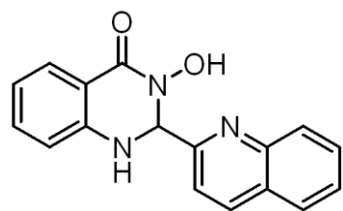
EML586



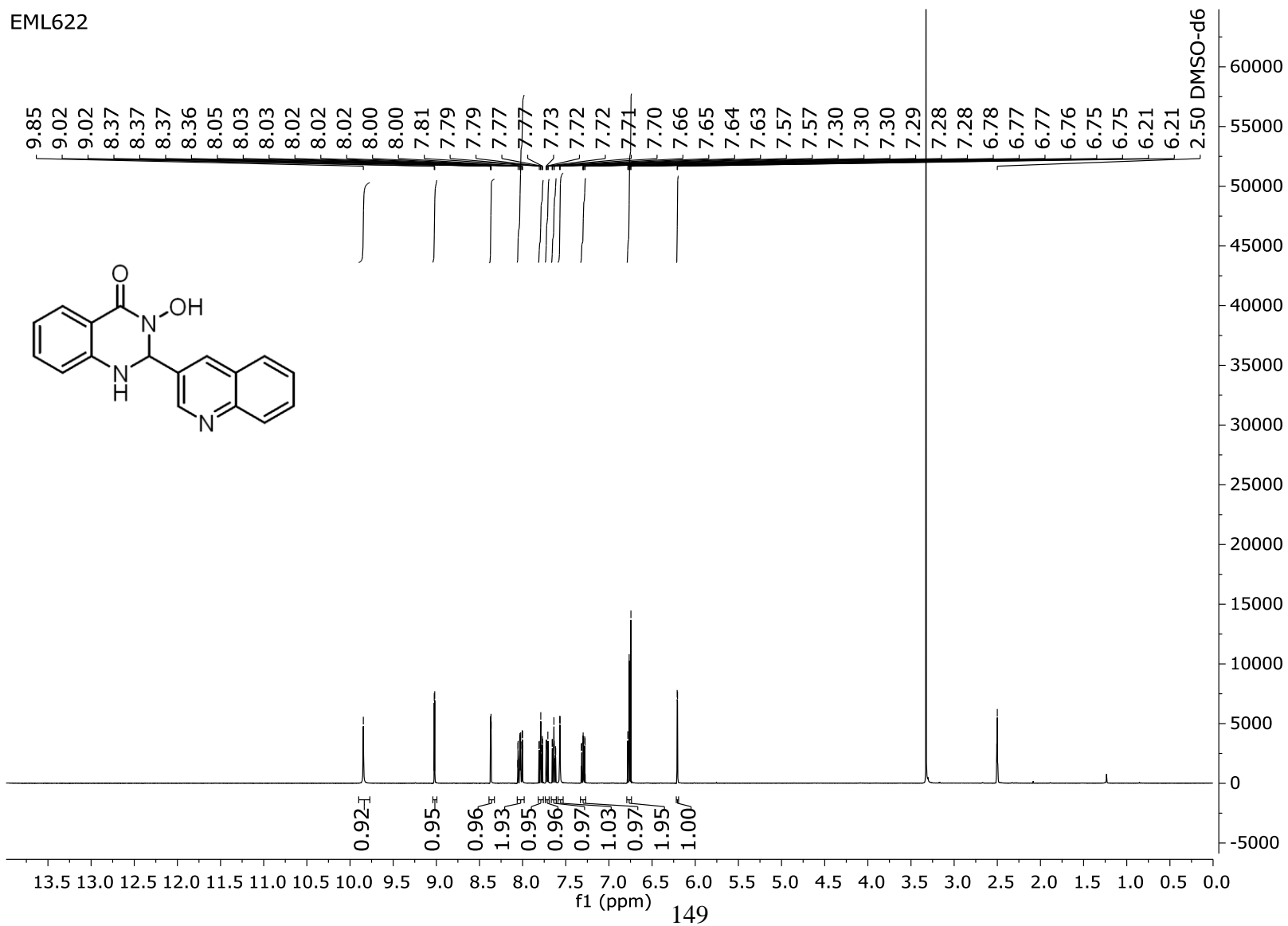
EML621



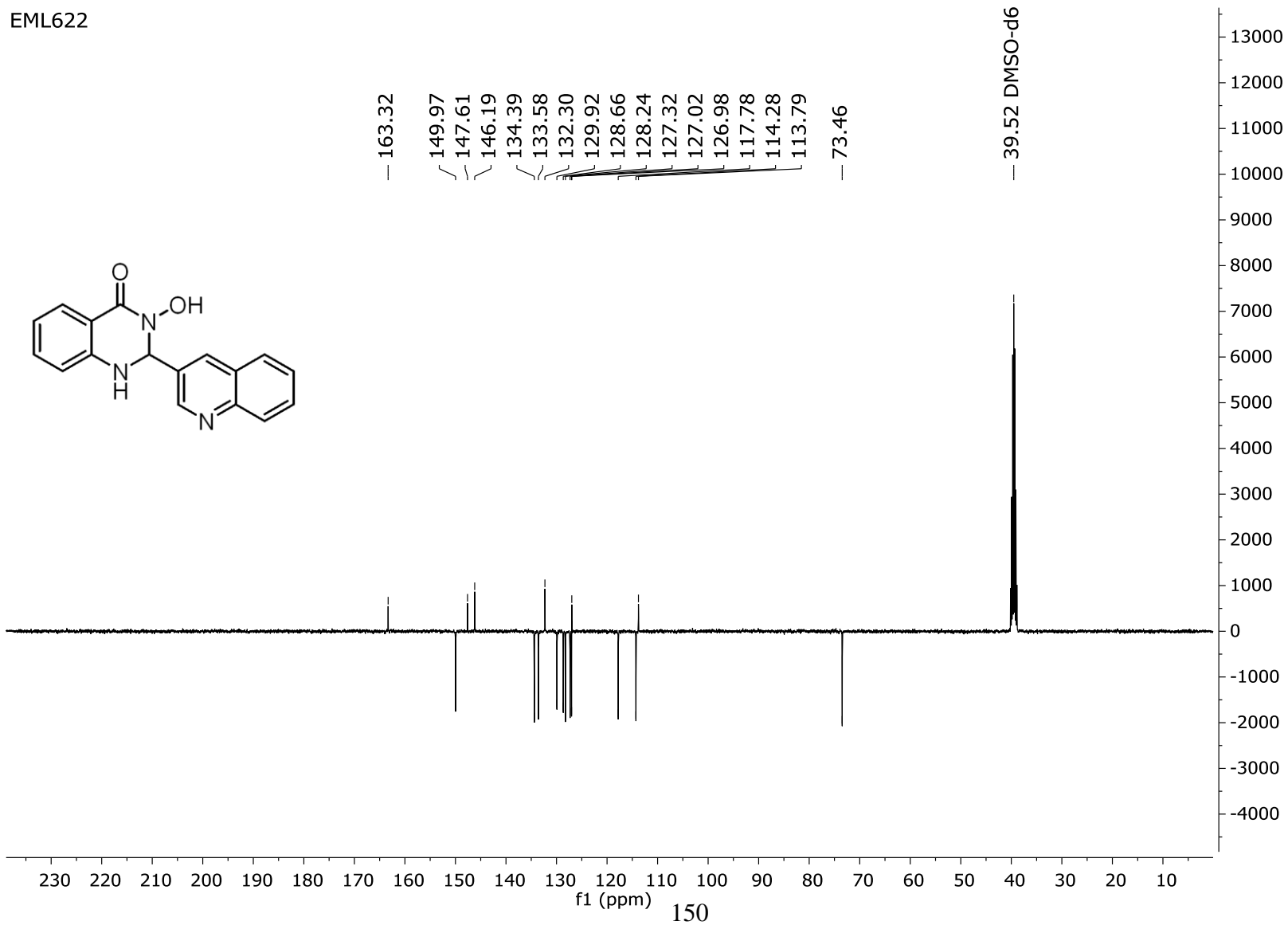
EML621



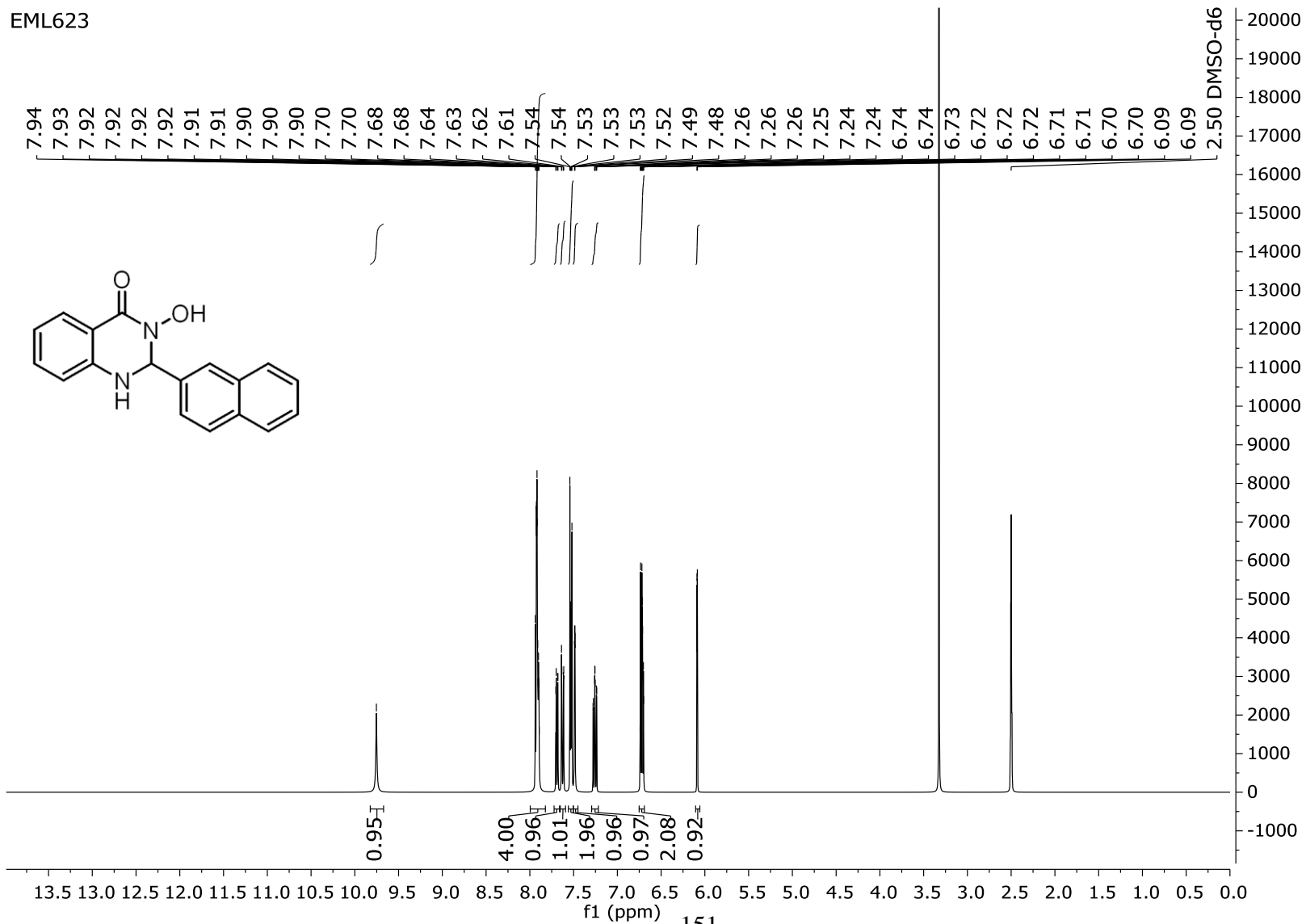
EML622



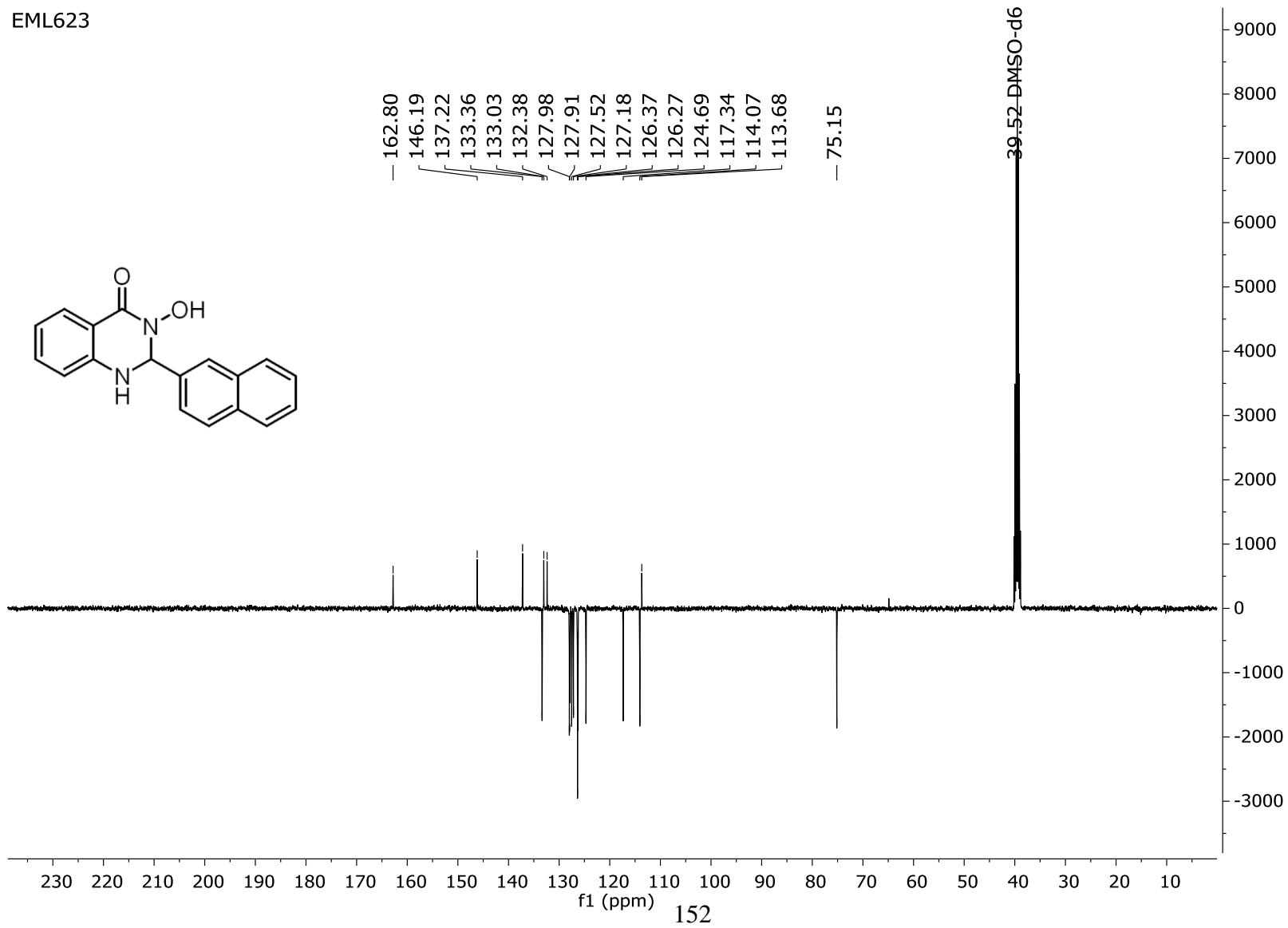
EML622



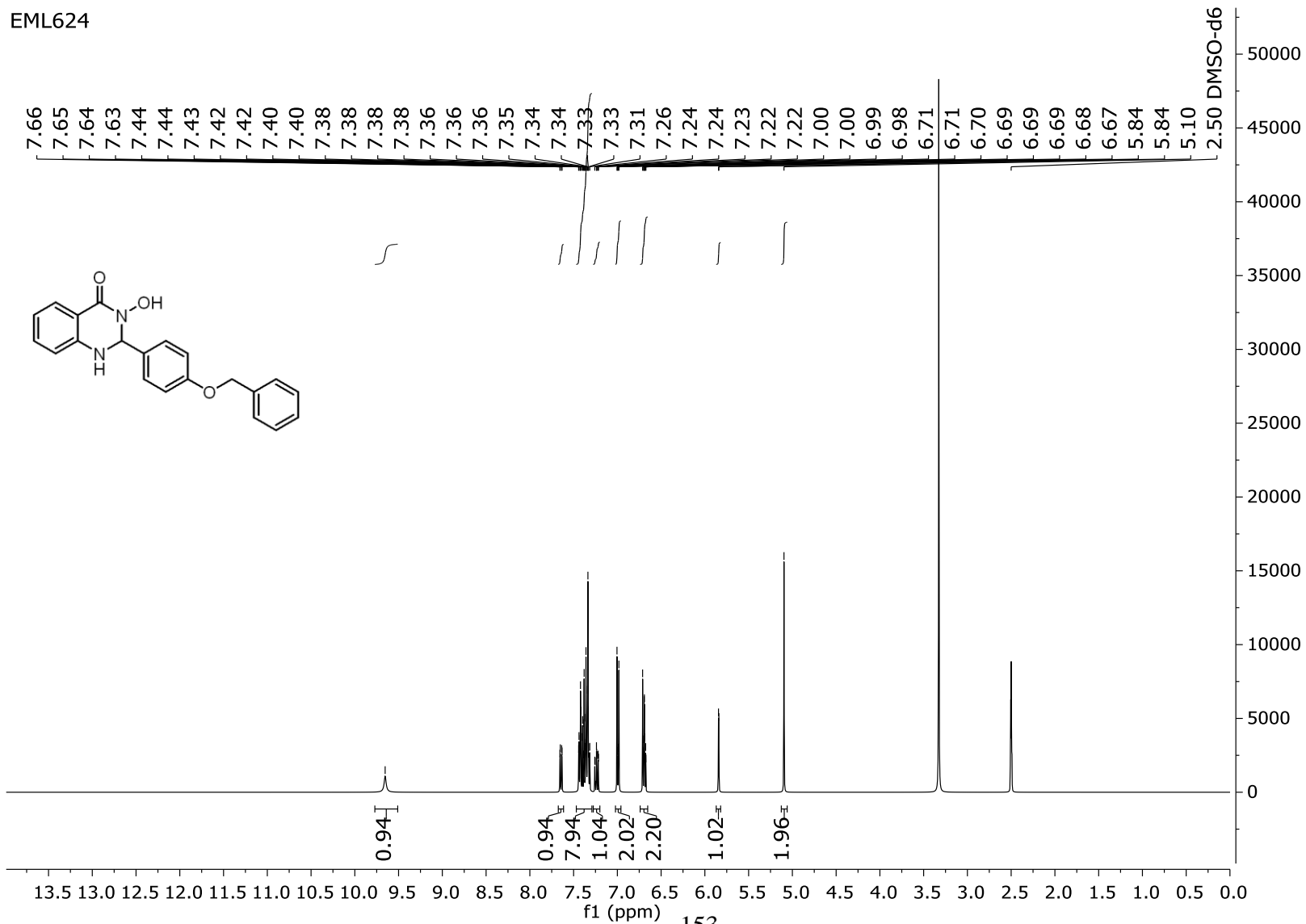
EML623



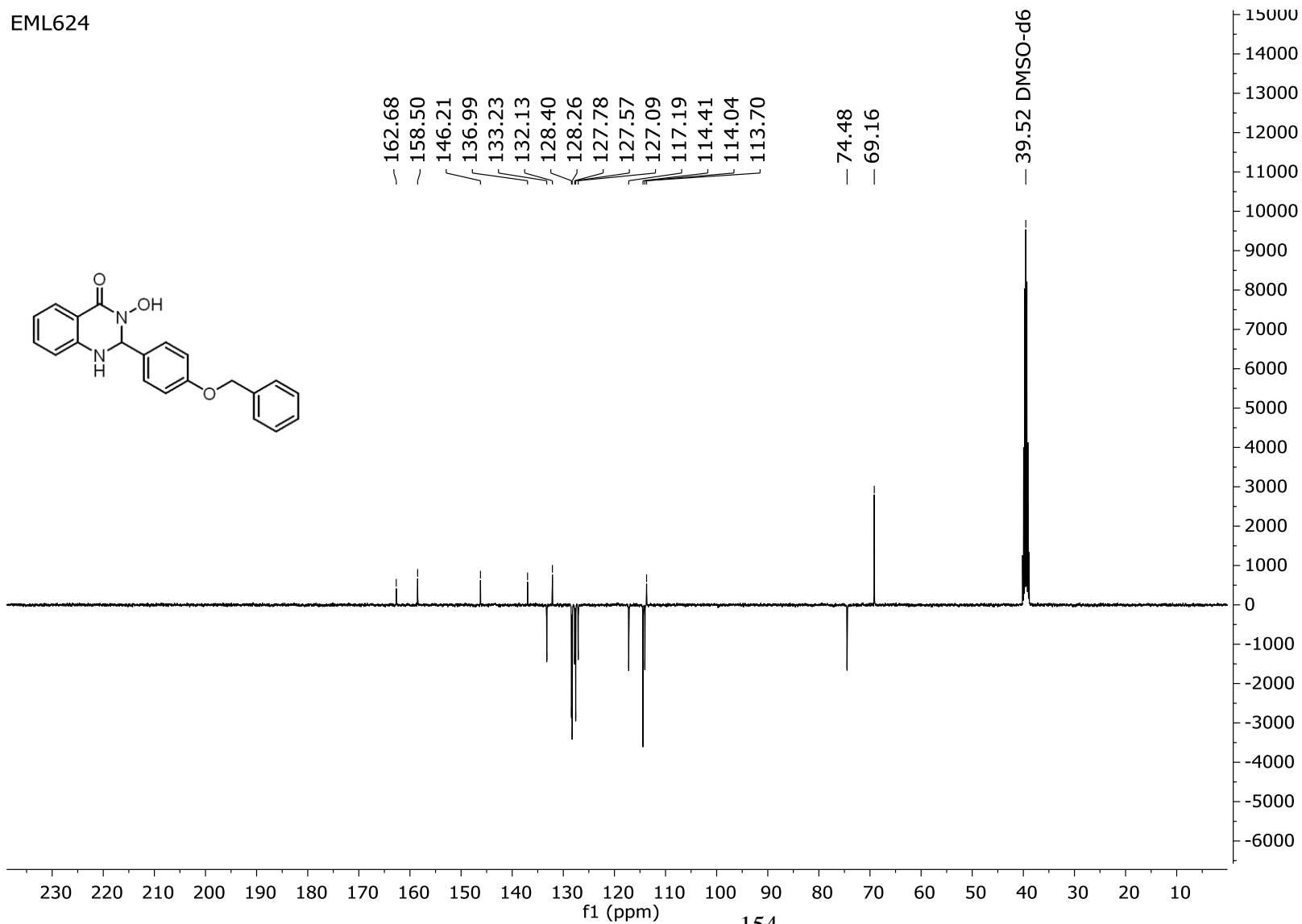
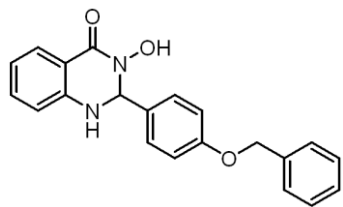
EML623



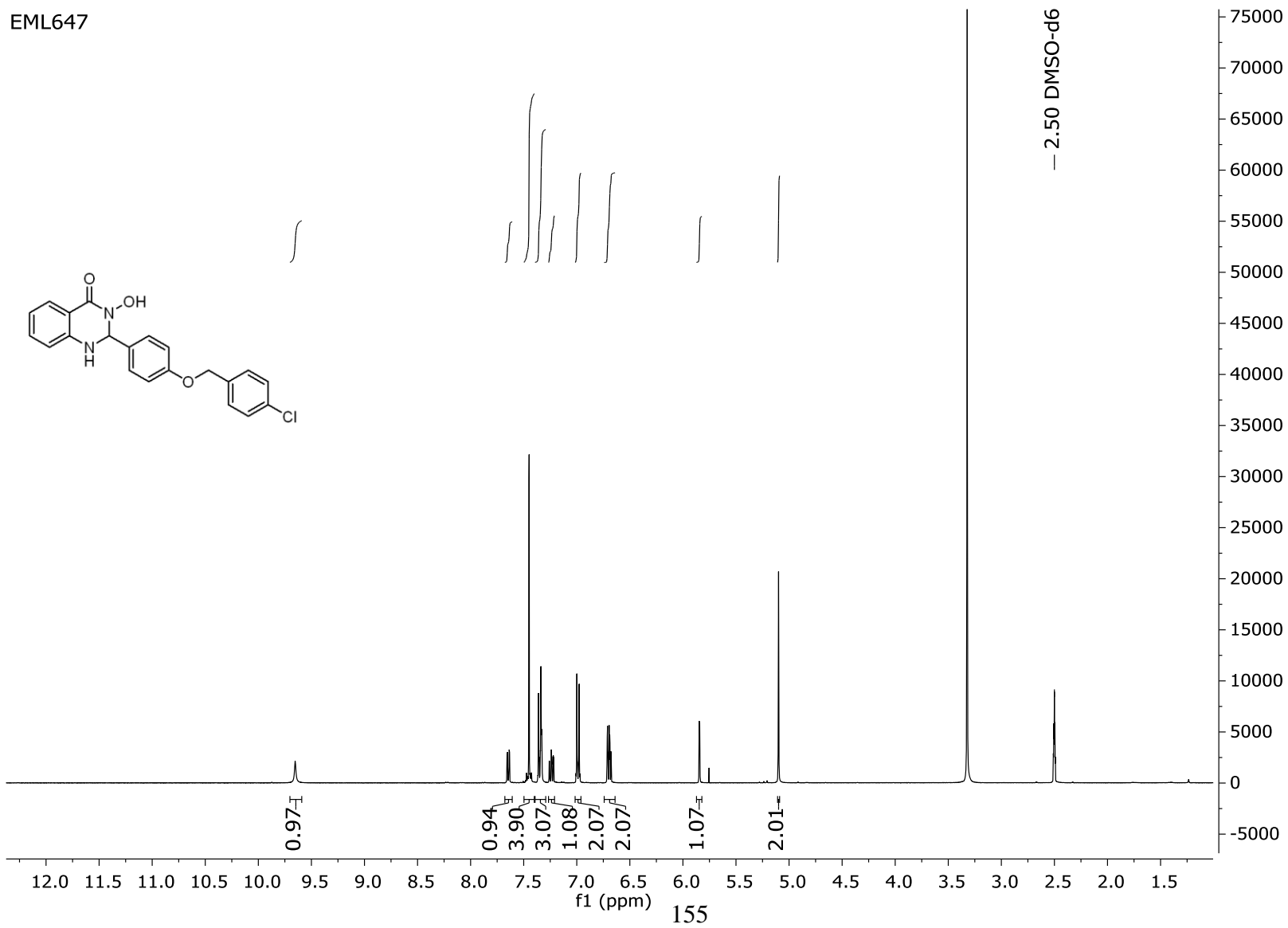
EML624



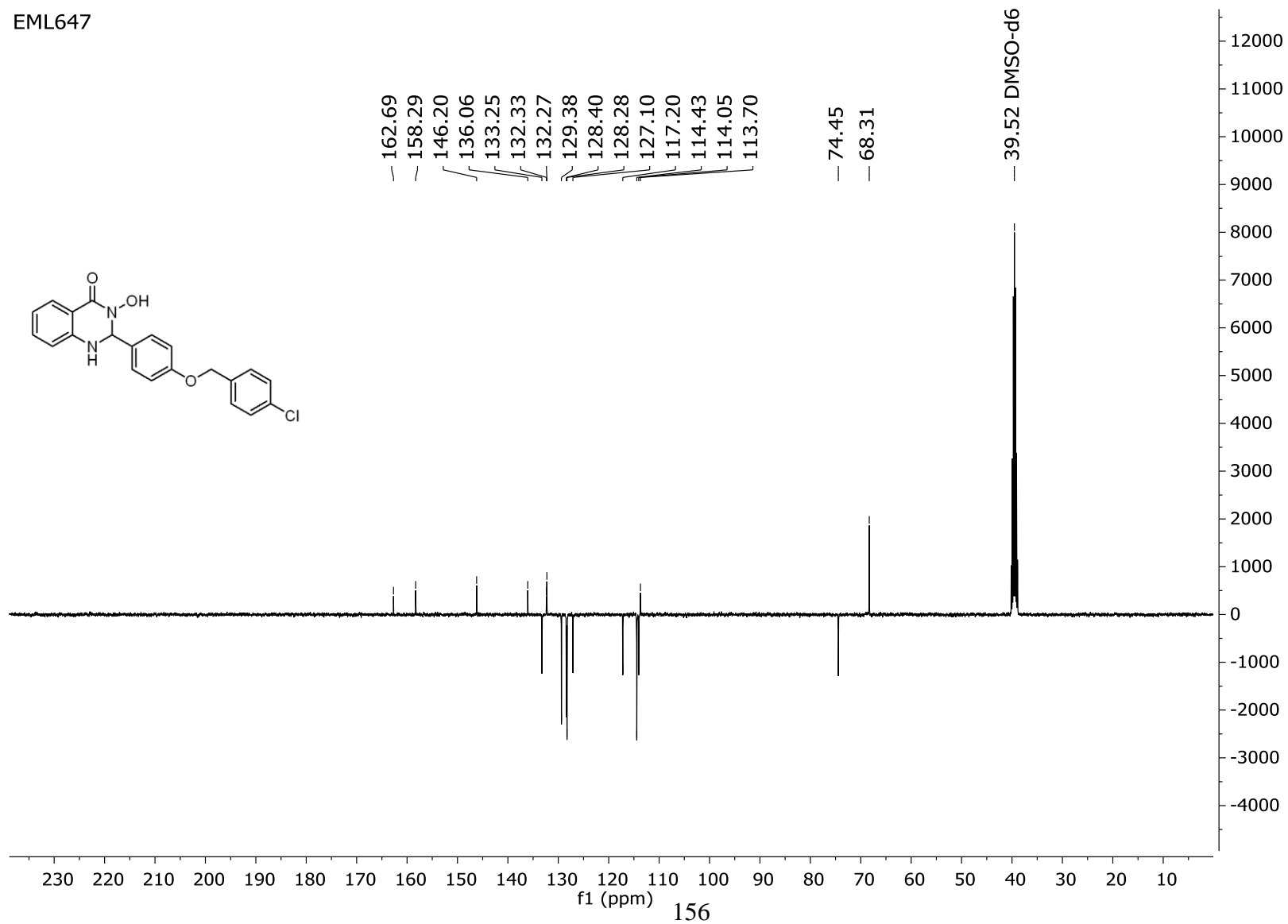
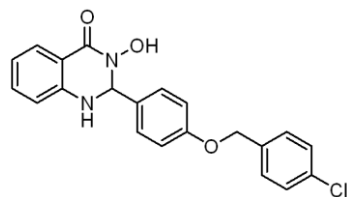
EML624



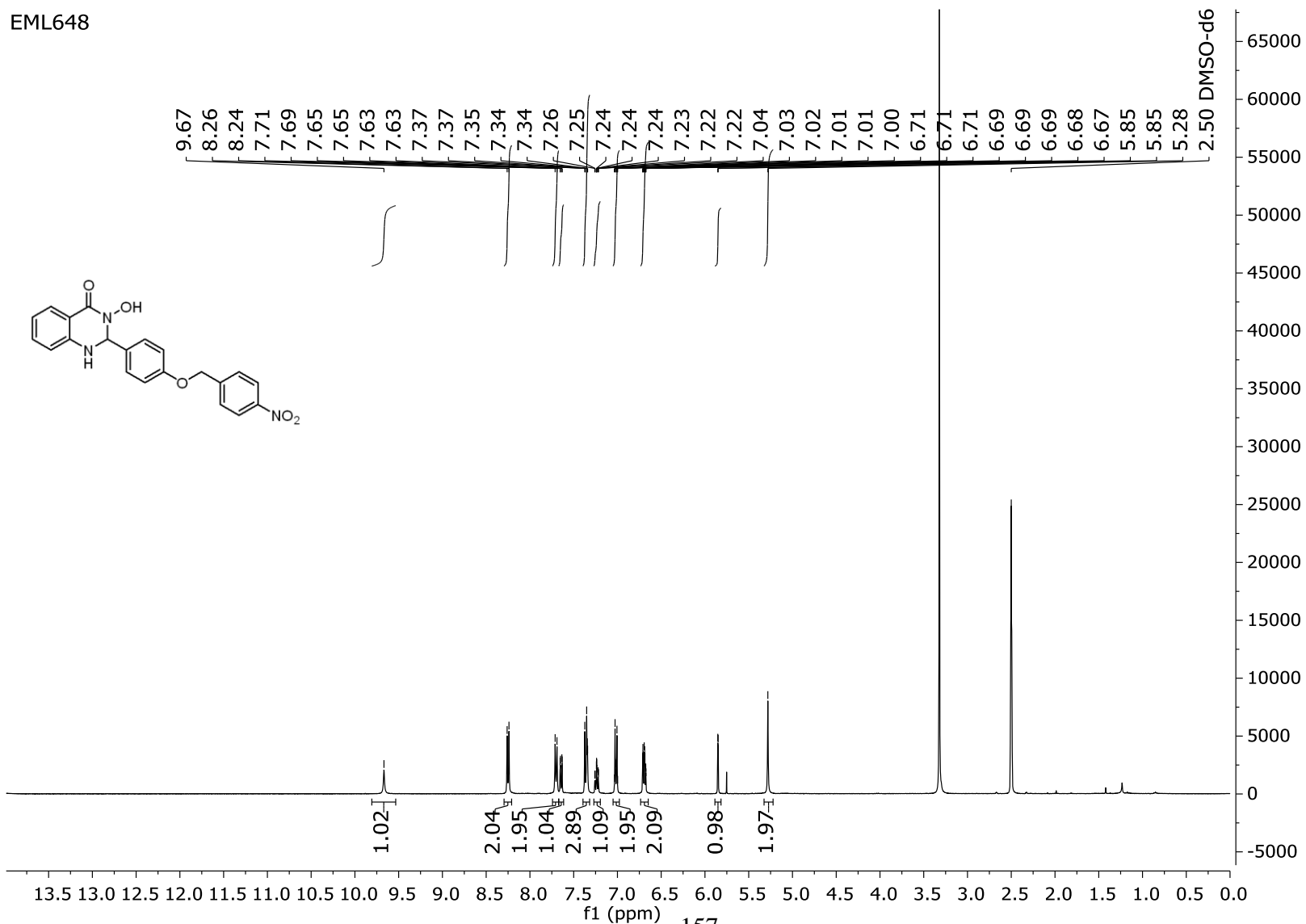
EML647



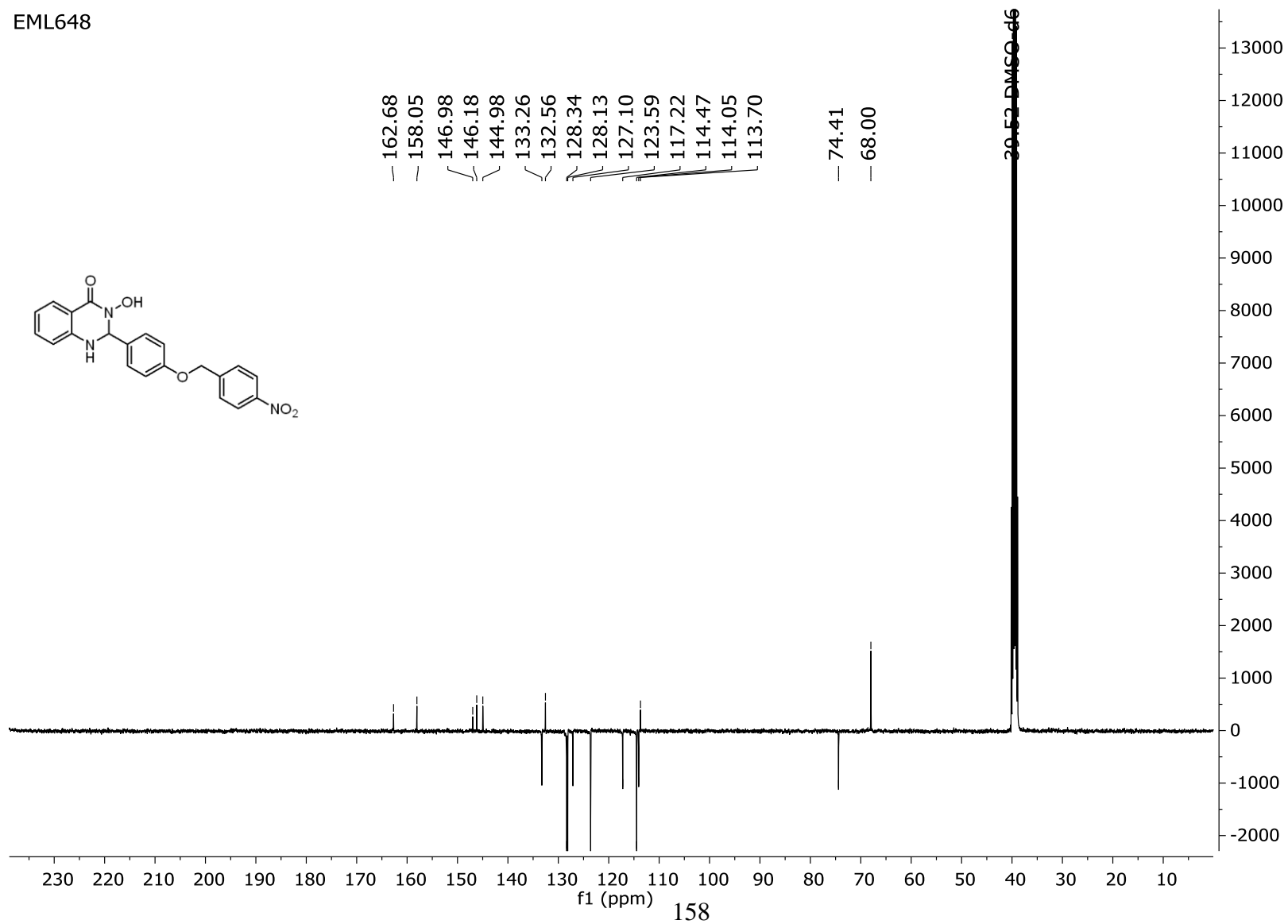
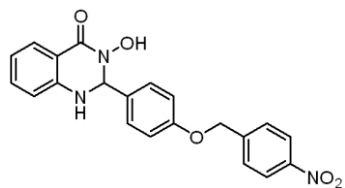
EML647



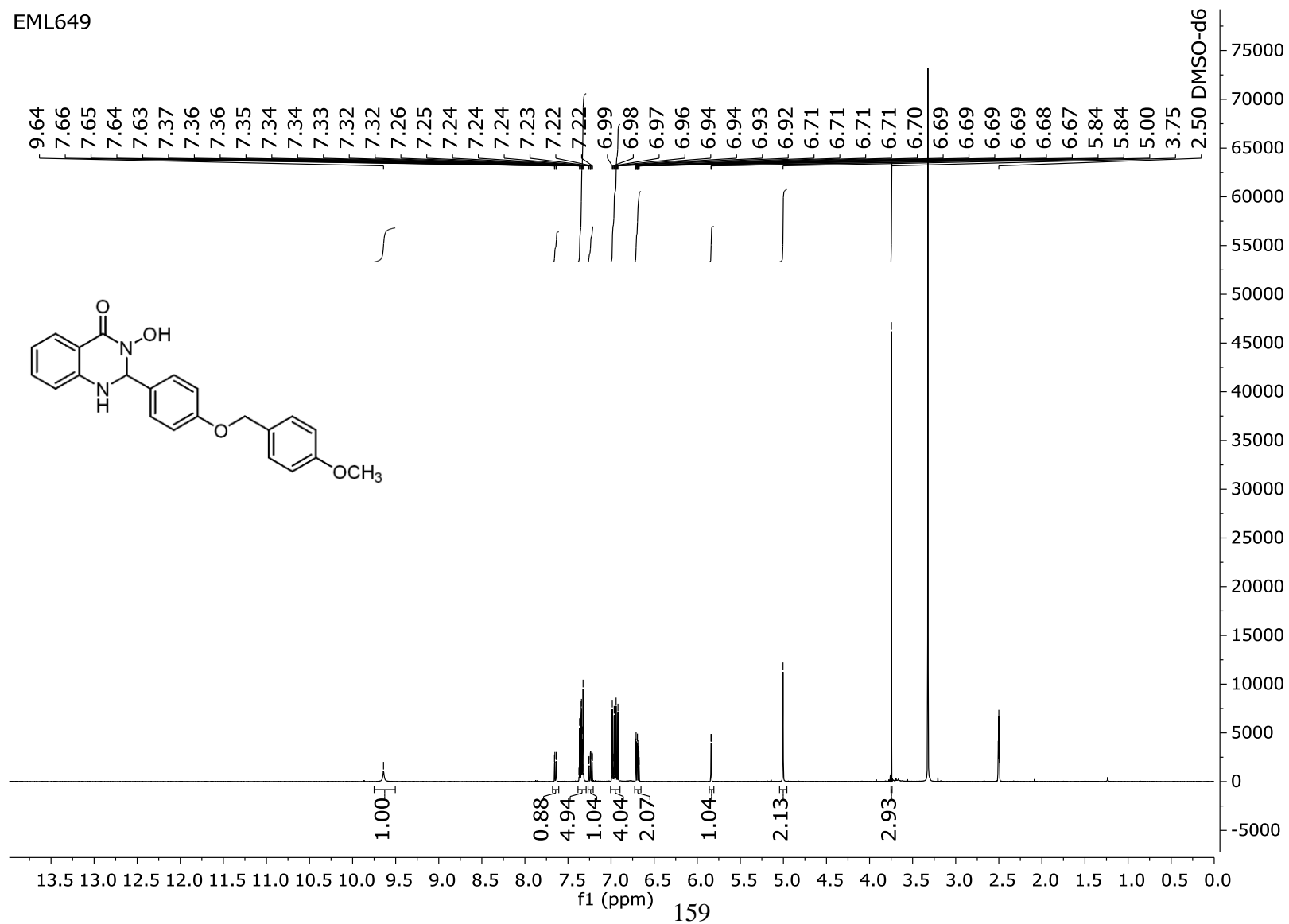
EML648



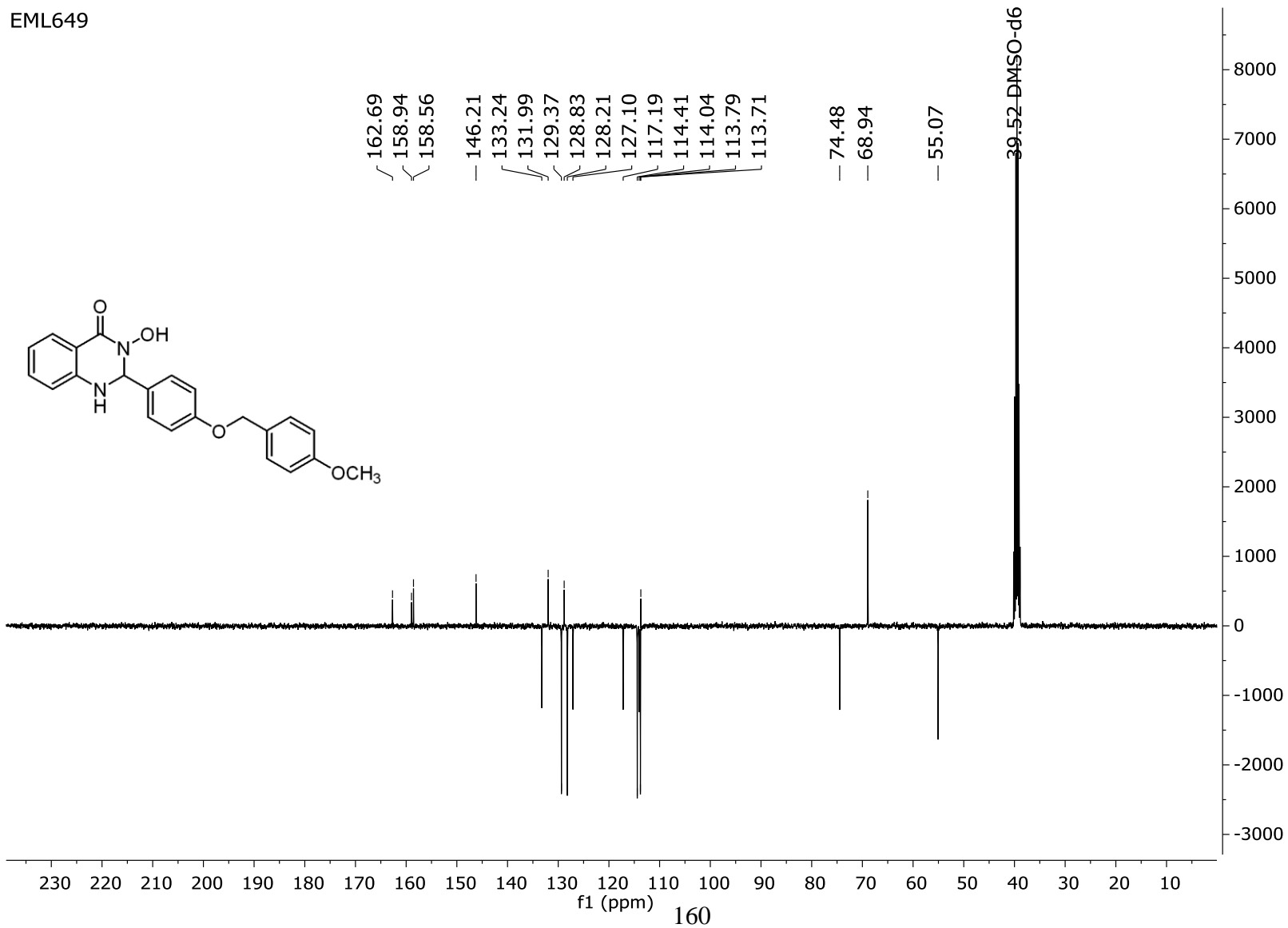
EML648



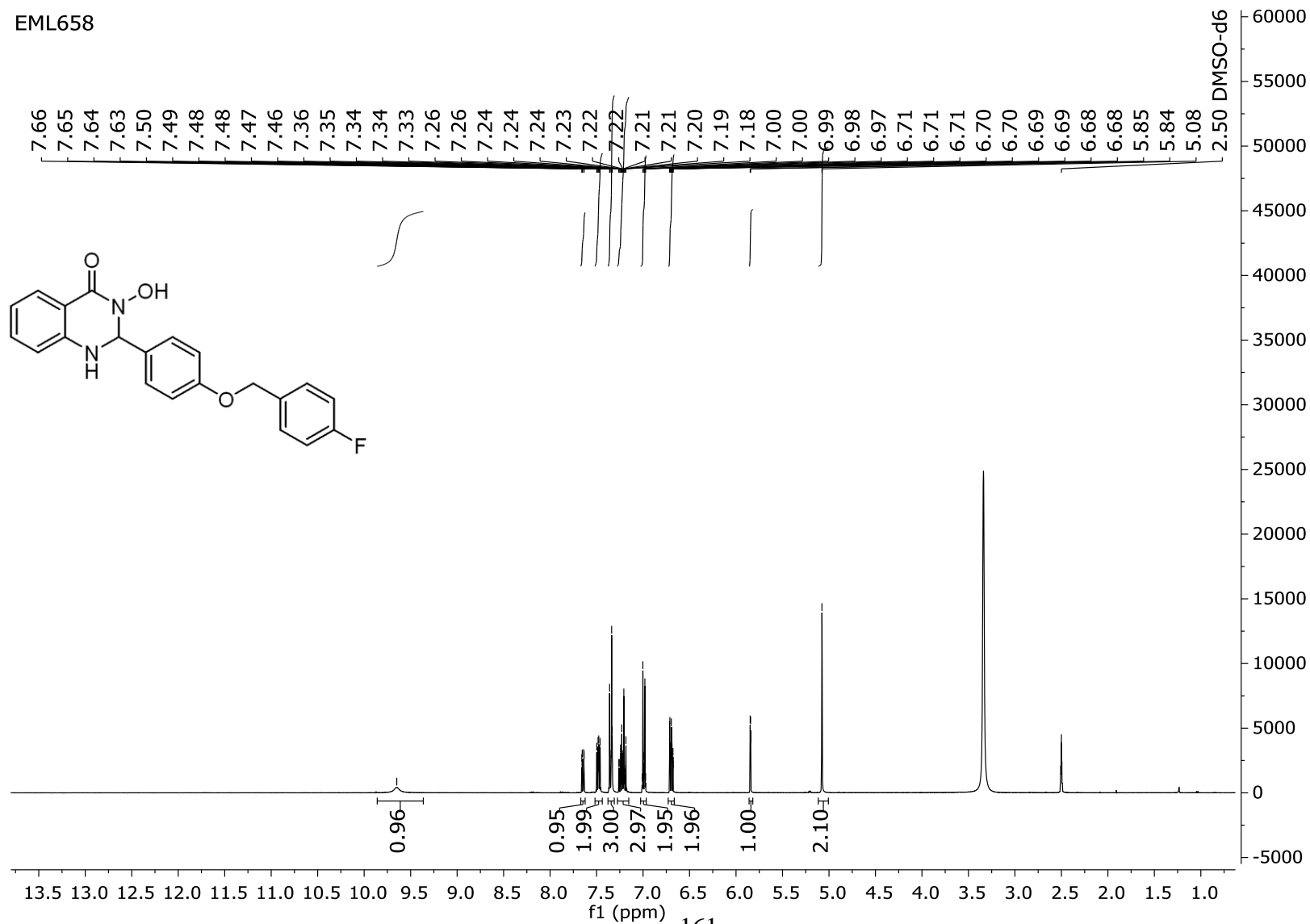
EML649



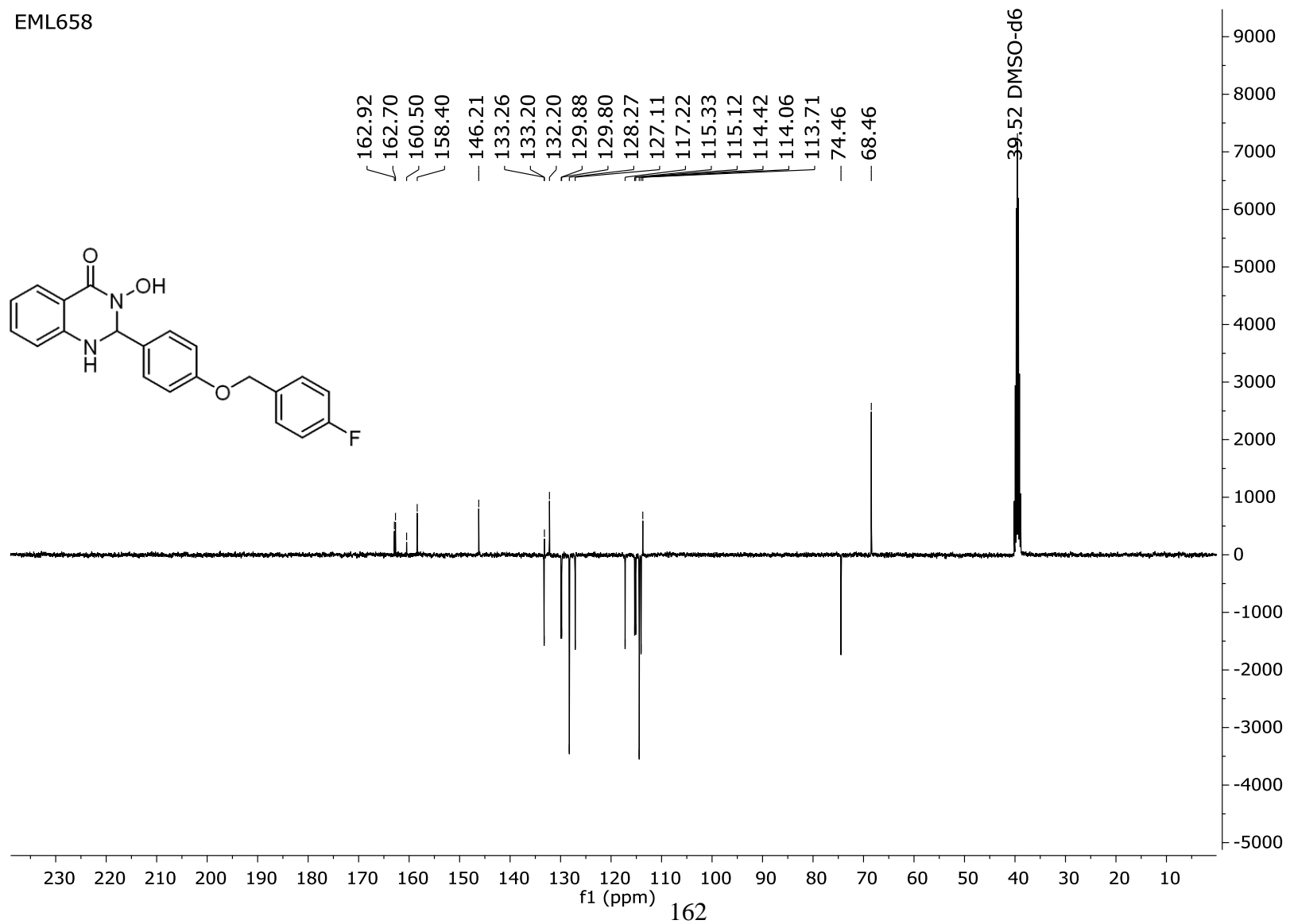
EML649



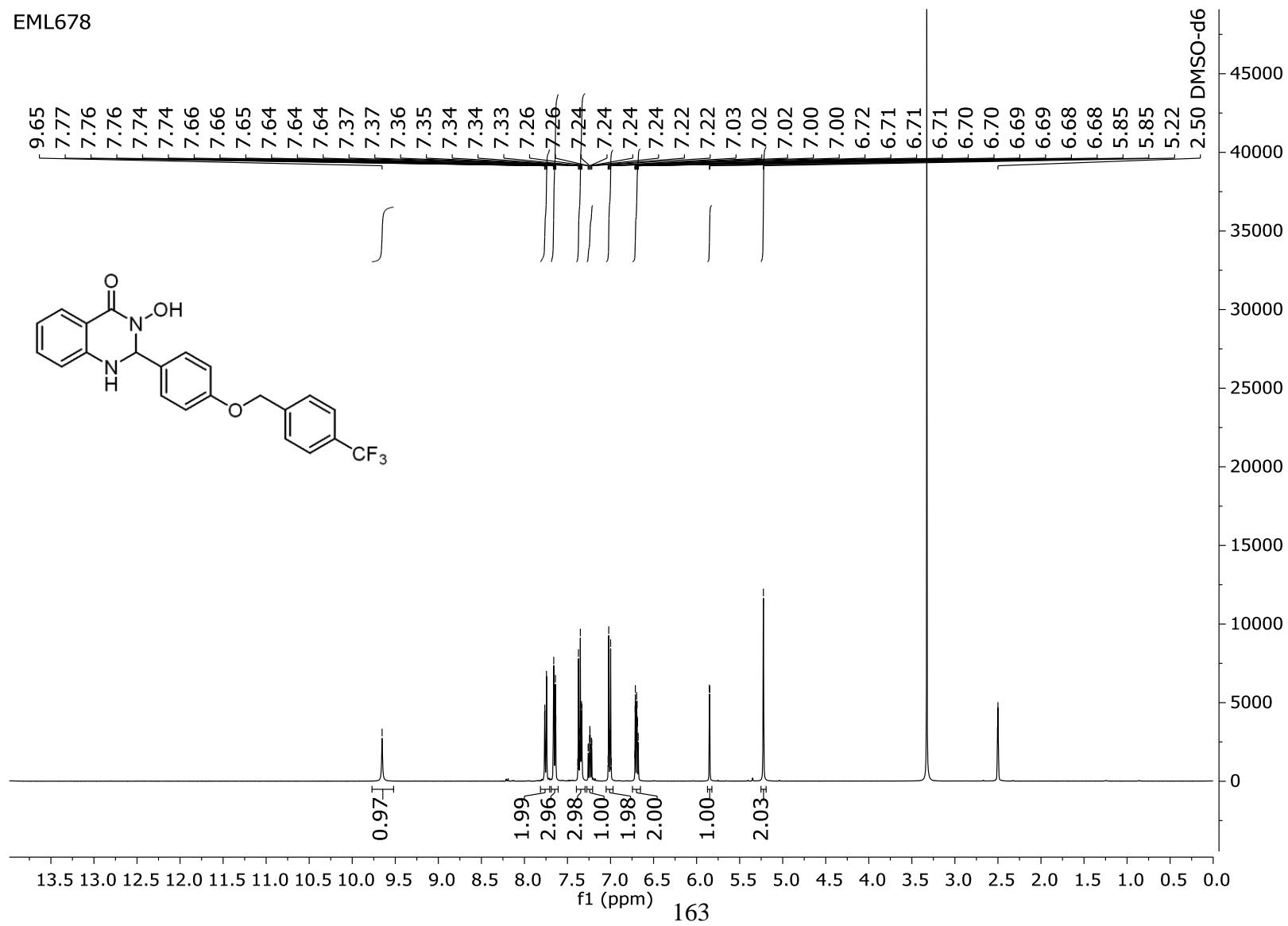
EML658



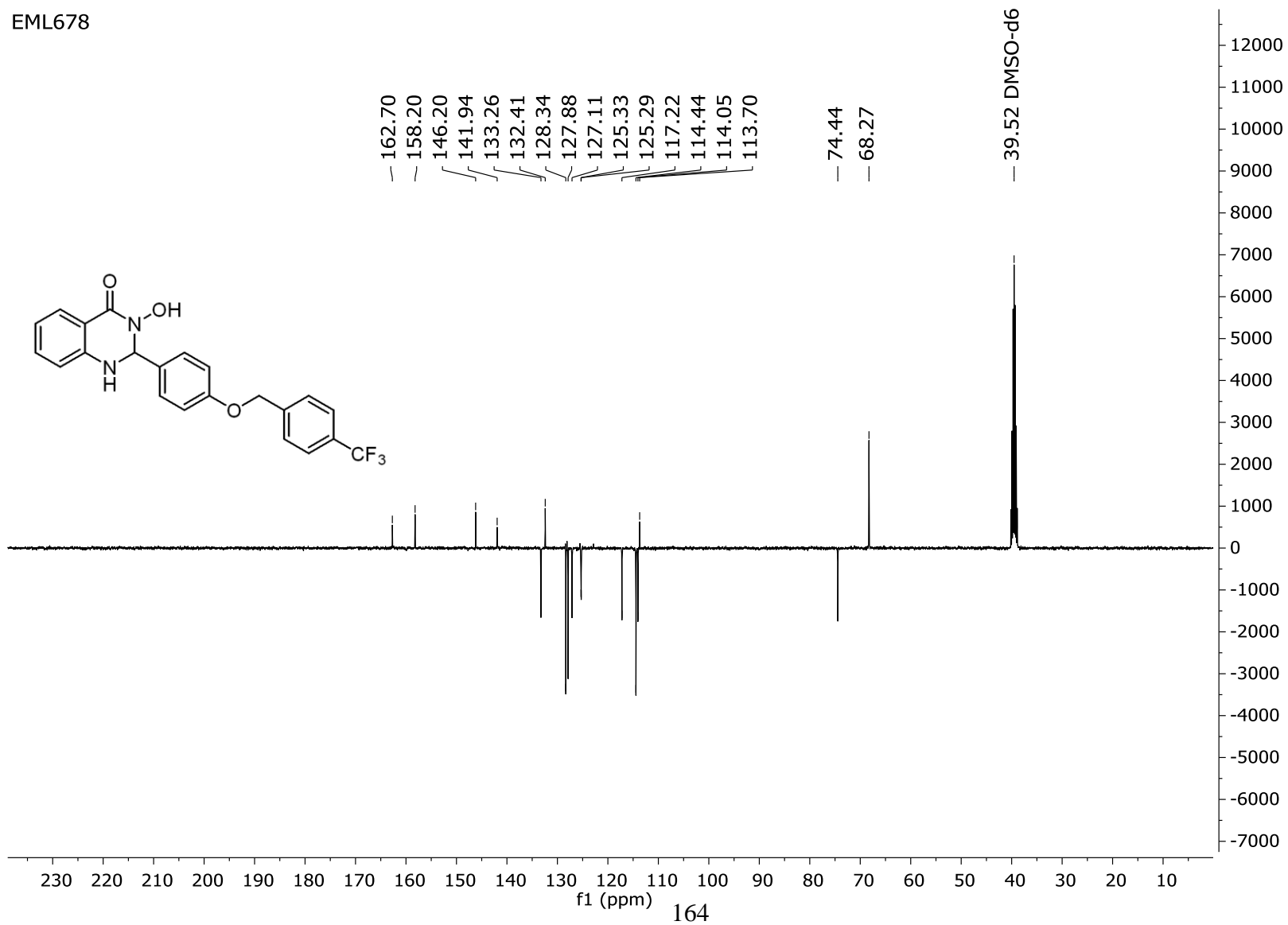
EML658



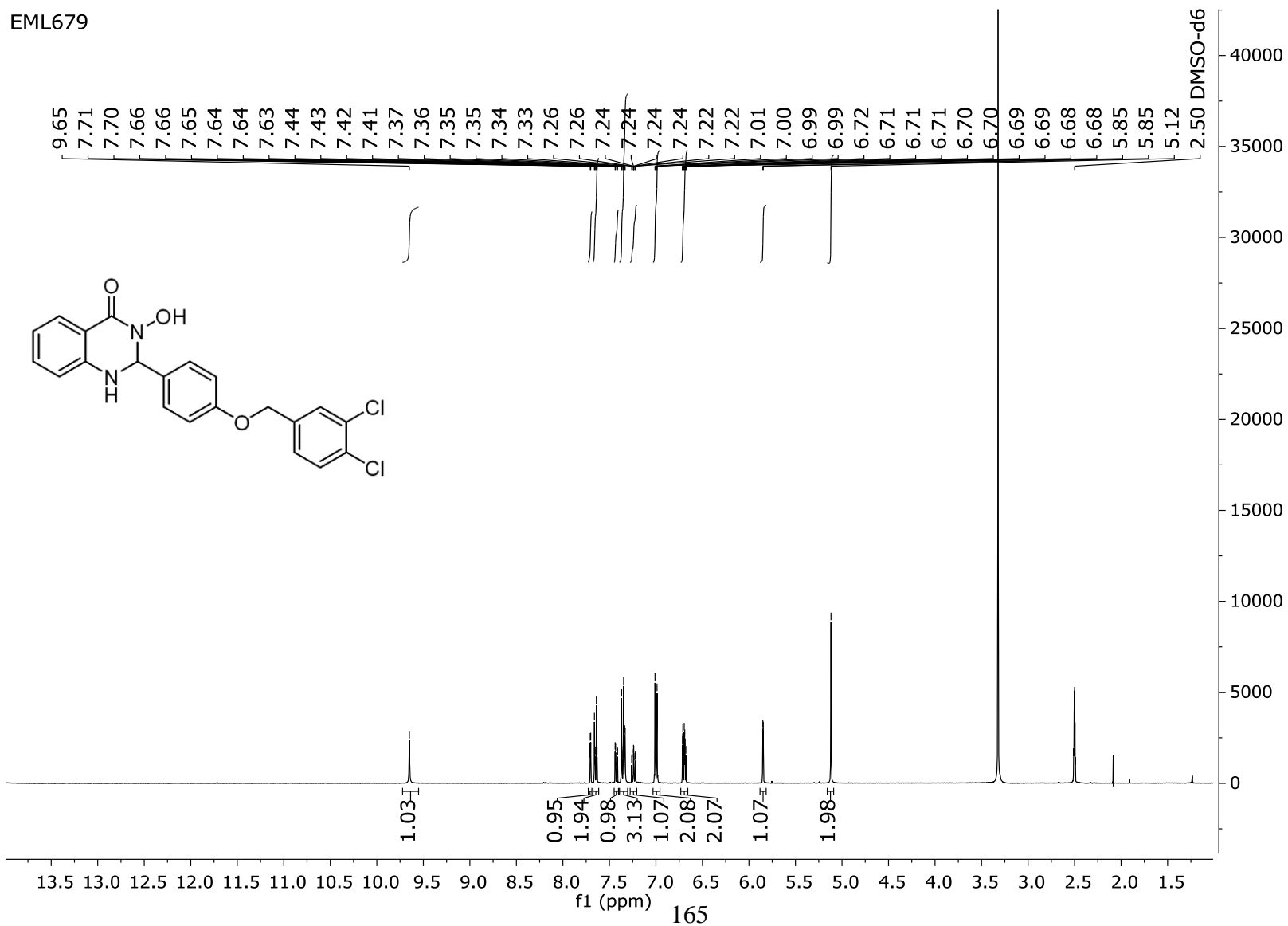
EML678



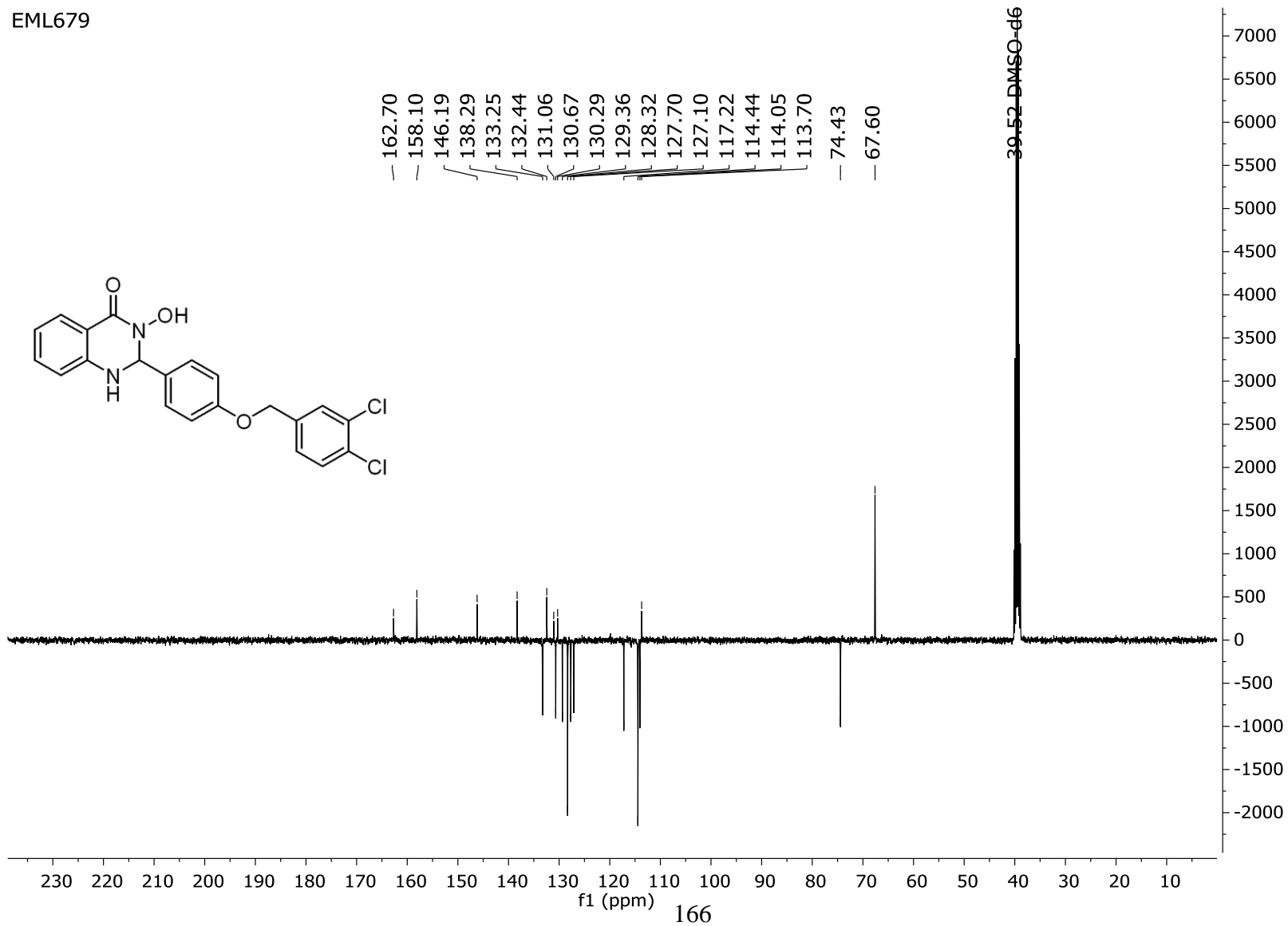
EML678



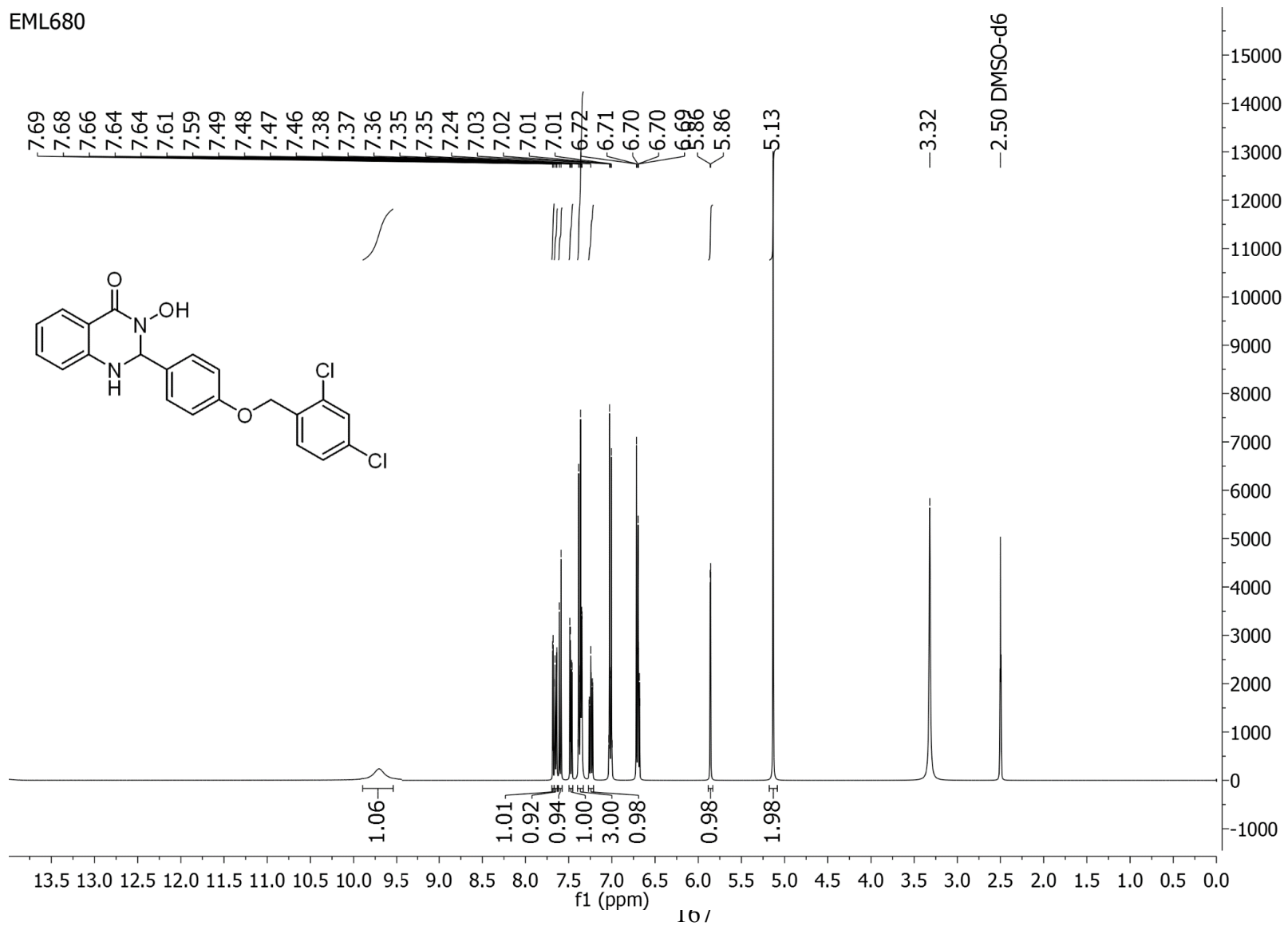
EML679



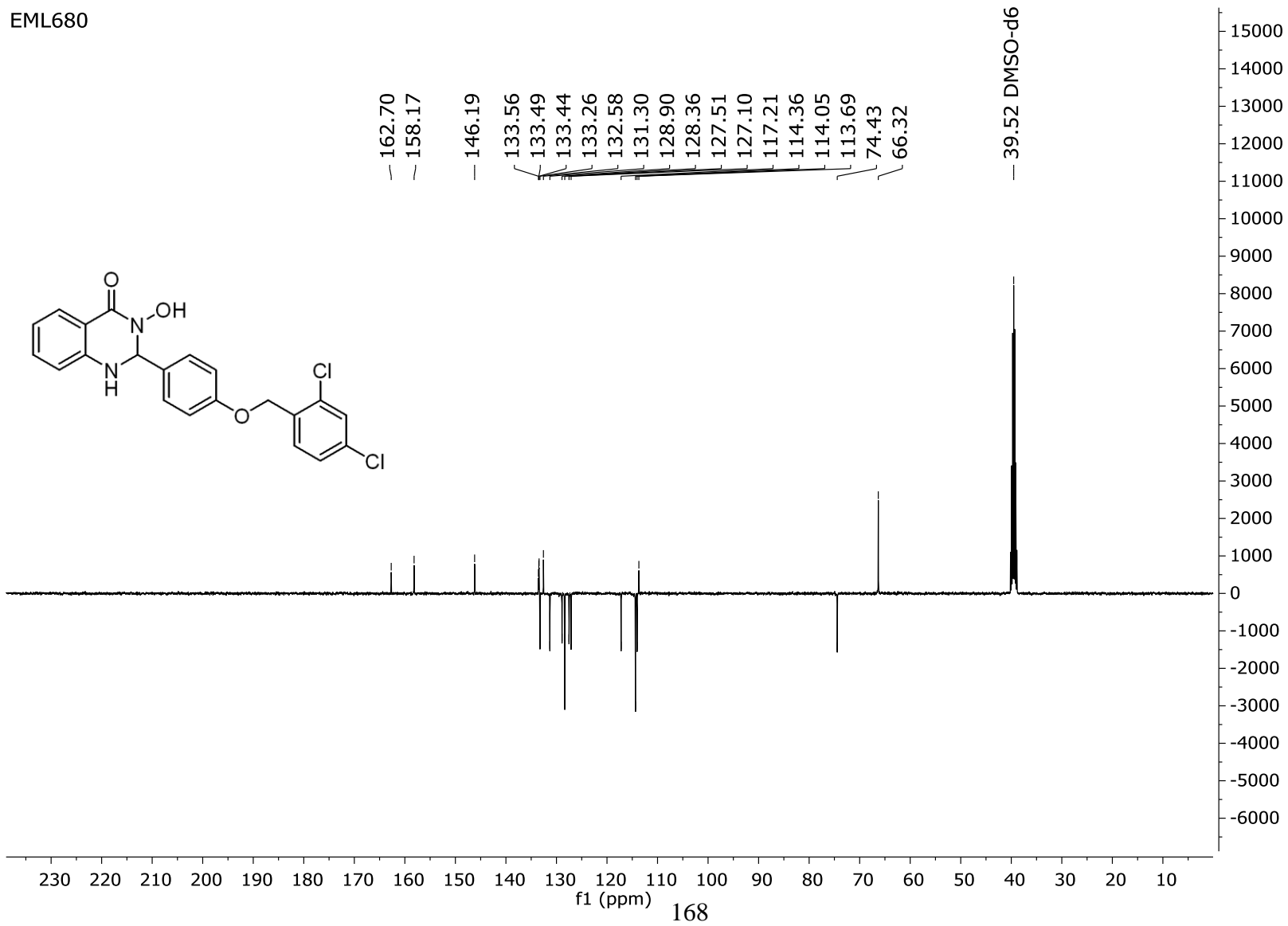
EML679



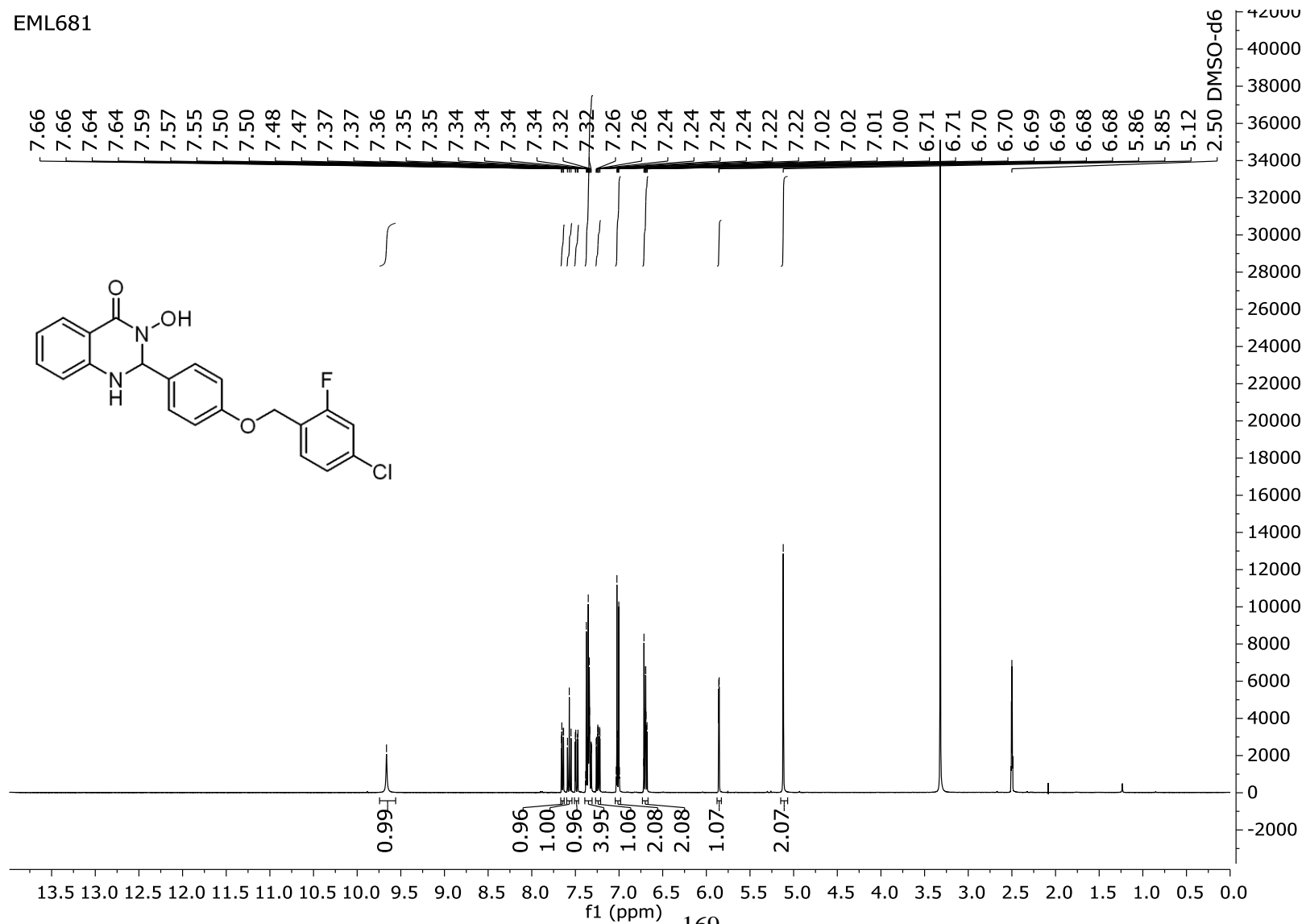
EML680



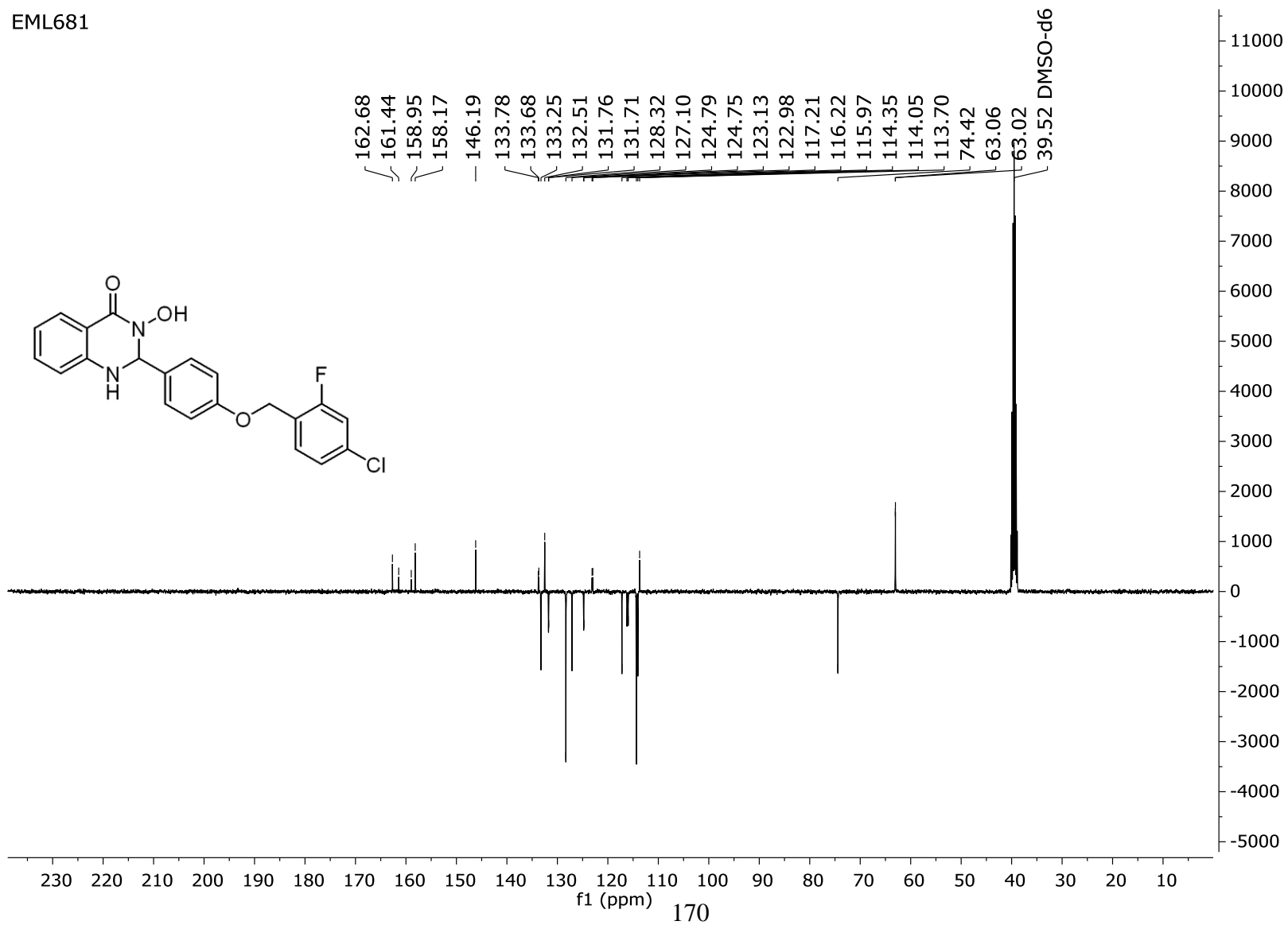
EML680



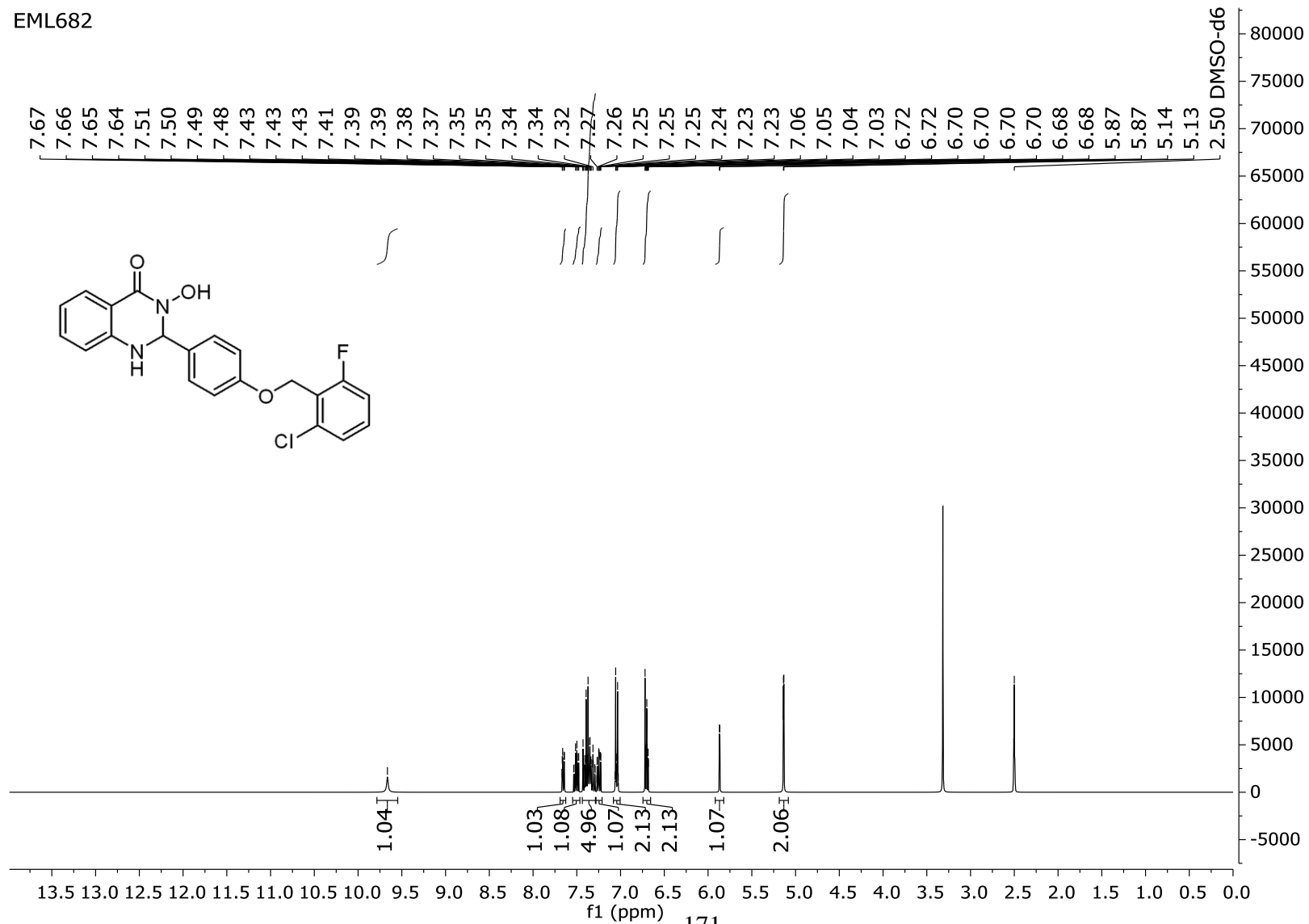
EML681



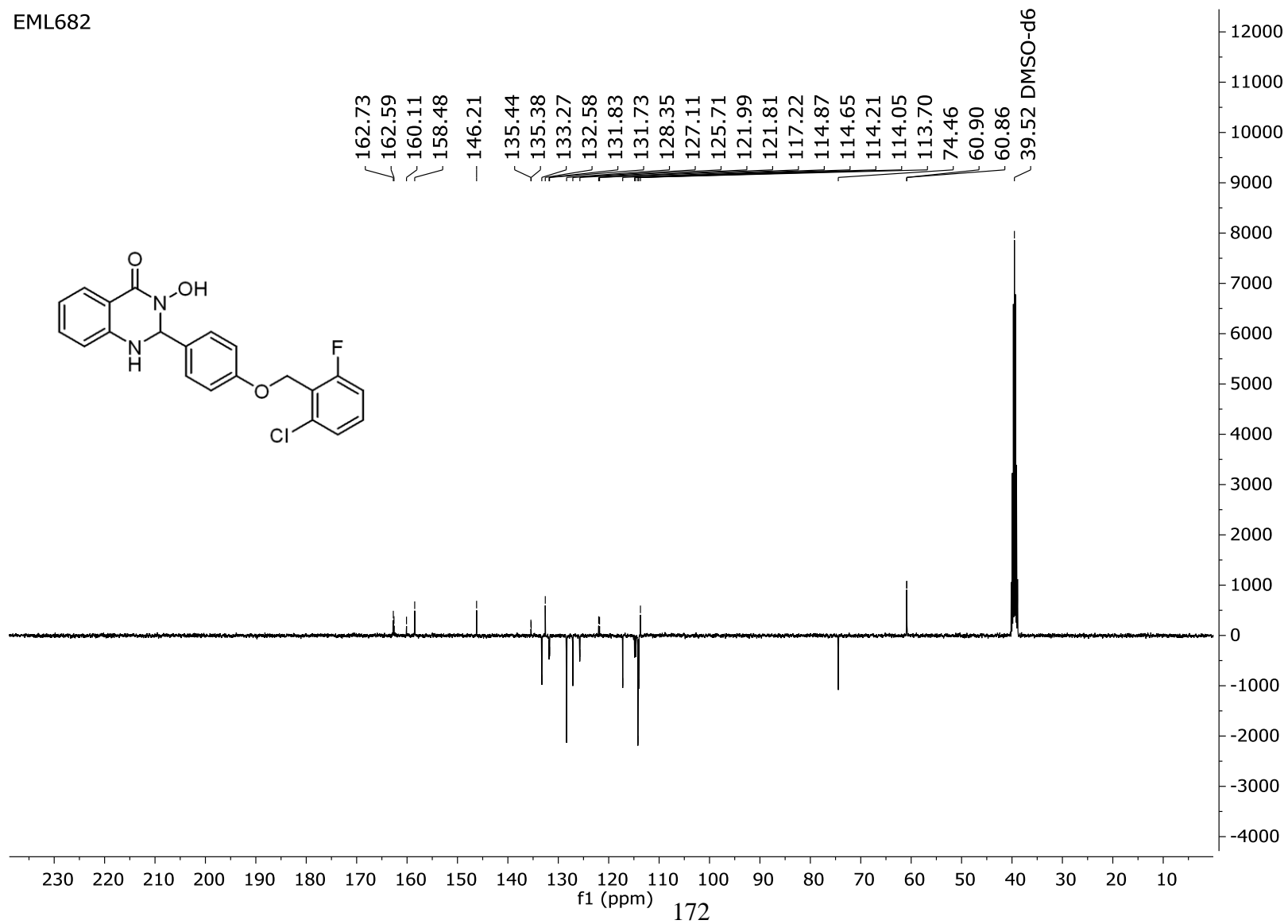
EML681



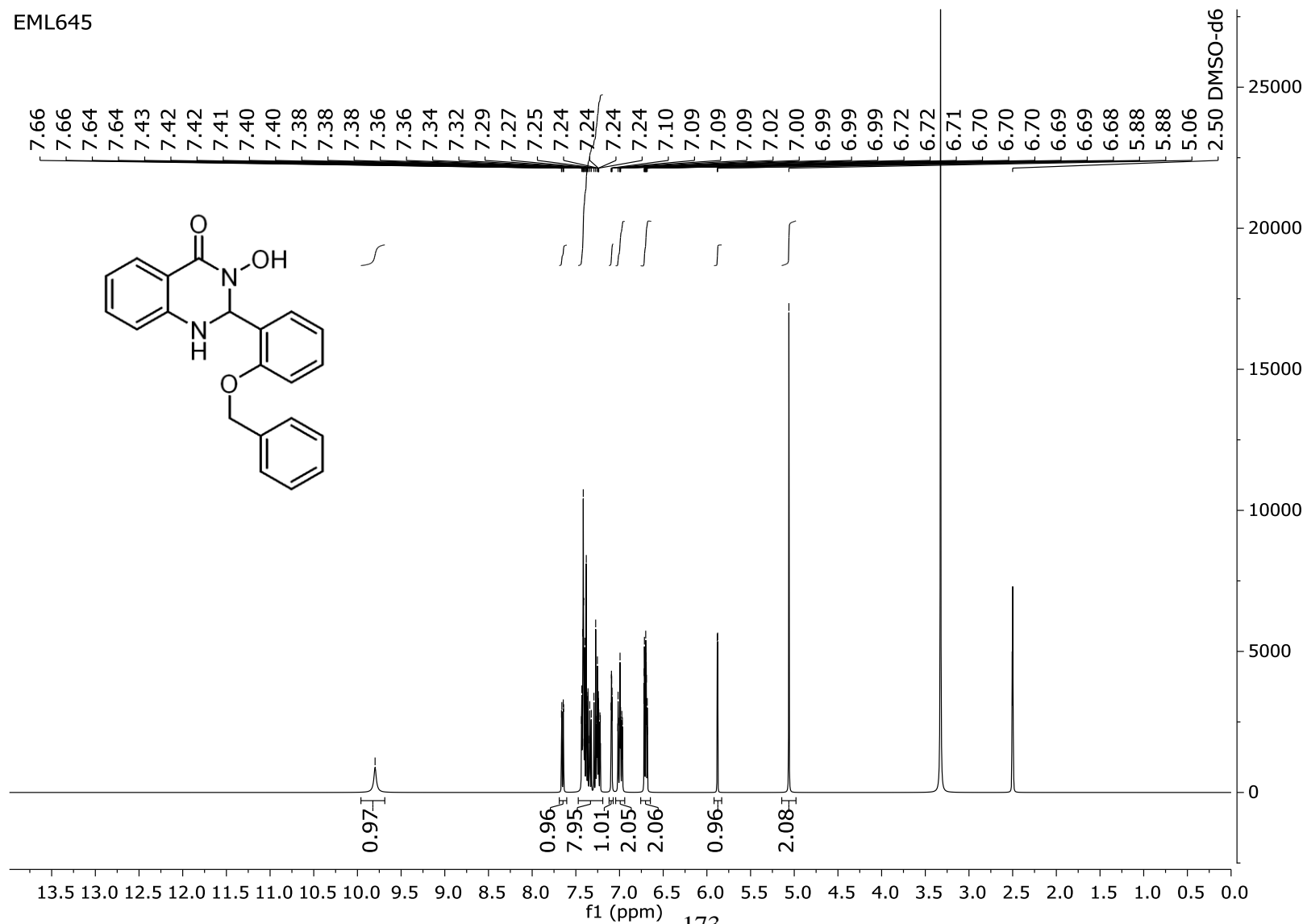
EML682



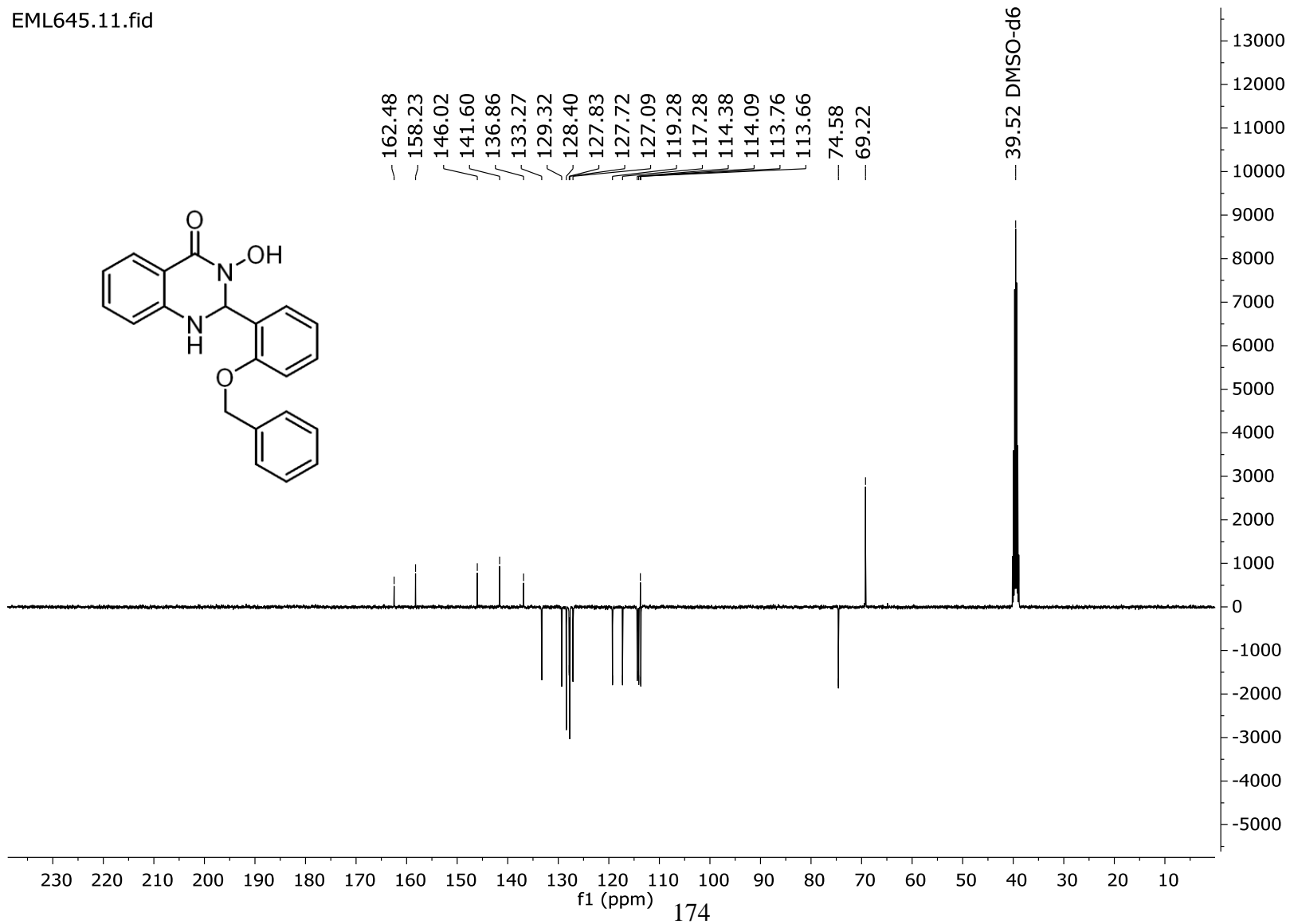
EML682

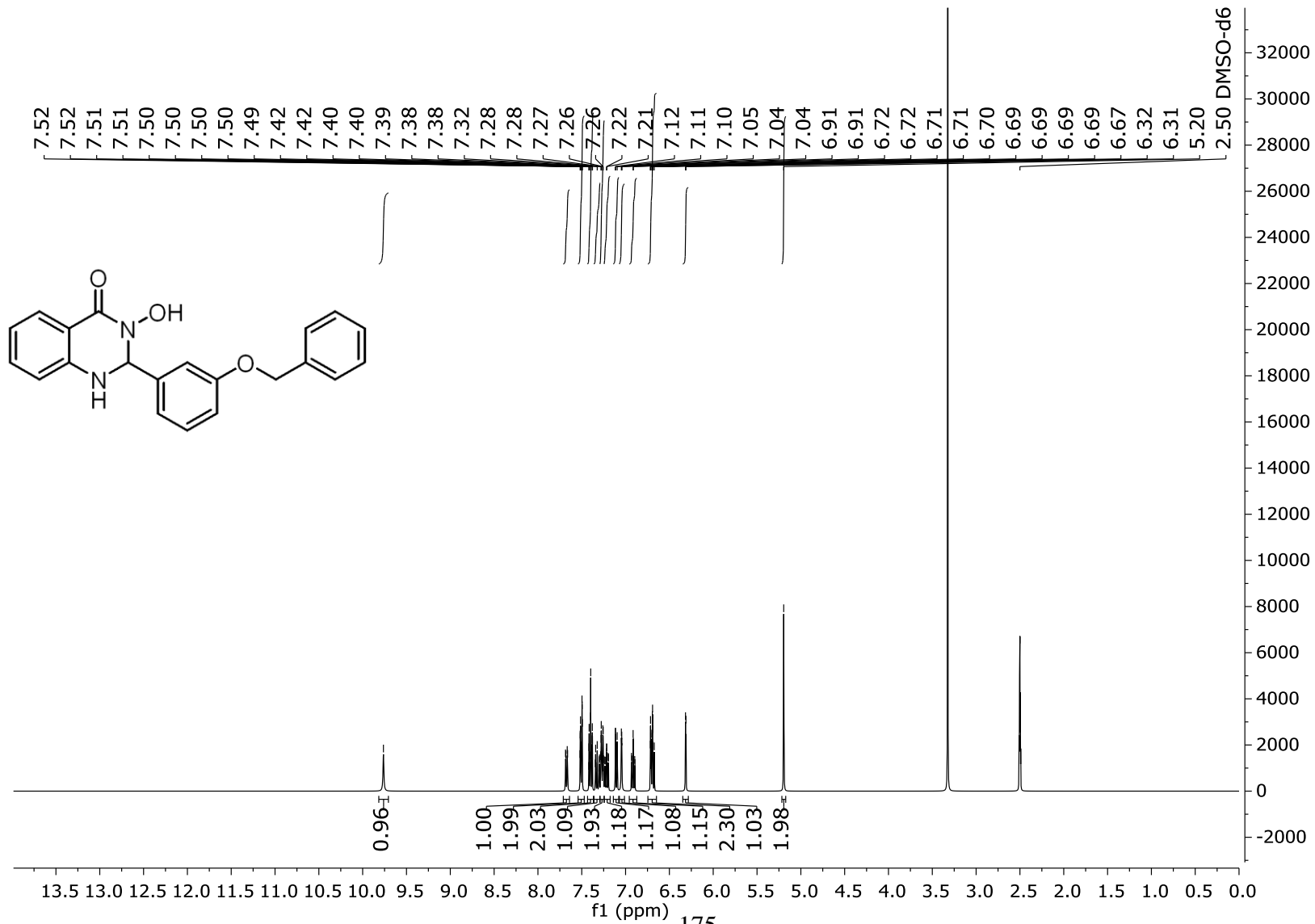


EML645

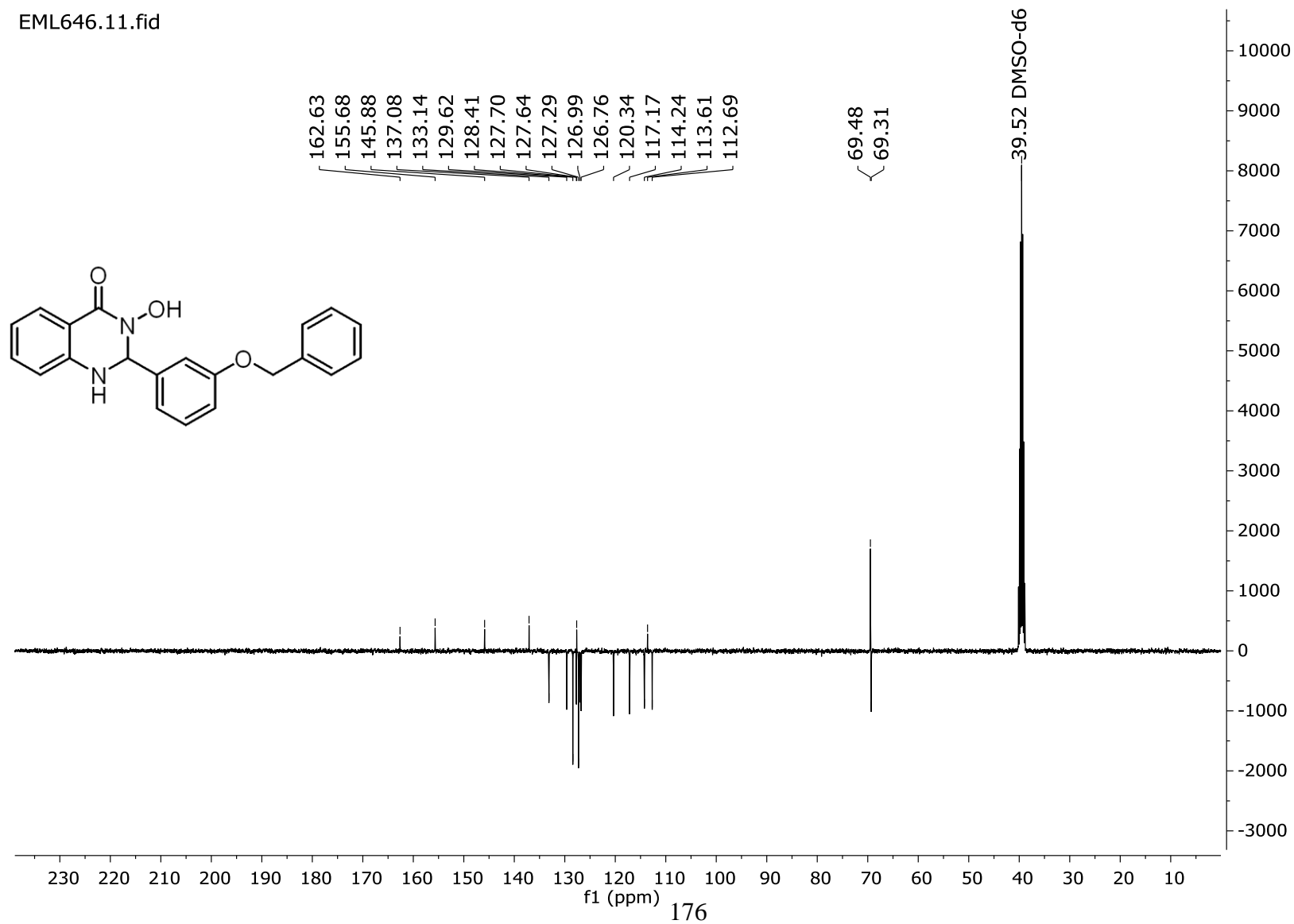


EML645.11.fid

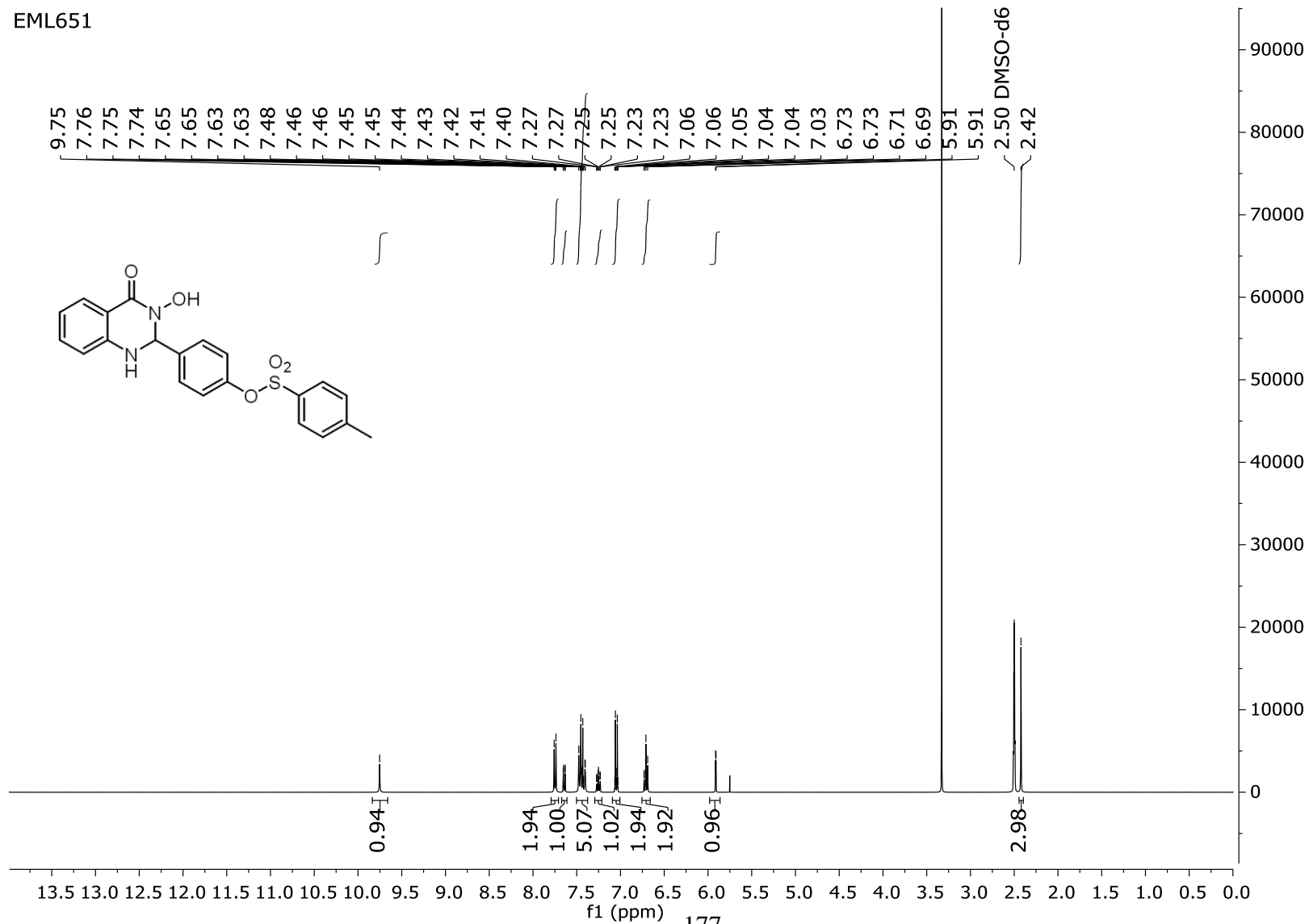




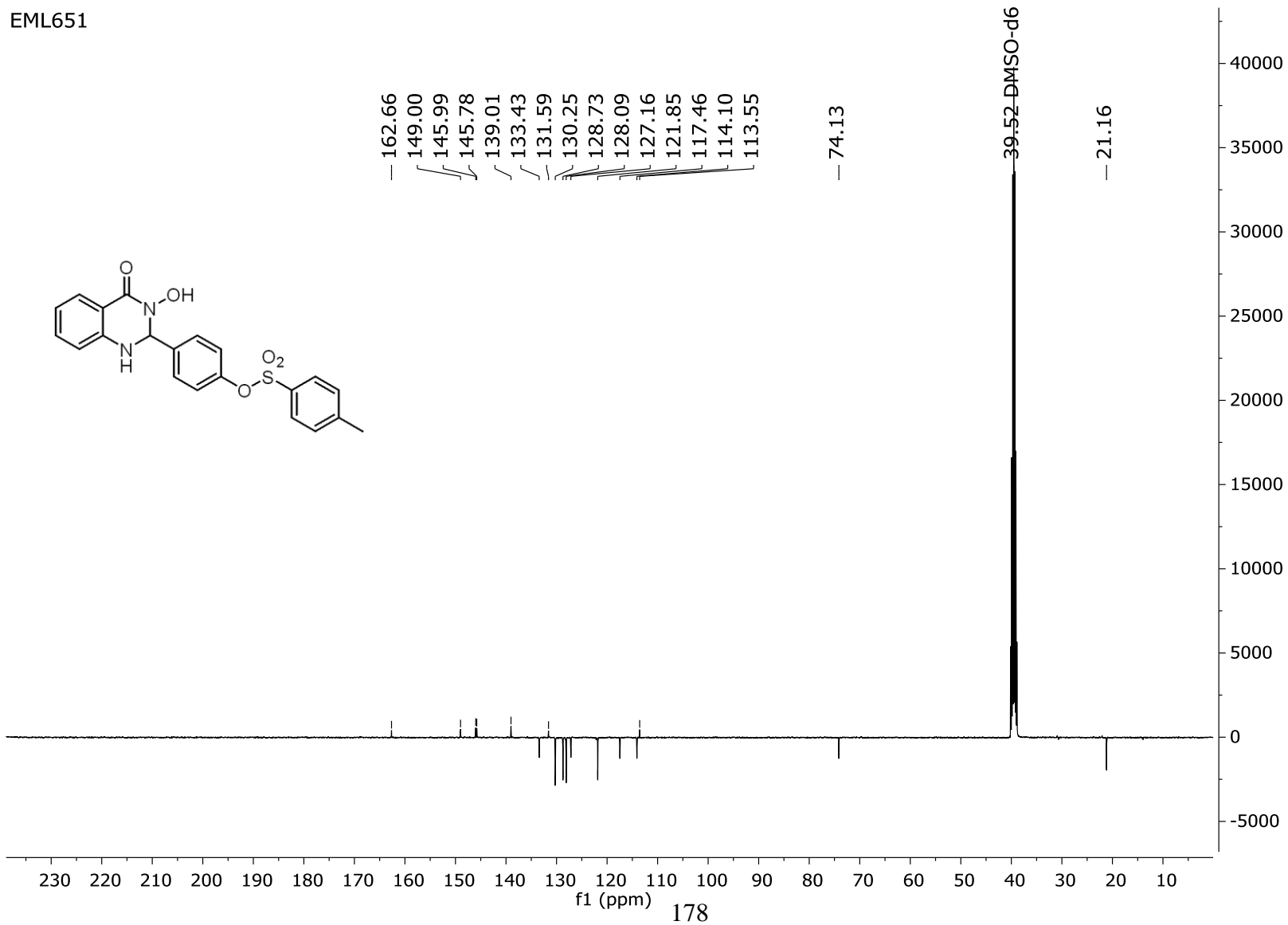
EML646.11.fid



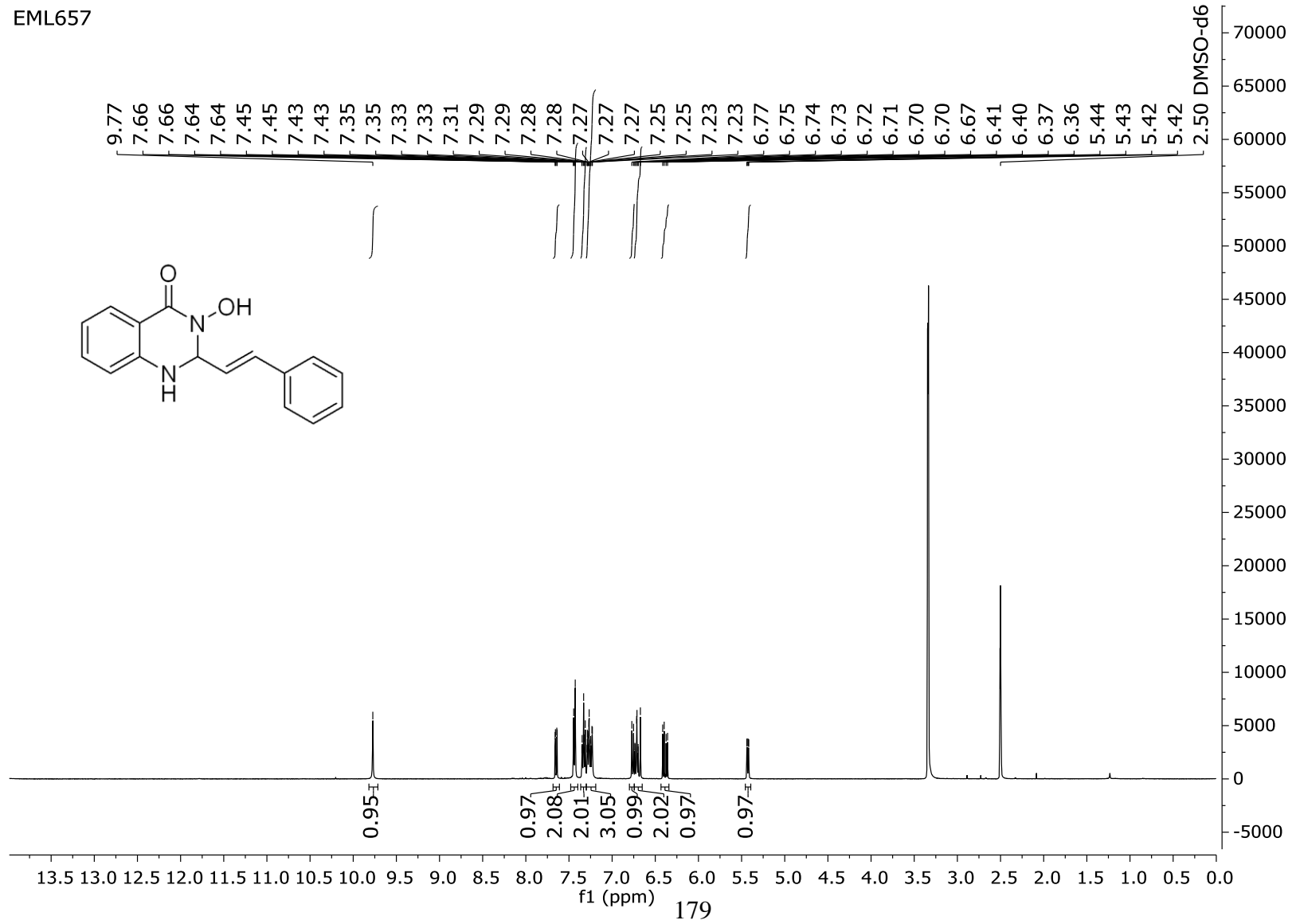
EML651



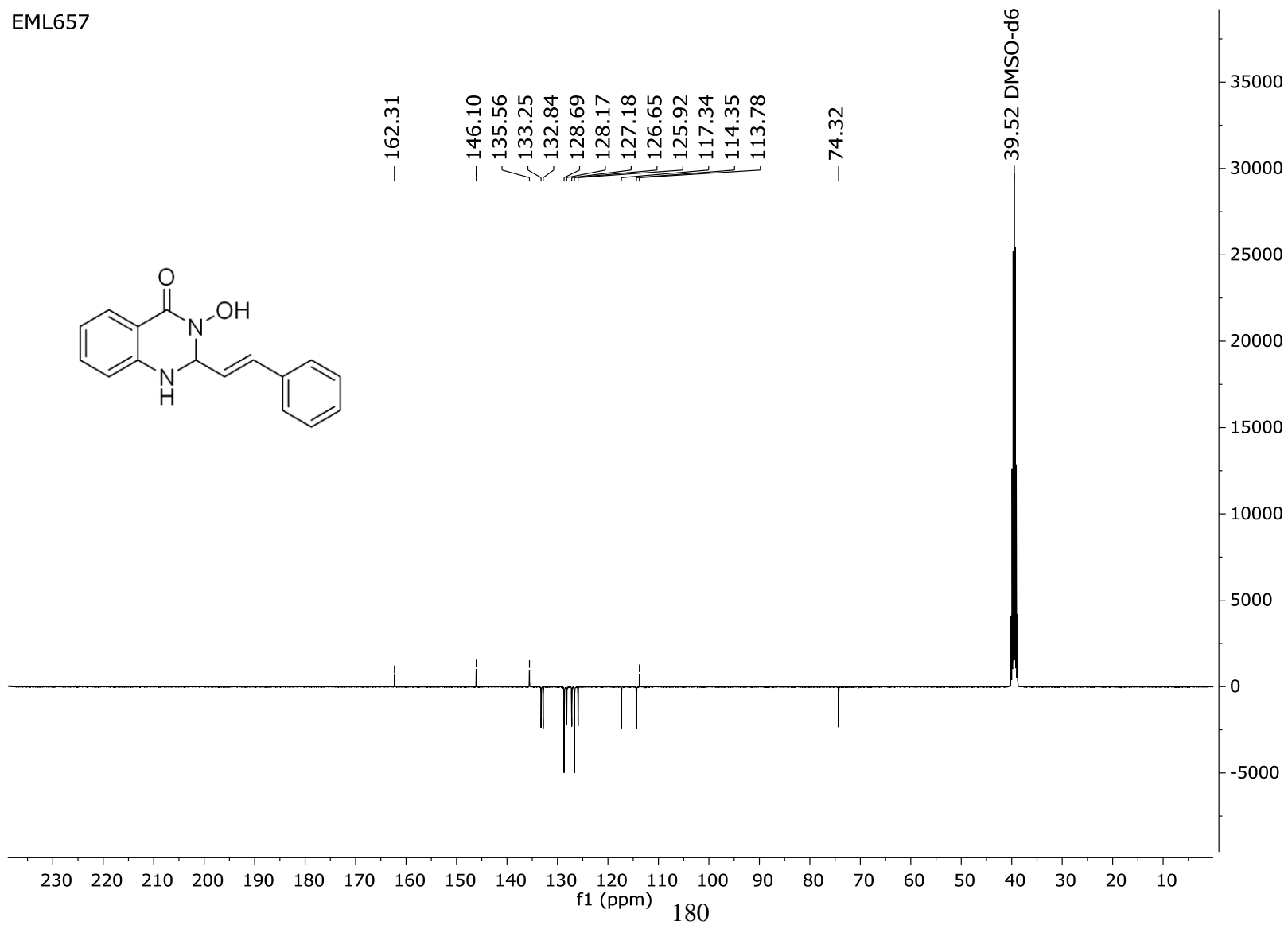
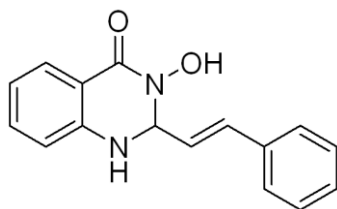
EML651



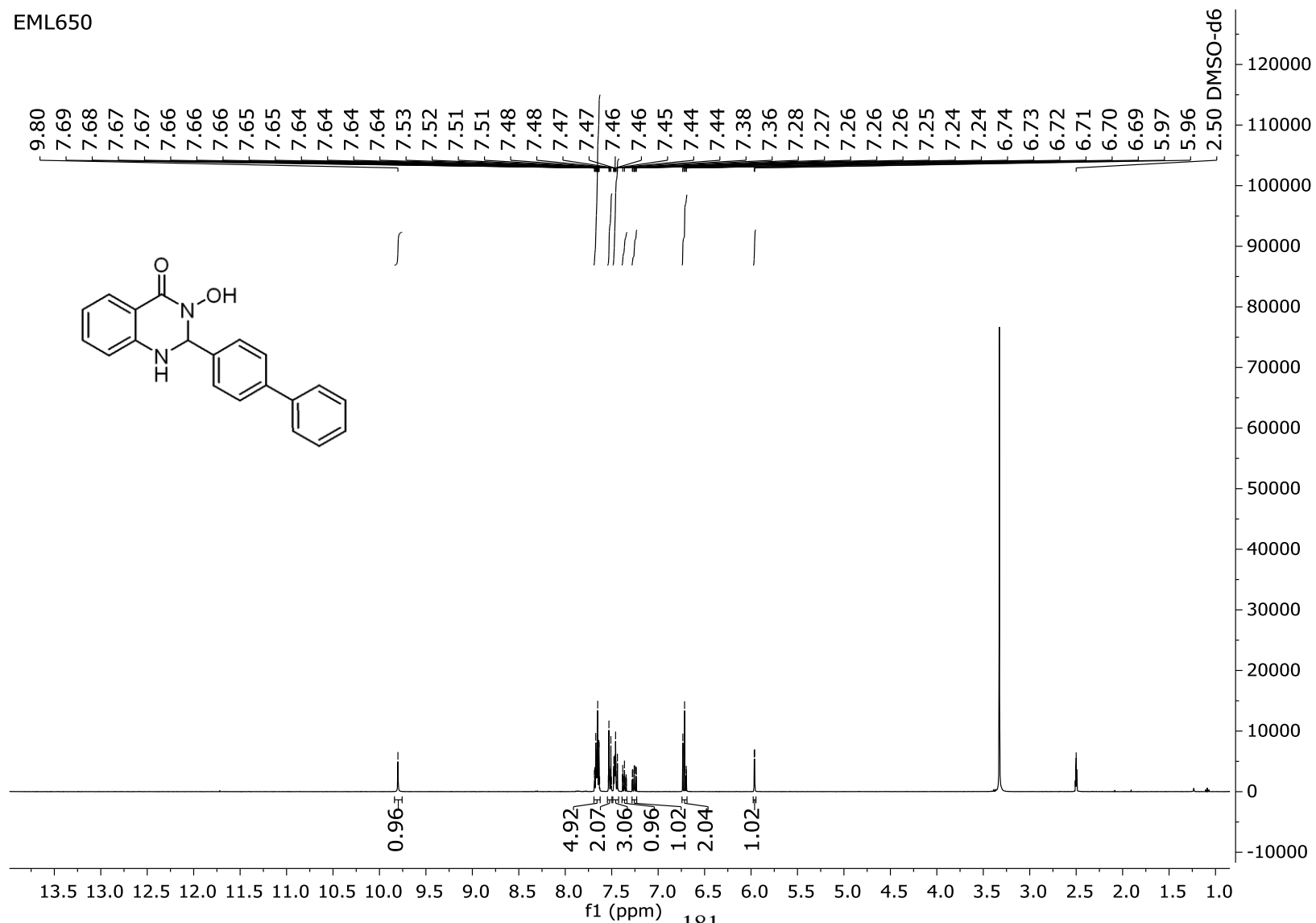
EML657



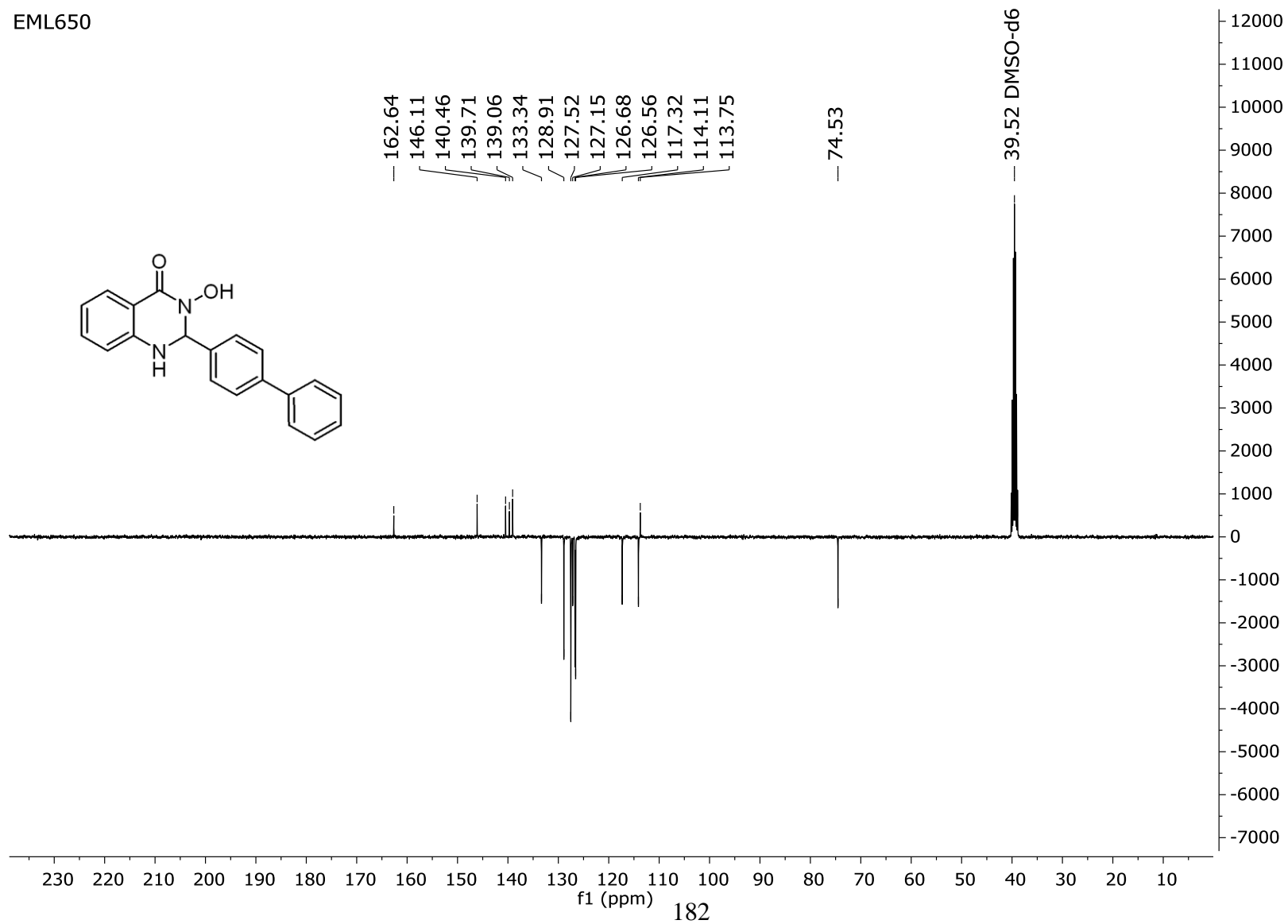
EML657



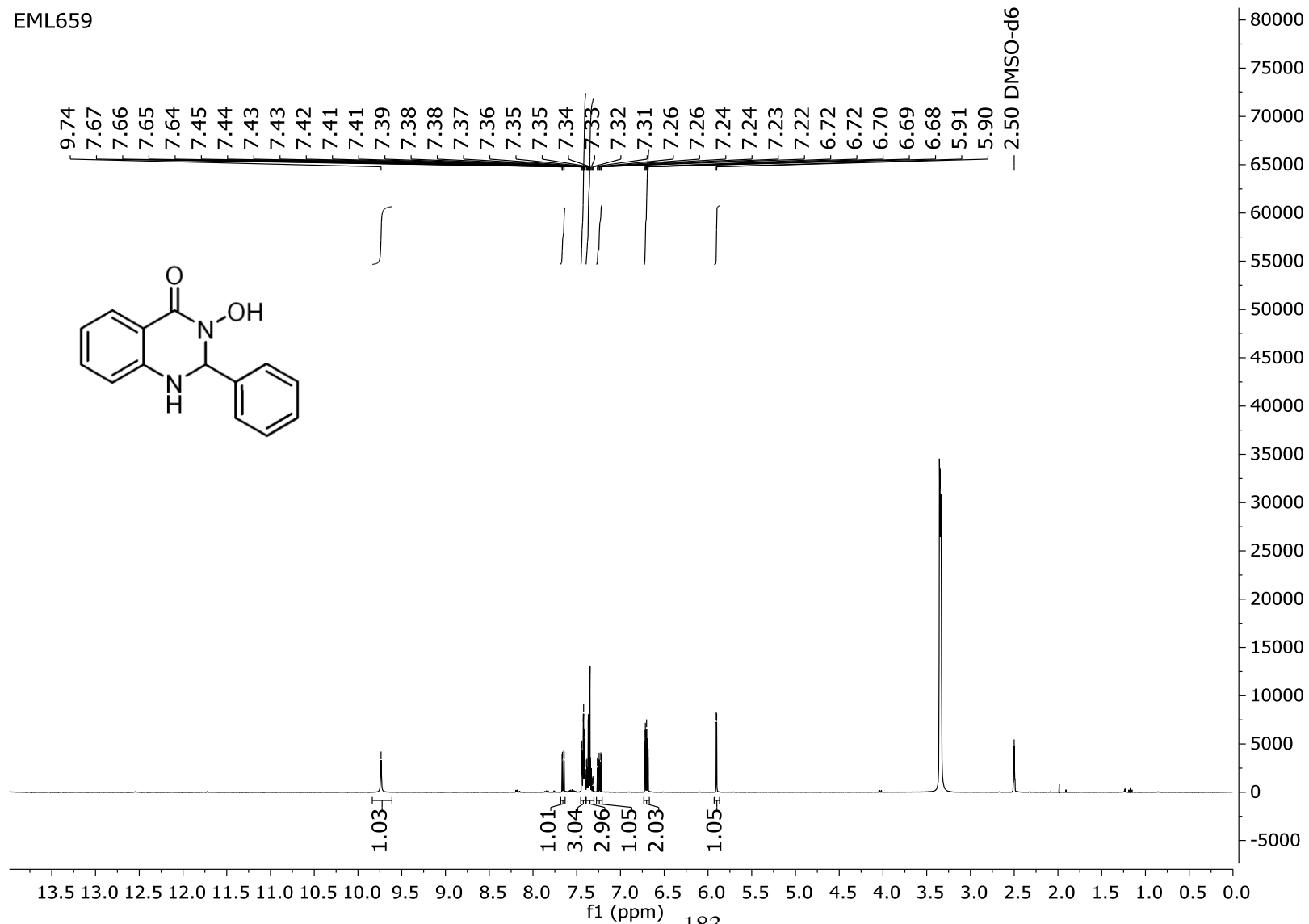
EML650



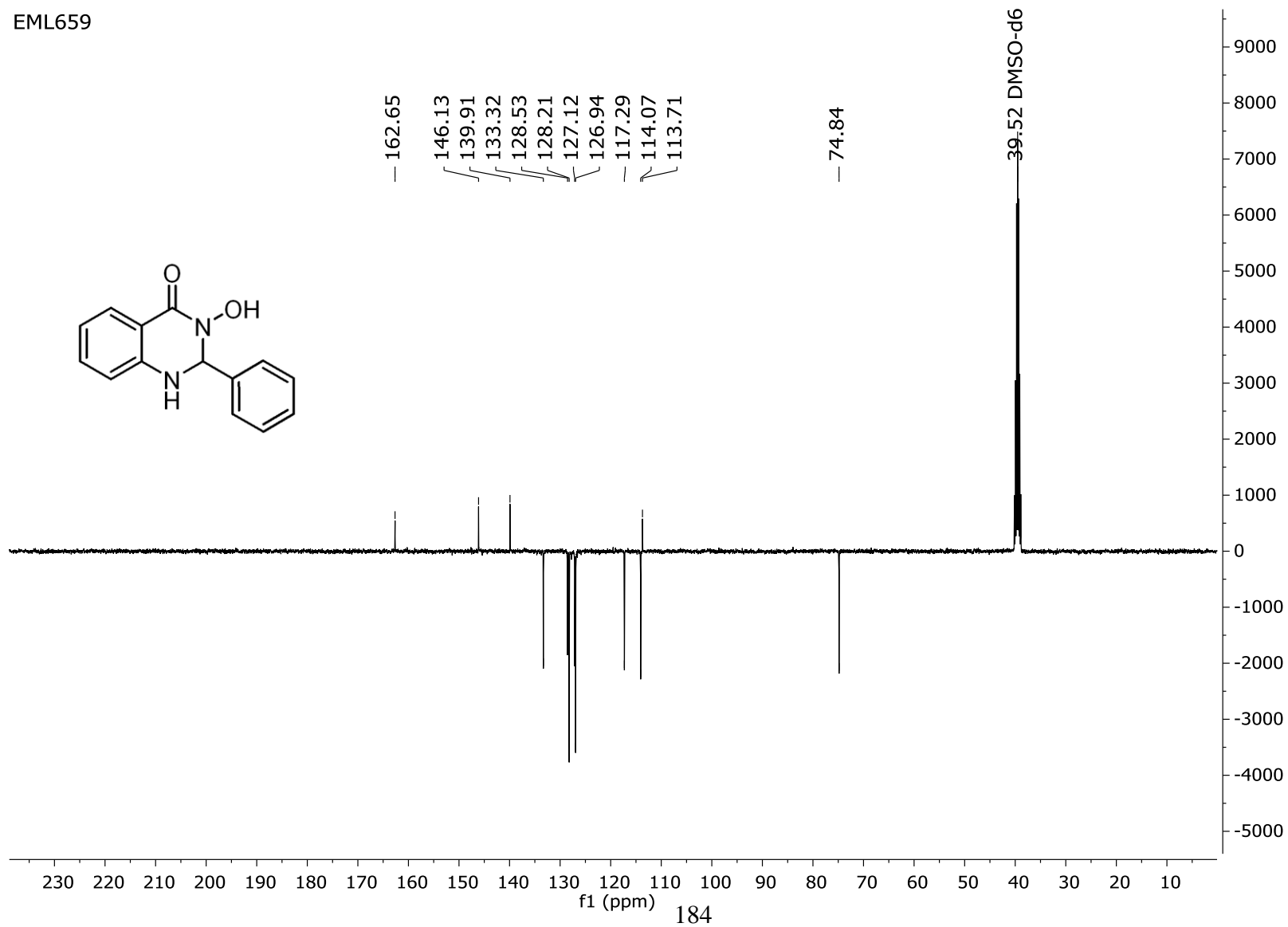
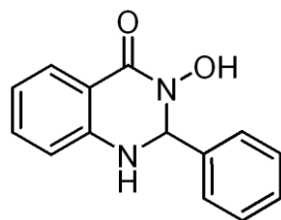
EML650



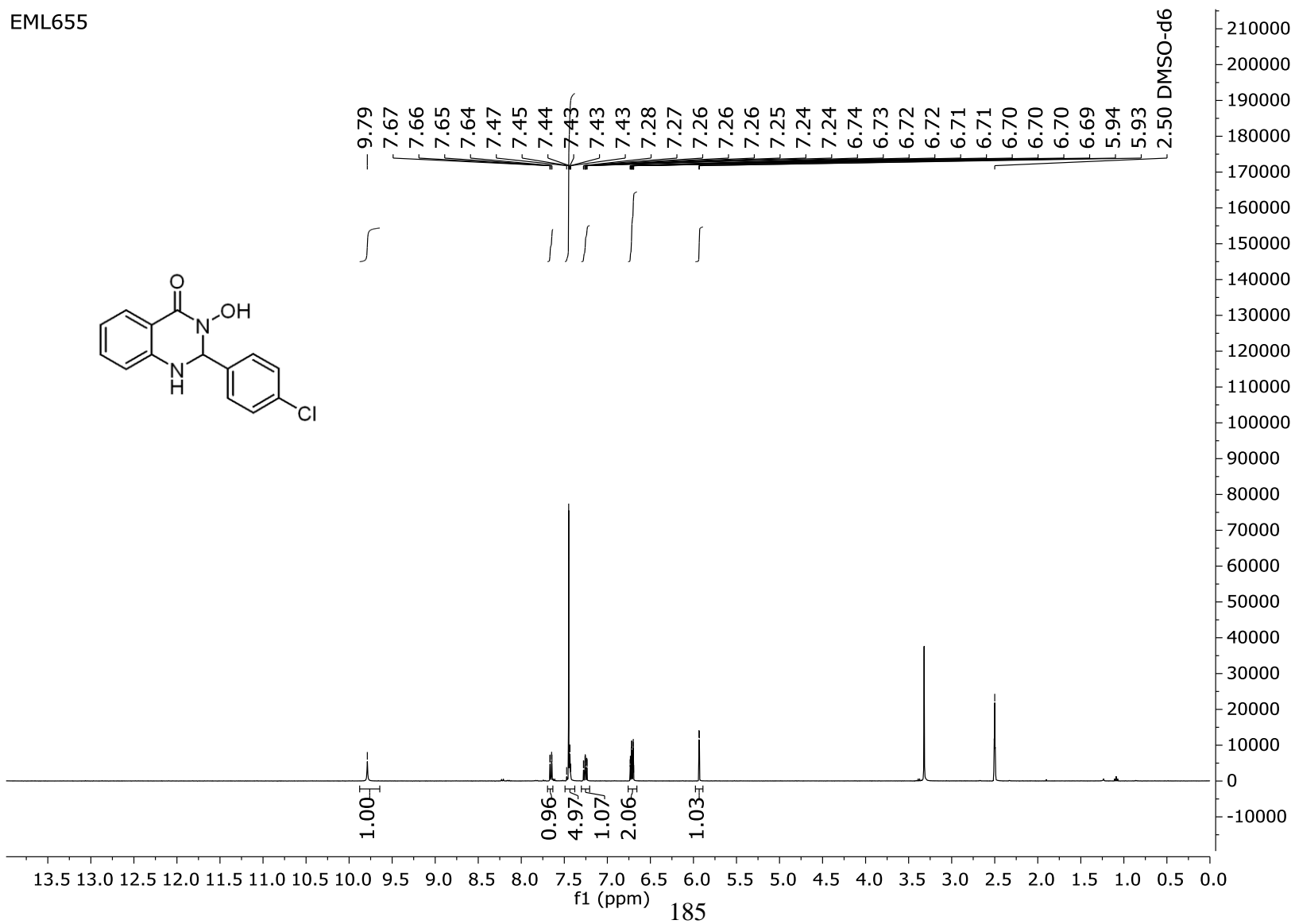
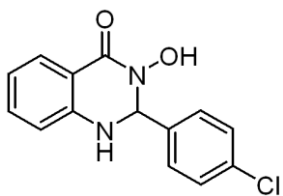
EML659



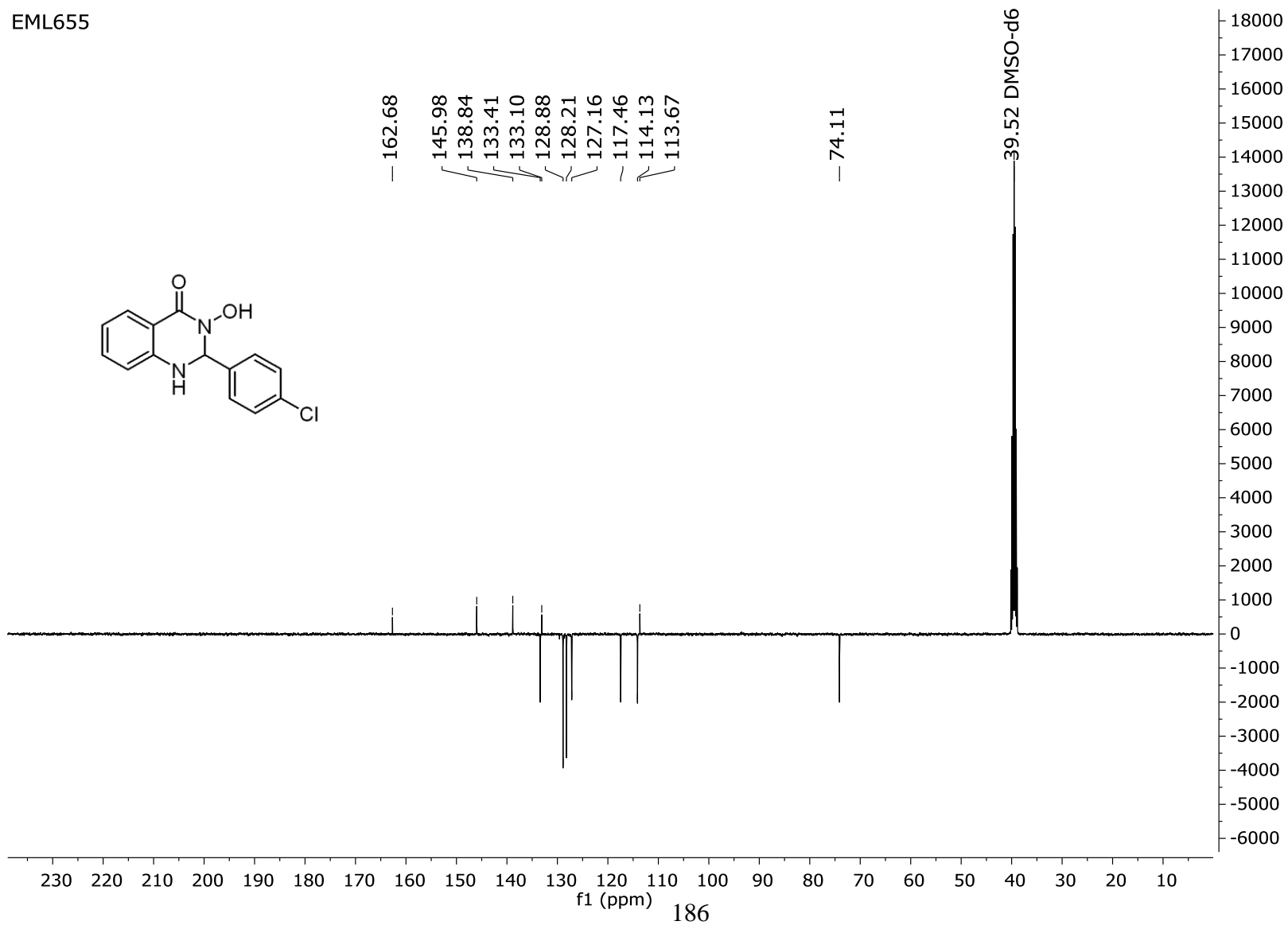
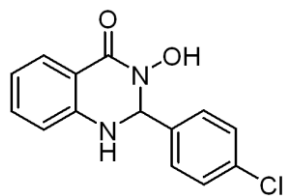
EML659



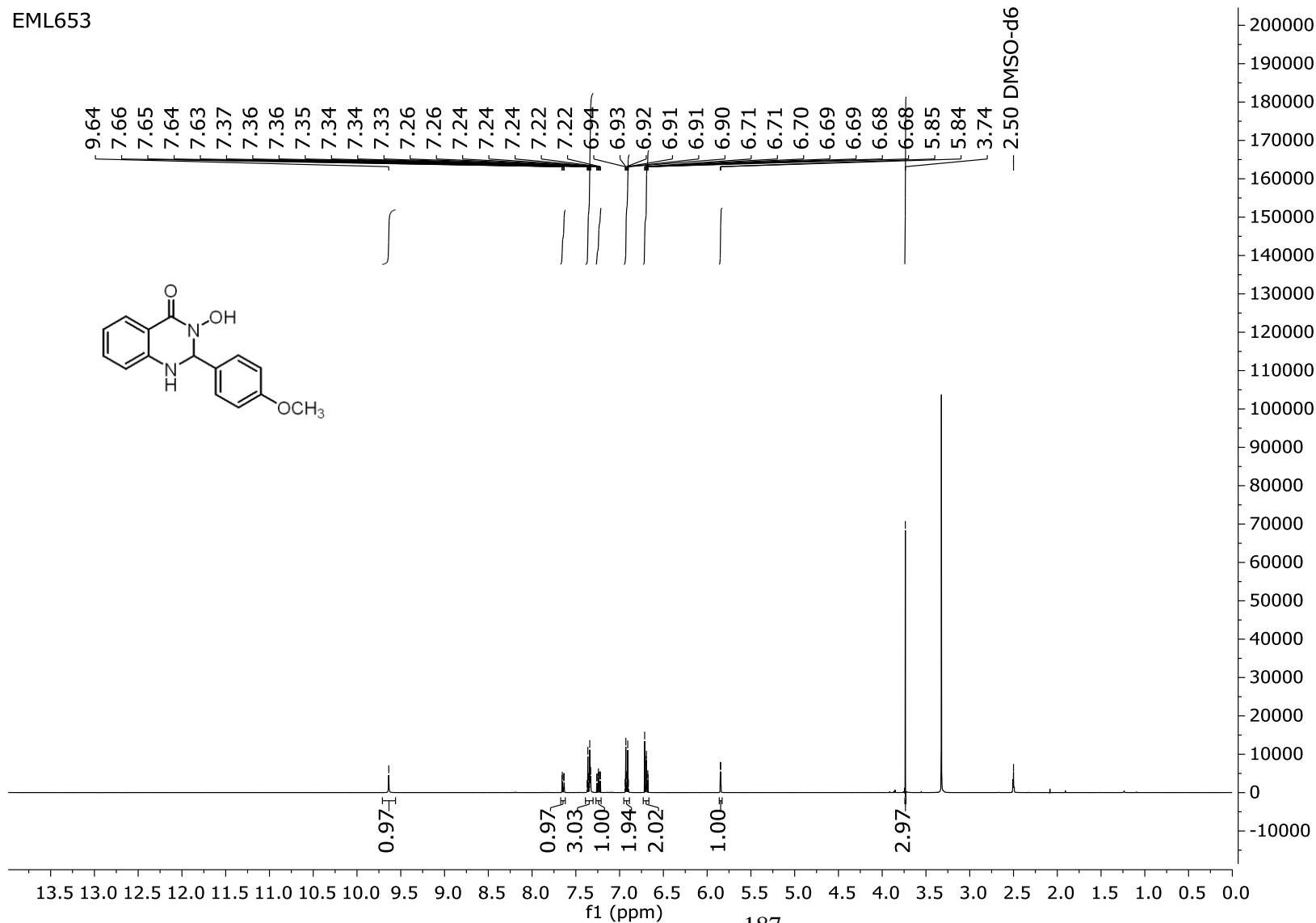
EML655



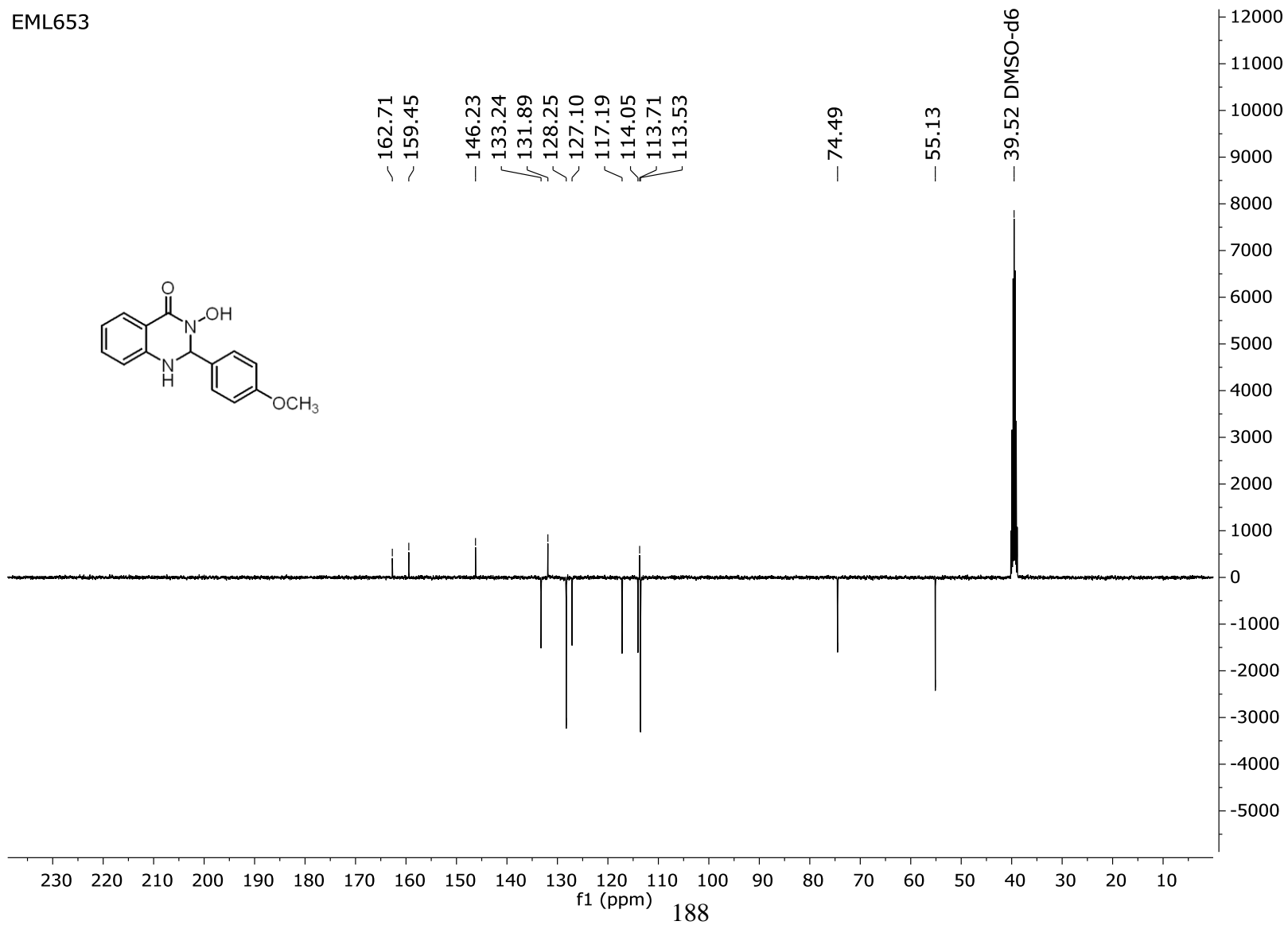
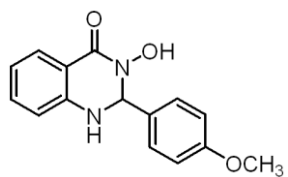
EML655



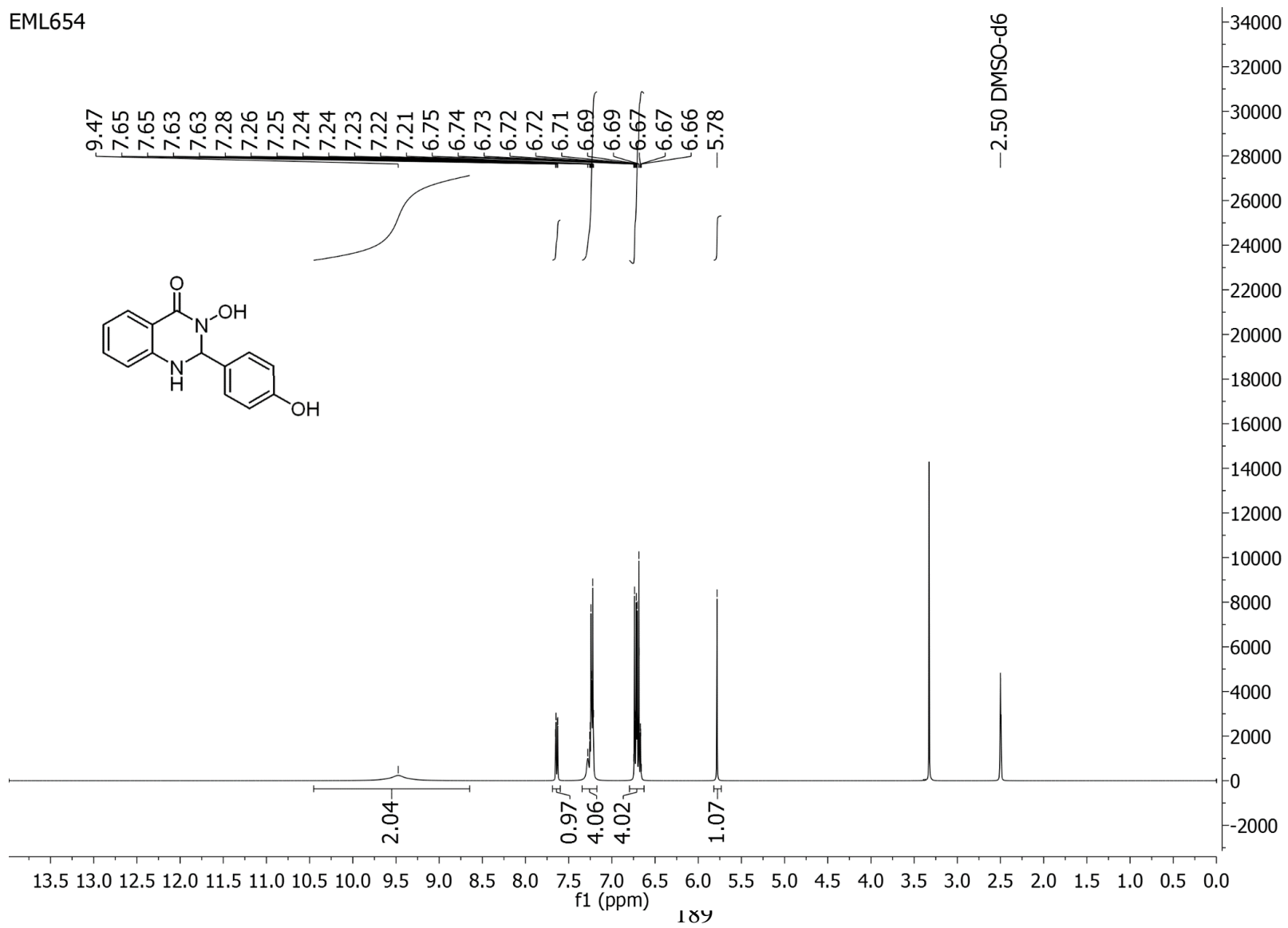
EML653



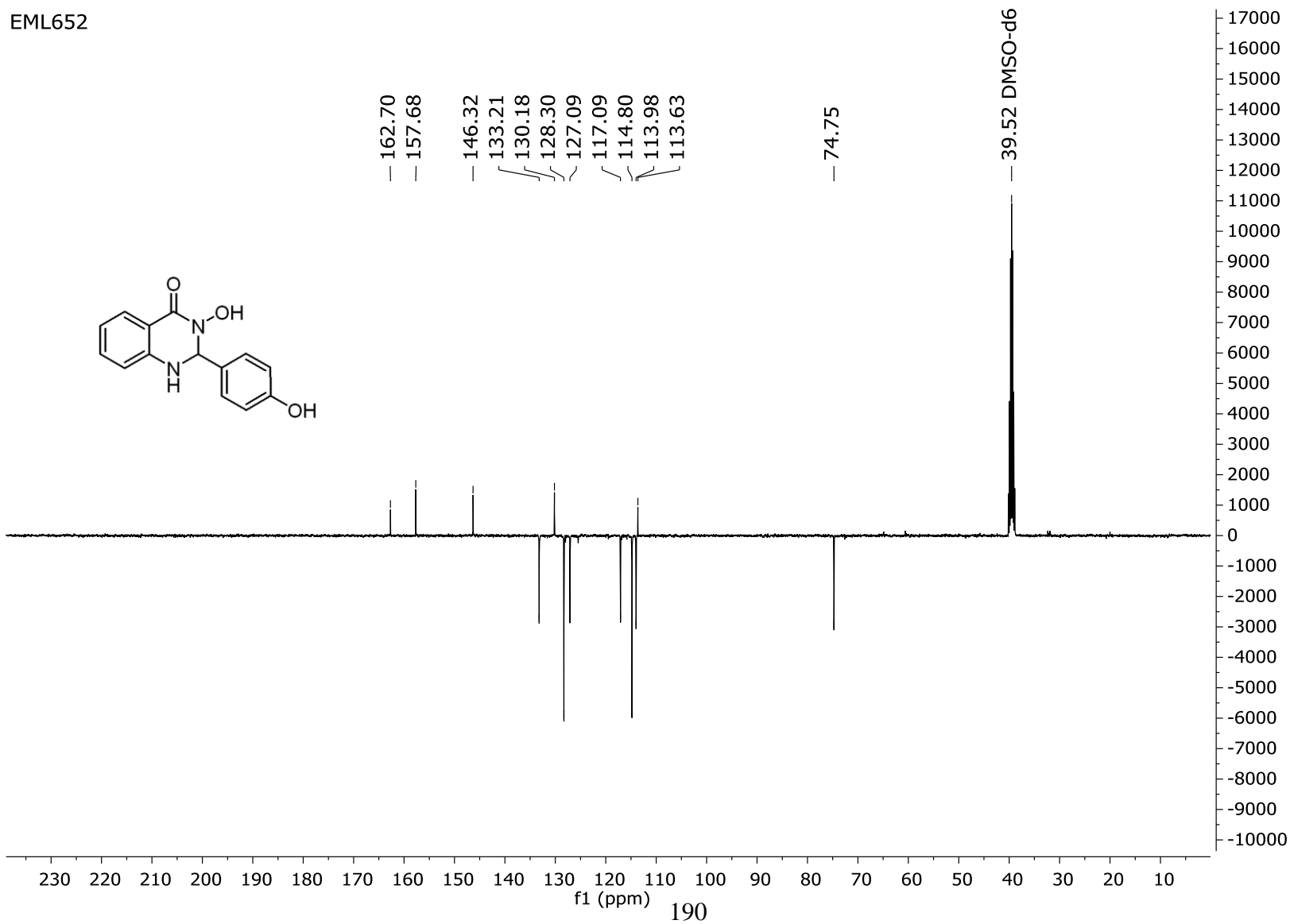
EML653



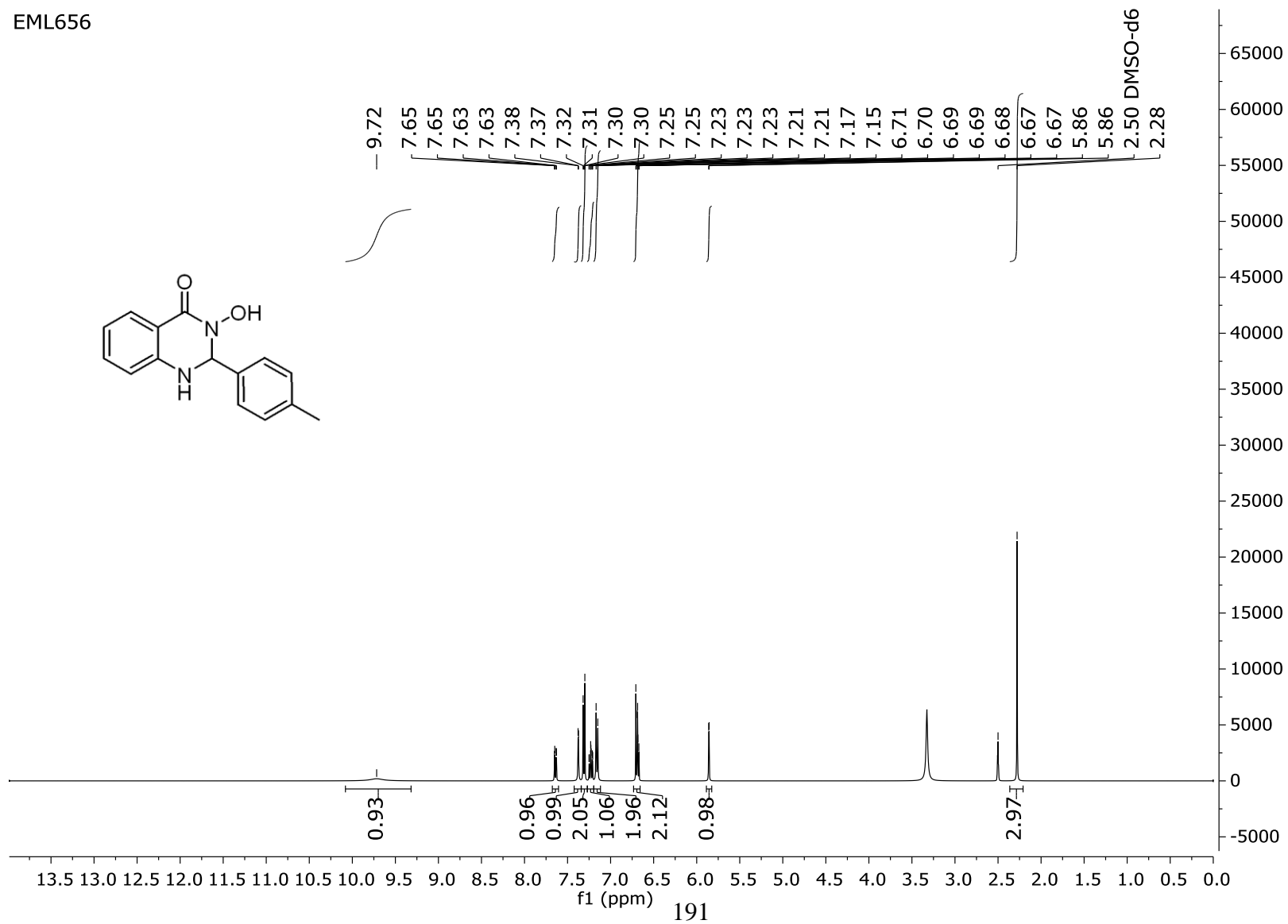
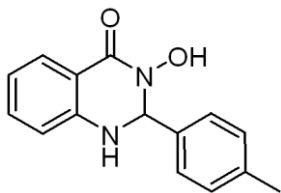
EML654



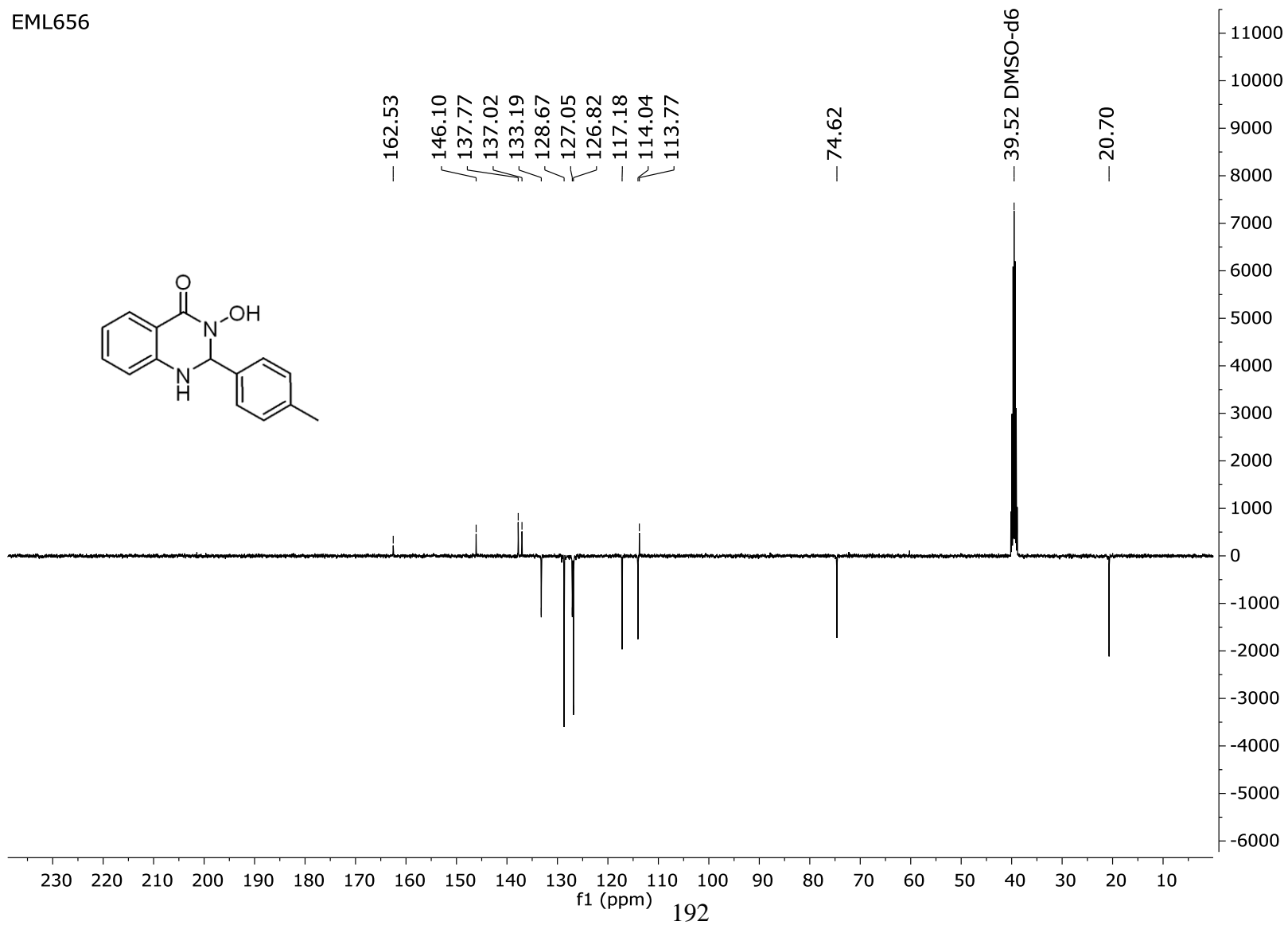
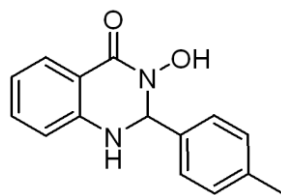
EML652



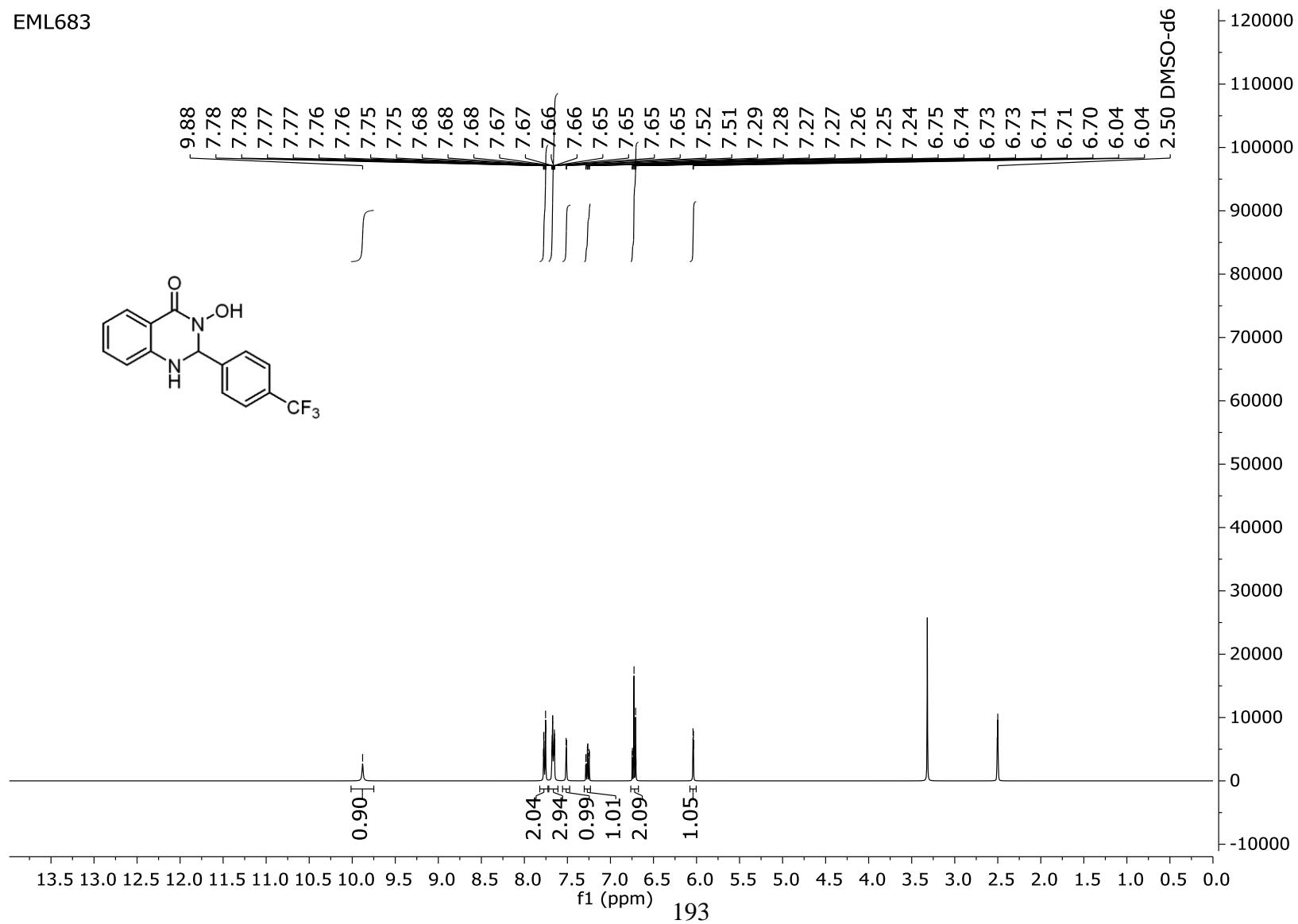
EML656



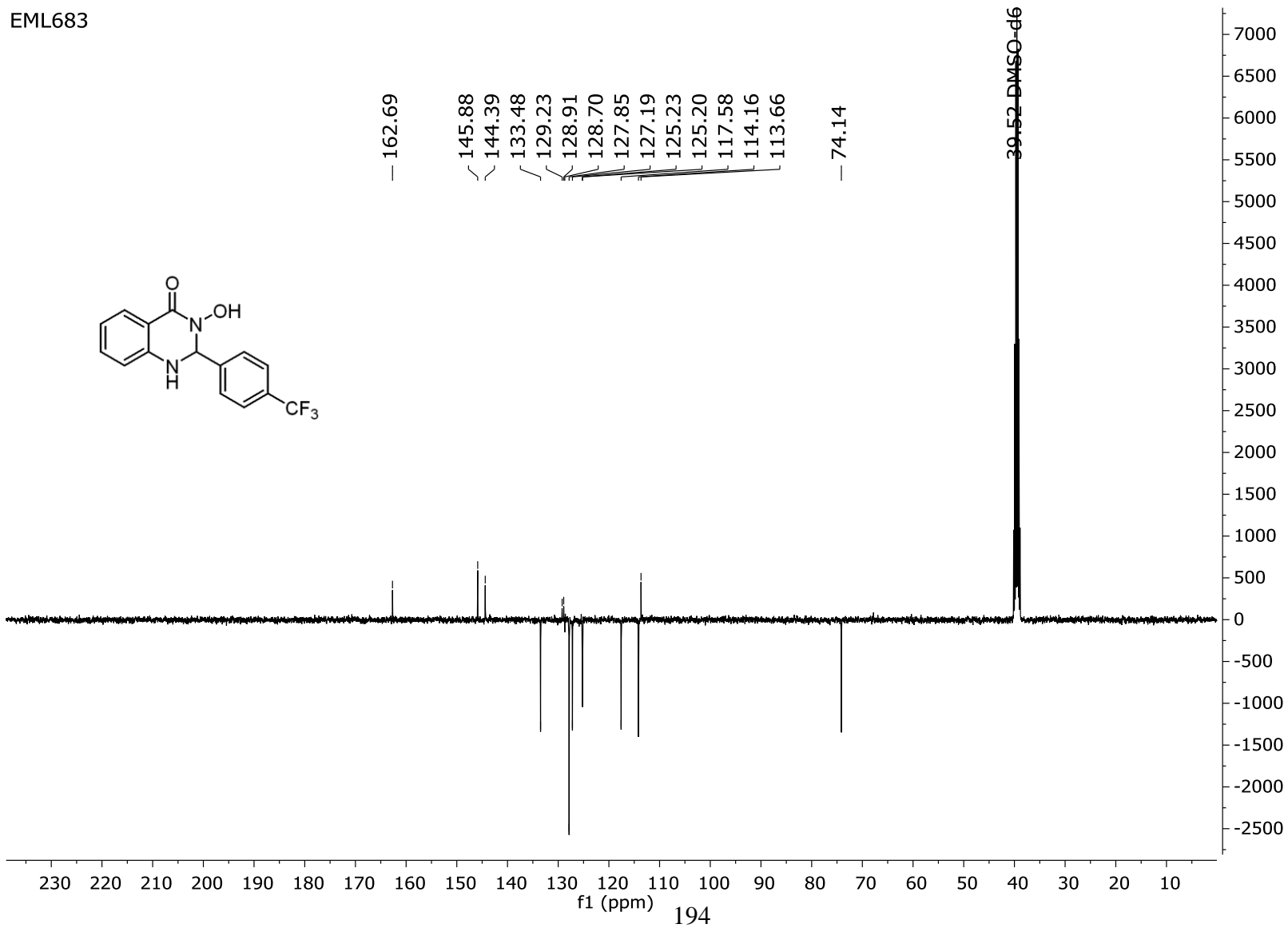
EML656



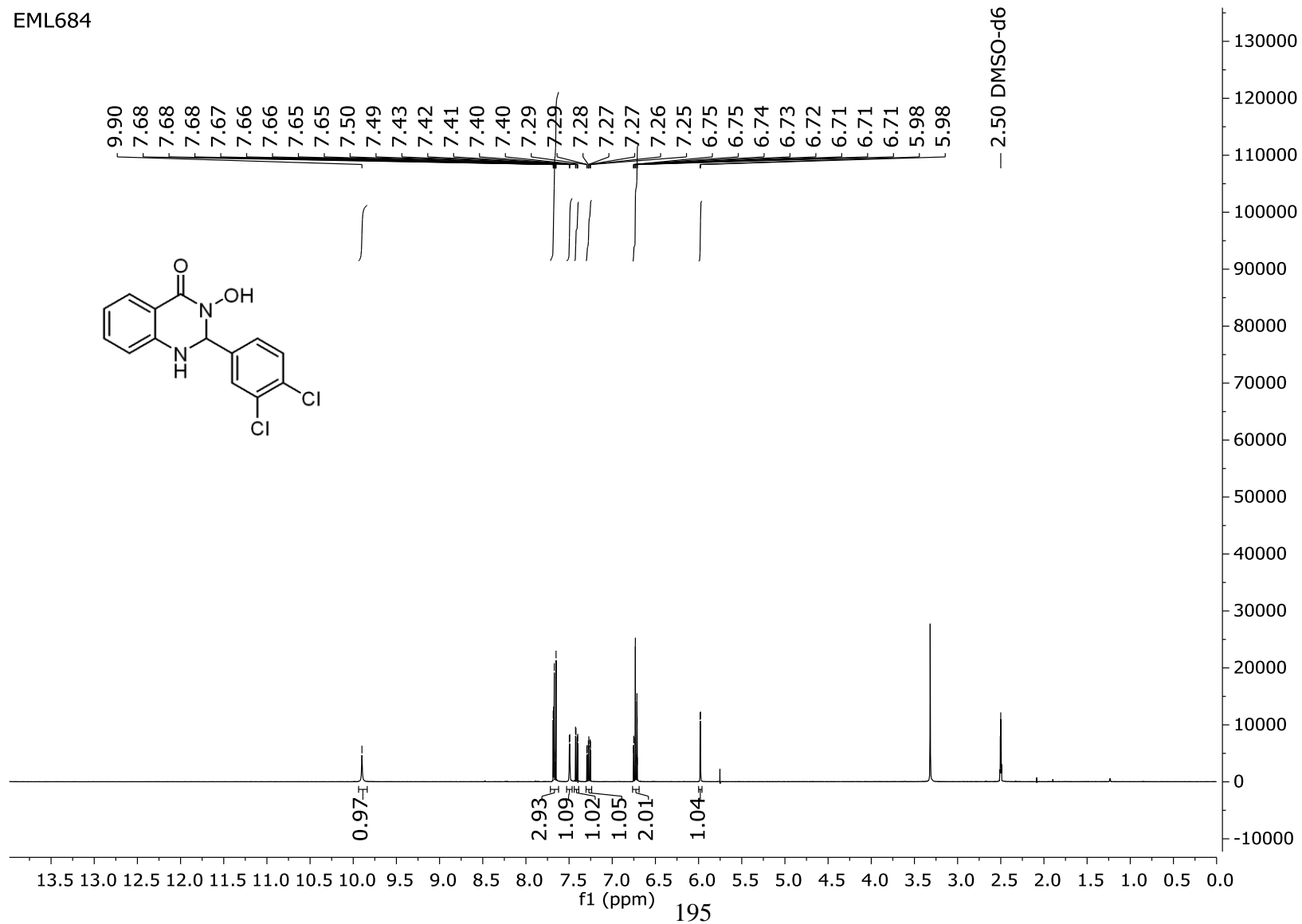
EML683



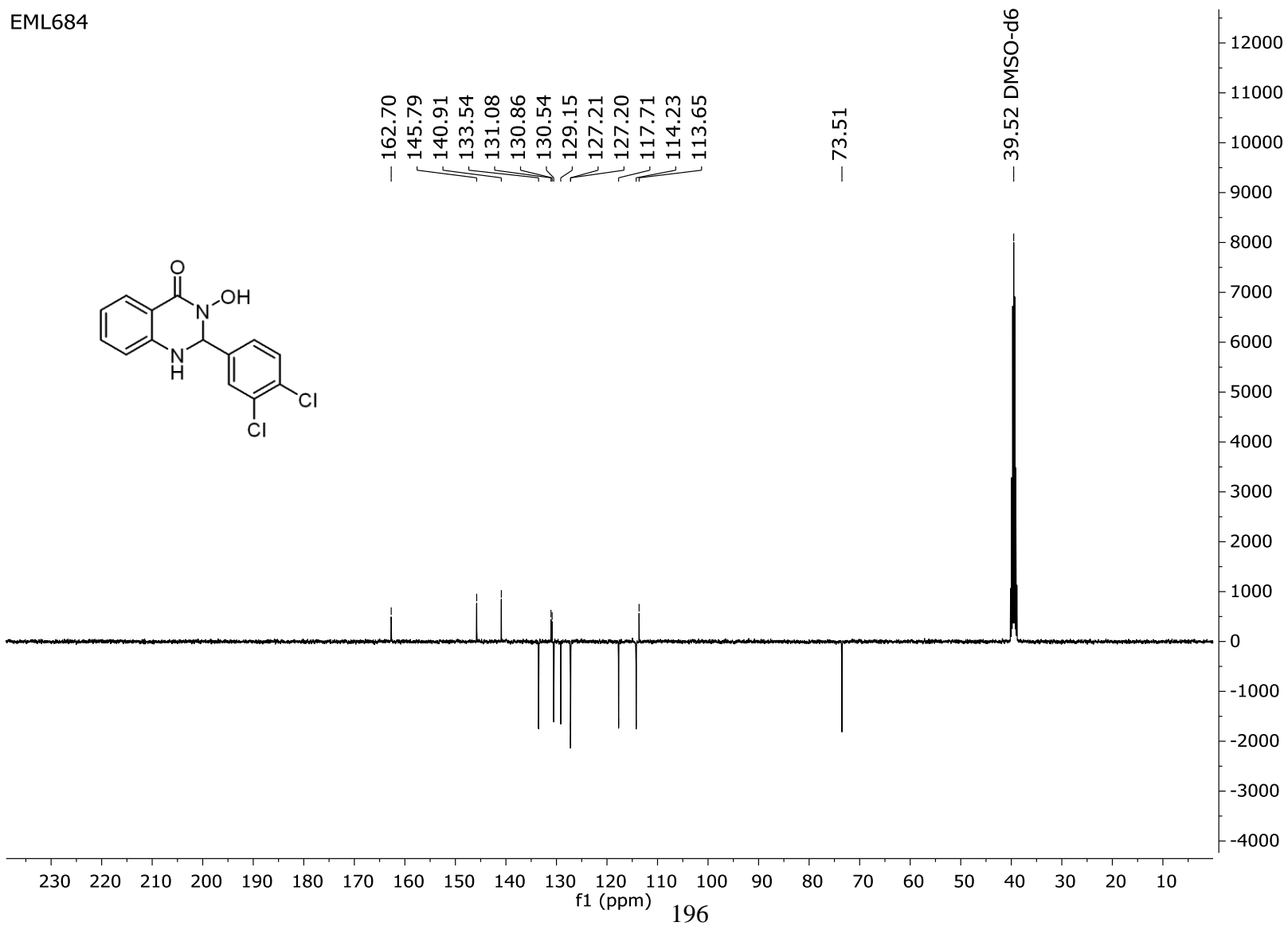
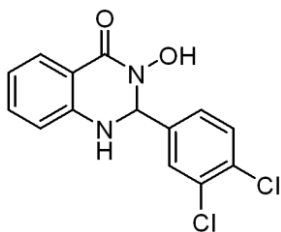
EML683



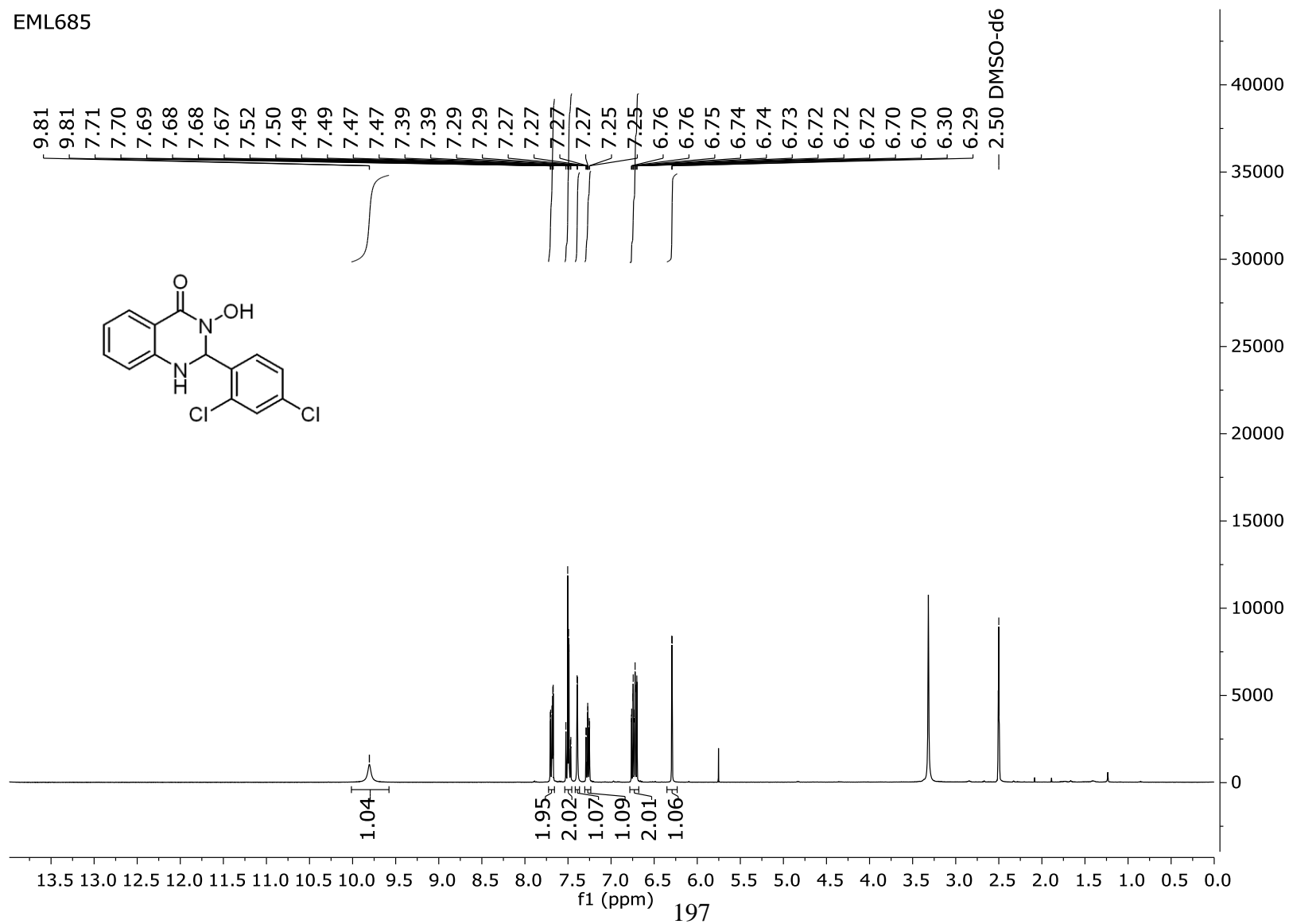
EML684



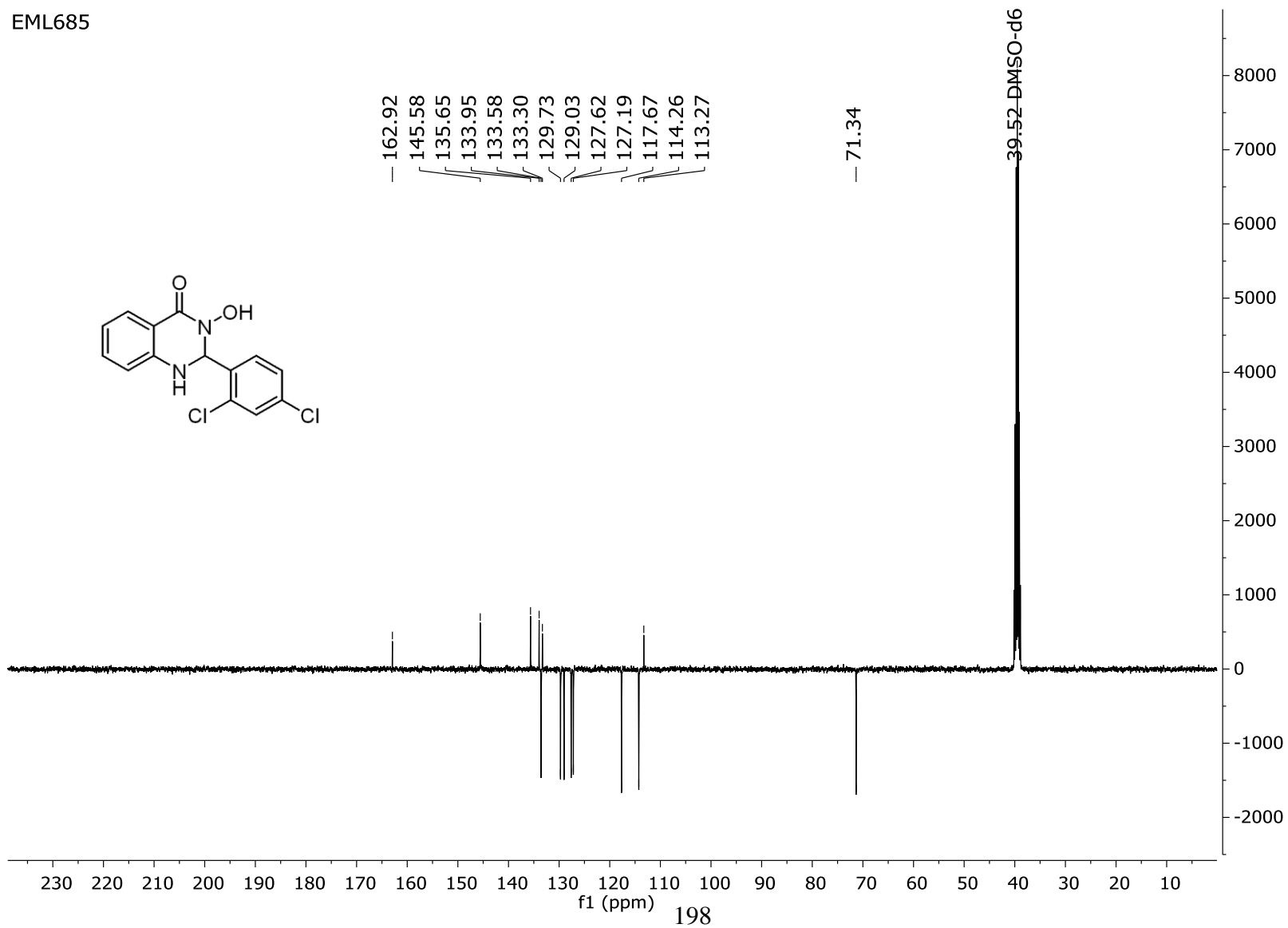
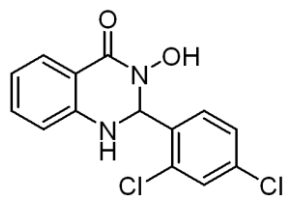
EML684



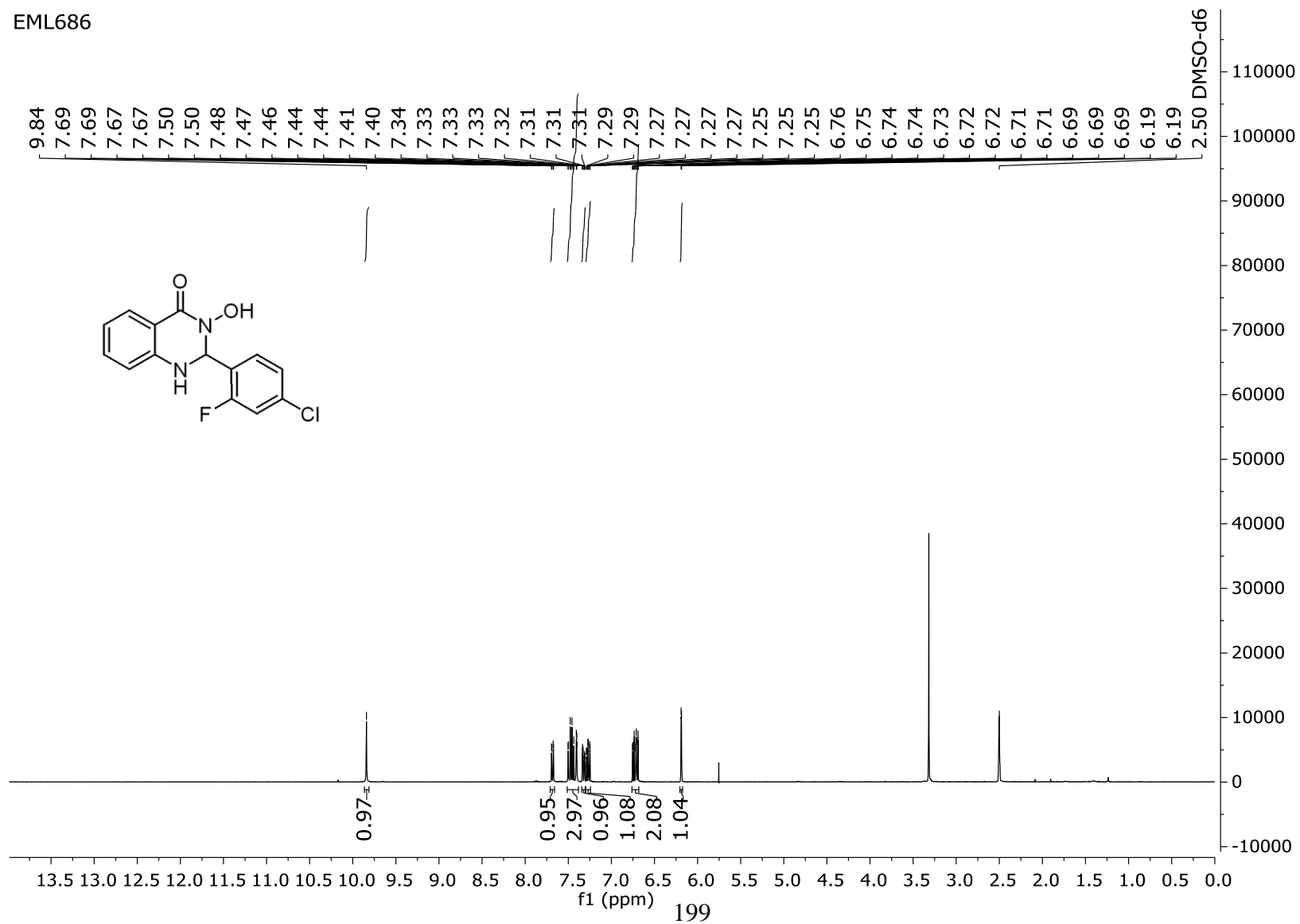
EML685



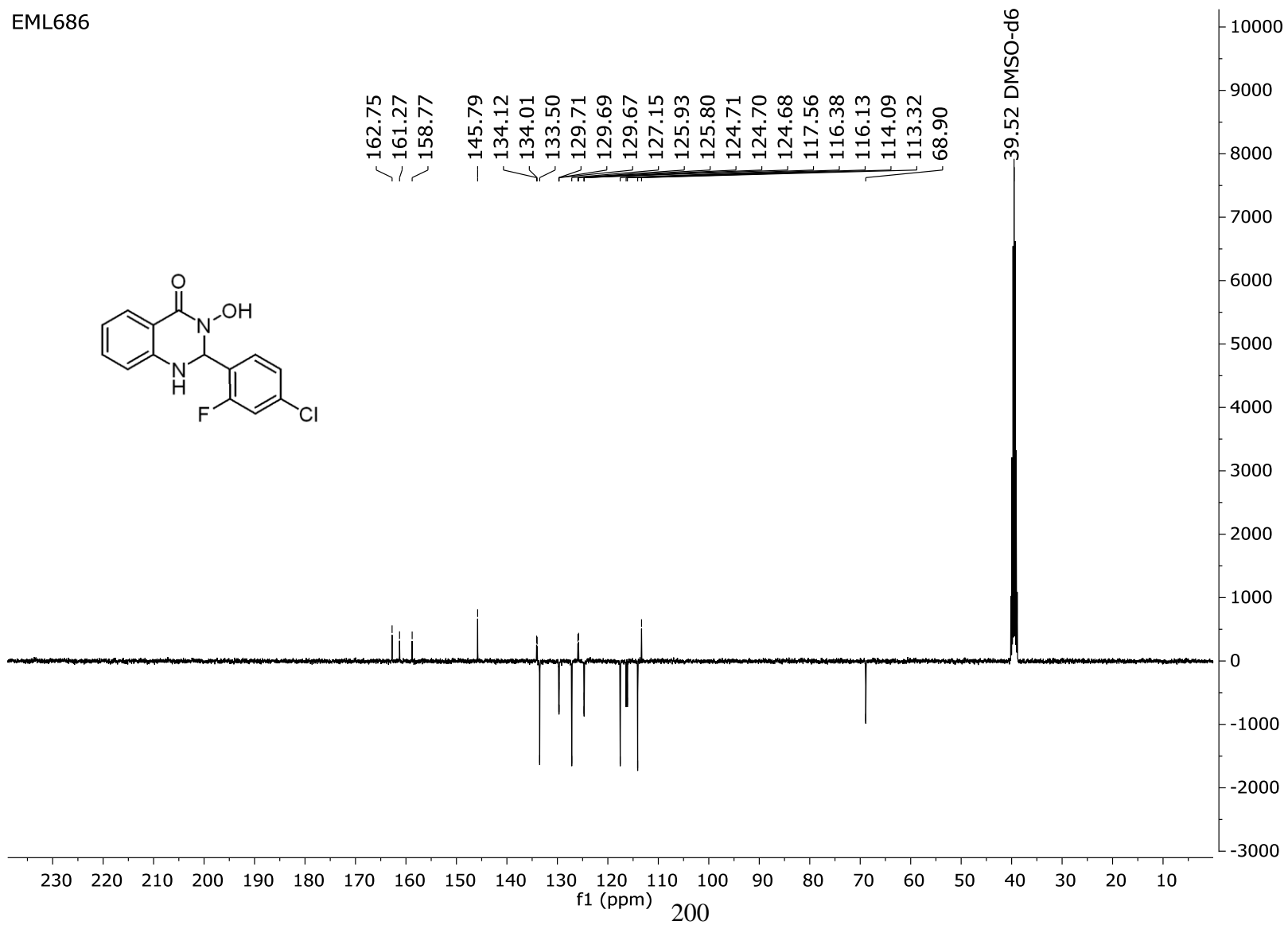
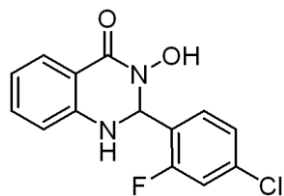
EML685



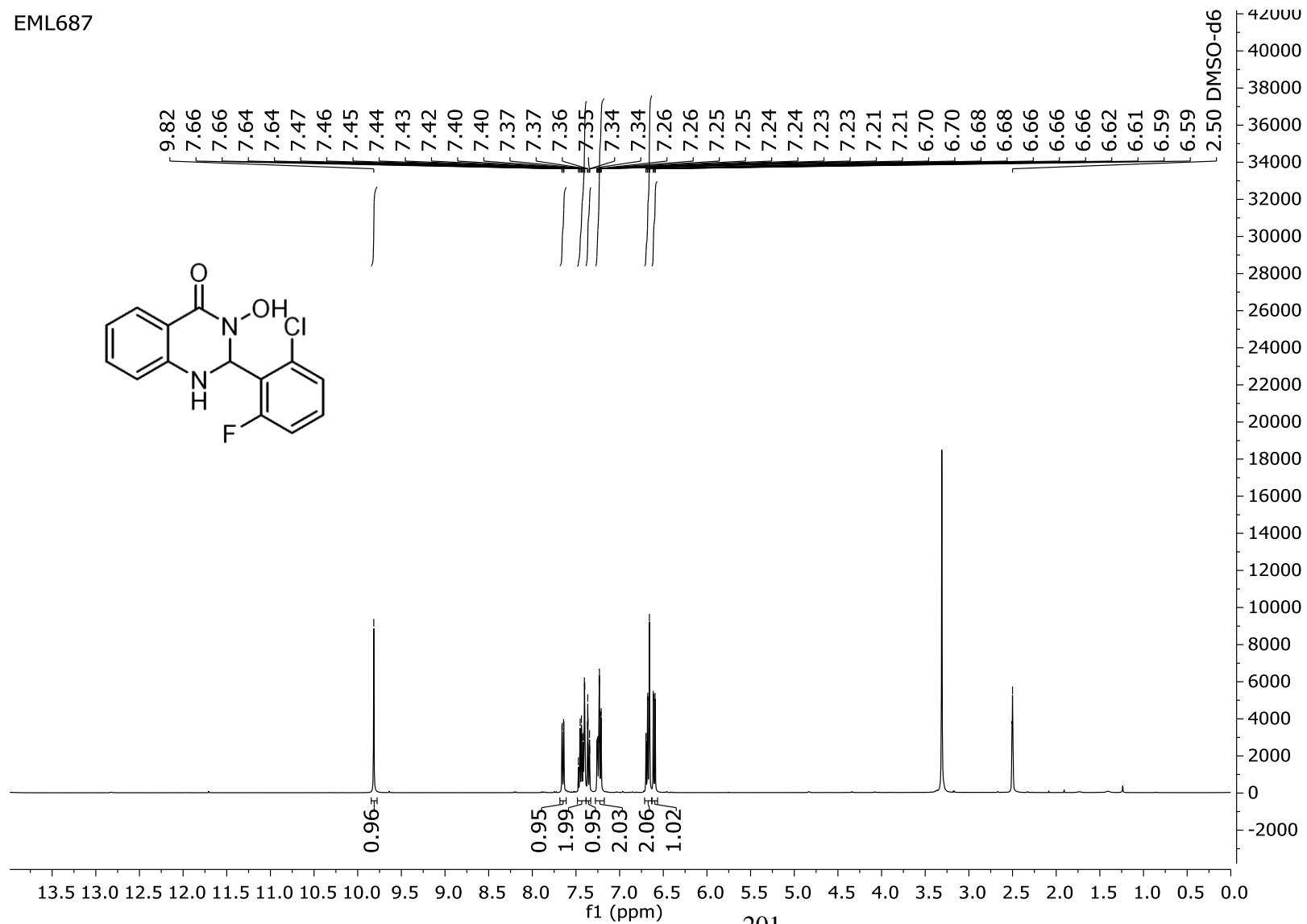
EML686



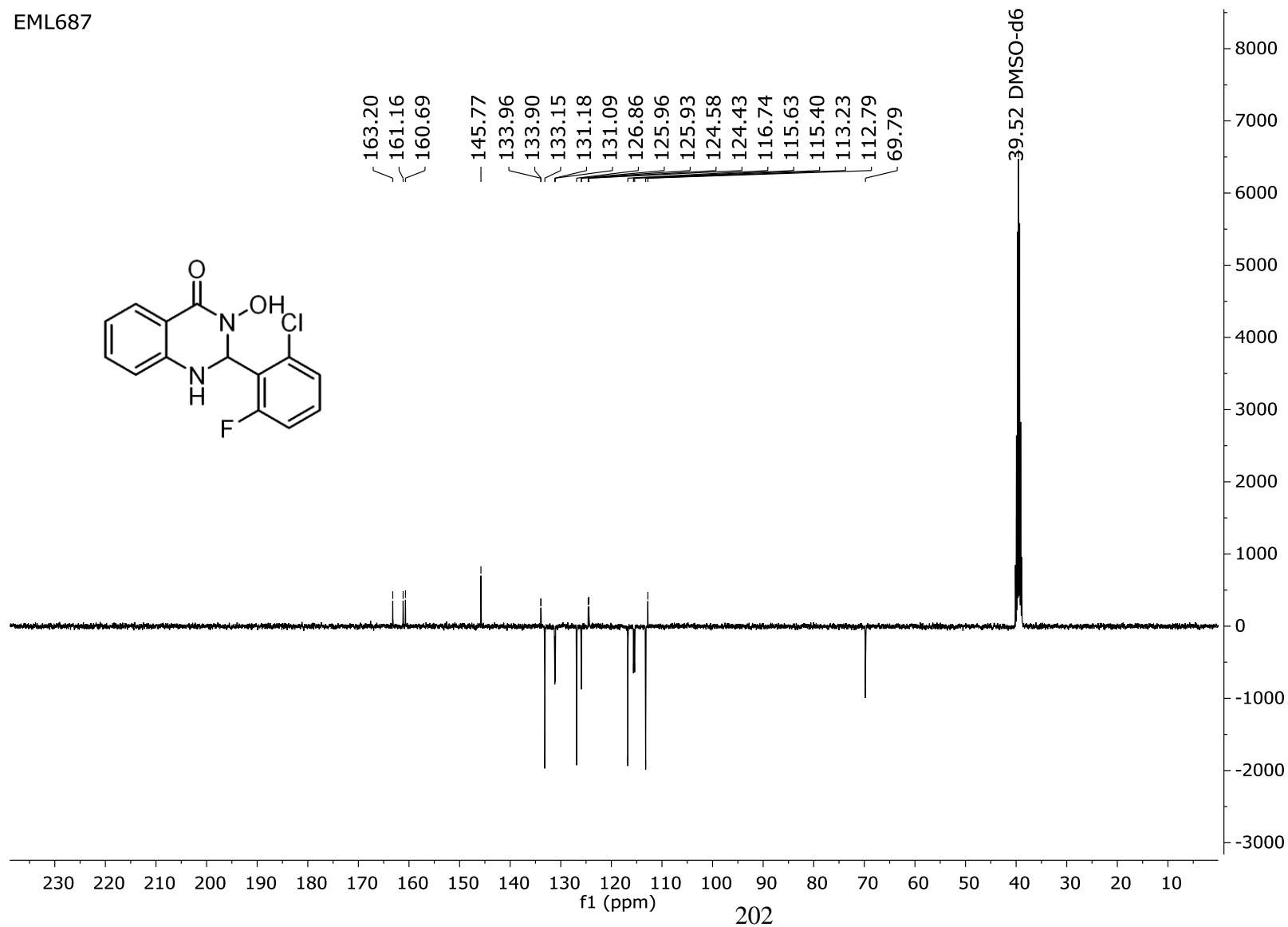
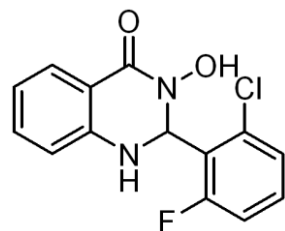
EML686



EML687



EML687



ACKNOWLEDGEMENTS

First and foremost I would like to express my sincere gratitude to Prof. Gianluca Sbardella and Prof. Sabrina Castellano for the continuous support of my Ph.D study and related research, for their patience, motivation, and immense knowledge. Their guidance helped me in all the time of research since I was just a Master's student.

I am very grateful to Professor Axel Imhof for giving me the opportunity to spend a period at LMU, for his help and guidance during my time in his lab. Special thank goes to Moritz Völker-Albert and Dr. Ignasi Forné for their support during my approach to the world of biology.

I am forever indebted to my academic supervisors, Dr. Ciro Milite, Dr. Monica Viviano and Dr. Alessandra Feoli, for their enthusiasm, guidance, and unrelenting support throughout this path. They have routinely gone beyond their duties being above all good friends.

I thank all my labmates for all the time we spent working together, for the laughing, the discussions, for all the fun we have had in these three years. In particular, I want to thank Cristina and Federica for their active role in the realization of this project.

I would like to thank my family for all their love and encouragement. I know I always have them to count on when times are rough.

And finally to Donatella, who has been by my side throughout this PhD, living every single minute of it always on my side. She helps me to be a better person and a better scientist.

REFERENCES

1. Copeland, R. A.; Solomon, M. E.; Richon, V. M., Protein methyltransferases as a target class for drug discovery. *Nat Rev Drug Discovery* **2009**, *8*.
2. Waddington, C. H., The epigenotype. 1942. *International journal of epidemiology* **2012**, *41* (1), 10-3.
3. Bird, A., Perceptions of epigenetics. *Nature* **2007**, *447* (7143), 396-398.
4. Kouzarides, T., Chromatin modifications and their function. *Cell* **2007**, *128* (4), 693-705.
5. Tan, S.; Davey, C. A., Nucleosome structural studies. *Current opinion in structural biology* **2011**, *21* (1), 128-136.
6. Yang, X.; Lay, F.; Han, H.; Jones, P. A., Targeting DNA methylation for epigenetic therapy. *Trends in pharmacological sciences* **2010**, *31* (11), 536-546.
7. Yoo, C. B.; Jones, P. A., Epigenetic therapy of cancer: past, present and future. *Nature reviews Drug discovery* **2006**, *5* (1), 37-50.
8. Bannister, A. J.; Kouzarides, T., Regulation of chromatin by histone modifications. *Cell research* **2011**, *21* (3), 381-395.
9. Jenuwein, T.; Allis, C. D., *Science* **2001**, 293.
10. Rotili, D.; Mai, A., Targeting Histone Demethylases: A New Avenue for the Fight against Cancer. *Genes & Cancer* **2011**, *2* (6), 663-679.
11. Margueron, R.; Trojer, P.; Reinberg, D., The key to development: interpreting the histone code? *Current opinion in genetics & development* **2005**, *15* (2), 163-176.
12. Lan, F.; Shi, Y., Epigenetic regulation: methylation of histone and non-histone proteins. *Science in China Series C: Life Sciences* **2009**, *52* (4), 311-322.
13. Benard, A.; Goossens-Beumer, I. J.; van Hoesel, A. Q.; de Graaf, W.; Horati, H.; Putter, H.; Zeestraten, E. C.; van de Velde, C. J.; Kuppen, P. J., Histone trimethylation at H3K4, H3K9 and H4K20 correlates with patient survival and tumor recurrence in early-stage colon cancer. *BMC cancer* **2014**, *14* (1), 1.
14. Martin, C.; Zhang, Y., The diverse functions of histone lysine methylation. *Nat Rev Mol Cell Biol* **2005**, *6* (11), 838-849.
15. Coppedè, F., The potential of epigenetic therapies in neurodegenerative diseases. *Frontiers in genetics* **2014**, *5*, 220.
16. Huang, B.; Yang, X.-D.; Lamb, A.; Chen, L.-F., Posttranslational modifications of NF- κ B: another layer of regulation for NF- κ B signaling pathway. *Cellular signalling* **2010**, *22* (9), 1282-1290.
17. Stark, G. R.; Wang, Y.; Lu, T., Lysine methylation of promoter-bound transcription factors and relevance to cancer. *Cell research* **2011**, *21* (3), 375-380.
18. Zhang, X.; Wen, H.; Shi, X., Lysine methylation: beyond histones. *Acta biochimica et biophysica Sinica* **2012**, *44* (1), 14-27.
19. Shi, Y.; Lan, F.; Matson, C.; Mulligan, P.; Whetstine, J. R.; Cole, P. A.; Casero, R. A.; Shi, Y., Histone demethylation mediated by the nuclear amine oxidase homolog LSD1. *Cell* **2004**, *119* (7), 941-53.

20. Karytinis, A.; Forneris, F.; Profumo, A.; Ciossani, G.; Battaglioli, E.; Binda, C.; Mattevi, A., A novel mammalian flavin-dependent histone demethylase. *Journal of Biological Chemistry* **2009**, *284* (26), 17775-17782.
21. Tsukada, Y.-i.; Fang, J.; Erdjument-Bromage, H.; Warren, M. E.; Borchers, C. H.; Tempst, P.; Zhang, Y., Histone demethylation by a family of JmjC domain-containing proteins. *Nature* **2006**, *439* (7078), 811-816.
22. Klose, R. J.; Kallin, E. M.; Zhang, Y., JmjC-domain-containing proteins and histone demethylation. *Nat Rev Genet* **2006**, *7* (9), 715-727.
23. Wang, Y.; Wysocka, J.; Sayegh, J.; Lee, Y.-H.; Perlin, J. R.; Leonelli, L.; Sonbuchner, L. S.; McDonald, C. H.; Cook, R. G.; Dou, Y., Human PAD4 regulates histone arginine methylation levels via demethyliminination. *Science* **2004**, *306* (5694), 279-283.
24. Zhang, X.; Bolt, M.; Guertin, M. J.; Chen, W.; Zhang, S.; Cherrington, B. D.; Slade, D. J.; Dreyton, C. J.; Subramanian, V.; Bicker, K. L., Peptidylarginine deiminase 2-catalyzed histone H3 arginine 26 citrullination facilitates estrogen receptor α target gene activation. *Proceedings of the National Academy of Sciences* **2012**, *109* (33), 13331-13336.
25. Chang, B.; Chen, Y.; Zhao, Y.; Bruick, R. K., JMJD6 is a histone arginine demethylase. *Science* **2007**, *318* (5849), 444-447.
26. Böttger, A.; Islam, M. S.; Chowdhury, R.; Schofield, C. J.; Wolf, A., The oxygenase Jmjd6—a case study in conflicting assignments. *Biochemical Journal* **2015**, *468* (2), 191-202.
27. Walport, L. J.; Hopkinson, R. J.; Chowdhury, R.; Schiller, R.; Ge, W.; Kawamura, A.; Schofield, C. J., Arginine demethylation is catalysed by a subset of JmjC histone lysine demethylases. *Nature Communications* **2016**, *7*.
28. Kim, S.; Benoiton, L.; Paik, W. K., ϵ -Alkyllysine PURIFICATION AND PROPERTIES OF THE ENZYME. *Journal of Biological Chemistry* **1964**, *239* (11), 3790-3796.
29. Humphrey, G. W.; Wang, Y.; Russanova, V. R.; Hirai, T.; Qin, J.; Nakatani, Y.; Howard, B. H., Stable histone deacetylase complexes distinguished by the presence of SANT domain proteins CoREST/kiaa0071 and Mta-L1. *Journal of Biological Chemistry* **2001**, *276* (9), 6817-6824.
30. Shi, Y.; Sawada, J.-i.; Sui, G.; Affar, E. B.; Whetstone, J. R.; Lan, F.; Ogawa, H.; Po-Shan Luke, M.; Nakatani, Y.; Shi, Y., Coordinated histone modifications mediated by a CtBP co-repressor complex. *Nature* **2003**, *422* (6933), 735-738.
31. Huang, J.; Sengupta, R.; Espejo, A. B.; Lee, M. G.; Dorsey, J. A.; Richter, M.; Opravil, S.; Shiekhata, R.; Bedford, M. T.; Jenuwein, T.; Berger, S. L., p53 is regulated by the lysine demethylase LSD1. *Nature* **2007**, *449* (7158), 105-108.
32. Wang, J.; Hevi, S.; Kurash, J. K.; Lei, H.; Gay, F.; Bajko, J.; Su, H.; Sun, W.; Chang, H.; Xu, G., The lysine demethylase LSD1 (KDM1) is required for maintenance of global DNA methylation. *Nature genetics* **2009**, *41* (1), 125-129.
33. Kontaki, H.; Talianidis, I., Lysine methylation regulates E2F1-induced cell death. *Molecular cell* **2010**, *39* (1), 152-160.
34. Ciccone, D. N.; Su, H.; Hevi, S.; Gay, F.; Lei, H.; Bajko, J.; Xu, G.; Li, E.; Chen, T., KDM1B is a histone H3K4 demethylase required to establish maternal genomic imprints. *Nature* **2009**, *461* (7262), 415-418.
35. Fang, R.; Barbera, A. J.; Xu, Y.; Rutenberg, M.; Leonor, T.; Bi, Q.; Lan, F.; Mei, P.; Yuan, G.-C.; Lian, C.; Peng, J.; Cheng, D.; Sui, G.; Kaiser, U. B.; Shi, Y.;

- Shi, Y. G., Human LSD2/KDM1b/AOF1 Regulates Gene Transcription by Modulating Intragenic H3K4me2 Methylation. *Molecular Cell* **2010**, *39* (2), 222-233.
36. Forneris, F.; Binda, C.; Battaglioli, E.; Mattevi, A., LSD1: oxidative chemistry for multifaceted functions in chromatin regulation. *Trends in biochemical sciences* **2008**, *33* (4), 181-189.
37. Stavropoulos, P.; Blobel, G.; Hoelz, A., Crystal structure and mechanism of human lysine-specific demethylase-1. *Nature structural & molecular biology* **2006**, *13* (7), 626-632.
38. Yang, M.; Gocke, C. B.; Luo, X.; Borek, D.; Tomchick, D. R.; Machius, M.; Otwinowski, Z.; Yu, H., Structural basis for CoREST-dependent demethylation of nucleosomes by the human LSD1 histone demethylase. *Molecular cell* **2006**, *23* (3), 377-387.
39. Fang, R.; Chen, F.; Dong, Z.; Hu, D.; Barbera, A. J.; Clark, E. A.; Fang, J.; Yang, Y.; Mei, P.; Rutenberg, M., LSD2/KDM1B and its cofactor NPAC/GLYR1 endow a structural and molecular model for regulation of H3K4 demethylation. *Molecular cell* **2013**, *49* (3), 558-570.
40. Hojfeldt, J. W.; Agger, K.; Helin, K., Histone lysine demethylases as targets for anticancer therapy. *Nat Rev Drug Discov* **2013**, *12* (12), 917-930.
41. Lee, M. G.; Wynder, C.; Schmidt, D. M.; McCafferty, D. G.; Shiekhattar, R., Histone H3 lysine 4 demethylation is a target of nonselective antidepressive medications. *Chemistry & biology* **2006**, *13* (6), 563-567.
42. Binda, C.; Valente, S.; Romanenghi, M.; Pilotto, S.; Cirilli, R.; Karytinis, A.; Ciossani, G.; Botrugno, O. A.; Forneris, F.; Tardugno, M., Biochemical, structural, and biological evaluation of tranlycypromine derivatives as inhibitors of histone demethylases LSD1 and LSD2. *Journal of the American Chemical Society* **2010**, *132* (19), 6827-6833.
43. Morera, L.; Lübbert, M.; Jung, M., Targeting histone methyltransferases and demethylases in clinical trials for cancer therapy. *Clinical Epigenetics* **2016**, *8* (1), 57.
44. Klose, R. J.; Zhang, Y., Regulation of histone methylation by demethylination and demethylation. *Nature reviews Molecular cell biology* **2007**, *8* (4), 307-318.
45. Takeuchi, T.; Yamazaki, Y.; Katoh-Fukui, Y.; Tsuchiya, R.; Kondo, S.; Motoyama, J.; Higashinakagawa, T., Gene trap capture of a novel mouse gene, jumonji, required for neural tube formation. *Genes & development* **1995**, *9* (10), 1211-1222.
46. Loenarz, C.; Schofield, C. J., Expanding chemical biology of 2-oxoglutarate oxygenases. *Nature chemical biology* **2008**, *4* (3), 152-156.
47. Schofield, C. J.; Ratcliffe, P. J., Oxygen sensing by HIF hydroxylases. *Nature reviews Molecular cell biology* **2004**, *5* (5), 343-354.
48. Schofield, C. J.; Ratcliffe, P. J., Signalling hypoxia by HIF hydroxylases. *Biochemical and biophysical research communications* **2005**, *338* (1), 617-626.
49. Kaelin, W. G.; Ratcliffe, P. J., Oxygen sensing by metazoans: the central role of the HIF hydroxylase pathway. *Molecular cell* **2008**, *30* (4), 393-402.
50. Cloos, P. A. C.; Christensen, J.; Agger, K.; Helin, K., Erasing the methyl mark: histone demethylases at the center of cellular differentiation and disease. *Genes & Development* **2008**, *22* (9), 1115-1140.

51. Pedersen, M. T.; Helin, K., Histone demethylases in development and disease. *Trends in cell biology* **2010**, *20* (11), 662-671.
52. Clifton, I. J.; McDonough, M. A.; Ehrismann, D.; Kershaw, N. J.; Granatino, N.; Schofield, C. J., Structural studies on 2-oxoglutarate oxygenases and related double-stranded β -helix fold proteins. *Journal of Inorganic Biochemistry* **2006**, *100* (4), 644-669.
53. McDonough, M. A.; Loenarz, C.; Chowdhury, R.; Clifton, I. J.; Schofield, C. J., Structural studies on human 2-oxoglutarate dependent oxygenases. *Current Opinion in Structural Biology* **2010**, *20* (6), 659-672.
54. Johansson, C.; Tumber, A.; Che, K.; Cain, P.; Nowak, R.; Gileadi, C.; Oppermann, U., The roles of Jumonji-type oxygenases in human disease. *Epigenomics* **2014**, *6* (1), 89-120.
55. Hausinger, R. P., Fe (II)/ α -ketoglutarate-dependent hydroxylases and related enzymes. *Critical reviews in biochemistry and molecular biology* **2004**, *39* (1), 21-68.
56. Whetstine, J. R.; Nottke, A.; Lan, F.; Huarte, M.; Smolikov, S.; Chen, Z.; Spooner, E.; Li, E.; Zhang, G.; Colaiacovo, M., Reversal of histone lysine trimethylation by the JMJD2 family of histone demethylases. *Cell* **2006**, *125* (3), 467-481.
57. Cloos, P. A.; Christensen, J.; Agger, K.; Maiolica, A.; Rappsilber, J.; Antal, T.; Hansen, K. H.; Helin, K., The putative oncogene GASC1 demethylates tri- and dimethylated lysine 9 on histone H3. *Nature* **2006**, *442* (7100), 307-311.
58. Yue, W. W.; Hozjan, V.; Ge, W.; Loenarz, C.; Cooper, C.; Schofield, C. J.; Kavanagh, K. L.; Oppermann, U.; McDonough, M. A., Crystal structure of the PHF8 Jumonji domain, an N ϵ -methyl lysine demethylase. *FEBS letters* **2010**, *584* (4), 825-830.
59. Horton, J. R.; Upadhyay, A. K.; Qi, H. H.; Zhang, X.; Shi, Y.; Cheng, X., Enzymatic and structural insights for substrate specificity of a family of jumonji histone lysine demethylases. *Nature structural & molecular biology* **2010**, *17* (1), 38-43.
60. Ponnaluri, V. C.; Vavilala, D. T.; Putty, S.; Gutheil, W. G.; Mukherji, M., Identification of non-histone substrates for JMJD2A–C histone demethylases. *Biochemical and biophysical research communications* **2009**, *390* (2), 280-284.
61. Berry, W. L.; Janknecht, R., KDM4/JMJD2 Histone Demethylases: Epigenetic Regulators in Cancer Cells. *Cancer Res.* **2013**, *73* (10), 2936-2942.
62. Katoh, M.; Katoh, M., Identification and characterization of JMJD2 family genes in silico. *International journal of oncology* **2004**, *24* (6), 1623-1628.
63. Hillringhaus, L.; Yue, W. W.; Rose, N. R.; Ng, S. S.; Gileadi, C.; Loenarz, C.; Bello, S. H.; Bray, J. E.; Schofield, C. J.; Oppermann, U., Structural and evolutionary basis for the dual substrate selectivity of human KDM4 histone demethylase family. *Journal of Biological Chemistry* **2011**, *286* (48), 41616-41625.
64. Ng, S. S.; Kavanagh, K. L.; McDonough, M. A.; Butler, D.; Pilka, E. S.; Lienard, B. M.; Bray, J. E.; Savitsky, P.; Gileadi, O.; Von Delft, F., Crystal structures of histone demethylase JMJD2A reveal basis for substrate specificity. *Nature* **2007**, *448* (7149), 87-91.
65. Rose, N. R.; Thalhammer, A.; Seden, P. T.; Mecinović, J.; Schofield, C. J., Inhibition of the histone lysine demethylase JMJD2A by ejection of structural Zn (II). *Chemical Communications* **2009**, (42), 6376-6378.

66. Jack, A. P.; Bussemer, S.; Hahn, M.; Pünzeler, S.; Snyder, M.; Wells, M.; Csankovszki, G.; Solovei, I.; Schotta, G.; Hake, S. B., H3K56me3 is a novel, conserved heterochromatic mark that largely but not completely overlaps with H3K9me3 in both regulation and localization. *PLoS one* **2013**, *8* (2), e51765.
67. Kim, J.; Daniel, J.; Espejo, A.; Lake, A.; Krishna, M.; Xia, L.; Zhang, Y.; Bedford, M. T., Tudor, MBT and chromo domains gauge the degree of lysine methylation. *EMBO reports* **2006**, *7* (4), 397-403.
68. Huang, Y.; Fang, J.; Bedford, M. T.; Zhang, Y.; Xu, R.-M., Recognition of histone H3 lysine-4 methylation by the double tudor domain of JMJD2A. *Science* **2006**, *312* (5774), 748-751.
69. Lee, J.; Thompson, J. R.; Botuyan, M. V.; Mer, G., Distinct binding modes specify the recognition of methylated histones H3K4 and H4K20 by JMJD2A-tudor. *Nature structural & molecular biology* **2008**, *15* (1), 109-111.
70. Musselman, C. A.; Kutateladze, T. G., PHD fingers: epigenetic effectors and potential drug targets. *Molecular interventions* **2009**, *9* (6), 314.
71. Iwamori, N.; Zhao, M.; Meistrich, M. L.; Matzuk, M. M., The testis-enriched histone demethylase, KDM4D, regulates methylation of histone H3 lysine 9 during spermatogenesis in the mouse but is dispensable for fertility. *Biology of reproduction* **2011**, *84* (6), 1225-1234.
72. Loh, Y.-H.; Zhang, W.; Chen, X.; George, J.; Ng, H.-H., Jmjd1a and Jmjd2c histone H3 Lys 9 demethylases regulate self-renewal in embryonic stem cells. *Genes & development* **2007**, *21* (20), 2545-2557.
73. Black, J. C.; Allen, A.; Van Rechem, C.; Forbes, E.; Longworth, M.; Tschop, K.; Rinehart, C.; Quiton, J.; Walsh, R.; Smallwood, A.; Dyson, N. J.; Whetstine, J. R., Conserved antagonism between JMJD2A/KDM4A and HP1gamma during cell cycle progression. *Mol Cell* **2010**, *40* (5), 736-48.
74. Mallette, F. A.; Mattioli, F.; Cui, G.; Young, L. C.; Hendzel, M. J.; Mer, G.; Sixma, T. K.; Richard, S., RNF8- and RNF168-dependent degradation of KDM4A/JMJD2A triggers 53BP1 recruitment to DNA damage sites. *The EMBO Journal* **2012**, *31* (8), 1865-1878.
75. Johmura, Y.; Sun, J.; Kitagawa, K.; Nakanishi, K.; Kuno, T.; Naiki-Ito, A.; Sawada, Y.; Miyamoto, T.; Okabe, A.; Aburatani, H.; Li, S.; Miyoshi, I.; Takahashi, S.; Kitagawa, M.; Nakanishi, M., SCF(Fbxo22)-KDM4A targets methylated p53 for degradation and regulates senescence. *Nat Commun* **2016**, *7*, 10574.
76. Hancock, R. L.; Masson, N.; Dunne, K.; Flashman, E.; Kawamura, A., The activity of JmjC histone lysine demethylase KDM4A is highly sensitive to oxygen concentrations. *ACS Chemical Biology* **2017**.
77. Dialynas, G. K.; Vitalini, M. W.; Wallrath, L. L., Linking Heterochromatin Protein 1 (HP1) to cancer progression. *Mutation Research/Fundamental and Molecular Mechanisms of Mutagenesis* **2008**, *647* (1-2), 13-20.
78. Albert, M.; Helin, K., Histone methyltransferases in cancer. *Seminars in Cell & Developmental Biology* **2010**, *21* (2), 209-220.
79. Wei, Y.; Xia, W.; Zhang, Z.; Liu, J.; Wang, H.; Adsay, N. V.; Albarracin, C.; Yu, D.; Abbuzzese, J. L.; Mills, G. B.; Bast, R. C.; Hortobagyi, G. N.; Hung, M.-C., Loss of trimethylation at lysine 27 of histone H3 is a predictor of poor outcome in breast, ovarian, and pancreatic cancers. *Molecular Carcinogenesis* **2008**, *47* (9), 701-706.

80. Ellinger, J.; Kahl, P.; Mertens, C.; Rogenhofer, S.; Hauser, S.; Hartmann, W.; Bastian, P. J.; Büttner, R.; Müller, S. C.; von Ruecker, A., Prognostic relevance of global histone H3 lysine 4 (H3K4) methylation in renal cell carcinoma. *International journal of cancer* **2010**, *127* (10), 2360-2366.
81. Tamagawa, H.; Oshima, T.; Shiozawa, M.; Morinaga, S.; Nakamura, Y.; Yoshihara, M.; Sakuma, Y.; Kameda, Y.; Akaike, M.; Masuda, M.; Imada, T.; Miyagi, Y., The global histone modification pattern correlates with overall survival in metachronous liver metastasis of colorectal cancer. *Oncology reports* **2012**, *27* (3), 637-42.
82. Manuyakorn, A.; Paulus, R.; Farrell, J.; Dawson, N. A.; Tze, S.; Cheung-Lau, G.; Hines, O. J.; Reber, H.; Seligson, D. B.; Horvath, S.; Kurdistani, S. K.; Guha, C.; Dawson, D. W., Cellular Histone Modification Patterns Predict Prognosis and Treatment Response in Resectable Pancreatic Adenocarcinoma: Results From RTOG 9704. *Journal of Clinical Oncology* **2010**, *28* (8), 1358-1365.
83. Song, J. S.; Kim, Y. S.; Kim, D. K.; Jang, S. J., Global histone modification pattern associated with recurrence and disease-free survival in non-small cell lung cancer patients. *Pathology international* **2012**, *62* (3), 182-190.
84. Liu, Y.; Zheng, P.; Liu, Y.; Ji, T.; Liu, X.; Yao, S.; Cheng, X.; Li, Y.; Chen, L.; Xiao, Z., An epigenetic role for PRL-3 as a regulator of H3K9 methylation in colorectal cancer. *Gut* **2013**, *62* (4), 571-581.
85. Northcott, P. A.; Nakahara, Y.; Wu, X.; Feuk, L.; Ellison, D. W.; Croul, S.; Mack, S.; Kongkham, P. N.; Peacock, J.; Dubuc, A., Multiple recurrent genetic events converge on control of histone lysine methylation in medulloblastoma. *Nature genetics* **2009**, *41* (4), 465-472.
86. Shi, L.; Sun, L.; Li, Q.; Liang, J.; Yu, W.; Yi, X.; Yang, X.; Li, Y.; Han, X.; Zhang, Y., Histone demethylase JMJD2B coordinates H3K4/H3K9 methylation and promotes hormonally responsive breast carcinogenesis. *Proceedings of the National Academy of Sciences* **2011**, *108* (18), 7541-7546.
87. Kawazu, M.; Saso, K.; Tong, K. I.; McQuire, T.; Goto, K.; Son, D. O.; Wakeham, A.; Miyagishi, M.; Mak, T. W.; Okada, H., Histone demethylase JMJD2B functions as a co-factor of estrogen receptor in breast cancer proliferation and mammary gland development. *PLoS One* **2011**, *6* (3), e17830.
88. Wissmann, M.; Yin, N.; Muller, J. M.; Greschik, H.; Fodor, B. D.; Jenuwein, T.; Vogler, C.; Schneider, R.; Gunther, T.; Buettner, R.; Metzger, E.; Schule, R., Cooperative demethylation by JMJD2C and LSD1 promotes androgen receptor-dependent gene expression. *Nat Cell Biol* **2007**, *9* (3), 347-53.
89. Young, L. C.; Hendzel, M. J., The oncogenic potential of Jumonji D2 (JMJD2/KDM4) histone demethylase overexpression 1. *Biochemistry and Cell Biology* **2012**, *91* (6), 369-377.
90. Liu, G.; Bollig-Fischer, A.; Kreike, B.; van de Vijver, M. J.; Abrams, J.; Ethier, S. P.; Yang, Z. Q., Genomic amplification and oncogenic properties of the GASC1 histone demethylase gene in breast cancer. *Oncogene* **2009**, *28* (50), 4491-4500.
91. Yang, Z. Q.; Imoto, I.; Fukuda, Y.; Pimkhaokham, A.; Shimada, Y.; Imamura, M.; Sugano, S.; Nakamura, Y.; Inazawa, J., Identification of a novel gene, GASC1, within an amplicon at 9p23-24 frequently detected in esophageal cancer cell lines. *Cancer Res* **2000**, *60* (17), 4735-9.

92. Rui, L.; Emre, N. C.; Kruhlak, M. J.; Chung, H. J.; Steidl, C.; Slack, G.; Wright, G. W.; Lenz, G.; Ngo, V. N.; Shaffer, A. L.; Xu, W.; Zhao, H.; Yang, Y.; Lamy, L.; Davis, R. E.; Xiao, W.; Powell, J.; Maloney, D.; Thomas, C. J.; Moller, P.; Rosenwald, A.; Ott, G.; Muller-Hermelink, H. K.; Savage, K.; Connors, J. M.; Rimsza, L. M.; Campo, E.; Jaffe, E. S.; Delabie, J.; Smeland, E. B.; Weisenburger, D. D.; Chan, W. C.; Gascoyne, R. D.; Levens, D.; Staudt, L. M., Cooperative epigenetic modulation by cancer amplicon genes. *Cancer Cell* **2010**, *18* (6), 590-605.
93. Toyokawa, G.; Cho, H.-S.; Iwai, Y.; Yoshimatsu, M.; Takawa, M.; Hayami, S.; Maejima, K.; Shimizu, N.; Tanaka, H.; Tsunoda, T.; Field, H. I.; Kelly, J. D.; Neal, D. E.; Ponder, B. A. J.; Maehara, Y.; Nakamura, Y.; Hamamoto, R., The Histone Demethylase JMJD2B Plays an Essential Role in Human Carcinogenesis through Positive Regulation of Cyclin-Dependent Kinase 6. *Cancer Prevention Research* **2011**, *4* (12), 2051-2061.
94. Kim, T.-D.; Shin, S.; Berry, W. L.; Oh, S.; Janknecht, R., The JMJD2A demethylase regulates apoptosis and proliferation in colon cancer cells. *Journal of Cellular Biochemistry* **2012**, *113* (4), 1368-1376.
95. Zhang, Q.-J.; Chen, H.-Z.; Wang, L.; Liu, D.-P.; Hill, J. A.; Liu, Z.-P., The histone trimethyllysine demethylase JMJD2A promotes cardiac hypertrophy in response to hypertrophic stimuli in mice. *The Journal of clinical investigation* **2011**, *121* (6), 2447-2456.
96. Chen, Z.; Zang, J.; Kappler, J.; Hong, X.; Crawford, F.; Wang, Q.; Lan, F.; Jiang, C.; Whetstone, J.; Dai, S., Structural basis of the recognition of a methylated histone tail by JMJD2A. *Proceedings of the National Academy of Sciences* **2007**, *104* (26), 10818-10823.
97. Rose, N. R.; Ng, S. S.; Mecinovic, J.; Liénard, B. t. M.; Bello, S. H.; Sun, Z.; McDonough, M. A.; Oppermann, U.; Schofield, C. J., Inhibitor Scaffolds for 2-Oxoglutarate-Dependent Histone Lysine Demethylases. *Journal of medicinal chemistry* **2008**, *51* (22), 7053-7056.
98. Hamada, S.; Suzuki, T.; Mino, K.; Koseki, K.; Oehme, F.; Flamme, I.; Ozasa, H.; Itoh, Y.; Ogasawara, D.; Komaarashi, H., Design, synthesis, enzyme-inhibitory activity, and effect on human cancer cells of a novel series of jumonji domain-containing protein 2 histone demethylase inhibitors. *Journal of medicinal chemistry* **2010**, *53* (15), 5629-5638.
99. Rose, N. R.; Woon, E. C. Y.; Tumber, A.; Walport, L. J.; Chowdhury, R.; Li, X. S.; King, O. N. F.; Lejeune, C.; Ng, S. S.; Krojer, T.; Chan, M. C.; Rydzik, A. M.; Hopkinson, R. J.; Che, K. H.; Daniel, M.; Strain-Damerell, C.; Gileadi, C.; Kochan, G.; Leung, I. K. H.; Dunford, J.; Yeoh, K. K.; Ratcliffe, P. J.; Burgess-Brown, N.; von Delft, F.; Muller, S.; Marsden, B.; Brennan, P. E.; McDonough, M. A.; Oppermann, U.; Klose, R. J.; Schofield, C. J.; Kawamura, A., Plant Growth Regulator Daminozide Is a Selective Inhibitor of Human KDM2/7 Histone Demethylases. *Journal of Medicinal Chemistry* **2012**, *55* (14), 6639-6643.
100. Mackeen, M. M.; Kramer, H. B.; Chang, K.-H.; Coleman, M. L.; Hopkinson, R. J.; Schofield, C. J.; Kessler, B. M., Small-molecule-based inhibition of histone demethylation in cells assessed by quantitative mass spectrometry. *Journal of proteome research* **2010**, *9* (8), 4082-4092.
101. Thalhammer, A.; Mecinović, J.; Loenarz, C.; Tumber, A.; Rose, N. R.; Heightman, T. D.; Schofield, C. J., Inhibition of the histone demethylase JMJD2E

by 3-substituted pyridine 2, 4-dicarboxylates. *Organic & biomolecular chemistry* **2011**, *9* (1), 127-135.

102. Chang, K. H.; King, O. N.; Tumber, A.; Woon, E. C.; Heightman, T. D.; McDonough, M. A.; Schofield, C. J.; Rose, N. R., Inhibition of histone demethylases by 4-carboxy-2, 2'-bipyridyl compounds. *ChemMedChem* **2011**, *6* (5), 759-764.

103. King, O. N.; Li, X. S.; Sakurai, M.; Kawamura, A.; Rose, N. R.; Ng, S. S.; Quinn, A. M.; Rai, G.; Mott, B. T.; Beswick, P.; Klose, R. J.; Oppermann, U.; Jadhav, A.; Heightman, T. D.; Maloney, D. J.; Schofield, C. J.; Simeonov, A., Quantitative high-throughput screening identifies 8-hydroxyquinolines as cell-active histone demethylase inhibitors. *PLoS One* **2010**, *5* (11), e15535.

104. Feng, T.; Li, D.; Wang, H.; Zhuang, J.; Liu, F.; Bao, Q.; Lei, Y.; Chen, W.; Zhang, X.; Xu, X., Novel 5-carboxy-8-HQ based histone demethylase JMJD2A inhibitors: Introduction of an additional carboxyl group at the C-2 position of quinoline. *European journal of medicinal chemistry* **2015**, *105*, 145-155.

105. England, K. S.; Tumber, A.; Krojer, T.; Scozzafava, G.; Ng, S. S.; Daniel, M.; Szykowska, A.; Che, K.; von Delft, F.; Burgess-Brown, N. A., Optimisation of a triazolopyridine based histone demethylase inhibitor yields a potent and selective KDM2A (FBXL11) inhibitor. *MedChemComm* **2014**, *5* (12), 1879-1886.

106. Rüger, N.; Roatsch, M.; Emmrich, T.; Franz, H.; Schüle, R.; Jung, M.; Link, A., Tetrazolylhydrazides as selective fragment-like inhibitors of the JumonjiC-domain-containing histone demethylase KDM4A. *ChemMedChem* **2015**, *10* (11), 1875-1883.

107. Sakurai, M.; Rose, N. R.; Schultz, L.; Quinn, A. M.; Jadhav, A.; Ng, S. S.; Oppermann, U.; Schofield, C. J.; Simeonov, A., A miniaturized screen for inhibitors of Jumonji histone demethylases. *Molecular BioSystems* **2010**, *6* (2), 357-364.

108. Nielsen, A. L.; Kristensen, L. H.; Stephansen, K. B.; Kristensen, J. B.; Helgstrand, C.; Lees, M.; Cloos, P.; Helin, K.; Gajhede, M.; Olsen, L., Identification of catechols as histone-lysine demethylase inhibitors. *FEBS letters* **2012**, *586* (8), 1190-1194.

109. Kim, S.-H.; Kwon, S. H.; Park, S.-H.; Lee, J. K.; Bang, H.-S.; Nam, S.-J.; Kwon, H. C.; Shin, J.; Oh, D.-C., Tripartin, a histone demethylase inhibitor from a bacterium associated with a dung beetle larva. *Organic letters* **2013**, *15* (8), 1834-1837.

110. Kwolek-Mirek, M.; Zdrag-Tecza, R.; Bartosz, G., Ascorbate and thiol antioxidants abolish sensitivity of yeast *Saccharomyces cerevisiae* to disulfiram. *Cell biology and toxicology* **2012**, *28* (1), 1-9.

111. Azad, G. K.; Tomar, R. S., Ebselen, a promising antioxidant drug: mechanisms of action and targets of biological pathways. *Molecular biology reports* **2014**, *41* (8), 4865-4879.

112. Chu, C.-H.; Wang, L.-Y.; Hsu, K.-C.; Chen, C.-C.; Cheng, H.-H.; Wang, S.-M.; Wu, C.-M.; Chen, T.-J.; Li, L.-T.; Liu, R., KDM4B as a target for prostate cancer: structural analysis and selective inhibition by a novel inhibitor. *Journal of medicinal chemistry* **2014**, *57* (14), 5975-5985.

113. Kim, T.-D.; Fuchs, J. R.; Schwartz, E.; Abdelhamid, D.; Etter, J.; Berry, W. L.; Li, C.; Ihnat, M. A.; Li, P.-K.; Janknecht, R., Pro-growth role of the JMJD2C histone demethylase in HCT-116 colon cancer cells and identification of curcuminoids as JMJD2 inhibitors. *Am J Transl Res* **2014**, *6* (3), 236-47.

114. Baell, J. B., Feeling nature's PAINS: natural products, natural product drugs, and Pan Assay Interference Compounds (PAINS). *J Nat Prod* **2016**, 79.
115. McAllister, T. E.; England, K. S.; Hopkinson, R. J.; Brennan, P. E.; Kawamura, A.; Schofield, C. J., Recent Progress in Histone Demethylase Inhibitors. *J Med Chem* **2016**, 59 (4), 1308-29.
116. Holdgate, G.; Geschwindner, S.; Breeze, A.; Davies, G.; Colclough, N.; Temesi, D.; Ward, L., Biophysical Methods in Drug Discovery from Small Molecule to Pharmaceutical. In *Protein-Ligand Interactions: Methods and Applications*, Williams, M. A.; Daviter, T., Eds. Humana Press: Totowa, NJ, 2013; pp 327-355.
117. Couture, J.-F.; Collazo, E.; Ortiz-Tello, P. A.; Brunzelle, J. S.; Trievel, R. C., Specificity and mechanism of JMJD2A, a trimethyllysine-specific histone demethylase. *Nature structural & molecular biology* **2007**, 14 (8), 689-695.
118. Kawamura, A.; Tumber, A.; Rose, N. R.; King, O. N.; Daniel, M.; Oppermann, U.; Heightman, T. D.; Schofield, C., Development of homogeneous luminescence assays for histone demethylase catalysis and binding. *Analytical biochemistry* **2010**, 404 (1), 86-93.
119. Taouji, S.; Dahan, S.; Bossé, R.; Chevet, E., Current Screens Based on the AlphaScreen™ Technology for Deciphering Cell Signalling Pathways. *Current genomics* **2009**, 10 (2), 93-101.
120. Rose, N. R.; Woon, E. C.; Kingham, G. L.; King, O. N.; Mecinovic, J.; Clifton, I. J.; Ng, S. S.; Talib-Hardy, J.; Oppermann, U.; McDonough, M. A.; Schofield, C. J., Selective inhibitors of the JMJD2 histone demethylases: combined nondenaturing mass spectrometric screening and crystallographic approaches. *J Med Chem* **2010**, 53 (4), 1810-8.
121. Congreve, M.; Carr, R.; Murray, C.; Jhoti, H., A 'rule of three' for fragment-based lead discovery? *Drug Discov Today* **2003**, 8 (19), 876-7.
122. Jhoti, H.; Williams, G.; Rees, D. C.; Murray, C. W., The 'rule of three' for fragment-based drug discovery: where are we now? *Nature Reviews Drug Discovery* **2013**, 12 (8), 644-644.
123. Nielsen, T. E.; Schreiber, S. L., Towards the optimal screening collection: a synthesis strategy. *Angewandte Chemie International Edition* **2008**, 47 (1), 48-56.
124. Morwick, T.; Berry, A.; Brickwood, J.; Cardozo, M.; Catron, K.; DeTuri, M.; Emeigh, J.; Homon, C.; Hrapchak, M.; Jacober, S.; Jakes, S.; Kaplita, P.; Kelly, T. A.; Ksiazek, J.; Liuzzi, M.; Magolda, R.; Mao, C.; Marshall, D.; McNeil, D.; Prokopowicz, A., III; Sarko, C.; Scouten, E.; Sledziona, C.; Sun, S.; Watrous, J.; Wu, J. P.; Cywin, C. L., Evolution of the Thienopyridine Class of Inhibitors of IκB Kinase-β: Part I: Hit-to-Lead Strategies. *J. Med. Chem.* **2006**, 49 (10), 2898-2908.
125. Morwick, T.; Büttner, F. H.; Cywin, C. L.; Dahmann, G.; Hickey, E.; Jakes, S.; Kaplita, P.; Kashem, M. A.; Kerr, S.; Kugler, S.; Mao, W.; Marshall, D.; Paw, Z.; Shih, C.-K.; Wu, F.; Young, E., Hit to Lead Account of the Discovery of Bisbenzamide and Related Ureidobenzamide Inhibitors of Rho Kinase. *Journal of Medicinal Chemistry* **2010**, 53 (2), 759-777.
126. Christie, R. M.; Moss, S., Cyclization of Schiff bases containing amide or hydroxamic acid groups to 1,2-dihydroquinazolin-4-ones; thermal decomposition reactions of the 1,2-dihydroquinazolin-4-ones. *J. Chem. Soc., Perkin Trans. 1* **1985**, (12), 2779-83.

127. Delpivo, C.; Micheletti, G.; Boga, C., A green synthesis of quinoxalines and 2,3-dihydropyrazines. *Synthesis* **2013**, *45* (11), 1546-1552.
128. Zhang, C.; Xu, Z.; Zhang, L.; Jiao, N., Et₃N-catalyzed oxidative dehydrogenative coupling of α -unsubstituted aldehydes and ketones with aryl diamines leading to quinoxalines using molecular oxygen as oxidant. *Tetrahedron* **2012**, *68* (26), 5258-5262.
129. Knapp, S.; Ziv, J.; Rosen, J. D., Synthesis of the food mutagens MeIQx and 4,8-DiMeIQx by copper(I)-promoted quinoxaline formation. *Tetrahedron* **1989**, *45* (5), 1293-8.
130. Rajulu, G. G.; Bhojya Naik, H. S.; Viswanadhan, A.; Thiruvengadam, J.; Rajesh, K.; Ganesh, S.; Jagadheshan, H.; Kesavan, P. K., New hydroxamic acid derivatives of fluoroquinolones: synthesis and evaluation of antibacterial and anticancer properties. *Chem Pharm Bull (Tokyo)* **2014**, *62* (2), 168-75.
131. De, S. K.; Stebbins, J. L.; Chen, L. H.; Riel-Mehan, M.; Machleidt, T.; Dahl, R.; Yuan, H.; Emdadi, A.; Barile, E.; Chen, V.; Murphy, R.; Pellicchia, M., Design, synthesis, and structure-activity relationship of substrate competitive, selective, and in vivo active triazole and thiadiazole inhibitors of the c-Jun N-terminal kinase. *J Med Chem* **2009**, *52* (7), 1943-52.
132. Sheng, C.; Che, X.; Wang, W.; Wang, S.; Cao, Y.; Miao, Z.; Yao, J.; Zhang, W., Design and synthesis of novel triazole antifungal derivatives by structure-based bioisosterism. *Eur. J. Med. Chem.* **2011**, *46* (11), 5276-5282.
133. Sandmeyer, T., Über Isonitrosoacetanilide und deren Kondensation zu Isatinen. *Helvetica Chimica Acta* **1919**, *2* (1), 234-242.
134. Kansy, M.; Senner, F.; Gubernator, K., Physicochemical High Throughput Screening: Parallel Artificial Membrane Permeation Assay in the Description of Passive Absorption Processes. *J. Med. Chem.* **1998**, *41* (7), 1007-1010.
135. Ottaviani, G.; Martel, S.; Carrupt, P.-A., Parallel Artificial Membrane Permeability Assay: A New Membrane for the Fast Prediction of Passive Human Skin Permeability. *Journal of Medicinal Chemistry* **2006**, *49* (13), 3948-3954.
136. Ng, S. S.; Kavanagh, K. L.; McDonough, M. A.; Butler, D.; Pilka, E. S.; Lienard, B. M. R.; Bray, J. E.; Savitsky, P.; Gileadi, O.; von, D. F.; Rose, N. R.; Offer, J.; Scheinost, J. C.; Borowski, T.; Sundstrom, M.; Schofield, C. J.; Oppermann, U., Crystal structures of histone demethylase JMJD2A reveal basis for substrate specificity. *Nature (London, U. K.)* **2007**, *448* (7149), 87-91.
137. Pan, L.; Ho, Q.; Tsutsui, K.; Takahashi, L., Comparison of chromatographic and spectroscopic methods used to rank compounds for aqueous solubility. *Journal of pharmaceutical sciences* **2001**, *90* (4), 521-9.
138. Silber, B. M.; Rao, S.; Fife, K. L.; Gallardo-Godoy, A.; Renslo, A. R.; Dalvie, D. K.; Giles, K.; Freyman, Y.; Elepano, M.; Gever, J. R.; Li, Z.; Jacobson, M. P.; Huang, Y.; Benet, L. Z.; Prusiner, S. B., Pharmacokinetics and metabolism of 2-aminothiazoles with antiprion activity in mice. *Pharmaceutical research* **2013**, *30* (4), 932-50.
139. Kerns, E. H.; Di, L.; Carter, G. T., In vitro solubility assays in drug discovery. *Current drug metabolism* **2008**, *9* (9), 879-85.
140. Villar-Garea, A.; Israel, L.; Imhof, A., Analysis of histone modifications by mass spectrometry. *Curr Protoc Protein Sci* **2008**, *Chapter 14*, Unit 14.10.
141. Kruidenier, L.; Chung, C.-w.; Cheng, Z.; Liddle, J.; Che, K.; Joberty, G.; Bantscheff, M.; Bountra, C.; Bridges, A.; Diallo, H., A selective jumonji H3K27

- demethylase inhibitor modulates the proinflammatory macrophage response. *Nature* **2012**, 488 (7411), 404-408.
142. AIST: Integrated Spectral Database System of Organic Compounds. National Institute of Advanced Industrial Science and Technology (Japan).
143. Lin, C.-F.; Yang, J.-S.; Chang, C.-Y.; Kuo, S.-C.; Lee, M.-R.; Huang, L.-J., Synthesis and anticancer activity of benzyloxybenzaldehyde derivatives against HL-60 cells. *Bioorganic & medicinal chemistry* **2005**, 13 (5), 1537-1544.
144. Kafle, B.; Aher, N. G.; Khadka, D.; Park, H.; Cho, H., Isoxazol-5 (4H) one Derivatives as PTP1B Inhibitors Showing an Anti-Obesity Effect. *Chemistry—An Asian Journal* **2011**, 6 (8), 2073-2079.
145. Ilangoan, A.; Anandhan, K.; Kaushik, M. P., Facile and selective deprotection of PMB ethers and esters using oxalyl chloride. *Tetrahedron Letters* **2015**, 56 (9), 1080-1084.
146. Bhattarai, B. R.; Kafle, B.; Hwang, J.-S.; Khadka, D.; Lee, S.-M.; Kang, J.-S.; Ham, S. W.; Han, I.-O.; Park, H.; Cho, H., Thiazolidinedione derivatives as PTP1B inhibitors with antihyperglycemic and antiobesity effects. *Bioorganic & medicinal chemistry letters* **2009**, 19 (21), 6161-6165.
147. Hobson, A. D.; Harris, C. M.; van der Kam, E. L.; Turner, S. C.; Abibi, A.; Aguirre, A. L.; Bousquet, P.; Kebede, T.; Konopacki, D. B.; Gintant, G., Discovery of A-971432, an orally bioavailable selective sphingosine-1-phosphate receptor 5 (S1P5) agonist for the potential treatment of neurodegenerative disorders. *Journal of medicinal chemistry* **2015**, 58 (23), 9154-9170.
148. Ma, Y.; Sun, S. X.; Cheng, X. C.; Wang, S. Q.; Dong, W. L.; Wang, R. L.; Xu, W. R., Design and Synthesis of Imidazolidine-2, 4-Dione Derivatives as Selective Inhibitors by Targeting Protein Tyrosine Phosphatase-1B Over T-Cell Protein Tyrosine Phosphatase. *Chemical biology & drug design* **2013**, 82 (5), 595-602.
149. Luzzio, F. A.; Chen, J., Efficient Preparation and Processing of the 4-Methoxybenzyl (PMB) Group for Phenolic Protection Using Ultrasound. *J. Org. Chem.* **2008**, 73 (14), 5621-5624.
150. Turan, I. S.; Akkaya, E. U., Chemiluminescence Sensing of Fluoride Ions Using a Self-Immolative Amplifier. *Org. Lett.* **2014**, 16 (6), 1680-1683.
151. Quiroz-Florentino, H.; Hernandez-Benitez, R. I.; Avina, J. A.; Burgueno-Tapia, E.; Tamariz, J., Total synthesis of naturally occurring furan compounds 5-[[4-(4-hydroxybenzyl)oxy]methyl]-2-furaldehyde and pichiafuran C. *Synthesis* **2011**, (7), 1106-1112.
152. Mhaske, S. B.; Argade, N. P., Regioselective Quinazolinone-Directed Ortho Lithiation of Quinazolinoylquinoline: Practical Synthesis of Naturally Occurring Human DNA Topoisomerase I Poison Luotonin A and Luotonins B and E. *The Journal of Organic Chemistry* **2004**, 69 (13), 4563-4566.